GENERATION AND CHARACTERISATION OF LEUCINE-RICH REPEAT KINASE 2 (LRRK2) KNOCKOUT SH-SY5Y NEUROBLASTOMA CELLS AND INVESTIGATION OF THE EFFECTS OF EDIBLE BIRD'S NEST EXTRACT

By

JONG HUI LAN

A thesis submitted to

M. Kandiah Faculty of Medicine and Health Sciences,

Universiti Tunku Abdul Rahman,

in partial fulfilment of the requirements for the degree of

Doctor of Philosophy (Medical Science)

March 2026

ABSTRACT

GENERATION AND CHARACTERISATION OF LEUCINE-RICH REPEAT KINASE 2 (LRRK2) KNOCKOUT SH-SY5Y NEUROBLASTOMA CELLS AND INVESTIGATION OF THE EFFECTS OF EDIBLE BIRD'S NEST EXTRACT

Jong Hui Lan

Mutations in leucine-rich repeat kinase 2 (LRRK2) are a major genetic contributor to Parkinson's disease (PD), with pathogenic variants increasing kinase activity and motivating LRRK2 inhibition as a therapeutic strategy. However, abnormal phenotypes in LRRK2 knockout models raise safety concerns. Emerging evidence also implicates LRRK2 in cancer biology, with pathogenic mutations associated with increased malignancy risk, prompting investigation of LRRK2 inhibition in oncology.

The human neuroblastoma cell line SH-SY5Y is widely used in PD research but expresses LRRK2 at low levels, presenting challenges for gene knockout studies. In this study, an optimised strategy was developed to generate LRRK2 knockout SH-SY5Y (LKO) cells. A double-cut CRISPR/Cas9 system with multiple guide RNAs was employed, alongside optimisation of electroporation conditions, clonal expansion procedures, and sensitive protein detection methods. Successful knockout of LRRK2 was confirmed by PCR, Sanger sequencing, and Western blot analysis.

Phenotypic characterisation of LKO cells revealed marked morphological and functional alterations, including changes in cell morphology, adhesion, proliferation, senescence, autophagy, and mitochondrial respiration. LKO cells underwent conversion into intermediate (I-type) and substrate-adherent/Schwannian (S-type) neuroblastoma phenotypes and displayed hallmarks of cellular senescence, such as enlarged and flattened morphology, loss of neurite-like processes, increased substrate adhesion, reduced proliferation, elevated senescence-associated β-galactosidase activity, and decreased autophagic activity and mitochondrial respiration. Among the LKO clones, LKO1 (I-type) retained the ability to differentiate into N-type cells and dopaminergic neurons, making it suitable for PD-related studies and a potential model for investigating LRRK2-associated cancer stem cell-like properties. In contrast, LKO2 and LKO3 (S-type) provided insights into neuroblastoma cell plasticity.

Using LKO1 cells, the effects of edible bird's nest (EBN) acid extract were evaluated. The extract exhibited antioxidant activity but significantly stimulated cell proliferation and autophagy, suggesting that EBN may promote senescence evasion and support cancer cell growth. Despite its antioxidant properties, EBN may therefore be unsuitable as a complementary therapy for cancer patients.

Keywords: leucine-rich repeat kinase 2; knockout; neuroblastoma; edible bird's nest; senescence

Subject Area: RC321-571 Neurosciences

ACKNOWLEDGEMENTS

First and foremost, I would like to express my heartfelt gratitude to my supervisors, Academician Emeritus Professor Cheong Soon Keng and Professor Lam Sau Kuen, for their support, insightful guidance, and constructive feedback. Their thoughtful reviews of both the manuscripts and this thesis are sincerely appreciated.

I am also profoundly thankful to collaborators at the University of Hong Kong, Professor Jin Dong Yan and Dr Yuen Kit San, for their kindness, generosity, and understanding. I am especially grateful for their steadfast support during a pivotal stage of my research, where they generously hosted me in their laboratory for three months to acquire advanced training in the CRISPR/Cas9 genome editing technique. This thesis would not have been possible without their invaluable assistance in helping me overcome that critical hurdle.

Special thanks are extended to Dr Susan Hoe Ling Ling, Research Officer at the Molecular Pathology Unit, Cancer Research Centre, Institute for Medical Research (IMR), for her invaluable assistance with cell sorting. Her consistent encouragement, helpful suggestions, and meticulous proofreading of the manuscript were of great help and are sincerely appreciated.

I would also like to express my sincere gratitude to Prof. Emeritus Robert A. Ross of Fordham University for his invaluable insights in confirming the morphology of the LKO cells, which shaped the interpretation of the findings. In addition, I extend my heartfelt thanks to Prof. Dario Alessi of the University of Dundee for his insightful comments, constructive guidance on future directions for LRRK2 research, and his encouragement.

I would like to dedicate this thesis to my beloved husband, parents, and siblings, whose unwavering love and support have sustained me throughout this journey. A special debt of gratitude is owed to my husband for his enduring support, understanding, and encouragement, especially during the most challenging times.

My heartfelt thanks also go to my friends, whose tremendous moral support has meant so much during difficult moments. Lastly, to all those not mentioned by name but who contributed in various ways during times of need, please accept my sincere appreciation and thanks.

APPROVAL SHEET

This thesis entitled "**GENERATION AND CHARACTERISATION OF LEUCINE-RICH REPEAT KINASE 2 (LRRK2) KNOCKOUT SH-SY5Y NEUROBLASTOMA CELLS AND INVESTIGATION OF THE EFFECTS OF EDIBLE BIRD'S NEST EXTRACT**" was prepared by JONG HUI LAN and submitted as partial fulfilment of the requirements for the degree of Doctor of Philosophy (Medical Science) at Universiti Tunku Abdul Rahman.

Approved by:

_____

(Academician Emeritus Prof. Dr. Cheong Soon Keng) Date: 28/10/2025
Academician Emeritus Professor/Supervisor
Department of Medicine
M. Kandiah Faculty of Medicine and Health Sciences
Universiti Tunku Abdul Rahman

_____

(Prof. Dr. Lam Sau Kuen) Date: 28/10/2025
Professor/Co-supervisor
Department of Pre-clinical Sciences
M. Kandiah Faculty of Medicine and Health Sciences
Universiti Tunku Abdul Rahman

M. KANDIAH FACULTY OF MEDICINE AND HEALTH SCIENCES

UNIVERSITI TUNKU ABDUL RAHMAN

Date: 28/10/2025

SUBMISSION OF THESIS

It is hereby certified that **Jong Hui Lan** (ID No:) has completed this thesis entitled "GENERATION AND CHARACTERISATION OF LEUCINE-RICH REPEAT KINASE 2 (LRRK2) KNOCKOUT SH-SY5Y NEUROBLASTOMA CELLS AND INVESTIGATION OF THE EFFECTS OF EDIBLE BIRD'S NEST EXTRACT" under the supervision of Academician Emeritus Prof. Dr. Cheong Soon Keng from the Department of Medicine, M. Kandiah Faculty of Medicine and Health Sciences, and Prof. Dr. Lam Sau Kuen from the Department of Pre-clinical Sciences, M. Kandiah Faculty of Medicine and Health Sciences.

I understand that the University will upload a soft copy of my thesis in PDF format into the UTAR Institutional Repository, which may be made accessible to the UTAR community and the public.

Yours truly,

_____

Jong Hui Lan

DECLARATION

I, JONG HUI LAN, hereby declare that the thesis is based on my original work except for quotations and citations which have been duly acknowledged. I also declare that it has not been previously or concurrently submitted for any other degree at UTAR or other institutions.

_____

(JONG HUI LAN)

Date: 28/10/2025

TABLE OF CONTENTS

LIST OF TABLES

LIST OF FIGURES

LIST OF ABBREVIATIONS

BSA	Bovine serum albumin
CAA	Cellular antioxidant activity
CAM	Complementary and alternative medicine
Cas9	CRISPR-associated protein 9
CRISPR	Clustered regularly interspaced short palindromic repeats
DCFH-DA	Dichloro-dihydro-fluorescein diacetate
DPPH	2,2-diphenyl-1-picrylhydrazyl
EBN	Edible bird's nest
ECAR	Extracellular acidification rate
EDTA	Ethylenediaminetetraacetic acid
FACS	Fluorescence-activated cell sorting
FCCP	Carbonyl cyanide-4 (trifluoromethoxy) phenylhydrazone
GAPDH	Glyceraldehyde-3-Phosphate Dehydrogenase
GFP	Green fluorescence protein
gRNA	Guide RNA
I-type	Intermediate type
KO	Knockout
LKO	LRRK2 knockout SH-SY5Y
LRRK2	Leucine-rich repeat kinase 2
N-type	Neuronal type
OCR	Oxygen consumption rate
ORAC	Oxygen radical absorbance capacity
PAM	Protospacer adjacent motif

PBS	Phosphate-buffered saline
PCR	Polymerase chain reaction
PD	Parkinson's disease
PX458	pSpCas9(BB)-2A-GFP
SA-β-gal	Senescence-associated β-galactosidase
S-type	Substrate-adherent/ Schwannian type
WT	Wild type

CHAPTER 1.0

INTRODUCTION

Leucine-rich repeat kinase 2 (LRRK2) is a large, multi-domain protein possessing both kinase and GTPase activities, and is involved in a variety of cellular processes (Tolosa *et al.*, 2020). A growing body of evidence implicates LRRK2 in the pathogenesis of Parkinson's disease (PD). The heightened kinase activity associated with its pathogenic variants has attracted considerable interest from both academic and pharmaceutical communities, leading to intensified efforts to develop therapeutic strategies targeting LRRK2 kinase activity, particularly given that PD remains an incurable disorder (Kalogeropulou *et al.*, 2022, Cookson, 2010, U.S. National Library of Medicine, 2025a, U.S. National Library of Medicine, 2025d). However, the abnormal phenotypes observed in LRRK2 knockout animal models raise significant safety concerns that have yet to be fully addressed (Tong *et al.*, 2012, Hinkle *et al.*, 2012, Baptista *et al.*, 2013, Pellegrini *et al.*, 2018, Tong *et al.*, 2010). Despite these early concerns, LRRK2 continues to be a high-priority target for PD therapy, and significant efforts have been made to develop kinase inhibitors with improved safety profiles. Several LRRK2 kinase inhibitors have shown promise in preclinical studies, with some advancing to clinical trials (Taymans *et al.*, 2023, Azeggagh and Berwick, 2022, U.S. National Library of Medicine, 2025a, U.S. National Library of Medicine, 2025d). Nevertheless, concerns about adverse effects persist. While some studies have reported undesirable outcomes following LRRK2 kinase inhibition

(Fuji *et al.*, 2015, Fell *et al.*, 2015, Daher *et al.*, 2015), others have demonstrated that these effects are reversible upon drug withdrawal (Baptista *et al.*, 2020b, Bryce *et al.*, 2021) or have reported no significant side effects (Ho *et al.*, 2022, Andersen *et al.*, 2018).

Despite its well-established role in the pathogenesis of PD, accumulating evidence indicates that LRRK2 may also play a role in cancer biology. Pathogenic LRRK2 mutations, most notably the G2019S variant, have been associated with an increased risk of several malignancies in patients with PD, including skin cancer, colorectal cancer, leukaemia, hormone-related cancers, and breast cancer (Agalliu *et al.*, 2019, Agalliu *et al.*, 2015). Accordingly, as in PD, pharmacological inhibition of LRRK2 has been investigated as a potential therapeutic strategy in oncology, with studies demonstrating effects in clear cell renal cell carcinoma (Yang *et al.*, 2021), lung cancer (Wu *et al.*, 2023, Jiang *et al.*, 2019) and breast cancer cell lines (Jung *et al.*, 2021).

Owing to its human origin and neuronal characteristics, the SH-SY5Y human neuroblastoma cell line, established over five decades ago (BiedlerHelson and Spengler, 1973, Biedler *et al.*, 1978), has been widely utilised as a cellular model for PD (IoghenCeafalan and Popescu, 2023). Notably, SH-SY5Y cells have been extensively employed in studies of neurotoxicity and neurogenetics (IoghenCeafalan and Popescu, 2023, Kovalevich and Langford, 2013b). LRRK2 expression in SH-SY5Y cells is relatively low, mirroring the low endogenous levels observed in the human brain, particularly when compared to tissues such as the lungs and kidneys (The Human Protein Atlas, no date, Tong *et al.*, 2010). Accumulating evidence over the years has highlighted that genes with low expression levels should not be overlooked, as they can play critical roles in

regulating cellular functions, development, and disease processes (Hipp *et al.*, 2010, Li *et al.*, 2024a). Knocking out low-expression genes is inherently challenging due to minimal baseline activity and subtle functional effects, which often result in weak or absent phenotypes. For LRRK2, pronounced effects are mainly observed in high-expression tissues, while low-expression tissues show limited changes, likely due to genetic compensation and functional redundancy with LRRK1 (Biskup *et al.*, 2007, Fernández *et al.*, 2022, Giaime *et al.*, 2017, Tong *et al.*, 2010). These low-expression genes are often difficult to detect and quantify, making it challenging to confirm successful knockout (Biskup *et al.*, 2007, Fernández *et al.*, 2022). While knocking out low-expression genes remains a technical challenge, the advent of CRISPR/Cas9 genome editing technology has significantly facilitated this process.

CRISPR/Cas9 is a revolutionary, Nobel Prize-winning genome editing technology (Ledford and Callaway, 2020) that has been widely adopted by laboratories worldwide since its first successful application in mammalian cells in 2013 (Ran *et al.*, 2013). Due to its high efficiency, precision, and ease of use, CRISPR/Cas9 has been employed across a broad range of research fields, including neurodegenerative diseases such as PD, to facilitate genetic manipulation in both cellular and animal models. Its applications include gene knock-in and knockout (Xu and Li, 2020). In this context, the present study aims to establish a cellular model of LRRK2 knockout using SH-SY5 cells and CRISPR/Cas9 technology, with the goal of investigating the potential adverse effects associated with the loss of LRRK2. While the model has notable limitations, it nonetheless offers a valuable and accessible platform for

preliminary screening and mechanistic studies, helping to bridge the gap between simpler *in vitro* models and more complex *in vivo* models.

Edible bird's nest (EBN) is a functional food widely consumed around the world, particularly within the Chinese community (Zulkefle *et al.*, 2024). Its reputed immune-boosting properties have made it a popular complementary and alternative medicine (CAM) among cancer patients seeking to mitigate the adverse effects of chemotherapy (Wong *et al.*, 2010, ShihChiang and Chan, 2009, Lim *et al.*, 2006, Zhao *et al.*, 2016). However, EBN has also been reported to stimulate the proliferation of various cell types (Roh *et al.*, 2012, Zainal Abidin *et al.*, 2011, Chua *et al.*, 2013, Albishtue *et al.*, 2018b), raising concerns about its appropriateness for consumption by cancer patients.

This study initially aimed to address the following research gaps: (i) whether LRRK2 knockout leads to deleterious effects, and (ii) whether EBN extracts can ameliorate these effects, specifically by evaluating the neuroprotective effects of EBN on LRRK2 knockout dopaminergic neurons differentiated from SH-SY5Y neuroblastoma cells. However, this study took an unexpected turn when the established LRRK2 knockout SH-SY5Y (LKO) cells exhibited unanticipated phenotypic changes, shifting from the neuronal (N-type) phenotype to either intermediate (I-type) or substrate-adherent/Schwannian (S-type) neuroblastoma subtypes. Among the three LKO clones generated, LKO1 displayed features consistent with I-type cells, whereas LKO2 and LKO3 exhibited characteristics typical of S-type cells. Given that LKO2 and LKO3 showed very slow or nearly no growth, they may not pose an immediate clinical concern, as they resemble therapy-induced senescent cells. However, senescent cells are known to elicit senescence-associated secretory phenotypes (SASP), which may promote

inflammation and other deleterious effects (Luo *et al.*, 2025); this aspect will be explored in future studies. While the neuronal properties and differentiation potential of LKO1 cells will be investigated separately, the focus of the present study shifted from assessing the neuroprotective effects of EBN to examining its impact on LKO1 cells. Specifically, this shift entailed investigating the potential anti-proliferative or pro-proliferative effects of EBN, namely, whether EBN may promote relapse in neuroblastoma patients undergoing chemotherapy, given that LKO1 likely possesses stem cell-like properties.

The study initially hypothesised that dopaminergic neurons differentiated from LRRK2 knockout SH-SY5Y would exhibit dysfunction in certain cellular processes and that EBN extracts might ameliorate these dysfunctions. However, this hypothesis was revised following an unexpected shift in the research direction. The new hypothesis proposed that EBN may exert pro-cancer, rather than anti-cancer, effects.

The overall objective of this study is to generate, validate, and characterise LRRK2 knockout SH-SY5Y neuroblastoma cells and to investigate the effects of EBN extracts using this knockout model. The specific aims are: (i) to knock out the LRRK2 gene in SH-SY5Y neuroblastoma cells using CRISPR/Cas9 genome editing; (ii) to validate the LRRK2 knockout model; (iii) to characterise the LRRK2 knockout SH-SY5Y neuroblastoma cells; and (iv) to investigate the effects of EBN extracts on the LRRK2 knockout SH-SY5Y neuroblastoma model. The general objective and specific aims of the study were achieved, and the outcomes were organised into three parts, each illustrated by a corresponding graphical abstract (Figure 1.1–1.3).

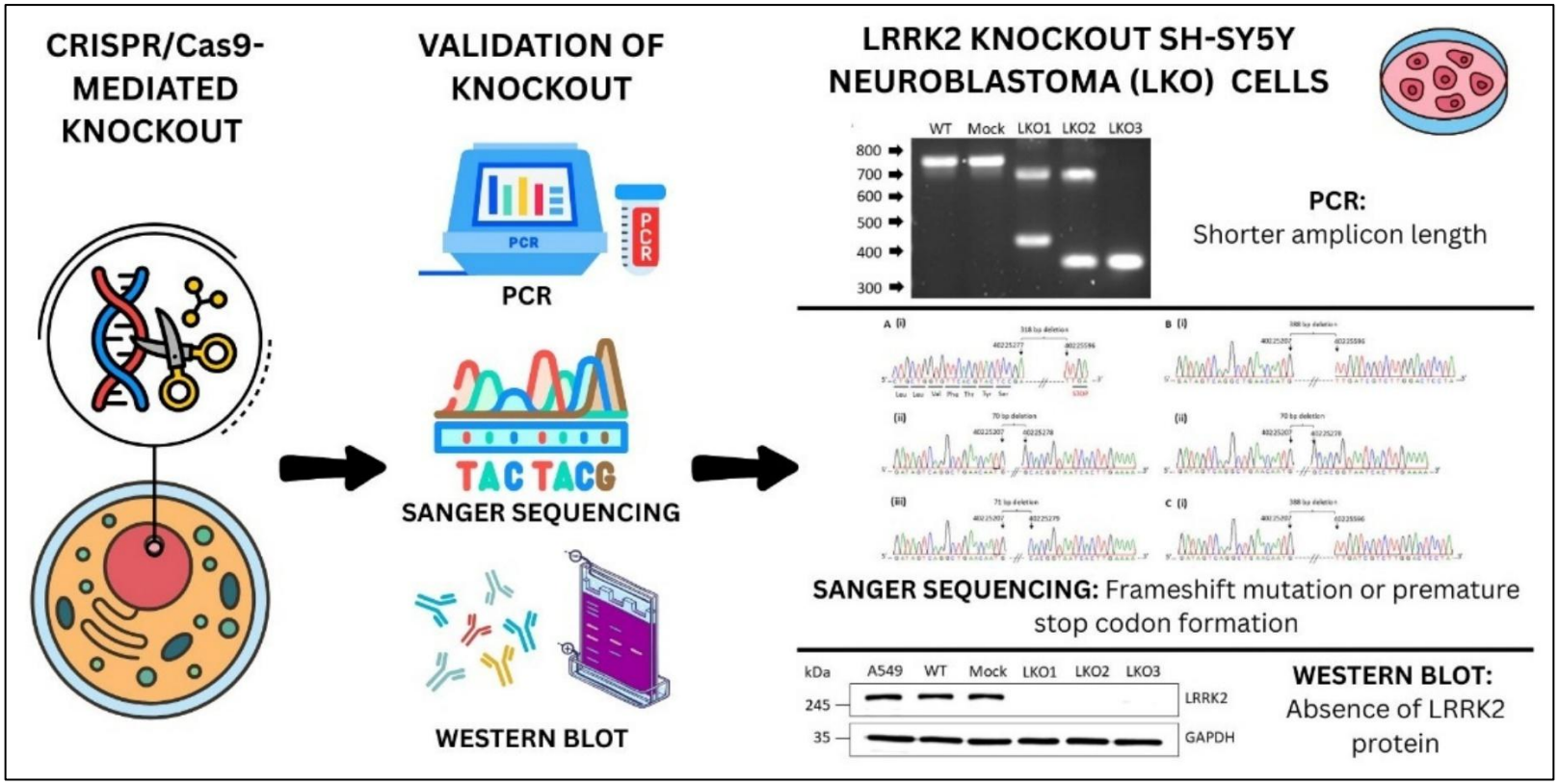

Figure 1.1: Graphical abstract illustrating the generation of LRRK2 knockout SH-SY5Y neuroblastoma cells using CRISPR/Cas9 genome editing, and their validation by PCR, Sanger sequencing, and Western blot analysis

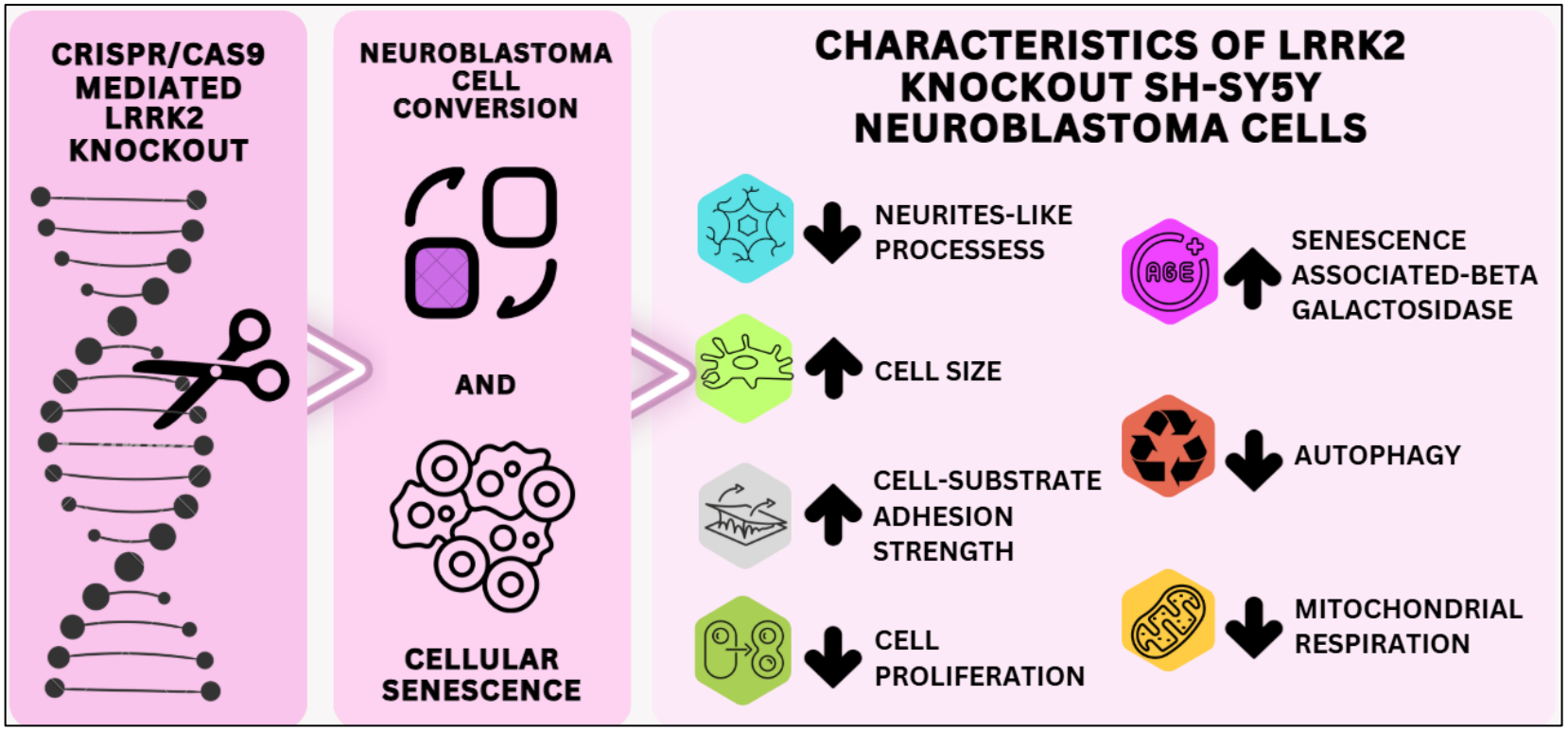

Figure 1.2: Graphical abstract illustrating the characteristics of LRRK2 knockout SH-SY5Y neuroblastoma cells, which underwent cellular conversion and senescence, characterised by reduced neurite-like processes, cell proliferation, autophagy, and mitochondrial respiration, alongside increased cell size, cell-substrate adhesion strength, and senescence-associated β-galactosidase activity

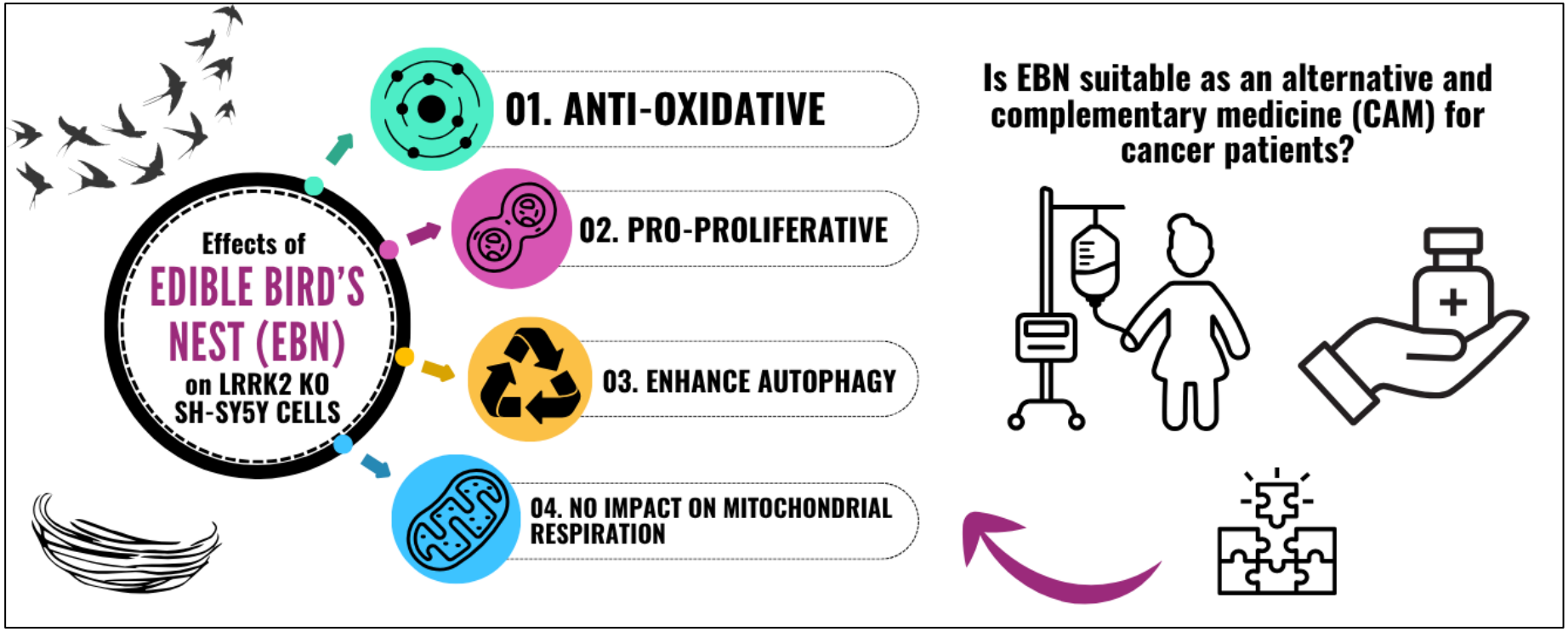

Figure 1.3: Graphical abstract illustrating the effects of EBN extract on LRRK2 knockout SH-SY5Y neuroblastoma cells, including anti-oxidative and pro-proliferative effects, enhancement of autophagy, and no observable impact on mitochondrial respiration

CHAPTER 2.0

LITERATURE REVIEW

2.1 Leucine-rich repeat kinase 2 (LRRK2)

2.1.1 Overview of LRRK2

Leucine-rich repeat kinase 2 (LRRK2), pronounced as "Lark 2," is also known as Dardarin, a name derived from the Basque word *dardara*, meaning "tremor" (Paisán-Ruíz *et al.*, 2004). The *LRRK2* gene is located within the PARK8 locus, which was identified in 2002 (Funayama *et al.*, 2002). Two years later, LRRK2 was linked to Parkinson's disease (PD), marking a breakthrough in the field (Paisán-Ruíz *et al.*, 2004, Zimprich *et al.*, 2004). Over the past 23 years, significant progress has been made in LRRK2 research (Table 2.1), establishing it as a promising therapeutic target. Notably, clinical trials for the LRRK2 inhibitor (DNL151) are currently underway and are expected to conclude by 2028.

LRRK2 is a large, multifunctional protein (286 kDa) composed of multiple domains. Located on chromosome 12, it spans 144 kb and contains 51 exons. LRRK2 belongs to the ROCO family, characterised by the presence of a Ras of complex proteins (ROC)/ GTPase domain, followed by a COR (C-terminal of ROC) domain (Bosgraaf and Van Haastert, 2003). The LRRK2 protein consists of seven domains: the armadillo repeat domain (ARM), ankyrin repeat domain (ANK), leucine-rich repeat domain (LRR), ROC, COR, kinase domain (KIN), and WD40 repeat (WD40) (Zimprich *et al.*, 2004, Mata *et al.*, 2006) (Figure 2.1).

Of these, four are involved in protein-protein interactions: ARM, ANK, LRR, and WD40, while ROC, COR, and KIN function as catalytic domains (Chen and Wu, 2018, Tolosa *et al.*, 2020). While the LRRK2 protein has been associated with a range of cellular processes involved in PD pathogenesis, its precise physiological function remains elusive. Nonetheless, evidence accrued over the years has demonstrated that LRRK2 plays a critical role in regulating synaptic function, autophagy, mitochondrial function, cytoskeletal dynamics, vesicle trafficking, lysosomal function, immune responses, and oxidative stress (Tolosa *et al.*, 2020).

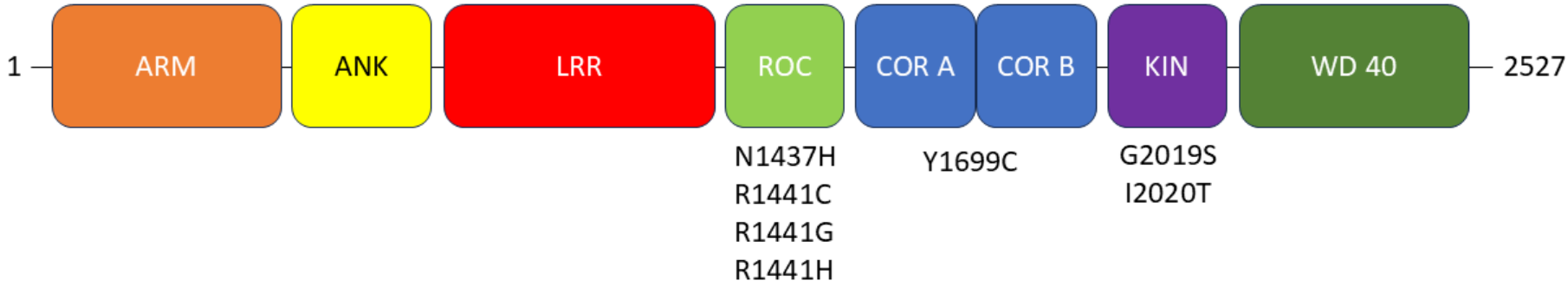

Figure 2.1: Domain structure of LRRK2, indicating the locations of pathogenic variants. ARM, armadillo repeat; ANK, ankyrin repeat; LRR, leucine-rich repeat; ROC, Ras of complex proteins domain; COR, C-terminal of ROC; KIN, kinase domain; WD40, WD40 domain

Table 2.1: Timeline of the major achievements in LRRK2 research from 2002 to 2025

Year	Achievement(s)	Reference(s)
2002	Discovery of the PARK8 locus	(Funayama *et al.*, 2002)
2004	Identification of LRRK2 as a genetic risk factor for PD	(Zimprich *et al.*, 2004, Paisán-Ruíz *et al.*, 2004)
2006	Pathogenic LRRK2 variants display increased kinase activity	(West *et al.*, 2005, Gloeckner *et al.*, 2006, Greggio *et al.*, 2006, Smith *et al.*, 2006)
2009	GWAS identified PD risk-associated SNPs at the LRRK2 locus	(Satake *et al.*, 2009)
2009 - 2010	Identification of surrogate substrates and pS910/935 LRRK2 phosphosites as markers supporting drug development research	(Cuny, 2009, Covy and Giasson, 2009, Nichols *et al.*, 2009, Klein *et al.*, 2009, Greggio *et al.*, 2009, KamikawajiIto and Iwatsubo, 2009, Liu *et al.*, 2010a, Gloeckner *et al.*, 2010, Pedro *et al.*, 2010, Lee *et al.*, 2010, Liu *et al.*, 2010b, Dzamko *et al.*, 2010, Li *et al.*, 2010, Pungaliya *et al.*, 2010)
2011	Identification of the first LRRK2 kinase inhibitor	(Deng *et al.*, 2011)
2016	Discovery of Rab proteins as substrates of LRRK2	(Steger *et al.*, 2016)
2017	First-in-human LRRK2 inhibitor (DNL201) clinical trial	(U.S. National Library of Medicine, 2020)

2019	First-in-human antisense oligonucleotide targeting LRRK2 (BIIB094) clinical trial	(U.S. National Library of Medicine, 2025c)
2020	Biogen and Denali announced a collaboration to co-develop and commercialise an LRRK2 inhibitor (DNL151)	(Biogen, 2020)
2022-2028	Phase 2a and Phase 2b clinical trials for DNL151 have commenced	(U.S. National Library of Medicine, 2025a, U.S. National Library of Medicine, 2025d)

Abbreviations: PARK8, autosomal dominant PD 8; GWAS, genome-wide association studies; SNPs, single nucleotide polymorphisms; pS910/ 935 LRRK2, the phosphorylated form of LRRK2 at serine 910 and 935; Rab, Ras-associated binding

2.1.2 LRRK2 variants

LRRK2 has been implicated in the pathogenesis of PD for over two decades, during which several variations in the gene have been identified (Taymans *et al.*, 2023). While the majority of these variants enhance kinase activity and reduce GTPase activity, thereby increasing the risk of developing PD and being classified as pathogenic, a minority are considered either protective variants or of uncertain significance.

Pathogenic LRRK2 variants are the most common cause of autosomal dominant PD. These variants are primarily found in the central core/ catalytic domains of the LRRK2 protein, specifically within the kinase and GTPase domains (Gilsbach and Kortholt, 2014). Interestingly, a plethora of evidence suggests that LRRK2 variants vary across geographical regions and ethnic/racial groups. For instance, G2019S is the most common variant observed in Caucasian populations (e.g., Ashkenazi Jews and North American Berber Arabs), but it is less frequently found in Asian populations. In contrast, G2385R and R1628P are the most common variants in Asian populations, including those in Malaysia (Simpson *et al.*, 2022, Gopalai *et al.*, 2014).

According to the Movement Disorder Society Genetic Mutation Database (https://www.mdsgene.org/), out of 211 PD-associated variants, 25 are classified as pathogenic or likely pathogenic. To date, only seven variants of LRRK2 have been confirmed to be pathogenic, including N1437H, R1441C/H/G, Y1699C, G2019S and I2020T. Among them, the G2019S is the most common and strongly associated with PD (Krüger *et al.*, 2025, Coku *et al.*, 2022). Recently, Coku *et al.* identified two novel pathogenic LRRK2 variants, H230R and A1440P (Coku *et al.*, 2022). Pathogenic LRRK2 variants alter the structure and function of the

protein (Ito and Utsunomiya-Tate, 2023). However, the exact pathophysiological mechanisms underlying these mutations remain unclear. The prevailing hypothesis is that these variants enhance kinase activity, leading to the hyperphosphorylation of substrate proteins, such as the Rab GTPase family members (Rab3A/B/C/D, Rab5A/B, Rab8A/B, Rab10, Rab12, Rab29, Rab35, and Rab43) (SeolNam and Son, 2019). This heightened kinase activity disrupts multiple cellular processes, including vesicle trafficking, cytoskeletal dynamics (Boecker *et al.*, 2021, Civiero *et al.*, 2018), autophagy (Boecker *et al.*, 2021), and mitochondrial function (Ho *et al.*, 2018, Williamson *et al.*, 2023), ultimately resulting in the degeneration of dopaminergic neurons in the substantia nigra (Krüger *et al.*, 2025, Ito and Utsunomiya-Tate, 2023).

On the other hand, studies have shown that the LRRK2 N551K and R1398H variants are protective, as individuals with these variants exhibit a reduced risk of PD across various populations, including White, Arab-Bebber, and Asian (Gopalai *et al.*, 2019, Ross *et al.*, 2011). In contrast to the alterations observed in pathogenic LRRK variants, the R1398H variant has been shown to enhance GTPase activity, Wnt signalling, and axon outgrowth, key processes vital for neuronal function (Nixon-Abell *et al.*, 2016). Additionally, Toh *et al.* demonstrated that the protective variants N551K and R1398H could suppress the phenotypic effects induced by the pathogenic LRRK2 variant G2019S (Toh *et al.*, 2021)

2.1.3 Functions of LRRK2

2.1.3.1 Autophagy

Autophagy, derived from the Greek words "auto" (self) and "phagy" (eating), refers to the process of "self-eating." It is a vital catabolic process that helps maintain cellular homeostasis by degrading and recycling dysfunctional or damaged proteins and organelles, especially during periods of stress or starvation. The resulting breakdown products are recycled to support essential cellular functions. Post-mitotic cells, such as neurons and muscle cells, rely heavily on autophagy (Gómez-Virgilio *et al.*, 2022, MadureiraConnor-Robson and Wade-Martins, 2020).

A growing body of evidence suggests that LRRK2 plays a critical role in regulating autophagy. Pathogenic variants of LRRK2 are thought to disrupt this process, leading to the accumulation of misfolded proteins and the formation of aggregates, which, in turn, contribute to the degeneration of dopaminergic neurons in the substantia nigra, a hallmark of PD (Pang *et al.*, 2022, MadureiraConnor-Robson and Wade-Martins, 2020, Gómez-Virgilio *et al.*, 2022). Neuronal cell and animal models carrying the G2019S variant (a LRRK2 pathogenic mutation associated with a significant increase in kinase activity) have been widely used in numerous studies to investigate this hypothesis. However, the outcomes of the studies have been conflicting.

Several previous studies have suggested that increased kinase activity in cell and animal models carrying LRRK2 pathogenic variants impairs autophagy. Specifically, it has been demonstrated that the G2019S variant interferes with the endo-lysosomal pathway in astrocytes, reducing their capacity to internalise and degrade α-synuclein (Streubel-Gallasch *et al.*, 2021). Yadavalli and

Ferguson further demonstrated that lysosomal degradative activity is suppressed in macrophages carrying the kinase-hyperactive G2019S variant (Yadavalli and Ferguson, 2023). Additionally, increased LRRK2 kinase activity in neurons carrying G2019S was found to disrupt neuronal autophagy by interfering with autophagosome transport and maturation. This effect was reversed by pharmacological inhibition of LRRK2 (Boecker *et al.*, 2021). Recombinant G2019S cell lines exhibited an accumulation of α-synuclein, accompanied by altered lysosomal morphology and functionality. Inhibition of kinase activity promoted autolysosome formation and increased lysosomal activity, thereby enhancing the clearance of α-synuclein (Obergasteiger *et al.*, 2020). Furthermore, LRRK2 has also been shown to regulate mitochondrial autophagy, or mitophagy. In G2019S knock-in mice, basal mitophagy was inversely correlated with kinase activity, and treatment with GSK3357679A, a CNS-penetrant LRRK2 kinase inhibitor, rescued the mitophagy defects observed in these mice (Singh *et al.*, 2021). Similarly, another LRRK2 kinase inhibitor, GSK2578215A, was found to induce mitophagy in neuroblastoma SH-SY5Y cells (Saez-Atienzar *et al.*, 2014). In addition, Hsieh *et al.* demonstrated that LRRK2 G2019S disrupts the arrest of mitochondrial motility, thereby delaying the initiation of mitophagy (Hsieh *et al.*, 2016).

On the other hand, there are also evidences suggesting that LRRK2 pathogenic variants promote autophagy, and that inhibition of LRRK2 kinase activity impairs this process. For instance, Tong *et al.* demonstrated that the loss of LRRK2 led to disruption of the protein degradation pathway in aged mice, as evidenced by the accumulation and aggregation of α-synuclein and ubiquitinated proteins (Tong *et al.*, 2010). A subsequent study revealed age-dependent,

biphasic changes in autophagic activity in the absence of LRRK2 (Tong *et al.*, 2012). Another study found that constitutive silencing of LRRK2 resulted in early deregulation of glucocerebrosidase activity, followed by late-stage impairment of both macroautophagy and chaperone-mediated autophagy (Albanese *et al.*, 2021). Several other studies have also demonstrated that mitophagy is enhanced in various models carrying LRRK2 pathogenic variants, including G2019S and R1441C, such as fibroblasts from PD patients, rat dopaminergic neuron cultures (SuGuo and Qi, 2015), and transgenic mice (Ramonet *et al.*, 2011).

2.1.3.2 Mitochondrial functions

Mitochondria are crucial for generating the energy needed to support essential cellular processes. Neurons are highly susceptible to mitochondrial dysfunction due to their unique bioenergetic and morphological characteristics. Their long, unmyelinated axonal arbors require substantial energy, making them especially dependent on mitochondrial function. Numerous studies have established that mitochondrial dysfunction is a central feature of PD (Beal, 2005). LRRK2 affect several aspects of mitochondrial function, including fission and fusion, mitophagy, oxidative stress, mitochondrial trafficking, and calcium homeostasis (SinghZhi and Zhang, 2019, Pacelli *et al.*, 2015).

Mitochondrial dynamics, including fission and fusion, are essential for maintaining mitochondrial health and function (Liu *et al.*, 2020). These processes, along with mitochondrial transport, enable long-distance energy transfer, which is vital for axonal and synaptic function (SinghZhi and Zhang, 2019, LarsenHanss and Krüger, 2018). Pathogenic LRRK2 variants impair

mitochondrial fission and fusion. Studies have shown that overexpressing G2019S or R1441C variants in various neuronal cell models, such as neuroblastoma SH-SY5Y and primary cortical neurons, induces mitochondrial fragmentation via the mitochondrial dynamin-like protein, DRP1 (Wang *et al.*, 2012, Ho *et al.*, 2018, Niu *et al.*, 2012, Ho *et al.*, 2019). This disrupts mitochondrial dynamics, leading to neuronal cell death. In contrast, the LRRK2 variant E193K prevents mitochondrial fission by altering LRRK2 binding to DRP1 (Perez Carrion M, 2018). Furthermore, treatment with P110, a selective peptide inhibitor of DRP1, has been shown to reduce mitochondrial fragmentation and correct excessive autophagy in G2019S-expressing cells and PD patient fibroblasts (Su and Qi, 2013).

Mitophagy is the process by which dysfunctional or excessive mitochondria are eliminated to maintain optimal mitochondrial function. Mitochondrial homeostasis is regulated through a balance between mitochondrial removal and production. Pathogenic variants of LRRK2 have been shown to disturb this equilibrium by either impairing or enhancing mitophagy, leading to increased cellular stress and neuronal cell death (SinghZhi and Zhang, 2019, Juárez-Flores *et al.*, 2018, Wang *et al.*, 2023b). Neurons carrying the R1441C variant exhibit impaired mitophagy, and treatment with MLi-2, a LRRK2 kinase inhibitor, does not fully restore mitophagy defects (Williamson *et al.*, 2023). However, mitophagy defects in LRRK2 G2019S mice can be rescued with the LRRK2 kinase inhibitor GSK3357679A (Singh *et al.*, 2021). LRRK2 knockdown or inhibition in fibroblasts from PD patients carrying the G2019S mutation has also been shown to reverse mitophagy impairments (Wauters *et al.*, 2020). Additionally, LRRK2 inhibition with PF-06447475 improved mitophagy in a

mouse model of 1-methyl-4-phenyl-1,2,3,6-tetrahydropyridine (MPTP)-induced PD (Filippone *et al.*, 2024). Beyond impairing mitophagy, pathogenic LRRK2 variants have also been shown to enhance mitophagy in various cellular and animal models (SuGuo and Qi, 2015, Ramonet *et al.*, 2011).

Oxidative stress, resulting from an imbalance between reactive oxygen species (ROS) production and antioxidant defences, is another consequence of LRRK2 mutations. Mitochondria produce ROS as byproducts of oxidative phosphorylation, and these ROS can damage cellular biomolecules (Juan *et al.*, 2021). Studies have linked pathogenic LRRK2 variants to increased oxidative stress. For example, ROS levels are elevated in neural stem cells with the R1441G mutation, whereas LRRK2 knockout cells show low ROS levels (Bahnassawy *et al.*, 2013). Expression of G2019S and R1441C variants in yeast cells also stimulates ROS production (PereiraMartins and Saraiva, 2014). Additionally, LRRK2 pathogenic variants are associated with mitochondrial DNA damage in iPSC-derived neural cells from individuals with G2019S or R1441C mutations, likely due to oxidative stress (Sanders *et al.*, 2014). Elevated oxidative stress markers have also been found in the cerebrospinal fluid of healthy individuals with these variants (Loeffler *et al.*, 2017).

Axonal transport is critical for neuronal health, as it delivers proteins and organelles and removes waste products. LRRK2 variants can impair mitochondrial axonal transport, particularly in dopaminergic neurons, which have long and complex axonal structures requiring efficient mitochondrial trafficking to maintain energy supply (Hung, 2021, Maday *et al.*, 2014). iPSC-derived dopaminergic neurons with the G2019S variant exhibit mitochondrial distribution and trafficking abnormalities linked to reduced sirtuin deacetylase

activity and nicotinamide adenine dinucleotide levels (Schwab *et al.*, 2017). In another study, G2019S disrupted mitochondrial motility by impairing its interaction with Miro, delaying the arrest of damaged mitochondria and the initiation of mitophagy (Hsieh *et al.*, 2016). Additionally, the LRRK2 R1441C variant induces mitochondrial trafficking defects in SH-SY5Y neuroblastoma cells, which can be alleviated with the GTP-binding inhibitor 68 and FX2149 (Thomas *et al.*, 2017).

LRRK2 also regulates mitochondrial calcium levels, and pathogenic variants can impair mitochondrial calcium handling, contributing to dysfunction, particularly in neurons that require tight calcium regulation (SinghZhi and Zhang, 2019). Mouse cortical neurons expressing G2019S or R1441C show reduced calcium buffering capacity, leading to increased mitophagy and dendritic shortening (Cherra III *et al.*, 2013). Furthermore, both variants increase mitochondrial calcium uptake in cortical neurons and PD patient fibroblasts, contributing to dendritic degeneration (Verma *et al.*, 2017).

2.1.3.3 Cytoskeletal dynamics

Cytoskeleton dynamics involve the continuous assembly and disassembly of protein filaments in response to cellular signals. This dynamic process enables key functions such as cell motility, shape changes, and intracellular transport. In neurons, cytoskeleton dynamics are essential for processes like dendritic and axonal growth, synaptic vesicle transport, and synaptic plasticity (Civiero *et al.*, 2018). Several lines of evidence indicate that LRRK2 play a role in the modulation of actin and tubulin dynamics, hence affecting neurite outgrowth

(Esteves and Cardoso, 2017). Neurite retraction is a prominent feature of degenerative phenotypes in neurons and has been extensively reported in various animal and cell models carrying LRRK2 variants (Lobbestael *et al.*, 2020). For instance, neuroblastoma SH-SY5Y cells transfected with the pathogenic G2019S variant exhibited significant neurite shortening (Plowey *et al.*, 2008). Similarly, LRRK2 G2019S transgenic mice showed reduced dendritic arborisation and fewer dendritic spines (Winner *et al.*, 2011). However, a recent study reported conflicting results, where overexpression of LRRK2 G2019S did not induce neurite retraction or impair neurite outgrowth in either cell culture or *in vivo* models (Lobbestael *et al.*, 2020). LRRK2 is known to interact with microtubules, the cytoskeletal structures that serve as highways for vesicular transport in neurons (Gandhi *et al.*, 2008, Civiero *et al.*, 2018). It plays a key role in regulating the stability and dynamics of microtubules, which are essential for the long-range transport of synaptic vesicles along the axon and dendrites to synaptic sites (Gillardon, 2009, Civiero *et al.*, 2018). In addition to microtubules, LRRK2 interacts with the actin cytoskeleton, which is involved in the short-range movement of vesicles, particularly during synaptic vesicle recycling and vesicle docking at the synapse. LRRK2 modulates actin dynamics by influencing actin-binding proteins, which in turn affect vesicle movement and fusion with the presynaptic membrane (Caesar *et al.*, 2015, Meixner *et al.*, 2011, Civiero *et al.*, 2018). Pathogenic LRRK2 variants have been shown to disrupt vesicle transport. Godena *et al.* demonstrated that the R1441C and Y1699C mutations cause locomotor deficits in *Drosophila* by impairing axonal transport through their association with acetylated microtubules (Godena *et al.*, 2014). Additionally, the anterograde axonal transport of synaptic vesicle precursor proteins was

disrupted in iPSC-derived neurons expressing the LRRK2 pathogenic variant R1441H (DouAiken and Holzbaur, 2024).

2.1.3.4 Immune responses

Compelling evidence suggests that LRRK2 plays a crucial role in modulating inflammatory responses in both the central and peripheral nervous systems (RussoBubacco and Greggio, 2022, WallingsHerrick and Tansey, 2020). LRRK2 is highly expressed in various immune cells, including B cells, T cells, monocytes, and macrophages (Cook *et al.*, 2017, Ahmadi Rastegar *et al.*, 2022). Beyond its role in neuroinflammation, LRRK2 has been implicated in several immune-related disorders, such as inflammatory bowel diseases (Sun *et al.*, 2024, Cabezudo *et al.*, 2023, Herrick and Tansey, 2021) and systemic lupus erythematosus (Zhang *et al.*, 2019, Zhang *et al.*, 2017). Additionally, LRRK2 plays a role in the immune response to bacterial infections, including *Mycobacterium tuberculosis* (Weindel *et al.*, 2020), *Salmonella typhimurium* (Liu *et al.*, 2017, Shutinoski *et al.*, 2019, Zhu *et al.*, 2025, Härtlova *et al.*, 2018) and *Mycobacterium leprae* (Dallmann-Sauer *et al.*, 2023, Wallings and Tansey, 2019), where it influences pathogen clearance and inflammatory signalling.

Pathogenic LRRK2 variants are strongly linked to PD, with increased kinase activity exacerbating both neuroinflammation and systemic inflammation. Dysregulated LRRK2 function disrupts proinflammatory mediator secretion, phagocytosis, and immune cell migration, highlighting its role as a key link between immune dysfunction and neurodegeneration. Microglia and astrocytes from animals expressing the LRRK2 G2019S and R1441G variants exhibit

heightened secretion of proinflammatory cytokines, including interleukin-1β, tumour necrosis factor-α and interferon-γ (An *et al.*, 2024, Ho *et al.*, 2024, GillardonSchmid and Draheim, 2012, Panagiotakopoulou *et al.*, 2020), as well as increased chemokine release (Caesar *et al.*, 2014). These inflammatory changes contribute to both PD development and progression. Notably, pharmacological inhibition of LRRK2 kinase activity using inhibitors such as LRRK2-IN-1 (Luerman *et al.*, 2014, Moehle *et al.*, 2012), GSK2578215A (Kim *et al.*, 2019) and Sunitinib (Moehle *et al.*, 2012) as well as LRRK2 knockout (Kim *et al.*, 2019, RudykDwyer and Hayley, 2019, Yan and Liu, 2017) significantly reduces proinflammatory cytokine and chemokine levels.

Phagocytosis is essential for immune defence and tissue homeostasis, allowing immune cells to engulf and degrade pathogens, cellular debris, and misfolded proteins. In the brain, microglia play a crucial role in clearing toxic protein aggregates, including misfolded α-synuclein, a hallmark of PD. The role of LRRK2 in microglial phagocytosis remains controversial, with conflicting findings. Some studies report that microglia and macrophages from PD patients carrying the LRRK2 G2019S mutation exhibit increased phagocytic activity, while LRRK2 deficiency leads to reduced phagocytosis (Kim *et al.*, 2018a). Conversely, other studies suggest that LRRK2 deficiency enhances microglial phagocytosis. For example, Feng *et al.* reported that LRRK2-deficient microglia exhibited increased phagocytosis following α-synuclein exposure in mice (Feng *et al.*, 2023). Similarly, LRRK2 knockout microglia showed an enhanced ability to clear α-synuclein, likely due to an increase in Rab5-positive endosomes, which are essential for early endocytic trafficking (Maekawa *et al.*, 2016). Adding to this inconsistency, a study found that human iPSC-derived microglia-

like cells (iMGLs) with the LRRK2 G2019S mutation demonstrated impaired phagocytosis in response to inflammatory stimuli, an effect observed exclusively in male PD patient-derived iMGLs but not in female patient-derived cells (Ohtonen *et al.*, 2023).

Previous studies suggest that LRRK2 regulates immune cell migration, though findings remain conflicting. Moehle *et al.* reported that myeloid cells expressing the G2019S LRRK2 mutation exhibit enhanced migration due to interactions between LRRK2 and actin-regulatory proteins that control chemotaxis. Notably, LRRK2 kinase inhibitors can disrupt this interaction (Moehle *et al.*, 2015). Conversely, Choi *et al.* found that microglia carrying the G2019S LRRK2 mutation displayed impaired migration, while LRRK2 knockdown enhanced their motility (Choi *et al.*, 2015). Similarly, Ma *et al.* demonstrated that LRRK2-null microglia migrated more efficiently and travelled longer distances toward a fractalkine source (Ma *et al.*, 2016).

2.1.3.5 Synaptic functions

Robust evidence indicates that LRRK2 plays a critical role in regulating synaptic function by modulating several key processes, including synaptic vesicle dynamics, synaptic plasticity, cytoskeletal stability, and autophagy (Pischedda and Piccoli, 2021, Kuhlmann and Milnerwood, 2020, Mancini *et al.*, 2020, Lamonaca and Volta, 2020). Previous studies have shown that the R1441C and G2019S LRRK2 mutations disrupt the organisation of glutamatergic α-amino-3-hydroxy-5-methyl-4-isoxazolepropionic acid (AMPA) receptors. These mutations are also associated with a reduced frequency of miniature excitatory

postsynaptic currents, alterations in dendritic spine nano-architecture, and changes in single-synapse currents (Chen *et al.*, 2020a). Skiteva *et al.* further demonstrated that the G2019S mutation impairs glutamatergic synaptic transmission in dopaminergic neurons. Specifically, G2019S mice exhibited reduced protein expression of the presynaptic glutamatergic marker, vesicular glutamate transporter 1 (VGLUT1), along with decreased levels of GluA1 and GluN1 subunits of AMPA and N-methyl-d-aspartate (NMDA) receptors, respectively (Skiteva *et al.*, 2022). The pathogenic G2019S variant of LRRK2 has additionally been implicated in microglial dysfunction, notably altering synaptic pruning and contributing to dopaminergic fibre loss *in vivo* (Zhang *et al.*, 2022b). Moreover, this mutation induces aberrant synaptic changes in spiny projection neurons under stress conditions (Guevara *et al.*, 2020). Tombesi *et al.* demonstrated a role for LRRK2 in brain-derived neurotrophic factor (BDNF)-mediated synaptic signalling. Specifically, the G2019S mutation led to altered phosphorylation of proteins involved in postsynaptic structural organisation, while LRRK2 knockout resulted in impaired BDNF-dependent spinogenesis (Tombesi *et al.*, 2024). Furthermore, the D620N missense mutation in vacuolar protein sorting 35 (VPS35), also associated with PD, has been shown to interact with LRRK2 pathways. Kadgien *et al.* reported that this mutation increases phosphorylation of Rab10, a key substrate of LRRK2. Although LRRK2 kinase inhibition reversed Rab10 phosphorylation, it did not normalise the elevated glutamate release or surface GluA1 expression (KadgienKamesh and Milnerwood, 2021). In contrast, Bu *et al.* demonstrated that treatment with the LRRK2 kinase inhibitor MLi-2 restored

striatal dopamine function in mice carrying the VPS35 D620N mutation (Bu *et al.*, 2023).

2.1.4 The roles of LRRK2 in cancers

Despite its well-established role in the pathogenesis of Parkinson's disease, increasing evidence suggests that LRRK2 may also be involved in cancer biology. Recent studies have implicated LRRK2 in cellular pathways relevant to oncogenesis, although its precise role in tumour initiation and progression remains incompletely understood.

Accumulating evidence indicates that dysregulation of LRRK2 is associated with an increased risk of several cancer types. Notably, pathogenic LRRK2 mutations, particularly the G2019S variant, have been linked to elevated cancer risk in patients with Parkinson's disease, including skin cancer, colorectal cancer, leukaemia, hormone-related cancers, and breast cancer (Agalliu *et al.*, 2019, Agalliu *et al.*, 2015). Mechanistically, Wang et al. demonstrated that LRRK2 G2019S promotes colorectal tumorigenesis by fostering a pro-inflammatory intestinal microenvironment, and proposed inhibition of LRRK2 kinase activity as a potential therapeutic strategy (Wang *et al.*, 2024b). In line with these findings, several studies have reported anti-cancer effects following LRRK2 knockdown. For example, Wu et al. showed that knockdown of LRRK2 suppresses lung cancer growth through modulation of the toll-like receptor 4 (TLR4)/nuclear factor kappa-light-chain-enhancer of activated B cells (NF-κB) signalling pathway and the NLRP3 inflammasome (Wu *et al.*, 2023). Similarly, LRRK2 knockdown has been shown to attenuate proliferation in clear cell renal

cell carcinoma (Yang *et al.*, 2021), lung cancer (Jiang *et al.*, 2019) and breast cancer cell lines (Jung *et al.*, 2021). However, the role of LRRK2 in cancer appears to be context-dependent. In contrast to the predominantly anti-tumorigenic effects reported above, Lebovitz et al. demonstrated that loss of LRRK2 promotes carcinogen-induced lung tumorigenesis, suggesting a potential tumour-suppressive function under specific conditions (Lebovitz *et al.*, 2021).

Beyond point mutations, structural alterations in LRRK2 have also been implicated in cancer. Copy number variations, including both gene amplification and whole-gene deletion, have been associated with poor prognosis in multiple human malignancies, prompting Lopez et al. to propose LRRK2 inhibition as a therapeutic strategy for LRRK2-amplified tumours (Lopez *et al.*, 2020). Consistent with this, somatic mutations in LRRK2 have been frequently identified in breast cancer (Parrilla Castellar *et al.*, 2020). Nevertheless, not all studies support a cancer-predisposing role for LRRK2 variants. For instance, Allegra et al. reported no association between the LRRK2 G2019S mutation and cancer risk in an Italian cohort (Allegra *et al.*, 2014), highlighting potential population-specific effects and underscoring the complexity of LRRK2's role in cancer biology.

2.1.5 LRRK2 knockout models

Since increased LRRK2 kinase activity disrupts multiple cellular processes and contributes to the pathogenesis of PD, inhibiting LRRK2 kinase activity has emerged as a promising therapeutic strategy and a major focus of ongoing

research. To support these efforts, numerous LRRK2 knockout cell lines and animal models have been developed over the years.

2.1.5.1 Cell lines

Although cell lines have reduced complexity and limited physiological relevance compared to animal models, they are widely used to generate preliminary data and establish proof-of-concept findings before more extensive investigations. Over the years, researchers have developed LRRK2 knockout cell lines from various cell types, including human iPSCs, HEK-293/ HEK-293T, SH-SY5Y, RAW 264.7, and BV2 cells (Table 2.2), to better understand LRRK2's physiological roles. Most of these knockout models were generated using CRISPR/Cas genome editing technology, enabling precise gene disruption. The functional changes observed in these models have been instrumental in uncovering LRRK2's role in key cellular processes such as mitochondrial function, immune responses, oxidative stress, and apoptosis.

Among these cell lines, the neuroblastoma-derived SH-SY5Y is widely used in PD research due to its several advantages. While iPSCs derived from PD patient fibroblasts offer a physiologically relevant model that retains patient-specific genetic variants, they are costly to maintain, labour-intensive to culture, and require careful handling, despite ongoing efforts to simplify their culturing process (Chang *et al.*, 2015, Ghaedi and Niklason, 2016, Cheng *et al.*, 2023). Conversely, LRRK2 knockout SH-SY5Y cells are significantly more cost-effective and easier to maintain. Unlike HEK-293/ HEK-293T cells, which are easier to transfect and culture but lack neuronal properties (IoghenCeafalan and

Popescu, 2023), SH-SY5Y cells possess neuronal characteristics, making them particularly relevant for PD research. Additionally, while LRRK2 knockout BV2 microglial cells and RAW 264.7 macrophages are useful for studying neuroinflammation-related processes, such as aggregate clearance (Gao *et al.*, 2023), LRRK2 knockout SH-SY5Y cells offer broader research applications, including synaptic transmission studies. SH-SY5Y cells are also widely used to investigate cellular responses to neurotoxicants and genetic mutations linked to PD (Xu *et al.*, 2021, Rakotoarisoa *et al.*, 2019, Luo and Sakamoto, 2023, RamalingamHuh and Lee, 2019, Rodríguez-Losada *et al.*, 2020, Zhao *et al.*, 2020).

Table 2.2 LRRK2 knockout cell lines

No.	Cell line	Method of genetic modification	Genetic modification(s)	Functional change(s)	Reference
1	Human induced pluripotent stem cell (iPSC)	CRISPR/Cas9	• C11-LRRK2-KO1: Deletion of 2 base pairs in LRRK2 exon 9 • C11-LRRK2-KO2: insertion of 13 base pairs in LRRK2 exon 9	N/A	(Chen *et al.*, 2020b)
2	Human induced pluripotent stem cell (iPSC)	CRISPR/Cas9	• 19877 bp deletion	N/A	(Beylina *et al.*, 2021)
3	Human embryonic kidney cell line 293 (HEK-293)	CRISPR/Cas9	• Disruption of the start codon (ATG) in LRRK2 exon 1	Resistant to rotenone-induced oxidative stress, mitochondrial damage, and apoptosis *in vitro*	(Quintero-Espinosa *et al.*, 2023)
4	Human neuroblastoma cell line (SH-SY5Y)	CRISPR/Cas9	• N/A	Reduced Akt and Erk1 phosphorylation in response to BDNF stimulation	(Tombesi *et al.*, 2024)
5	Microglial cells (BV2)	CRISPR/Cas9	• Premature stop codons within the ORF of LRRK2 • Deletion of a length of genomic DNA including 5'UTR and LRRK2 exon 1	Longer cellular processes, enhanced adhesion, and weakened migration capacity	(Zhang *et al.*, 2022a)

6	Murine macrophage cell line (RAW 264.7)	CRISPR/Cas9	N/A	Reduced pro-inflammatory cytokine release, increased chemokines, anti-inflammatory cytokines, and pleiotropic cytokines, with no effect on phagocytic activity	(Almudimeegh, 2022)
7	Murine macrophage cell line (RAW 264.7) *	ZFNs	N/A	N/A	(American Type Culture Collection, 2023)
8	Human embryonic kidney cell line 293, modified to express the SV40 large T antigen (HEK-293T) **	N/A	N/A	N/A	(FenicsBIO, 2025)

Abbreviation: N/A, not available; CRISPR/Cas9, clustered regularly interspaced short palindromic repeats and CRISPR-associated protein 9; ZFNs, zinc-finger nucleases; BDNF, brain-derived neurotrophic factor; Akt, Ak strain transforming (also known as protein kinase B, PKB); Erk, extracellular signal-regulated kinase; ORF, open reading frame

Note:

* This cell line is commercially available at the American Type Culture Collection (ATCC), USA

** This cell line is commercially available at the FenicsBIO, USA

2.1.5.2 Animal models

LRRK2 knockout animal models are essential for understanding both the normal function of LRRK2 and its role in PD pathology. Additionally, these models can be used to evaluate the risks associated with LRRK2 inhibition, as pharmacological LRRK2 inhibitors are being explored as potential therapeutic approaches for PD. Pathogenic LRRK2 variants cluster within the catalytic triad of the protein, with N1437H, R1441C, R1441G, and R1441H located in the Ras-of-complex (ROC) GTPase domain, G2019S and I2020T in the protein kinase domain, and Y1699C in the C-terminal of ROC (COR) domain (Abdalla-Carvalho *et al.*, 2010, Nguyen and Moore, 2017). Structurally, the LRRK2 gene is organized such that exons 29–31 encode the ROC GTPase domain, while exons 38–44 encode the MAPKKK (kinase) domain (Nuytemans *et al.*, 2008, Abdalla-Carvalho *et al.*, 2010).

Numerous LRRK2 knockout models have been developed using homologous recombination in embryonic stem cells and Cre-LoxP-mediated exon deletion (Table 2.3), with many targeting LRRK2 exon 41 (Hinkle *et al.*, 2012, Russo *et al.*, 2019, RudykDwyer and Hayley, 2019, Dächsel *et al.*, 2010). This focus arises because exon 41 encodes the kinase domain, where G2019S, the most common and extensively studied pathogenic variant, is located. This mutation increases LRRK2 kinase activity and is strongly associated with PD risk (Lesage *et al.*, 2007). Additionally, some animal models have been designed with disruptions in LRRK2 exon 29 and exon 30, as these exons encode the GTPase domain, which harbours several other pathogenic variants (Tong *et al.*, 2012, Østergaard, 2024, Tong *et al.*, 2010). To investigate the effects of complete LRRK2 loss, researchers often delete exon 1 or exon 2, ensuring a full and

effective knockout of gene function (Pellegrini *et al.*, 2018, Tong *et al.*, 2012, Härtlova *et al.*, 2018, Ludtmann *et al.*, 2019, Russo *et al.*, 2019, Tong *et al.*, 2010).

LRRK2 knockout models have shown that the loss of LRRK2 leads to abnormalities in multiple peripheral organs, including the lungs, kidneys, and liver. It also disrupts autophagic activity and perturbs metabolic and immune homeostasis (Table 2.3). However, the full extent of these detrimental effects remains unclear. Despite these uncertainties, several pharmacological LRRK2 inhibitors have been evaluated. While some studies have reported undesirable side effects from LRRK2 inhibition (Fuji *et al.*, 2015, Fell *et al.*, 2015, Daher *et al.*, 2015), others have shown that these effects are reversible upon drug withdrawal (Baptista *et al.*, 2020b, Bryce *et al.*, 2021) or that no significant adverse effects were observed (Ho *et al.*, 2022, Andersen *et al.*, 2018). Notably, LRRK2 inhibitors such as DNL201 and DNL151 have progressed to clinical trials (U.S. National Library of Medicine, 2020, Biogen, 2020, U.S. National Library of Medicine, 2025a), with Phase 2a and Phase 2b trials for DNL151 still ongoing. Could DNL151 be the long-awaited cure for PD? The results of these clinical trials, expected by 2028, will provide crucial insights.

Table 2.3 LRRK2 knockout animal models

No.	Animal model	Method of genetic modification	Genetic modification(s)	Phenotypic/ functional change(s)	Reference
1	C57BL/6J mice	Homologous recombination in ES cells and Cre-LoxP mediated exon deletion	Deletion of LRRK2 exon 41	i. Abnormal exploratory activity ii. Enhanced motor performance iii. Degeneration in the kidney iv. Enhancement of autophagic activity and accumulation of autofluorescent material	(Hinkle *et al.*, 2012)
2	Long Evans rat	N/A	N/A	2 months of age: i. Abnormal kidney staining patterns and/or morphologic changes that were associated with higher serum phosphorus, creatinine, cholesterol, and sorbitol dehydrogenase, and lower serum sodium and chloride ii. Pronounced changes in urine specific gravity, total volume, urine potassium, creatinine, sodium, and chloride 16 months of age: i. Abnormal kidney, lung, and liver phenotype	(Baptista *et al.*, 2013)

3	C57BL/6J mice	Homologous recombination in ES cells and Cre-LoxP mediated exon deletion	Deletion of the second coding exon of LRRK2	Mice: i. Differentially expressed vesicular trafficking and protein translation proteins in kidneys ii. Deregulation of proteins important for translational, lysosomal and cytoskeletal function iii. Accumulation of endo-lysosomal clusters in kidneys Epithelial kidney cells: i. Lysosomal dysregulation	(Pellegrini *et al.*, 2018)
4	B6/129 mice	Homologous recombination in ES cells and Cre-LoxP mediated exon deletion	i. Disruption in LRRK2 promoter and exon 1 ii. Disruption in LRRK2 exon 29 and 30	i. Gross morphological abnormalities of the kidney ii. Ratio of kidney/body weight is increased at 1, 4, and 7 months, but drastically decreased at 20 months iii. Expression of kidney injury molecule-1 is up-regulated iv. Age-dependent bi-phasic alterations of the autophagic activity in kidneys	(Tong *et al.*, 2012)
5	B6/129 mice	Homologous recombination in ES cells and Cre-LoxP mediated exon deletion	i. Disruption in LRRK2 promoter and exon 1 ii. Disruption in LRRK2 exon 29 and 30	i. Accumulation and aggregation of α-synuclein and ubiquitinated proteins in kidneys at 20 months ii. Impairment of autophagy–lysosomal iii. Enhancement of apoptotic cell death, inflammatory responses, and oxidative damage	(Tong *et al.*, 2010)

6	Long Evans rat	N/A	N/A	i. Significant weight gain ii. Significant increases in insulin and insulin-like growth factors iii. Displayed kidney morphological and histopathological alterations in the renal tubule epithelial cells iv. Significant decreases of lipocalin-2, in both the urine and plasma v. Significant alterations in the cellular composition of the spleen vi. Subtle differences in response to dual infection with rat-adapted influenza virus (RAIV) *and Streptococcus pneumoniae*	(Ness *et al.*, 2013)
7	Drosophila melanogaster (G7459)	P-element imprecise excision	N/A	i. Exhibited severely impaired locomotive activity ii. Degeneration of dopaminergic neurons	(Lee *et al.*, 2007)
8	C57BL/6J mice	Homologous recombination in ES cells and Cre-LoxP mediated exon deletion	i. Deletion of LRRK2 exon 2 ii. Deletion of LRRK2 exon 41	i. Attenuated induction of mitochondrial superoxide dismutase-2 in response to α-synuclein pre-formed fibrils	(Russo *et al.*, 2019)

9	C57BL/6N mice	N/A	Deletion of LRRK2 exon 41	i. Prevented paraquat-induced signs of sickness, inflammation, and peripheral toxicity ii. Reduced signs of illness, motivational and home-cage activity deficits induced by paraquat iii. Blunted the corticosterone elevation induced by paraquat	(RudykDwyer and Hayley, 2019)
10	C57BL/6J mice	Homologous recombination in ES cells and Cre-LoxP mediated exon deletion	Deletion of LRRK2 exon 2	i. Targeted Mtb to phagolysosomes and limits Mtb replication ii. Enhanced phagosome maturation in macrophages iii. Enhanced innate immunity to Mtb *in vivo*	(Härtlova *et al.*, 2018)
11	C57BL/6J mice	Homologous recombination in ES cells and Cre-LoxP mediated exon deletion	Deletion of LRRK2 exon 41	Homozygous KO i. Increase in mean process length and branching in both hippocampal and midbrain primary neurons Heterozygous KO i. No change in either neuritic outgrowth or branching	(Dächsel *et al.*, 2010)
12	C57BL/6J mice	Homologous recombination in ES cells and Cre-LoxP mediated exon deletion	Deletion of LRRK2 exon 2	i. Impaired mitochondrial Ca^{2+} extrusion via $Na^{+}/Ca2^{+}/Li^{+}$ exchanger ii. Lowered mitochondrial permeability transition pore opening threshold iii. Increased cell death	(Ludtmann *et al.*, 2019)
13	C57BL/6 mice	Homologous recombination in ES cells	Deletion of partial LRRK2 exon 39,	i. No major abnormalities and live to adulthood ii. The dopaminergic system is normal	(Andres-Mateos *et al.*, 2009)

			complete deletion of LRRK2 exon 40 and introduction of a stop codon into the coding sequences	iii.	No significant difference in the susceptibility of LRRK2 KO and wild-type mice to MPTP	
14	Long Evans rat	N/A	Deletion of 10 bp in LRRK2 exon 30	i. ii.	Increases sensitivity to wavelength information Affects visual processing at a developmental level rather than an acute deficiency of LRRK2	(Østergaard, 2024)

Abbreviation: N/A, information is not available; ES cells, embryonic stem cells; Mtb, *Mycobacterium tuberculosis*; MPTP, 1-methyl-4-phenyl-1,2,3,6-tetrahydropyridine

2.2 Neuroblastoma cell line (SH-SY5Y)

2.2.1 Overview of SH-SY5Y

The SH-SY5Y neuroblastoma cell line is a thrice-subcloned derivative of the parental SK-N-SH cell line. SK-N-SH was originally established in 1970 from metastatic cells in the bone marrow aspirate of a four-year-old female (BiedlerHelson and Spengler, 1973). This neuroblast-like cell line was sequentially subcloned into SH-SY, then SH-SY5, and ultimately SH-SY5Y (Biedler *et al.*, 1978). More than five decades after its establishment, the SH-SY5Y cell line has become a widely used model for PD research, valued for its human origin and neuronal characteristics.

Compared to primary neurons, SH-SY5Y cells are relatively easy and cost-effective to culture, express various human-specific proteins and isoforms absent in rodent primary cells, are amenable to genetic manipulation, and can undergo large-scale expansion before differentiation. Additionally, they can be differentiated into dopaminergic neurons, making them particularly relevant for PD studies (Kovalevich and Langford, 2013b, IoghenCeafalan and Popescu, 2023, Rodríguez-Losada *et al.*, 2020). These properties make SH-SY5Y cells a valuable tool for investigating the mechanisms of PD and testing potential therapies.

Despite their advantages, SH-SY5Y cells have notable limitations, including their cancerous origin, genomic instability (IoghenCeafalan and Popescu, 2023, Hoffmann *et al.*, 2023), potential conversion to an epithelial phenotype (IoghenCeafalan and Popescu, 2023, RossSpengler and Biedler, 1983), and low expression of certain PD-related proteins, such as LRRK2 (Snoderly-Foster and Olivas, 2022). These factors can limit their applicability in specific studies.

However, SH-SY5Y cells remain a valuable and accessible platform for initial screenings and mechanistic studies, bridging the gap between simpler *in vitro* systems and more complex *in vivo* models.

2.2.2 Applications of SH-SY5Y cells in PD research

2.2.2.1 Neurogenetic models

SH-SY5Y cells have been widely used as a neurogenetic model, particularly in the study of neurodegenerative diseases such as PD. Their human origin, neuronal characteristics, and adaptability make them an ideal platform for investigating the genetic mechanisms underlying neurodegeneration. SH-SY5Y cells are highly accessible for various genetic manipulations, including stable transgene integration, overexpression of genes or gene variants, gene knockdown or silencing (e.g., via siRNA or shRNA), and gene knockout (e.g., using CRISPR-Cas9). Such genetic modifications allow researchers to explore the roles of disease-associated genes, study pathogenic mutations, and develop potential gene-targeted therapies for neurodegenerative conditions.

A previous study demonstrated that expressing the LRRK2 G2385R variant, a PD-associated mutation prevalent in the Asian population, in SH-SY5Y cells leads to increased mitochondrial reactive oxygen species (ROS) production, caspase-3/7 activation, and enhanced poly-ADP ribose polymerase (PARP) cleavage, ultimately resulting in neurotoxicity. Notably, the study also found that curcumin treatment could reverse the neurodegeneration caused by LRRK2 G2385R, highlighting its potential as a therapeutic strategy (Zhang *et al.*, 2021). Additionally, Anantha *et al.* demonstrated that nucleoside diphosphate kinase A (NME1) promotes neurite outgrowth in SH-SY5Y cells overexpressing human

wild-type α-synuclein (the primary component of Lewy bodies and a key pathological hallmark of synucleinopathies, including PD), as well as in SH-SY5Y cells carrying the LRRK2 G2019S pathogenic variant (Anantha *et al.*, 2022). Moreover, Potdar *et al.* reported that SH-SY5Y cells expressing the LRRK2 I1371V variant exhibit higher autophosphorylation of phospho-LRRK2 (pLRRK2) at serine1292 and serine935, along with increased substrate phosphorylation of Rab8A and Rab10. These findings provide insights into the potential role of this variant in dopaminergic neuron development and survival, suggesting a link between LRRK2 dysfunction and impaired neurogenesis in PD (Potdar *et al.*, 2024).

Apart from gene overexpression, SH-SY5Y cells are also commonly used for gene knockdown and silencing studies. Snoderly-Foster and Olivas demonstrated that knocking down the two human Pumilio homologs (Pumilio 1 and Pumilio 2) in SH-SY5Y cells led to increased SNCA and LRRK2 mRNA levels, as well as elevated α-synuclein protein expression. These findings suggest that Pumilio proteins normally repress these PD-associated genes, highlighting their potential regulatory role in neurodegeneration (Snoderly-Foster and Olivas, 2022). Additionally, siRNA-mediated silencing of N-acylphosphatidylethanolamines-specific phospholipase D (NAPE-PLD) in SH-SY5Y cells led to a significant accumulation of non-metabolized NAPEs, a shift of LRRK2 from the membrane to the cytosol, and a reduction in total LRRK2 content. These results imply that NAPE-PLD activity may regulate LRRK2 localization by modulating membrane NAPE levels (Palese *et al.*, 2021). Furthermore, Wang *et al.* reported that Hox transcript antisense intergenic RNA (HOTAIR) knockdown in SH-SY5Y cells protected against 1-methyl-4-

phenylpyridinium (MPP^+)-induced neuronal apoptosis by inhibiting caspase 3 activity. This finding suggests that inhibiting HOTAIR expression could serve as an effective disease-modifying strategy in PD (Wang *et al.*, 2017).

Beyond gene knockdown or silencing, SH-SY5Y cells are also frequently used in gene knockout studies. Kim *et al.* reported that CRISPR/Cas9-mediated knockout of glucocerebrosidase 1 (GBA1) in SH-SY5Y cells resulted in a decrease in α-synuclein tetramers and related multimers, while increasing α-synuclein monomers. This finding provides mechanistic insights into how GBA1 regulates the formation of α-synuclein multimers and suggests potential therapeutic opportunities for PD and dementia with Lewy bodies (Kim *et al.*, 2018b). In another study, Haque *et al.* demonstrated that CRISPR/Cas9-mediated knockout of G protein-coupled receptor 4 (GPR4) in SH-SY5Y cells decreased the Bax/Bcl-2 ratio and ROS generation, while stabilizing the mitochondrial membrane potential, thereby protecting the cells from MPP^+ or hydrogen peroxide-induced apoptotic cell death. These findings indicate that GPR4 could be a promising therapeutic target for PD (Haque *et al.*, 2020).

2.2.2.2 Neurotoxicity models

In addition to its role as a neurogenetic model, the SH-SY5Y cell line is widely used as an *in vitro* neurotoxicity model for studying PD, owing to its neuronal characteristics and responsiveness to neurotoxic agents. SH-SY5Y cells are particularly effective for modeling the effects of neurotoxic substances such as paraquat, 1-methyl-4-phenylpyridinium (MPP^+), 6-hydroxydopamine (6-OHDA), and rotenone. Studies using these neurotoxins in SH-SY5Y cells provide valuable insights into the molecular mechanisms underlying PD and

help identify potential therapeutic targets. Additionally, the SH-SY5Y cell line has been used to screen and identify neuroprotective treatments for PD.

Paraquat, one of the most widely used herbicides in the world, is a potent neurotoxin that has been linked to an increased risk of PD (Tong *et al.*, 2022). A previous study demonstrated that naringenin, a natural flavonoid, exhibits neuroprotection in paraquat-treated SH-SY5Y cells by increasing cell viability, reducing oxidative stress, and elevating mitochondrial membrane potential and cellular ATP levels (Ahmad *et al.*, 2021). Furthermore, Carneiro *et al.* showed that paraquat-induced neurotoxicity in SH-SY5Y cells could be partially prevented by psychostimulants such as amphetamine or methylphenidate (Carneiro *et al.*, 2024). Additionally, Gopar-Cuevas *et al.* found that autophagy inducers, i.e., metformin and trehalose, reduced dopaminergic cell death induced by paraquat in SH-SY5Y cells (Gopar-Cuevas *et al.*, 2023).

The neurotoxin 6-hydroxydopamine (6-OHDA) is widely used to induce models of PD, effectively replicating the key cellular processes involved in the disorder, such as oxidative stress, neurodegeneration, neuroinflammation, and neuronal death through apoptosis (Hernandez-BaltazarZavala-Flores and Villanueva-Olivo, 2017). Cirmi *et al.* reported the neuroprotective effects of a flavonoid-rich mandarin orange juice extract in 6-OHDA-treated SH-SY5Y cells. Pre-incubation with the mandarin orange juice extract significantly inhibited apoptosis in these cells by blocking caspase 3 and modulating the expression of the p53, Bax, and Bcl-2 genes (Cirmi *et al.*, 2021). Similarly, another natural product, silk fibroin, was shown to inhibit cell death in 6-OHDA-treated SH-SY5Y cells (Ceccarini *et al.*, 2025). Additionally, O'Mahony *et al.* demonstrated

that TMP269, a class-IIa histone deacetylase inhibitor, offers protection against 6-OHDA-induced neurite injury in SH-SY5Y cells (O'Mahony *et al.*, 2025).

Rotenone is one of the most widely used insecticides and piscicides globally. It is also commonly employed as a neurotoxin in various animal and cell models to induce PD-relevant pathology and behavioral phenotypes. Rotenone selectively induces dopaminergic neurotoxicity by inhibiting mitochondrial complex I, which leads to the generation of oxidative stress and subsequent oxidative damage (Lawana and Cannon, 2020). Soni *et al.* reported that auranofin-loaded chitosan-lipid hybrid nanoparticles inhibit rotenone-induced ROS generation and apoptosis in SH-SY5Y cells by blocking glycogen synthase kinase-3 beta (GSK-3β) (Soni *et al.*, 2025). In another study, a potent leonurine-based therapeutic molecule, MJ210, was shown to significantly enhance the survival of SH-SY5Y cells treated with rotenone. MJ210 prevented apoptosis, reduced reactive oxygen species, alleviated mitochondrial dysfunction, and attenuated neuroinflammation through the ERK1/2-P38-JNK and P65-NFκB signaling pathways (Gupta *et al.*, 2025). Additionally, Anandan *et al.* demonstrated that shikonin, a naphthoquinone compound extracted from the *Lithospermum erythrorhizon* herb, alleviates rotenone-induced neurotoxicity in SH-SY5Y cells by inhibiting apoptosis via the IGF-1R/PI3K/AKT pathway (Anandan *et al.*, 2025).

1-methyl-4-phenyl-1,2,3,6-tetrahydropyridine (MPTP) is a neurotoxin that induces Parkinsonism through its conversion to MPP^+ by glial monoamine oxidase. MPP^+ selectively accumulates in dopaminergic neurons, where it inhibits mitochondrial complex I, leading to oxidative stress and ultimately cell death (Przedborski *et al.*, 2000). A previous study demonstrated that curcumin,

a primary bioactive compound in turmeric, protects SH-SY5Y cells from MPP^+-induced toxicity by modulating the transient receptor potential cation channel subfamily V member 4 (TRPV4) (Çınar and Yıldızhan, 2025). Furthermore, Liu *et al.* showed that Mastoparan-M, a polypeptide derived from the venom of the *Vespa magnifica* wasp, significantly improves cell viability and mitochondrial membrane potential in MPP^+-treated SH-SY5Y cells. This suggests the Mastoparan-M's potential as a promising therapeutic candidate for PD (Liu *et al.*, 2025).

2.3 CRISPR/Cas9 genome editing technology

2.3.1 Overview of CRISPR/Cas9

CRISPR stands for clustered regularly interspaced short palindromic repeats, while Cas9 refers to CRISPR-associated protein 9, a nuclease enzyme. CRISPR was first discovered in the *Escherichia coli* genome by Japanese researchers in 1987 (Ishino *et al.*, 1987). Subsequently, CRISPR was identified in many other bacteria and archaea (Mojica *et al.*, 2000). However, the function of CRISPR remained unclear until 2007, when Barrangou *et. al.* from the yogurt industry demonstrated that CRISPR serves as a bacterial adaptive immune defence mechanism, protecting *Streptococcus thermophilus* from viral attacks (Barrangou *et al.*, 2007). Its first application in eukaryotic cells was reported in 2013 (Cong *et al.*, 2013). Today, CRISPR/Cas9 has become an indispensable tool in numerous laboratories, particularly those of molecular biologists worldwide.

CRISPR/Cas9 is a revolutionary genome-editing technology that enables precise, permanent modifications to DNA by harnessing the cell's double-strand break (DSB) repair mechanisms, namely non-homologous end joining (NHEJ) and homology-directed repair (HDR). NHEJ is a canonical DSB repair pathway in cells, but due to its error-prone nature, it often results in insertions or deletions (indels), leading to frameshift mutations or the generation of a premature stop codon, and consequently gene knockout. In contrast, HDR uses a donor template for DSB repair, ensuring precision and making it ideal for gene knock-in applications (Ran *et al.*, 2013). In contrast to earlier gene-editing tools such as zinc finger nucleases (ZFNs) and transcription activator-like effector nucleases (TALENs), CRISPR/Cas9 offers several advantages, including high specificity, efficiency, ease of use, and versatility. These qualities have made it widely applicable in genetic research and have led to its rapid adoption by the scientific community for targeting, editing, and modifying the genomes of various cells and organisms (Doudna and Charpentier, 2014).

Since Cas9 can bind to DNA at sites defined by the guide RNA sequence and the protospacer adjacent motif (PAM), CRISPR/Cas9 technology offers broad applications beyond permanent DNA modifications. These applications, which include human gene therapy, agriculture (e.g., crop and animal modifications), synthetic biology (e.g., pathway engineering), programmable RNA targeting, viral and pathogen gene disruption, ecological vector control (e.g., mosquito sterilisation), and drug target screening, were outlined by Nobel laureates, Jennifer A. Doudna and Emmanuelle Charpentier (Doudna and Charpentier, 2014). Both were awarded the Nobel Prize in Chemistry in 2020 for their groundbreaking discovery of CRISPR (Ledford and Callaway, 2020).

2.3.2 Mechanism of CRISPR/Cas9

The CRISPR/Cas9 system consists of two essential components: Cas9 and guide RNA. Cas9 is a DNA endonuclease responsible for cleaving the target DNA to create a double-stranded break, earning it the nickname "molecular scissors". The guide RNA (gRNA) is a short RNA sequence that directs the Cas9 enzyme to a specific DNA sequence in the genome for editing. The gRNA is composed of two parts: the CRISPR RNA (crRNA) and the trans-activating RNA (tracrRNA). The crRNA contains the sequence that enables target DNA binding, while the tracrRNA acts as a scaffold and is common to all guide RNAs. Both the crRNA and tracrRNA can be produced independently, or they can be engineered into a single guide RNA (sgRNA) (Jinek *et al.*, 2012).

CRISPR/Cas9-mediated genome editing involves three crucial steps: recognition, cleavage, and repair. The process begins with the gRNA recognising the target sequence in the gene of interest through complementary base pairing, guiding the Cas9 protein to the specific DNA sequence. Cas9 then makes a double-stranded break at a site three to four base pairs upstream of the PAM (Jinek *et al.*, 2012). The PAM is a short, conserved DNA sequence (usually two to six base pairs in length) located downstream of the targeted cleavage region. The PAM sequence can vary depending on the bacterial species (Jamal *et al.*, 2016). For *Streptococcus pyogenes* Cas9, the PAM is a 5'-NGG-3' sequence, where N represents any nucleotide. PAM is essential for Cas9 recognition, as without it, Cas9 cannot identify the target sequences, even if the sequences are fully complementary to the gRNA (Sternberg *et al.*, 2014).

Following cleavage, the double-stranded break is repaired by one of two mechanisms: non-homologous end joining (NHEJ) or homology-directed repair

(HDR) (Ran *et al.*, 2013) (Figure 2.2). In the NHEJ mechanism, DNA fragments are rejoined through an enzymatic process without the need for exogenous homologous DNA. Although NHEJ is error-prone, it is the predominant repair mechanism in active cells and is active throughout the cell cycle. Due to its error-prone nature, NHEJ often leads to random insertions or deletions (indels) within a coding exon, which can result in frameshift mutations or the creation of premature stop codons. In contrast, HDR is a precise repair mechanism that requires homologous DNA templates (Ran *et al.*, 2013). HDR is most active during the late S and G2 phases of the cell cycle (Liu *et al.*, 2019).

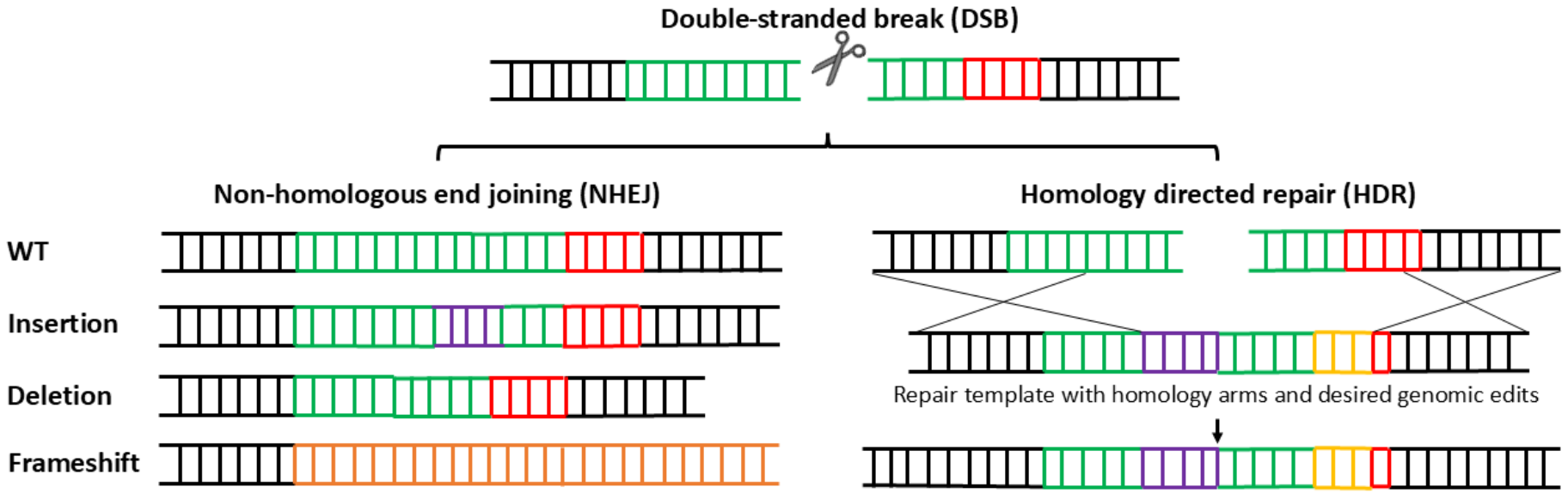

Figure 2.2: Schematic illustration of DNA double-strand break repair mechanisms activated following Cas9-mediated cleavage, namely non-homologous end joining and homology-directed repair

2.3.3 Applications of CRISPR/ Cas9 in PD research

Since its first application in mammalian cells in 2013 (Ran *et al.*, 2013), CRISPR/Cas9-mediated genome editing technology has revolutionised PD research, accelerating the development of various cell and animal models, enabling the study of gene function and key disease mechanisms. Additionally, CRISPR/Cas9 has significantly advanced the exploration of direct therapeutic strategies to correct pathogenic genes (Pinjala *et al.*, 2023, Rahman *et al.*, 2022).

Researchers have employed CRISPR/Cas9 to generate various LRRK2 knockout cell lines, including neuroblastoma, HEK-293, RAW264.7, and BV2 cells, to investigate the genetic underpinnings at the cellular level (reviewed in Section 2.1.4.1). In addition, CRISPR/Cas9 has been used to create knockout models for several other genes implicated in the pathogenesis of PD, including the glucocerebrosidase (*GBA*), the α-synuclein (*SNCA*) and the Parkinson protein 2 (*PARK2*) genes. For instance, Jiang *et al.* utilised CRISPR/Cas9 to generate DNase hypersensitive site (DHS) knockout SH-SY5Y cells and replace rs12411216, a functional single-nucleotide polymorphism (SNP) of the *GBA* gene. The CRISPR/Cas9-edited SH-SY5Y cells were crucial in confirming that the distal regulatory SNP rs12411216 influences the expression and enzymatic activity of the *GBA* gene, thereby promoting α-synuclein aggregation (Jiang *et al.*, 2020). In another study, Inoue *et al.* generated an α-synuclein null human induced pluripotent stem cell (hiPSC) line by introducing a frameshift mutation into the *SNCA* alleles using CRISPR/Cas9. The resulting *SNCA* knockout hiPSC-derived dopaminergic neurons exhibited reduced vulnerability to MPP^+. This *SNCA* knockout hiPSC line could serve as a valuable tool for investigating the physiological role of α-synuclein and exploring PD pathology (Inoue *et al.*,

2023). Another research group also used hiPSCs as a model to study PD pathology, creating PARK2 knock-in and knockout (KIKO) hiPSCs using CRISPR/Cas9. The PARK2 gene encodes parkin, an E3 ubiquitin ligase involved in mitophagy. Mutations in PARK2 are typically considered loss-of-function mutations, leading to impaired parkin activity and, consequently, defective mitophagy. The researchers found a significant reduction in the expression of ghrelin receptors (GHSR) in PD-specific hiPSC-derived dopaminergic neurons from patients with PARK2 mutations, compared to neurons from healthy controls. They further observed that GHSR expression was recapitulated in isogenic PARK2 KIKO iPSC-derived dopaminergic neurons. They concluded that the downregulation of GHSR in dopaminergic neurons may contribute to the initial neuronal dysfunction, potentially leading to extrapyramidal symptoms in PD (Suda *et al.*, 2018).

In addition to generating knockout cell models, CRISPR/Cas9 has also been used to create knock-in cell models and to correct gene mutations. Previously, the Cre-LoxP recombination system was employed to correct gene mutations. However, a major limitation of the Cre-LoxP system is that the residual LoxP site in an intron near the mutation correction site may potentially affect gene expression (Zou *et al.*, 2011). Qing *et al.* reported the development of a footprint-free LRRK2 G2019S isogenic hiPSC line using both CRISPR/Cas9 and piggyBac technologies. These hiPSCs are free from the residual LoxP site, thus overcoming the issue encountered by Zou *et al.* The dopaminergic neurons derived from the edited hiPSCs displayed reduced neurite complexity, a key indicator of neuronal dysfunction (Qing *et al.*, 2017, Zou *et al.*, 2011). Besides human iPSCs, CRISPR/Cas9 has also been used to generate knock-in models in

marmoset ESCs and iPSCs. The common marmoset, a non-human primate species, is widely used for comprehensive modelling of genetic mutations. Marmoset ESCs and iPSCs edited to carry the LRRK2 G2019S mutation exhibited increased kinase activity and intracellular ROS, alongside a decrease in neuronal viability and neurite complexity. These changes successfully recapitulated the phenotypes observed in dopaminergic neurons derived from iPSCs of PD patients carrying the LRRK2 G2019S mutation (Vermilyea *et al.*, 2020). Aside from generating knock-in models, CRISPR/Cas9 has also been employed to correct disease-causing gene mutations. For instance, Barbuti *et al.* successfully corrected the A30P point mutation in the *SNCA* gene using patient-derived iPSC clones. To isolate single-cell, isogenic, gene-corrected iPSC clones, a quadruple selection strategy (QSS) was implemented. This approach involved antibiotic selection, single-cell FACS sorting, PCR amplification with restriction enzyme-based clonal screening, and confirmation via Sanger sequencing. Dopaminergic neurons differentiated from the corrected iPSCs exhibited reduced α-synuclein protein levels, highlighting the therapeutic potential of precise gene correction in PD (Barbuti *et al.*, 2020).

Beyond creating knockout and knock-in cell models, CRISPR/Cas9 has also been explored for its use as a therapeutic strategy. The Synergistic Activation Mediator (SAM) system, also known as CRISPR activation (CRISPRa), utilises catalytically inactive Cas9/ dead Cas9 (dCas9), fused to transcriptional activators to induce gene expression at a specific location. Narváez-Pérez *et al.* reported the use of CRISPR/Cas9-directed SAM to activate the endogenous tyrosine hydroxylase gene in astrocytes, leading to the generation of dopamine in the striatum of 6-OHDA hemiparkinsonian rats. The lesioned rats that

received edited astrocytes exhibited significant improvements in motor behaviour compared to rats receiving non-edited astrocytes, which did not produce dopamine (Narváez-Pérez *et al.*, 2024). Furthermore, CRISPR/Cas9 technology has also been adapted to repress gene expression through a method known as CRISPR interference (CRISPRi). In this approach, a catalytically inactive Cas9 (dCas9) is fused to a transcriptional repressor, allowing for targeted inhibition of gene activity. For example, Sastre *et al.* employed dCas9 fused to the Krüppel-associated box (KRAB) repressor domain to suppress α-synuclein expression in iPSC-derived neuronal cultures from a patient carrying an *SNCA* genomic triplication. This targeted repression led to reduced oxidative stress and mitochondrial DNA damage, highlighting the potential of CRISPRi as a precision medicine strategy for PD through selective modulation of *SNCA* gene expression (Sastre *et al.*, 2023). Similarly, another group of researchers employed the CRISPRi approach to modulate *SNCA* gene expression, but with a distinct strategy. Instead of targeting the KRAB repressor domain, they developed an all-in-one lentiviral system targeting DNA methylation within intron 1 of the *SNCA* gene. In this system, dCas9 was fused to the catalytic domain of DNA methyltransferase 3A (DNMT3A). Editing iPSCs derived from a patient with *SNCA* triplication using this system successfully rescued disease-related phenotypes. Specifically, the elevated mitochondrial reactive oxygen species (ROS) production was reduced, and impaired cellular viability was restored (Kantor *et al.*, 2018).

2.4 Edible bird's nest (EBN)

2.4.1 Overview of EBN

Edible bird's nest (EBN), also known as the "Caviar of the East," is a highly valued medicinal delicacy consumed worldwide, particularly within the Chinese community. Its consumption has long symbolised wealth, power, and prestige, and it has been used medicinally in traditional Chinese medicine since as early as the Tang (618–907 AD) and Song (960–1279 AD) dynasties (Koon and Cranbrook, 2002). EBN is produced from the saliva of swiftlets, specifically those belonging to the genus *Aerodramus*. The majority of EBN traded globally comes from two species: *Aerodramus fuciphagus* and *Aerodramus maximus* (Marcone, 2005). These nests are commonly harvested from caves in Southeast Asian countries such as Indonesia, Malaysia, Thailand, Vietnam, and the Philippines.

EBN is considered one of the most expensive animal-derived products (Zulkefle *et al.*, 2024). Due to overharvesting and the resulting decline in cave nest availability, paired with rising global demand and increasing prices, EBN farming has emerged in many countries. This practice involves constructing buildings to attract swiftlets, allowing them to build nests that can be harvested sustainably (Connolly, 2016, MaimunHana and Choon, 2024). EBN is mainly composed of protein, carbohydrate, minerals, ash, fat, and moisture. The percentage of each of these components in EBN differs depending on factors such as production site, swiftlet species, and geographical origin. Production site refers to the environment where EBN is collected, either natural caves or man-made swiftlet houses, while geographical origin indicates the country or region from which the EBN originates (Quek *et al.*, 2018b, Quek *et al.*, 2018a, Seow *et*

al., 2016, Guo *et al.*, 2017, Huda *et al.*, 2008, SaengkrajangMatan and Matan, 2013). The quality of EBN is often closely linked to these factors, which can significantly influence its market value (Guo *et al.*, 2017). In addition, other variables such as the swiftlet nesting season, harvesting period, habitat conditions, and food availability can also impact EBN quality (Quek *et al.*, 2018b, NorhayatiAzman and Nazaimoon, 2010).

Protein is the most abundant component found in edible bird's nest (EBN), followed by carbohydrates, ash, and fat (Quek *et al.*, 2018b, SaengkrajangMatan and Matan, 2013). Among the carbohydrate components, sialic acid is particularly prominent and is considered one of the key bioactive constituents of EBN (Daud *et al.*, 2021, PozsgayJennings and Kasper, 1987). Sialic acid plays a crucial role in brain development and cognition (Wang and Brand-Miller, 2003, Wang, 2009) and has therefore been extensively studied for its role in mediating the health benefits of EBN (Xie *et al.*, 2018, Careena *et al.*, 2018, Qian *et al.*, 2025). Additionally, sialic acid has become an important marker compound for grading and authenticating EBN, helping to ensure both its safety and quality (Chan *et al.*, 2013, Yang *et al.*, 2014). Standardising sialic acid content is particularly crucial for the export of EBN to international markets (Thavamanithevi *et al.*, 2014, Looi and Omar, 2016). A total of 22 amino acids have been identified in EBN, although the presence of some varies depending on the country of origin (Hun *et al.*, 2015, SaengkrajangMatan and Matan, 2013, Marcone, 2005). Sodium, potassium, magnesium, and calcium are the predominant minerals present, with trace amounts of iron, zinc, copper, and phosphorus also detected (SaengkrajangMatan and Matan, 2013, NorhayatiAzman and Nazaimoon, 2010). The moisture content of EBN is

typically high, likely due to the elevated humidity characteristic of the tropical climates in Southeast Asian countries (Quek *et al.*, 2018b).

2.4.2 Beneficial properties of EBN

EBN has been extensively studied for its potential health benefits in recent years. A wide range of bioactivities has been reported, including antioxidant (Table 2.4), pro-proliferative, neuroprotective, immunomodulatory, antiviral, osteoprotective, chondroprotective, anticoagulant, anti-diabetic, sexual function-enhancing, skin-lightening, and anti-wrinkle effects (Table 2.5). Among these, the antioxidant properties of EBN are the most frequently reported. Oxidative stress occurs when there is an imbalance between the production of reactive oxygen species (ROS) and the body's ability to neutralise them with antioxidants. This imbalance can lead to cellular damage, contributing to the development of various chronic diseases and ageing-related conditions (Pizzino *et al.*, 2017). A substantial body of evidence supports the classification of EBN as a functional food with potent antioxidant properties (Table 2.4).

Various biochemical assays, such as DPPH, ABTS, FRAP, and ORAC, have been utilised to assess the antioxidant activity of different EBN extracts (Table 2.4). For example, Ghassem *et al.* demonstrated that EBN fractions derived from pepsin-trypsin hydrolysates exhibited significant radical-scavenging activity and promising antioxidant potential, as evidenced by results from the ORAC, ABTS, FRAP, and DPPH assays (Ghassem *et al.*, 2017). Similarly, Chantakun and Benjakul demonstrated that protein hydrolysates derived from EBN co-products treated with ultrasound exhibited high antioxidant activity, as evaluated by

ORAC, ABTS, FRAP, and DPPH assays (Chantakun and Benjakul, 2022). EBN co-products or by-products refer to the discarded materials generated during the cleaning and processing of EBN, which typically include feathers, glycoproteins, eggshells, and other residues (Cao *et al.*, 2022, Chantakun and Benjakul, 2022, Ling *et al.*, 2020). Enzymatic hydrolysis of these by-products has been shown to enhance their antioxidant activity significantly (Ling *et al.*, 2020), presenting a promising strategy for the sustainable utilisation of EBN waste. Furthermore, Cao *et al.* employed response surface methodology to isolate peptides from EBN co-products with good antioxidant properties (Cao *et al.*, 2022).

In addition to biochemical assays, the DCFH-DA assay has been employed to evaluate the antioxidant capacity of EBN at the cellular level (Table 2.4). The DCFH-DA assay offers greater biological relevance than biochemical antioxidant activity assays, as it accounts for cellular uptake, metabolism, and the intracellular localisation of antioxidant compounds (Wolfe and Liu, 2007). Murugan *et al.* demonstrated that EBN aqueous extract protects human umbilical vein endothelial cells (HUVECs) from high glucose-induced oxidative damage, as evidenced by reduced intracellular ROS levels measured using the DCFH-DA assay (Murugan *et al.*, 2020). Similarly, Yew *et al.* reported that EBN attenuates ROS accumulation in 6-OHDA-challenged SH-SY5Y cells, suggesting its potential as a nutraceutical for protecting against oxidative stress-related neurodegenerative disorders such as PD (Yew *et al.*, 2014). Consistent with these findings, other studies have shown that EBN extracts mitigate ROS production in HepG2 cells exposed to hydrogen peroxide, a known inducer of oxidative stress (YidaImam and Ismail, 2014, Fan *et al.*, 2021a).

For *in vivo* investigations, biological samples such as serum, aortic rings, and brain homogenates from animal models (e.g., rats and mice) have been collected to evaluate antioxidant activity and detect oxidative stress markers using biochemical assays and Western blot analysis (Table 2.4). Careena *et al.* assessed ROS levels in brain lysates via DCFH-DA assays and estimated lipid peroxidation using the TBARS assay. Their findings indicated that pretreatment with EBN significantly reduced ROS production in a lipopolysaccharide-induced neuroinflammation model in Wistar rats (Careena *et al.*, 2018). Similarly, Yida *et al.* demonstrated that EBN mitigated high-fat diet-induced oxidative stress, as evidenced by decreased levels of serum and hepatic oxidative markers measured using ABTS and TBARS assays (Yida *et al.*, 2015a). Furthermore, Yew *et al.* reported that EBN upregulated glutathione peroxidase 1, an antioxidant enzyme predominantly localised around dopaminergic neurons in the substantia nigra of a 6-OHDA-induced PD mouse model (Yew *et al.*, 2018). In another study, Murugan *et al.* showed that EBN reduced high glucose-induced vascular superoxide production in the aorta of C57BL/6J mice, as determined by lucigenin-enhanced chemiluminescence, and inhibited the expression of oxidative stress-associated proteins NADPH oxidase 2 and nitrotyrosine (Murugan *et al.*, 2020)

Table 2.4 Antioxidant properties of EBN

No.	Type of EBN extract	Antioxidant evaluation method	Outcome(s) of study	Reference
1	Aqueous extract & enzyme extract (pancreatin)	DCFH-DA	EBN may serve as a promising nutraceutical candidate for protecting against oxidative stress-related neurodegenerative disorders, such as PD	(Yew *et al.*, 2014)
2	Aqueous extract & enzyme extract (pepsin, pancreatin & bile extracts)	ABTS, ORAC, DCFH-DA	Undigested EBN aqueous extract exhibited minimal antioxidant activity, whereas the digested samples demonstrated significantly enhanced antioxidant activities at comparable concentrations	(YidaImam and Ismail, 2014)
3	Raw EBN	ABTS	Evidence-based use of EBN as a dietary supplement for the prevention of obesity-related inflammation and oxidative stress in rats	(Yida *et al.*, 2015a)
4	Aqueous extract	ABTS, ORAC, SOD & ROS ELISA assay	Lactoferrin and ovotransferrin may exert synergistic or all-or-none antioxidant effects in EBN	(Hou *et al.*, 2015a)
5	Enzyme extract (pepsin, trypsin, pancreatin and mucosal peptidases)	DPPH, ABTS, FRAP, ORAC	EBN protein hydrolysates are a good source of natural antioxidants and hold potential for use as nutraceutical compounds	(Ghassem *et al.*, 2017)
6	Aqueous extract	DPPH & FRAP	The antioxidant activity of EBN varies depending on its production method, the swiftlet species, and the geographical origin	(Quek *et al.*, 2018b)

7	Aqueous extract	QuantiChrome™ TBARS assay kit, Enzychrom™ SOD assay kit, QuantiChrome™ antioxidant assay kit	EBN promoted the proliferation of uterine structures, as evidenced by the upregulation of steroid receptors, EGF, EGFR, VEGF, and PCNA expression in the uterus, along with increased plasma concentrations of antioxidants and reduced oxidative stress levels	(Albishtue *et al.*, 2018b)
8	Aqueous extract and enzyme extract (pancreatin)	Lipid hydroperoxide assay kit & measurement of GPX1 protein expression	EBN exerted neuroprotective effects by enhancing antioxidant enzyme activity and inhibiting microglial activation, NO production, and lipid peroxidation in a PD model	(Yew *et al.*, 2018)
9	Enzyme extract (pepsin & pancreatin)	DCFH-DA & TBARS	EBN inhibited LPS-induced upregulation of proinflammatory cytokines and oxidative stress markers	(Careena *et al.*, 2018)
10	Raw EBN & enzyme extract (alcalase)	DPPH, ABTS, FRAP	Both EBN and chicken eggs are good sources of protein and essential amino acids; however, EBN has demonstrated higher antioxidant activity	(Ali *et al.*, 2019)
11	Aqueous extract	Enzychrom™ SOD assay kit	EBN alleviated the detrimental effects of lead acetate-induced uterine toxicity, potentially by enhancing SOD activity and upregulating the expression of EGF, VEGF, and PCNA, which are associated with cell proliferation	(Albishtue *et al.*, 2019)
12	Enzyme extract (alcalase, papain & papaya juice)	DPPH	Enzymatic hydrolysis enhanced the functional properties of EBN, highlighting its potential to be developed as a natural antioxidant and anti-hyperglycaemic agent	(Zulkifli *et al.*, 2019)

13	Aqueous extract	DCFH-DA, LECL & measurement of NOX2, nitrotyrosine and SOD1 protein expression	EBN restored endothelial function and protected endothelial cells from high glucose-induced oxidative damage in HUVECs, isolated mouse aorta, and *db/db* diabetic mice by modulating ROS pathways, thereby increasing NO bioavailability	(Murugan *et al.*, 2020)
14	Enzyme extract (pancreatin & alcalase)	DPPH & FRAP	Enzymatic hydrolysis recovered EBN co-products from low-value sources, resulting in enhanced antioxidant activities	(Ling *et al.*, 2020)
15	Enzyme extract (the type of enzyme used is not stated)	DPPH	EBN enhanced DPPH radical scavenging activity in a concentration-dependent manner	(Kim *et al.*, 2021b)
16	Enzyme extract (papain) dissolved in ginger extract, mulberry leaf extract & cinnamon twig extract	DPPH & FRAP	EBN enzyme extract dissolved in mulberry leaf extract exhibited the highest antioxidant activity	(TangGoh and Sia, 2021)
17	Enzyme extract (simulated gastric and intestinal fluid)	DCFH-DA	Digested EBN exhibited significant antioxidant activity and a protective effect against H_2O_2-induced oxidative damage in cells	(Fan *et al.*, 2021a)
18	Aqueous extract	SOD assay kit	EBN protected the histomorphology of the rat uterus against cadmium toxicity by reducing cadmium accumulation and enhancing antioxidant activity	(Quddus *et al.*, 2021)

19	Enzyme extract (protease from *B. amyloliquefaciens*)	SOD1 ELISA kit, catalase activity colorimetric/ fluorometric assay kit, and GPX activity colorimetric assay kit	EBN effectively suppressed UVB-induced oxidative stress in the dorsal skin of hairless mice	(Kim *et al.*, 2021a)
20	Aqueous extract, acid extract (hydrochloric and acetic acid), base extract (sodium hydroxide), enzyme extract (pancreatin)	DPPH	Aqueous and acid extracts of farmed EBN exhibited higher antioxidant activity compared to those derived from cave EBN	(Napavichayanun *et al.*, 2021)
21	Enzyme extract (alcalase) with ultrasonication	DPPH, ABTS, FRAP & ORAC	EBN enzyme extracts treated with ultrasonication exhibited higher antioxidant activity compared to those without ultrasonication	(Chantakun and Benjakul, 2022)
22	Enzyme extract (Papain, acid protease, neutrase, alcalase, pepsin, and trypsin)	DPPH & ABTS	Purified peptides derived from EBN by-products showed potent antioxidant properties	(Cao *et al.*, 2022)
23	Enzyme extract (digestive enzyme mixtures)	ORAC, cellular ORAC, CellROX®	EBN enzyme extract protected human keratinocytes and 3D epithelium equivalents against UV- and arid environment–induced oxidative stress	(Wang *et al.*, 2023a)

		Orange and Green Reagent		
24	Aqueous extract, enzyme extract (pancreatin & alcalase) & bacterial-fermented extract (*L. helveticus*, *L. curvatus*, *and L. sakei*)	DPPH, ABTS, FRAP	Of all the extracts, the *L. curvatus*-fermented EBN extract showed the highest antioxidant activity	(Ter *et al.*, 2024)
25	Peptides derived from enzyme extract (alcalase)	DPPH & ABTS	Peptides (LFWSPSVYLK and GWPHLEDNYLDW) derived from EBN showed high antioxidant capacity	(Lee *et al.*, 2024)
26	Enzyme extract (papain & bromelain, and papaya, pineapple and cantaloupe juice)	ABTS, •OH-scavenging	Fruit juice-mediated hydrolysis of EBN enhanced the antioxidant, anti-tyrosinase, and wound-healing properties of the hydrolysates	(Nguyen *et al.*, 2024)
27	Bacterial-fermented extract (*B. amyloliquefaciens* & *B. natto*)	DPPH, ABTS, •OH-scavenging	The extract fermented with *B. amyloliquefaciens* and *B. natto* exhibited higher antioxidant activity than the extract fermented with *B. amyloliquefaciens* alone	(Li *et al.*, 2024b)

28	AEC-derived fractions from enzyme extract (pancreatin & alcalase)	DPPH, ABTS & FRAP	AEC fractionation can purify EBN and yield positively charged EBN fractions with antioxidant potential, which may be applied as functional food components to promote health benefits	(Mun *et al.*, 2024)

Abbreviations:

DCFH-DA, 2', 7'-dichlorofluorescein diacetate [cellular antioxidant assay]; ABTS, 2,2'-azino-bis(3-ethylbenzothiazoline-6sulfonic acid) [radical scavenging assay]; ORAC, oxygen radical absorbance capacity assay; SOD, superoxide dismutase; ROS, reactive oxygen species; ELISA, enzyme-linked immunosorbent assay; DPPH, 2,2-diphenyl-1-picrylhydrazyl [free radical scavenging activity assay]; FRAP, ferric reducing antioxidant power; TBARS, thiobarbituric acid reactive substances assay; EGF, epidermal growth factor; EGFR, epidermal growth factor receptor; VEGF, vascular endothelial growth factor; PCNA, proliferating cell nuclear antigen; GPX1, glutathione peroxidase 1; NO, nitric oxide; HUVECs, human umbilical vein endothelial cells; LPS, lipopolysaccharide; LECL, lucigenin-enhanced chemiluminescence assay; NOX2, NADPH oxidase 2; H_2O_2, hydrogen peroxide; •OH-scavenging, hydroxyl radical scavenging activity assay; UV, ultraviolet; AEC, anion exchange chromatography

Table 2.5 Beneficial properties of EBN

No.	Beneficial property of EBN	Type of EBN extract(s)	Outcome(s) of the study	Reference
1	Pro-proliferative	Acid extract (hydrochloric acid)	EBN enhanced the proliferation of Caco-2 cells	(Aswir Abd Rashed and Wan Nazaimoon, 2010)
2	Pro-proliferative	Aqueous extract	A low concentration of EBN in serum-containing medium can induce the proliferation of cultured rabbit corneal keratocytes	(Zainal Abidin *et al.*, 2011)
3	Pro-proliferative	Enzyme extract [Protamex (a blend of microbial endo-proteases)]	EBN promoted the proliferation of human adipose-derived stem cells by upregulating IL-6 and VEGF gene expression, mediated through the activation of NF-κB and AP-1 via the p44/42 MAPK and p38 MAPK signalling pathways	(Roh *et al.*, 2012)
4	Pro-proliferative	Aqueous extract	Supplementation with 0.5–1.0% EBN aqueous extract enhanced the proliferation of human articular chondrocytes	(Chua *et al.*, 2013)
5	Pro-proliferative	Aqueous extract	EBN enhanced the proliferation of B-lymphocytes	(Zhao *et al.*, 2016)
6	Pro-proliferative	Enzyme extract (patented method)	EBN enhanced the proliferation of normal human keratinocytes and normal human skin fibroblasts	(Terazawa and Shimoda, 2020)
7	Pro-proliferative	Acid extract (hydrochloric acid)	EBN promoted the L929 fibroblast cell growth	(Napavichayanun *et al.*, 2021)

8	Pro-proliferative	Enzyme extract (pepsin & pancreatin)	EBN promoted the proliferation of T-lymphocytes	(Dobutr *et al.*, 2022)
9	Neuroprotective	Aqueous extract & enzyme extract (pancreatin)	EBN may exert neuroprotective effects against 6-OHDA-induced dopaminergic neuron degeneration, primarily through the inhibition of apoptosis	(Yew *et al.*, 2014)
10	Neuroprotective	Raw EBN	EBN showed potential for neuroprotection against estrogen deficiency-associated damage, at least in part through modulation of the redox system and reduction of advanced glycation end-products	(Zhiping *et al.*, 2015)
11	Neuroprotective	Raw EBN	EBN treatment improved cognition and memory in ovariectomized female rats, suggesting it may serve as an effective alternative to estrogen therapy for menopause-related cognitive decline	(Hou *et al.*, 2017)
12	Neuroprotective	Enzyme extract (pepsin & pancreatin)	EBN significantly enhanced memory and demonstrated potent neuroprotective effects by inhibiting neuroinflammation and oxidative stress	(Careena *et al.*, 2018)
13	Neuroprotective	Aqueous extract	EBN significantly reduced beta-amyloid accumulation in the hippocampus, decreased acetylcholinesterase activity, and improved neurological scores and spatial memory in animals	(SirinupongChansuwan and Kaewkaen, 2024)
14	Immunomodulatory	Aqueous extract	EBN was a leading cause of food-induced anaphylaxis requiring hospitalisation among Chinese children in Singapore, with the reaction confirmed to be IgE-mediated and involving specific major allergens	(Goh *et al.*, 2000)
15	Immunomodulatory	Aqueous extract	The immunochemical properties of EBN allergens were characterised. EBN from different sources were found to be allergically distinct, and a 66-kDa protein was identified as the putative major allergen	(Goh *et al.*, 2001)

16	Immunomodulatory	Acid extract (hydrochloric acid)	EBN can reduce the production of the pro-inflammatory cytokine TNF-α in RAW 264.7 macrophages	(Aswir and Wan Nazaimoon, 2011)
17	Immunomodulatory	Acid extract (hydrochloric acid)	EBN exhibited anti-inflammatory properties in lipopolysaccharide-stimulated RAW 264.7 macrophages by inhibiting TNF-α and NO production without inducing significant cytotoxicity	(VimalaHussain and Nazaimoon, 2012)
18	Immunomodulatory	Raw EBN	EBN attenuated high-fat diet-induced inflammation by modulating the expression of hepatic inflammatory genes	(Yida *et al.*, 2015a)
19	Immunomodulatory	Aqueous extract	EBN can alleviate cyclophosphamide-induced intestinal immune injury by promoting B-cell proliferation, activation, and antibody secretion	(Zhao *et al.*, 2016)
20	Immunomodulatory	Aqueous extract	EBN exerted a protective effect against dextran sulfate sodium-induced colitis in mice, primarily by restoring the balance between T helper 17 and regulatory T cells	(Fan *et al.*, 2021b)
21	Immunomodulatory	Enzyme extract (pepsin & pancreatin)	EBN specifically promoted $CD3^+$ T-cell expansion and helped restore T-cell populations suppressed by immunosuppressive drugs, without significantly affecting B-cells or natural killer cells. In rats, oral EBN administration increased peripheral T-cell counts, influenced immune-related organs such as Peyer's patches and spleen, and elevated IL-2 levels, which correlated with T-cell proliferation	(Dobutr *et al.*, 2022)
22	Immunomodulatory	Aqueous extract	EBN attenuated sulfur dioxide-induced lung injury in mice by inhibiting inflammation and modulating immune balance	(Zeng *et al.*, 2022)
23	Immunomodulatory	Enzyme extract (pepsin & pancreatin)	EBN stimulated both MHC-II and costimulatory molecules, facilitating TCR/pMHC-II interactions and thereby promoting T-cell activation	(Dobutr *et al.*, 2023)

24	Antiviral	Enzyme extract (pancreatin)	EBN extract neutralised influenza virus infection in MDCK cells and inhibited the hemagglutination of influenza viruses with erythrocytes; however, it did not inhibit influenza virus sialidase activity	(Guo *et al.*, 2006)
25	Antiviral	Enzyme extract (pancreatin and neuraminidase)	EBN showed high neuraminidase inhibitory properties in both *in vitro* and *in vivo*	(Haghani *et al.*, 2016)
26	Antiviral	Enzyme extract (pancreatin and neuraminidase)	EBN can inhibit the influenza A virus as effectively as commercial antiviral agents	(Haghani *et al.*, 2017)
27	Antiviral	Aqueous extract	EBN inhibited apoptosis in cells following influenza A virus infection	(Nur AinAbdul Rahman and Aini, 2017)
28	Antiviral	Enzyme extract (pancreatin)	EBN exhibited a strong synergistic effect with either oseltamivir carboxylate or zanamivir, a competitive inhibitor of receptor-destroying neuraminidases, against the avian H5N1 virus	(Sriwilaijaroen *et al.*, 2024)
29	Osteoprotective	Enzyme extract (pancreatin)	EBN improved bone strength and calcium concentration, and increased dermal thickness in the femurs of ovariectomized rats, suggesting its potential effectiveness in mitigating bone loss and skin ageing in postmenopausal women	(Matsukawa *et al.*, 2011)
30	Osteoprotective	Enzyme extract (alcalase)	EBN enhanced bone quality and modulated inflammatory responses, indicating its potential as a beneficial alternative for osteoarthritis treatment	(Sulaiman *et al.*, 2024)
31	Chondroprotective	Aqueous extract	EBN reduced catabolic activity and enhanced cartilage extracellular matrix synthesis, suggesting its potential as a therapeutic agent for osteoarthritis	(Chua *et al.*, 2013)

32	Anti-diabetic	Raw EBN	EBN prevented the deterioration of metabolic indices and transcriptional alterations in insulin signalling genes induced by a high-fat diet	(Yida *et al.*, 2015c)
33	Anti-diabetic	Raw EBN	EBN improved metabolic indices and induced transcriptional changes in hepatic insulin signalling genes that promoted enhanced insulin sensitivity and glucose and lipid homeostasis, surpassing even the effects of estrogen	(Hou *et al.*, 2015b)
34	Anti-diabetic	Aqueous extract	EBN showed anti-diabetic effects by improving β-cell function and insulin sensitivity through the insulin-PI3K/Akt signalling pathway	(Choy *et al.*, 2021)
35	Skin-lightening	Aqueous extract	N-acetylneuraminic acid was the active ingredient in EBN that contributed to its skin-lightening properties	(Chan *et al.*, 2015)
36	Skin-lightening	Enzyme extract (simulated gastric and intestinal fluid)	EBN significantly inhibited tyrosinase activity in B16 cells	(Fan *et al.*, 2021a)
37	Skin-lightening	Enzyme extract (the type of enzyme used is not stated)	EBN reduced melanin content and downregulated the expression of melanogenesis-related genes, including MITF, TYR, TRP1, and TRP2	(Kim *et al.*, 2021b)
38	Skin-lightening	Enzyme extract (pepsin & pancreatin)	A <1 kDa fraction derived from EBN significantly inhibited tyrosinase activity and reduced melanin content by modulating the cAMP/MITF/TRP-1/TRP-2 signalling pathways involved in melanogenesis	(Yi *et al.*, 2023)
39	Skin-lightening	Enzyme extract (alcalase)	EBN reduced melanin content and inhibited tyrosinase activity, while also downregulating the expression of melanogenesis-related genes. Furthermore, the FRAF peptide derived from EBN bound to proteins involved in melanogenesis	(Bai *et al.*, 2024)

40	Anti-wrinkle	EBN extract (the type of extract is not specified)	EBN effectively reduced skin wrinkles in a randomised, double-blind, placebo-controlled, comparative study	(Kim *et al.*, 2022)
41	Anti-coagulant	Raw EBN	EBN may attenuate high-fat diet-induced hypercholesterolemia and coagulation, comparable to the effects of simvastatin, partly through the transcriptional regulation of coagulation-related genes	(Yida *et al.*, 2015b)
42	Anti-coagulant	Aqueous extract	EBN improved lipid and coagulation profiles, reduced hepatosteatosis, and stabilised atherosclerotic plaque formation in rabbits with hypercholesterolemia	(Mohamad Nasir *et al.*, 2023)
43	Sexual function-enhancing	Enzyme extract (pancreatin)	EBN may enhance sexual function in castrated male rats, potentially through testosterone-related mechanisms, suggesting its potential as an effective treatment for erectile dysfunction	(MaLiu and Dai, 2012)
44	Sexual function-enhancing	Aqueous extract	EBN increased sperm concentration and motility, as well as the levels of follicle-stimulating hormone and luteinizing hormone	(Jaffar *et al.*, 2021)

Abbreviations:

Caco-2, human colorectal adenocarcinoma cells; IL-6, interleukin-6; VEGF, vascular endothelial growth factor; NF-κB, nuclear factor kappa B; AP-1, activator protein-1; MAPK, mitogen-activated protein kinase; 6-OHDA, 6-hydroxydopamine; IgE, immunoglobulin E; TNF-α, tumour necrosis factor-α; NO, nitric oxide; IL-2, interleukin-2; MHC-II, major histocompatibility complex II; TCR, T-cell receptor; MDCK cells, Madin-Darby canine kidney cells; PI3K, phosphatidylinositol 3-kinase; Akt, protein kinase B; B16, murine melanoma cell line; MITF, microphthalmia

associated transcription factor; TYR, tyrosinase; TRP-1, tyrosinase related protein 1; TRP-2, tyrosinase related protein 2; cAMP, cyclic adenosine monophosphate

CHAPTER 3.0

MATERIALS AND METHODS

This study was conducted in four major phases: (i) generation of LRRK2 knockout SH-SY5Y neuroblastoma cells; (ii) screening and validation of the knockout clones; (iii) evaluation of phenotypic changes in the knockout clones; and (iv) assessment of the effects of edible bird's nest (EBN) extracts (Figure 3.1).

3.1 Cultivation of SH-SY5Y

The human neuroblastoma cell line (SH-SY5Y) was purchased from the American Type Culture Collection (ATCC, USA) and cultured in Dulbecco's Modified Eagle Medium: Nutrient Mixture F12 (DMEM/ F12) (Gibco, USA), supplemented with 10% (v/v) foetal bovine serum (FBS) (Tico Europe, Netherlands) and 1% (v/v) Penicillin/ Streptomycin (Sigma-Aldrich, USA). The culture was maintained in a humidified atmosphere of 95% (v/v) air / 5% (v/v) CO_2 at 37 °C. The media were changed every two to three days when they became acidic. When the cells reached 80 % confluency, they were subcultured into new culture vessels.

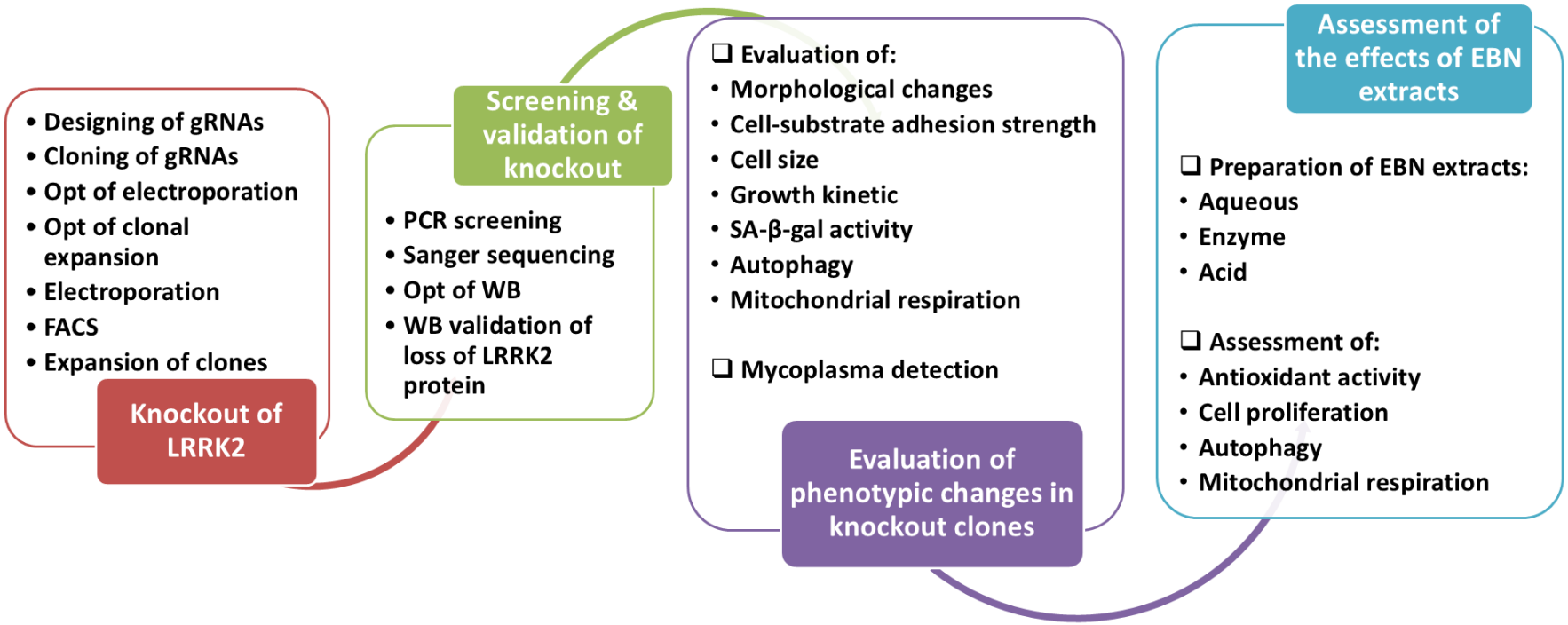

Figure 3.1: Schematic illustration of the four phases of the study and the corresponding experimental workflow. gRNAs, guide RNAs; Opt, optimisation; FACS, fluorescence-activated cell sorting; WB, Western blot; SA-β-gal, senescence-associated beta galactosidase; EBN, edible's bird's nest

3.2 Knockout of *LRRK2* gene using CRISPR/Cas9 genome editing tool

3.2.1 Design of gRNAs

gRNAs were designed using the web tool CHOPCHOP (https://chopchop.cbu.uib.no/), which identifies single gRNA targets for CRISPR/Cas systems. The parameters used for designing gRNAs to knock out LRRK2 are detailed in Table 3.1.

Table 3.1: The parameters used to design gRNAs

Parameter	Input
Target	LRRK2
In	Homo sapiens (hg38/GRCh38)
Using	CRISPR/Cas9
For	Knockout

Numerous web-based tools are available for gRNA design, each employing different algorithms to generate gRNA sequences and predict off-target sites. CHOPCHOP is one of the most highly recommended and commonly used tools (HwangSong and Bae, 2021). The gRNAs that fulfil the following criteria were selected:

i. 20 base pairs in length

ii. Target exon(s) in the early coding region

iii. Guanine-cytosine (GC) content of 40 - 60 %

iv. Low number of mismatches (i.e. number of off-target transcripts that the gRNA may bind to, outside of the target gene)

The three selected gRNAs used in this study are designated as gRNA1, gRNA2, and gRNA3. Their sequences and binding sites are presented in Figure 3.2.

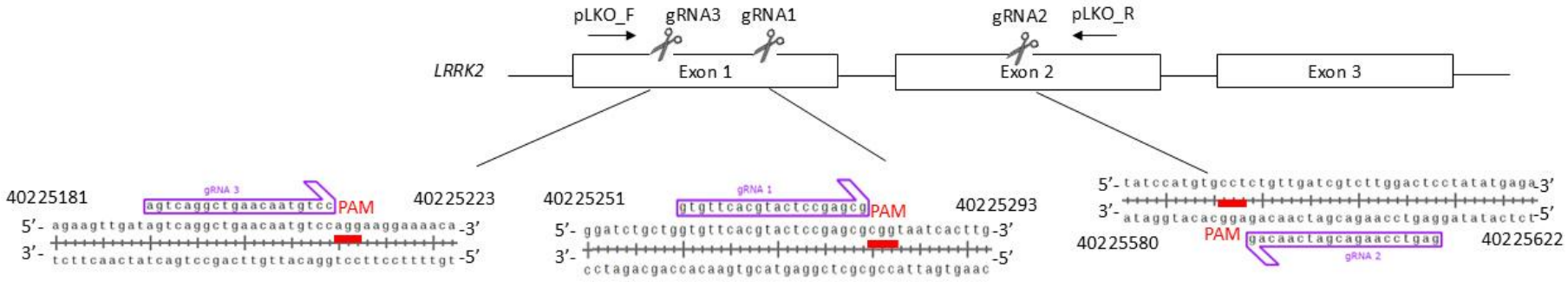

Figure 3.2: Sequence and binding sites of gRNA1, gRNA2 and gRNA3 in the exon 1 and 2 of the LRRK2 gene. PAM motifs are highlighted in red colour.

3.2.2 Cloning of gRNAs

PX458-gRNA1, PX458-gRNA2 and PX458-gRNA3 were constructed by inserting the respective gRNA sequence into pSpCas9(BB)-2A-GFP (PX458) plasmid. PX458 plasmids were a gift from Feng Zhang (Addgene plasmid # 48138; http://n2t.net/addgene:48138; RRID: Addgene_48138) (Ran *et al.*, 2013). The cloning of gRNAs involves the following steps:

i. Preparation of competent cells

ii. Digestion of PX458 plasmids

iii. Purification of the digested PX458 plasmids

iv. Annealing of gRNA oligos

v. Ligation of gRNA oligos and PX458 plasmids

vi. Transformation of ligation products into competent cells

vii. Extraction of PX458 plasmids

3.2.2.1 Preparation of competent cells

Escherichia coli (E. coli) DH5α cells were inoculated into 4 ml of Luria-Bertani (LB) broth (Condalab, Spain) and cultured overnight. Then, 2 ml of the overnight culture was transferred to 100 ml of LB broth and incubated at 37 °C until the optical density (OD) 550 reached between 0.3 and 0.5, measured using a spectrophotometer (Thermo Fisher Scientific, USA). The culture was then transferred to 50 ml centrifuge tubes and pelleted by centrifugation at 3500 x g for 5 minutes at 4 °C. After centrifugation, the supernatants were discarded, and

the cells were resuspended in 33 ml of ice-cold RF1 solution. The RF1 solution consisted of 100 mM potassium chloride (KCl) (Sigma-Aldrich, USA), 50 mM manganese (II) chloride tetrahydrate ($MnCl_2 \cdot 4H_2O$) (R&M Chemicals, UK), 30 mM potassium acetate (KAc) (R&M Chemicals, UK), 10 mM calcium chloride dihydrate ($CaCl_2 \cdot 2H_2O$) (R&M Chemicals, UK), and 15% (v/v) glycerol (Sigma-Aldrich, USA). The cell suspension was centrifuged again at 3500 x g for 5 minutes at 4 °C. The supernatant was removed, and the cells were resuspended in 8 ml of ice-cold RF2 solution, which contained 10 mM 3-morpholinopropanesulfonic acid (MOPS) (J&K Scientific, China), 10 mM potassium chloride (KCl) (Sigma-Aldrich, USA), 75 mM calcium chloride dihydrate ($CaCl_2 \cdot 2H_2O$) (R&M Chemicals, UK), and 15% (v/v) glycerol (Sigma-Aldrich, USA). The cell suspension was incubated on ice for 15 minutes. Subsequently, it was aliquoted into 1.5 ml microcentrifuge tubes and quickly frozen in liquid nitrogen before being stored at -80 °C.

3.2.2.2 Digestion of PX458 plasmids

Restriction enzyme digestion was performed to linearise PX458 plasmids. For each digestion reaction, 1 µg (1 unit) of *Bbs*I enzyme (New England Biolabs, USA) was added to a 1.5 ml microcentrifuge tube containing 5 µg of PX458 plasmids. The mixture was then incubated for 16 hours at 37 °C.

3.2.2.3 Purification of the digested PX458 plasmids

The digested PX458 plasmids were run on a 1% (w/v) agarose gel at 80 V for 30 minutes and purified using the Wizard SV Gel and PCR Clean-Up System

(Promega, USA) according to the manufacturer's instructions. Briefly, the DNA band was excised from the gel and placed in a 1.5 ml microcentrifuge tube. Membrane Binding Solution (10 µl per 10 mg of gel slice) was added, and the gel slice was vortexed and incubated at 65 °C until completely dissolved. The dissolved gel mixture was transferred to a Minicolumn assembly and incubated for 1 minute. After incubation, the Minicolumn assembly was centrifuged at 16,000 x g for 1 minute, and the flow-through was discarded. The Minicolumn was then reinserted into a collection tube.

Next, 700 µl of Membrane Wash Solution was added, and the Minicolumn assembly was centrifuged at 16,000 x g for 1 minute. The flow-through was discarded again, and the Minicolumn was reinserted into the collection tube. This step was repeated with 500 µl of Membrane Wash Solution, followed by centrifugation at 16,000 x g for 5 minutes. The collection tube was emptied, and the Minicolumn assembly was re-centrifuged for 1 minute to evaporate any residual ethanol. The Minicolumn was then transferred to a 1.5 ml microcentrifuge tube, 50 µl of nuclease-free water was added and incubated at room temperature for 1 minute, after which the Minicolumn was centrifuged at 16,000 x g for 1 minute to elute the plasmid. The purified plasmid was stored at -20 °C.

3.2.2.4 Annealing of gRNA oligos

The single-stranded gRNA oligos used in this study were synthesised by Integrated DNA Technologies (IDT, Singapore). The gRNAs sequence is as in Table 3.2.

Table 3.2: gRNAs sequence

gRNA	Sequence (5' - 3')
gRNA 1 sense	CACCGTGTTCACGTACTCCGAGCG
gRNA 1 anti-sense	AAACCGCTCGGAGTACGTGAACAC
gRNA 2 sense	CACCGAGTCCAAGACGATCAACAG
gRNA 2 anti-sense	AAACCTGTTGATCGTCTTGGACTC
gRNA 3 sense	CACCGAGTCAGGCTGAACAATGTCC
gRNA 3 anti-sense	AAACGGACATTGTTCAGCCTGACTC

Each pair of gRNA oligos was annealed in a thermal cycler (Applied Biosystems, USA) at 95 °C for 5 minutes, 90 °C for 5 minutes, 85 °C for 5 minutes, 80 °C for 5 minutes, 75 °C for 5 minutes, 70 °C for 5 minutes, 65 °C for 5 minutes and 60 °C for 20 minutes. Each annealing reaction consisted of 1.5 µl of 100 µM gRNA oligo (sense), 1.5 µl of 100 µM gRNA oligo (anti-sense), 1.0 µl of 10 X PCR buffer and 6.0 µl of nuclease-free water.

3.2.2.5 Ligation of gRNA oligos and PX458 plasmid

Each pair of annealed gRNA oligos was ligated into *Bbs*I-digested PX458 plasmid. The ligation reaction consisted of 4.0 µl annealed gRNA oligo (100 µM), 1.0 µl of *Bbs*I-digested PX458 plasmid, 1.0 µl of 10 X ligation buffer, 1.0 µl of T4 DNA ligase (Thermo Scientific, USA) and 3.0 µl of nuclease-free water. The ligation mix was incubated at room temperature for 10 minutes.

3.2.2.6 Transformation of ligation products into competent cells

Each ligation product was added to 100 µl of competent cells prepared in section 3.2.2.1, followed by incubation on ice for 30 minutes. The cells underwent heat shock at 42 °C for 90 seconds and were then chilled immediately on ice for 3 minutes. The competent cells were recovered in LB broth and incubated in a shaking incubator (IKA, Germany) at 37 °C for 1 hour. After recovery, the cells were spread on an LB agar plate containing Ampicillin (100 µg/ml) and incubated at 37 °C overnight. The following day, colonies were picked and inoculated into 1 ml of LB broth with Ampicillin (100 µg/ml), then incubated at 37 °C for 3 hours. After the incubation, 500 µl of the culture was harvested and sent to a service provider (Beijing Genomics Institute, China) for Sanger sequencing to verify the gRNA sequence in the PX458 plasmid. Once verification was completed, 100 µl of the culture was inoculated into 100 ml of LB broth with Ampicillin (100 µg/ml) and incubated at 37 °C overnight.

3.2.2.7 Extraction of PX458 plasmids

Plasmids were extracted from overnight culture using Nucleobond Xtra Midi Plus (Macherey-Nagel, Germany) following the manufacturer's protocol. Briefly, 100 ml culture was centrifuged at 6,000 x g for 10 minutes at 4 °C to pellet the cells. After centrifugation, the supernatant was completely discarded. The cell pellet was completely resuspended in 8 ml resuspension buffer and RNase A by vortexing the cells. Then, 8 ml lysis buffer was added to the suspension and mixed gently by inverting the tube 5 times. The mixture was incubated at room temperature for 5 minutes. Meanwhile, a NucleoBond Xtra

Column together with the inserted column filter were equilibrated with 12 ml equilibrium buffer. After 5 minutes of incubation, 8 ml neutralisation buffer was added to the suspension, and the lysate was mixed immediately by inverting the tube until the blue sample turned colourless completely. The lysate was applied to the equilibrated NucleoBond Xtra Column Filter. Next, the NucleoBond Xtra Column Filter and NucleoBond Xtra Column were washed with 5 ml equilibrium buffer. After washing, the NucleoBond Xtra Column Filter was pulled out and discarded. The NucleoBond Xtra Column was washed with 8 ml wash buffer, and the plasmid was eluted with 5 ml elution buffer. After elution, 3.5 ml room temperature isopropanol (Merck, USA) was added, and the mixture was vortexed and incubated for 2 minutes. Meanwhile, the plunger was removed from the 30 ml syringe, and NucleoBond Finaliser was attached to the syringe outlet. The precipitation mixture was added to the syringe, and the plunger was inserted. Holding the syringe vertically, the mixture was slowly pressed through the NucleoBond Finaliser, discarding the flow-through. The NucleoBond Finaliser was removed from the syringe, and the plunger was pulled out before reattaching the NucleoBond Finaliser. Then, 2 ml 70% (v/v) ethanol (Merck, USA) was added to the syringe, and, after inserting the plunger, the ethanol was pressed through the NucleoBond Finaliser slowly, discarding the flow-through. Air was pressed through the NucleoBond Finaliser as strongly as possible while touching a tissue with the tip of the NucleoBond Finaliser to soak up ethanol. This step was repeated until no ethanol leaked from the NucleoBond Finaliser. Then, the NucleoBond Finaliser was removed, and a 1 ml syringe plunger was pulled out before attaching the NucleoBond Finaliser to it. Next, 200 µl of nuclease-free water was pipetted into the syringe. The outlet of the NucleoBond

Finaliser was positioned vertically over a 1.5 ml microcentrifuge tube, and the plasmid was eluted slowly drop by drop by inserting the plunger. The first eluate was transferred back into the syringe and eluted into the same microcentrifuge tube a second time. The NucleoBond Finaliser was removed from the syringe, the plunger was pulled out to aspirate air, the NucleoBond Finaliser was reattached, and air was pressed out again to force out as much eluate as possible. Finally, the plasmid yield was determined using Nano Quant Plate on a microplate reader (Tecan, Switzerland), and plasmid integrity was confirmed by agarose gel electrophoresis. The extracted plasmid was kept in a -20 °C freezer until further use.

3.3 Electroporation of SH-SY5Y cells

3.3.1 Optimisation of electroporation protocol

The electroporation protocol has been optimised to determine the most effective parameters for SH-SY5Y cells. This optimisation is essential for achieving efficient genome editing while maintaining high cell viability. The Neon Transfection System (Thermo Fisher Scientific, USA) was utilised to electroporate the SH-SY5Y cells. Detailed optimisation parameters are provided in Table 3.3.

Table 3.3: Electroporation optimisation parameters

Sample	Well number	Pulse voltage (V)	Pulse width (ms)	Pulse number
1	A1	None (Control without electroporation)		
2	A2	1400	20	1
3	A3	1500	20	1
4	A4	1600	20	1
5	A5	1700	20	1
6	A6	1100	30	1
7	B1	1200	30	1
8	B2	1300	30	1
9	B3	1400	30	1
10	B4	1000	40	1
11	B5	1100	40	1
12	B6	1200	40	1
13	C1	1100	20	2
14	C2	1200	20	2
15	C3	1300	20	2
16	C4	1400	20	2
17	C5	850	30	2
18	C6	950	30	2
19	D1	1050	30	2
20	D2	1150	30	2
21	D3	1300	10	3
22	D4	1400	10	3
23	D5	1500	10	3
24	D6	1600	10	3

The cells were electroporated using the reagents and consumables provided in the Neon™ Transfection System 10 µl Kit and the Neon Transfection System (Thermo Fisher Scientific, USA), following the manufacturer's protocol. PX458

plasmids without gRNA were used for this optimisation. After electroporation, the cells were cultured in a CO_2 incubator for 72 hours to allow for recovery. After 72 hours of recovery, cells were observed under a fluorescence microscope with a FITC filter (Carl Zeiss, Germany), and images were captured for each well. Electroporation efficiency was evaluated based on the intensity of green fluorescence protein (GFP), while cell viability was assessed based on cell morphology. The optimal electroporation parameters for SH-SY5Y cells were identified. The optimal electroporation parameters for SH-SY5Y cells are 1400 V, 20 milliseconds, and 1 pulse.

3.3.2 Electroporation of PX458 plasmids into SH-SY5Y cells

To electroporate a larger number of cells, the Neon™ Transfection System 100 µl Kit was used instead of the 10 µl Kit. SH-SY5Y cells were electroporated using a Neon Transfection System according to the manufacturer's protocol (Thermo Fisher Scientific, USA). Briefly, SH-SY5Y cells were detached using trypsin-EDTA (Gibco, UK). After neutralisation, 10 µl of the cell suspension was used for cell counting with an automated cell counter (Thermo Fisher Scientific, USA) to determine cell density. Next, 500,000 cells per reaction were transferred to a 1.5 ml microcentrifuge tube, washed with 1 X PBS, and centrifuged at 300 x g for 5 minutes. Following centrifugation, the 1 X PBS was discarded and the cell pellet was resuspended in Resuspension Buffer R at a final density of 1.0 X 10^7 cells per ml. The cells were gently pipetted to obtain a single-cell suspension. A six-well plate was prepared by filling each well with 2 ml of culture media and pre-incubated in a CO_2 incubator. A Neon Tube was prepared with 3 ml of Buffer

E2, and the pulse conditions (1400 V, 20 milliseconds, 1 pulse) were set on the Neon transfection device. Each transfection reaction for LRRK2 knockout consisted of PX458-gRNA1 (6.67 μg), PX458-gRNA2 (6.67 μg) and PX458-gRNA3 (6.67 μg). A mock reaction with 20 μg PX458 (without gRNA) was also prepared as a negative control for genome editing. The plasmids were transferred to their respective 1.5 ml microcentrifuge tubes, and then the cells were added to the tubes containing the plasmids and gently mixed. A Neon Tip was fitted onto the Neon Pipette. The cells-plasmids mixture was aspirated into the Neon Tip using the Neon Pipette. The Neon Pipette with the sample was inserted into the Neon Tube placed in the Neon Pipette Station. The "Start" button on the Neon transfection device was pressed to deliver the electric pulse to the cells. After the electroporation, the Neon Pipette was removed from the Neon Pipette Station, and the sample in the Neon Tip was transferred into a prepared culture plate containing the pre-warmed media. The plate was gently rocked to ensure an even distribution of cells. Finally, the plate containing transfected cells was incubated in a CO_2 incubator for 72 hours to allow cell recovery.

3.4 Fluorescence-activated cell sorting (FACS)

Based on our observations, SH-SY5Y cells have considerable difficulty proliferating from a single cell. To maximise clone yield, both bulk sorting (sorting 100 or 200 cells into a 15 ml conical tube) and single-cell sorting (sorting individual cells into each well of a 96-well plate) were employed.

After 72 hours of recovery in a 6-well plate, the electroporated cells were brought to a cell sorting facility for FACS. The cells were harvested using

Accutase (Merck, USA) and subsequently washed with 1X PBS, followed by centrifugation at 300 x g for 5 minutes. After centrifugation, the supernatant was removed, and the cell pellet was resuspended in 1X sorting buffer, which consisted of 1X Hanks' balanced salt solution (HBSS) (Gibco, USA), 2% (v/v) FBS (Tico Europe, Netherlands) and 10 mM N-2-hydroxyethylpiperazine-N-ethanesulfonic acid (HEPES) (Sigma Aldrich, USA). The 1X sorting buffer was filtered through a 0.22 μm syringe filter before use. Cell counting was performed using an automated cell counter (Thermo Fisher Scientific, USA). The cells were then stained with 2 μg/ml propidium iodide (PI) (BD Biosciences, USA) for 10 minutes in the dark. PI was used to differentiate live cells from dead cells during sorting. Following staining, the cells were filtered through 40 μm cell strainers (BD Biosciences, USA) to obtain a single-cell suspension and transferred to 5 ml polypropylene round-bottom tubes (BD Biosciences, USA). Subsequently, the cells were sorted using the BD FACS Aria SORP cell sorter (BD Biosciences, USA) into a 96-well plate (one cell per well) and a 15 ml conical tube (100 or 200 cells per tube). An autoclaved and filtered 1X PBS solution (Biowest, USA) was used as the sheath buffer. The PI-negative and GFP-positive cells were collected. After sorting, the 96-well plate was transferred to a CO_2 incubator, while the 100 or 200 cells from the 15 ml conical tube were transferred to a 10 cm cell culture dish containing supplemented media and returned to the CO_2 incubator.

3.5 Cultivation and expansion of clones

3.5.1 Clones from bulk sorting

When the clones grew to an appropriate size, they were harvested from the 96-well plate using 0.25% (w/v) trypsin-EDTA (Gibco, USA) and transferred to a 24-well plate. The clones were then expanded by plating them into progressively larger vessels until there were sufficient cells for downstream assays.

3.5.2 Clones from single-cell sorting

When the clones grew to a reasonable size, they were isolated using the single-cell isolation technique (filter paper method) as described by Yuen *et al.* (Yuen *et al.*, 2017). The filter paper was punched using a paper puncher and autoclaved before use. Briefly, 0.25% (w/v) trypsin-EDTA (Gibco, USA) was pre-warmed, and the cells were washed once with 1X PBS. The trypsin-EDTA was applied to a filter paper, which was allowed to soak for 1 minute. Using sterile forceps, the filter paper was placed onto a clone, and the dish containing the clones was incubated at 37 °C for 1 minute. After incubation, the filter paper was removed with sterile forceps and placed into a 6-well plate pre-filled with medium. The filter paper was gently shaken in the medium to allow the cells to detach into the well. The plate containing the cells was then returned to the CO_2 incubator. The clones were subsequently expanded by plating them into progressively larger vessels until there were sufficient cells for downstream assays.

3.6 Verification of LRRK2 knockout

3.6.1 Extraction of total genomic DNA

Total genomic DNA was extracted using a Wizard Genomic DNA Extraction Kit (Promega, USA) according to the manufacturer's protocol. Briefly, cells were washed twice with 1X PBS and harvested by trypsinisation. Nuclei lysis solution (600 µl) was added to the cell pellets and mixed by pipetting. RNase solution (300 µl) was added to the cell lysates, mixed and incubated at 37 °C for 30 minutes. After cooling the cell lysates to room temperature, 200 µl protein precipitation solution was added. The cell lysates were vortexed, chilled on ice for 5 minutes and centrifuged at 16000 x g for 4 minutes. Following centrifugation, the supernatants were transferred to fresh 1.5 ml microcentrifuge tubes containing 600 µl isopropanol (Merck, USA) and gently mixed by inversion. The mixtures were centrifuged at 16000 x g for 1 minute. The supernatants were removed, and 600 µl of 70% (v/v) ethanol (Merck, USA) was added and mixed. The mixtures were centrifuged at 16000 x g for 1 minute. After centrifugation, the ethanol was aspirated, and the pellets were air-dried for 15 minutes. The DNA was rehydrated in 100 µl DNA rehydration solution for 10 minutes at room temperature. DNA concentration and purity were determined using Nano Quant Plate on a microplate reader (Tecan, Switzerland) and the DNA was stored at -20 °C until further use.

3.6.2 PCR

A pair of primers flanking the target site was used in the PCR:

pLKO_F: 5'-CTGAGCAGCGGACGTTCAT- 3'

pLKO_R: 5'-CTCTTCATCCCGTTTACATTGCG-3'

Each PCR reaction consisted of 12.5 µl of GoTaq Hot Start Master Mix (Promega, USA), 1.25 µl of 10 µM forward and reverse primer, 1 µl (100 ng) of DNA template and 9 µl nuclease-free water, for a final volume of 25 µl. The PCR reaction mix was mixed gently and centrifuged to bring the solution to the bottom of the tube. Subsequently, the PCR was performed on a Veriti 96-well thermal cycler (Thermo Fisher Scientific, USA) using the following cycling parameters: 95 °C for 2 minutes; 35 cycles of 95 °C for 15 seconds, 59.3 °C for 30 seconds and 72 °C for 1 minute; 72 °C for 5 minutes.

Based on the PCR verification, three representative LRRK2 knockout clones (designated LKO1, LKO2, and LKO3 hereafter) were selected for further validation.

3.6.3 TA cloning

TA cloning was performed using the pGEM-T Vector System (Promega, USA) following the manufacturer's protocol. Briefly, the ligation reactions were prepared and incubated at room temperature for 1 hour. Each ligation reaction consisted of 5 µl of 2 X ligation buffer, 1 µl of p-GEM T-Vector (50 ng), 1 µl of PCR product, 1 µl of T4 DNA ligase (3 Weiss unit) and 2 µl nuclease-free water. Then, 20 µl of isopropyl-β-d-thiogalactopyranoside (IPTG) (Biosynth

Carbosynth, UK) and 100 µl of 5-bromo-4-chloro-3-indolyl-beta-D-galacto-pyranoside (X-gal) were spread on an LB agar plate with Ampicillin (100 µg/ml). After 1 hour of incubation, the ligation products were added to 100 µl competent cells prepared in Section 3.2.2.1. The transformation was performed as in Section 3.2.2.6. After overnight incubation, the white colonies were picked from the plates, inoculated in 5 ml LB broth with Ampicillin (100 µg/ml) and cultured overnight.

3.6.4 Extraction of plasmids

The plasmids were extracted from 5 ml culture using FavorPrep™ Plasmid DNA Extraction Mini Kit (Favorgen, Taiwan), following the manufacturer's protocol. Briefly, the bacterial cultures were centrifuged at 11000 x g for 1 minute. The supernatants were completely discarded by aspiration. Then, 250 µl of FADP1 Buffer with RNase A was added to the cell pellets. The cells were completely resuspended by pipetting. Subsequently, 250 µl FADP2 Buffer was added, and the tubes were inverted 10 times. The mixtures were incubated at room temperature for 2 to 5 minutes. FADP3 Buffer (350 µl) was added, and the tubes were inverted 10 times immediately and centrifuged at 16000 x g for 10 minutes. Subsequently, the supernatants were transferred to the FADP columns and centrifuged at 11000 x g for 1 minute. The flow-through was discarded, and the columns were returned to the collection tubes. W1 Buffer (400 µl) was added to the FADP columns and centrifuged at 11000 x g for 30 seconds. The flow-through was discarded, and the columns were returned to the collection tubes. Wash Buffer (700 µl) was added to the FADP columns and centrifuged at 11000

x g for 30 seconds. The flow-through was discarded, and the columns were returned to the collection tubes. The FADP columns were centrifuged for an additional 3 minutes at 16000 x g. Then, the FADP columns were placed in 1.5 ml microcentrifuge tubes. Elution Buffer (50 µl) was added to the FADP columns and incubated for 1 minute. Finally, the FADP columns were centrifuged at 16000 x g for 1 minute to elute the plasmids. The plasmids were stored at -20 °C.

3.6.5 Sanger sequencing

The plasmids were sent to a service provider (Apical Pvt. Ltd., Malaysia) for Sanger sequencing. The primers for sequencing are listed in Section 3.6.2. Sanger sequencing results were analysed using Molecular Evolutionary Genetics Analysis (MEGA) software version 5.2. MEGA is an integrated tool for conducting sequence alignment. Manual alignments of sequences from wildtype and knockout clones were performed.

3.6.6 Extraction of protein lysates

Protein lysates were extracted from cells using NE-PER Nuclear and Cytoplasmic Extraction Reagents (Thermo Fisher Scientific, USA) with a protease inhibitor cocktail (Nacalai Tesque, Japan) following the manufacturer's instructions. Briefly, cells were harvested with Trypsin-EDTA (Gibco, UK) and washed with 1X PBS. After washing, the supernatants were aspirated to leave the cell pellets as dry as possible. Ice-cold CER I (260 µl) was added to the cell pellets in 1.5 ml microcentrifuge tubes. The tubes were mixed

vigorously at the highest setting for 15 seconds to fully resuspend the pellets, then incubated on ice for 30 minutes. Next, 14.3 µl of ice-cold CER II was added, and the tubes were mixed vigorously for another 15 seconds before being incubated on ice for 5 minutes. Following incubation, the tubes were centrifuged at 15,000 x g for 15 minutes. After centrifugation, the supernatants were discarded, and 130 µl of NER was added to the insoluble fractions (pellets). The tubes were mixed vigorously for 15 seconds and then incubated on ice, vortexing for 15 seconds every 10 minutes for a total of 40 minutes. After this incubation, the tubes were centrifuged again at 15,000 x g for 15 minutes. The supernatants were transferred to clean, pre-chilled 1.5 ml microcentrifuge tubes. The concentration of the protein lysates was quantified using Pierce 660 nm Protein Assay Reagent (Thermo Fisher Scientific, USA). After quantification, the protein lysates were stored at -20 °C.

3.6.7 Western blot

Twenty micrograms of each protein lysate, along with the ExcelBand™ 3-colour extra range protein marker (SMOBIO, Taiwan), were loaded onto a 4-20% (w/v) Tris-Glycine gel. The gel was run in 1X Tris-Glycine-Sodium Dodecyl Sulfate (TG-SDS) buffer (1st BASE, Singapore) using a vertical polyacrylamide gel electrophoresis system (Bio-Rad, USA) at 20 mA for 3 hours. Proteins were then transferred from the gel to a polyvinylidene fluoride (PVDF) membrane (Merck, USA) in 1X Tris-Glycine (TG) buffer (1st BASE, Singapore) using a wet transfer system (Bio-Rad, USA) at 30 V overnight at 4°C. After an overnight transfer, the sandwich was disassembled, and the ExcelBand™ marker was examined to

confirm complete transfer to the membrane. To verify the complete transfer of the large LRRK2 protein without over-transferring the smaller GAPDH protein, the membrane was stained with Ponceau S, while the gel was stained with Coomassie Blue. The presence of protein bands on the Coomassie Blue-stained gel indicates an incomplete transfer from the gel to the membrane. Conversely, the absence or minimal visibility of protein bands on the Ponceau S-stained membrane suggests either under-transfer or over-transfer of proteins. After this verification, the membrane was placed in a clean container and incubated with 5% (w/v) bovine serum albumin (BSA) (Merck, USA) in 1X Tris-Buffered Saline (1X TBST) at room temperature for 1 hour. Following this incubation, the membrane was cut and incubated with primary antibodies, i.e. anti-LRRK2 and anti-GAPDH antibodies (Abcam, UK) in separate containers overnight at 4°C with rocking. After overnight incubation, the primary antibody solutions were removed, and the membrane was washed three times with 1X TBST for 5 minutes each. The membrane was then incubated with goat anti-rabbit IgG (H+L) secondary antibody, HRP conjugate (Thermo Fisher Scientific, USA), at room temperature for 1.5 hours. After incubation, the secondary antibody solution was removed, and the membrane was washed three more times with 1X TBST for 5 minutes each. Finally, the membrane was incubated with WesternBright Sirius chemiluminescent HRP substrate (Advansta, USA) for 2 minutes, and images were captured using the Azure 600 Gel Imaging System (Azure, USA). Image capture parameters are detailed in Table 3.4.

Table 3.4: Image acquisition parameters for Western blot membranes using the Azure 600 Gel Imaging System

Parameter	Input
Protocol type	Chemi blot
Capture type	Manually image
Pixel binning	3 X 3
Exposure type	Manual
Channel name	Chemiluminescence
Imaging mode	Cumulative
Exposure interval	30 seconds
Maximum number of images	50
Light source	ECL
Filter	No filter
Aperture	Maximum
Tray type	Top shelf

3.7 Verification of gRNAs off-targets

Off-target effects are defined as unintended cleavages or genetic modifications at sites with sequences that are similar, but not identical, to the target site (Modrzejewski *et al.*, 2019). In this study, off-target prediction was performed using CHOPCHOP. According to CHOPCHOP, gRNA1 does not have any off-targets while gRNA2 and gRNA3 have 2 and 6 off-targets, respectively. PCR and Sanger sequencing were performed to evaluate the off-targets. gRNA2 and gRNA3 potential off-target locations, number of mismatches, sequences (as predicted by CHOPCHOP) and primers designed for validation, and the annealing temperature are detailed in Table 3.5.

3.7.1 Extraction of total genomic DNA

Total genomic DNA was extracted from the cells using the protocol outlined in Section 3.6.1.

3.7.2 PCR

Each PCR reaction consisted of 10 µl of 2 X Phusion High Fidelity PCR master mix (Thermo Fisher Scientific, USA), 2 µl of forward and reverse primers (10 µM), 1 µl of DNA template (100 ng) and 5 µl nuclease-free water, for a final volume of 20 µl. The PCR reaction mix was mixed gently and centrifuged to bring the solution to the bottom of the tube. Subsequently, the PCR was performed on a Veriti 96-well thermal cycler (Thermo Fisher Scientific, USA) using the following cycling parameters: 98 °C for 30 seconds; 35 cycles of 98 °C for 10 seconds, “xx” °C for 30 seconds and 72 °C for 30 seconds; 72 °C for 10 minutes. “xx” is the annealing temperature for each pair of primers, as indicated in Table 3.5.

Table 3.5: gRNA2 and gRNA3 potential off-target locations (No.1 and No. 2 to No.7, respectively), number of mismatches, sequences (as predicted by CHOPCHOP) and primers designed for validation, and the annealing temperature

No.	Location	Number of mismatches	Sequence (including mismatches*)	Primers	Annealing temperature (°C)
1	chr10:124442476	3	aAGaCCAAGACGAcCAACAGAGG	F: GATGTCAAGGCTGCAGTGAG R: GTTCACTCCCTTCTCCCCTC	63.0
2	chr10:75876195	3	AGTCAGcCTGAAgAgTGTCCTGG	F: CCTGACTGGGGAACACTGAT R: CCAAGGGAGAACTTCAAGAGCT	64.5
3	chr13:89431766	3	AGTgAaGCTGAACAATGTCtAGG	F: GCCAAAATACCAGCAACCTCA R: ACATAGTTGCCTCCTAGCCA	64.7
4	chr4:73126296	3	AGTCAGGCTGAAtAATacCCAGG	F: AGGCAGTGCAGAAGAGTGAT R: CACAACTGCTAATTTGGCCCT	64.3
5	chr4:83762058	3	CCAGGACATTGcTCAGCCTcACc	F: CAGGGTGCGCACATAAAGAC R: GCTGTGGCCATTTCTGAGCA	64.5
6	chr6:154976916	3	CCAcGAtATTGcTCAGCCTGACT	F: ACTCCAGTTACATGCCCAGC R: CTAAGACCACAGGCCAGACG	71.1
7	chr9:27216984	3	AGTCAaGCTttACAATGTCCAGG	F: CCCTCAAGTGCTCCTGGTTT R: CACGCATGGTAGTCGGTCAT	65.1

Note: * Mismatches are in lowercase.

3.7.3 Sanger sequencing

The PCR products were sent to a service provider (Apical Pvt. Ltd.) for Sanger sequencing. The primers for sequencing are listed in Table 3.5. Sanger sequencing results were analysed using Molecular Evolutionary Genetics Analysis (MEGA) software version 5.2. Manual alignments of sequences from the wildtype and knockout clones were performed.

3.8 Mycoplasma detection

Mycoplasma detection was performed using e-Myco Mycoplasma PCR Detection Kit (iNtRON Biotechnology, Korea) according to the manufacturer's protocol.

3.8.1 Preparation of samples

Briefly, the cells were harvested and counted using an automated cell counter (Thermo Fisher Scientific, USA). Aliquots of the cell suspension (50,000 cells per tube) were transferred to 1.5 ml microcentrifuge tubes and centrifuged at 300 x g for 5 minutes. The supernatants were carefully decanted, and the cells were resuspended in 1 ml of 1X PBS for washing, followed by centrifugation at 300 x g for 5 minutes. After centrifugation, the supernatants were discarded, and the cell pellets were resuspended in 100 µl of 1X PBS and heated at 95 °C for 10 minutes. The samples were then vortexed for 10 seconds and centrifuged at 12,000 x g for 2 minutes. The supernatants were transferred to new 1.5 ml microcentrifuge tubes, where they were used as templates for PCR.

3.8.2 PCR

An appropriate number of e-Myco™ Mycoplasma PCR Premix Tubes were prepared, including both positive and negative control tubes. Nuclease-free water (10 µl) was added to the RT-PCR premix tubes, followed by the addition of 10 µl DNA samples to each tube. For the control tubes, 1 µl of the positive control (provided in the kit) and nuclease-free water were added to the positive and negative control tubes, respectively. The blue pellets were dissolved by pipetting. PCR was performed on a Veriti 96-well thermal cycler (Thermo Fisher Scientific, USA) using the following cycling parameters: 94 °C for 1 minute; 35 cycles of 94 °C for 30 seconds, 60 °C for 20 seconds, and 72 °C for 1 minute; followed by a final extension at 72 °C for 5 minutes. The PCR products were run on a 2% (w/v) agarose gel, and the gel images were captured using the UVP Gel Imaging System (Analytik Jena, Germany).

3.9 Evaluation of phenotypic changes in LRRK2 knockout cells

Phenotypic changes of wild-type (WT), mock, LKO1, LKO2 and LKO3 cells were evaluated using the following assays:

i. Examination of morphological changes
ii. Measurement of cell size
iii. Evaluation of cell-substrate adhesion strength
iv. Assessment of growth kinetics
v. Senescence-associated β-galactosidase (SA-β-gal) staining
vi. Autophagy detection assay
vii. Assessment of mitochondrial respiration

3.9.1 Examination of morphological changes

Cell morphological changes were monitored and evaluated in every subculture. Images of cells were captured using the Invitrogen EVOS Cell Imaging System (Thermo Fisher Scientific, USA) at 400 X magnification. The cell morphological changes were then examined and recorded.

3.9.2 Measurement of cell size

Cell size was measured using the Invitrogen Countess II automated cell counter (Thermo Fisher Scientific, USA). The cell size changes were then evaluated and recorded.

3.9.3 Qualitative evaluation of cell-substrate adhesion strength

Cells were washed twice with 1X phosphate-buffered saline. The cell-substrate adhesion strength was qualitatively assessed by estimating the number of cells that remained adhered to the vessels. Dislodged cells were collected and combined with adherent cells, which were harvested using 0.25% (w/v) trypsin-EDTA (Gibco, USA) and subsequently returned to the cell culture vessels for further culture. Adhesion strength was categorised as follows: high adhesion was assigned when more than 80% of the cells remained attached after washing; medium indicated 50-80% cell retention; and low corresponded to fewer than 50% of cells remaining adherent.

3.9.4 Assessment of growth kinetics

Cell number was determined at the end of every passage (for 5 consecutive passages) using the Invitrogen Countess II automated cell counter (Thermo

Fisher Scientific, USA), and cumulative population doubling was calculated in relation to the cell number from the previous passage. The number of population doubling was calculated as described in (CristofaloVolker and Allen, 2000, Kurz *et al.*, 2004) using the formula below:

Population doubling = [In (number of cells harvested)- In (number of cells seeded)] / In 2

The images of cells were captured at 100 X magnification using the Invitrogen EVOS Cell Imaging System (Thermo Fisher Scientific, USA).

3.9.5 Senescence-associated β-galactosidase (SA-β-gal) staining

The cells were stained using the SA-β-gal Staining Kit (Cell Signalling Technology, USA) according to the manufacturer's instructions. Briefly, the cells were washed once with 2 ml of 1X PBS and then fixed for 15 minutes at room temperature in 1 ml of 1X fixative solution. After fixation, the cells were washed twice with 2 ml of 1X PBS. Next, 1 ml of freshly prepared staining solution was added to the wells, and the plate was sealed with parafilm to prevent evaporation, as evaporation can lead to crystal formation. The plate was incubated overnight at 37°C. The following morning, while the staining solution was still present, the cells were examined under a brightfield inverted microscope at 200 X magnification for the development of blue colouration. Then, the staining solution was removed, and the cells were washed with 1 ml of 1X PBS. An additional 1 ml of 1X PBS was added to the wells. Images of the cells were captured at 200 X magnification using the Invitrogen EVOS Cell Imaging System (Thermo Fisher Scientific, USA). The percentage of blue-stained cells

(SA-β-gal positive) relative to the total number of cells was determined by randomly selecting 10 microscopic fields for counting.

3.9.6 Autophagy detection assay

Autophagy detection was performed using the CYTO-ID Autophagy Detection Kit 2.0 (Enzo Life Sciences, USA) according to the manufacturer's protocol. Chloroquine, an anti-inflammatory drug used to treat or prevent malaria, was included in the assay as a positive control. Chloroquine suppresses inflammation by increasing lysosomal pH, which in turn inhibits lysosomal activity. Autophagy is a dynamic process where the accumulation of autophagosomes can either reflect increased autophagosome generation or a blocked conversion to autolysosomes. In this assay, chloroquine served to block the clearance of autophagosomes, thereby promoting their accumulation.

The cells were seeded in a 96-well plate at a density of 50,000 cells per well and cultured overnight. Following the overnight incubation, the cells were washed twice with 100 µl of 1X assay buffer. Next, 100 µl of dual-colour detection solution was added to the cells, and the plate was incubated in the dark at 37°C for 30 minutes. Following incubation, the cells were washed with 100 µl of 1X assay buffer, and fluorescence was measured at 480 nm excitation and 530 nm emission using a microplate reader (Tecan Spark, Switzerland). For nuclear staining, fluorescence was measured at 340 nm excitation and 480 nm emission. The increase in the green autophagy signal, normalised to the blue signal, reflects the accumulation of the probe within the cells, which results from the increase in autophagic vacuoles.

3.9.7 Assessment of mitochondrial respiration

Mitochondrial respiration in the cells was assessed by measuring the oxygen consumption rate (OCR) and extracellular acidification rate (ECAR) using the real-time cell metabolic analyser, the Seahorse XF HS Mini Analyser (Agilent, USA). The Seahorse XFp Cell Mito Stress Test Kit (Agilent, USA) was used according to the manufacturer's protocol.

3.9.7.1 Optimisation of cell seeding density

Cell seeding density is a critical parameter that must be empirically determined prior to assessing mitochondrial respiration. It is essential to first establish the basal respiration rates of the cells and ensure that the chosen seeding density yields OCR and ECAR values within the dynamic range of the instrument. The optimal seeding density varies by cell type, but generally, a density achieving 50 to 90 % confluency produces metabolic rates within the desired range. In this study, cell densities of 50,000, 100,000, 150,000, and 200,000 cells per well were tested, with optimisation performed according to the manufacturer's protocol.

The day before the assay, cells were seeded onto the Seahorse Poly-D-Lysine (PDL)-coated cell culture mini plate (Agilent, USA) and cultured overnight. The Seahorse XFp sensor cartridges (Agilent, USA) were hydrated with sterile water, and the Seahorse XF HS Mini Analyser was turned on and allowed to warm up overnight for a minimum of five hours. An aliquot of XF calibrant was pre-warmed in a non-CO_2 incubator at 37 °C overnight.

On the day of the assay, the assay medium was prepared by supplementing Seahorse XF DMEM with 1 mM pyruvate, 2 mM glutamine, and 10 mM glucose. The water in the Seahorse XFp sensor cartridges was replaced with a pre-

warmed XF calibrant, and the cells were washed with the assay medium. Both the Seahorse XFp sensor cartridges and the plates containing the washed cells were placed in a 37°C, non-CO_2 incubator for 45 minutes prior to the assay. Meanwhile, an assay template was designed on the Seahorse XF HS Mini analyser. The stock and working solutions of oligomycin (ATP synthase/ Complex V inhibitor), carbonyl cyanide-4 (trifluoromethoxy) phenylhydrazone (FCCP; uncoupling agent), and a mixture of rotenone (Rot; Complex I inhibitor) and antimycin A (AA; Complex III inhibitor) were prepared.

At the end of the 45-minute incubation, the working solutions of the compounds were loaded into the injection ports on the Seahorse XFp sensor cartridges. The Seahorse XFp sensor cartridges were then calibrated on the Seahorse XF HS Mini analyser. Before running the assay, the cells were washed again with the assay medium. After washing, the assay was initiated by loading the plates onto the Seahorse XF HS Mini analyser. Baseline measurement of OCR and ECAR was performed, followed by successive injections of 1.5 µM oligomycin, 1.0 µM FCCP and 0.5 µM Rot/ AA. At the end of the run, the data acquired were exported from the Seahorse XF HS Mini analyser.

To account for the differing proliferation rates among WT, mock and LKO1 cells, data were normalised to total protein content. Following completion of the assay, cells in each well were lysed using a lysis buffer [consisting of 10 mM Tris buffer and 0.1% (v/v) Triton X-100]. Total protein content was measured using the Pierce™ Bradford Plus Protein Assay Kit (Cat. No. 23236, Thermo Fisher Scientific, Waltham, MA, USA), following the manufacturer's instructions. Briefly, the media was removed from each well, and 20 µl of lysis buffer was added to each well, followed by incubation for 3 minutes at room temperature.

Subsequently, 130 µl of Bradford Plus Reagent was added to each well and mixed on a plate shaker (Cole-Parmer, USA) at 800 rpm for 30 seconds. The plate was then incubated at room temperature for 10 minutes. After incubation, the absorbance at 595 nm was measured using a microplate reader (Tecan Spark, Switzerland).

For the standard curve, BSA standards were prepared in concentrations of 0, 25, 125, 250, 500, 750, 1000, 1500, and 2000 µg/ml by diluting the BSA supplied with the kit. Twenty µl of each diluted BSA standard was added to a 96-well plate, followed by the addition of 130 µl of Bradford Plus Reagent. The plate was mixed on a shaker (Cole-Parmer, USA) at 800 rpm for 30 seconds and incubated at room temperature for 10 minutes. Absorbance at 595 nm was measured, and a standard curve was generated by plotting the average blank-corrected absorbance for each BSA concentration. The protein concentration of each sample was determined by comparing the measured absorbance to the standard curve.

The data exported from the Seahorse XF HS Mini analyser were normalised to total protein concentration. The normalised data were then imported into Agilent Seahorse Analytics (Agilent, USA), a web-based software, for analysis. Using the manufacturer's calculation matrix, the software was used to evaluate various parameters, including mitochondrial respiration, spare respiratory capacity, basal respiration, maximal respiration, proton leak, non-mitochondrial oxygen consumption, ATP-linked respiration, coupling efficiency percentage, and extracellular acidification rate. Additionally, an energy map was generated to visualise the OCR and ECAR.

3.9.7.2 Optimisation of FCCP concentration

The optimal final concentrations of oligomycin, FCCP and Rot/AA for achieving maximal effects are cell line-dependent and may be influenced by the type of assay medium used. Therefore, a titration experiment for each new cell line or assay medium is recommended. This is particularly important for FCCP, as its titration curve is often sharp, and excessive FCCP can diminish OCR responses. During the optimisation of cell seeding density, FCCP was unable to stimulate OCR. However, oligomycin effectively reduced OCR, while Rot/AA completely abolished it. Based on these findings, the FCCP concentration was subsequently optimised in this study. Four different concentrations of FCCP, i.e. 0.25 µM, 0.5 µM, 1.0 µM, and 2.0 µM, were tested. The cells were seeded on Seahorse Poly-D-Lysine (PDL) coated cell culture mini plates (Agilent, USA) at a density of 125,000 cells/ well and cultured overnight. The assay was performed as described in section 3.9.7.1 for the optimisation of the FCCP concentration.

3.9.7.3 Bioenergetic profiling

Briefly, cells were seeded onto Seahorse Poly-D-Lysine (PDL)-coated cell culture mini plates (Agilent, USA) at a density of 125,000 cells per well and cultured overnight. Based on the optimisation conducted in section 3.9.7.2, the optimal FCCP concentration was determined to be 2.0 µM. Therefore, 2.0 µM FCCP was used for bioenergetic profiling. The assay was performed as described in section 3.9.7.1 for bioenergetic profiling of WT, mock, and LKO1 cells.

3.10 Preparation of EBN extracts

A local EBN distributor, Royal Bird Nest Pte Ltd, generously supplied raw EBN. The finely ground raw EBN was added to distilled water at a concentration of 0.2 % (w/v) and allowed to elute for 24 hours at 4 °C.

3.10.1 Acid extract

Following elution, 0.4 M sulphuric acid (Merck, Germany) was added to the eluate. The mixture was heated in a water bath (Memmert, Germany) at 80 °C for 4 hours. After cooling to room temperature, the eluate was filtered through a filter paper (Advantec, USA), and the pH was adjusted to 7.0 by adding barium hydroxide (Nacalai Tesque, Japan). The resulting barium sulphate precipitate was removed by centrifugation at 3500 x g for 10 minutes. The supernatant was collected, aliquoted into freeze-dryer flasks, and pre-frozen overnight at -80 °C in a slightly sloped position. The following day, the freeze-dryer flasks were connected to a freeze dryer (LaboGene, Denmark), and the pre-frozen supernatant was freeze-dried until completely dry. The acid extract was collected, weighed, and stored at -20 °C.

3.10.2 Aqueous extract

Following elution, the eluate was heated in a water bath (Memmert, Germany) at 80 °C for 1 hour. After cooling to room temperature, it was filtered through a double-layer strainer. The supernatant was collected, freeze-dried, weighed, and stored at -20 °C.

3.10.3 Enzyme extract

Following elution, the eluate was heated in a water bath (Memmert, Germany) at 80 °C for 1 hour. After cooling to room temperature, the pancreatin enzyme (0.5 mg/ml) (Nacalai Tesque, Japan) was added, and the pH was adjusted to 8.5 - 9.0. The eluate was heated in the water bath at 45 °C for 4 hours. Subsequently, it was heated to 90 °C for 5 minutes to deactivate the pancreatin enzyme. After cooling to room temperature, the eluate was filtered through a filter paper (Advantec, USA). The supernatant was collected, freeze-dried, weighed and stored at -20 °C.

3.11 Evaluation of effects of EBN extracts

3.11.1 Antioxidant assays

3.11.1.1 DPPH free radical scavenging activity assay

Diluted EBN extracts (78, 156, 313, 625, 1250, 2500, 5000 μg/ml) and 10 mg/ml 2,2-diphenyl-1-picrylhydrazyl (DPPH) (Sigma Aldrich, USA) were prepared in methanol (Merck, USA), added to a microplate in triplicate wells and mixed. The mixtures were incubated at room temperature for 30 minutes in the dark. Fluorescence was measured at 480 nm excitation and 510 nm emission using a microplate reader (Tecan Infinite 200 Pro, Switzerland). The percentage of DPPH reduction was calculated using the following formula: [(mean fluorescence in control well - mean fluorescence in test well)/ mean fluorescence in control well] x 100.

3.11.1.2 Oxygen radical absorbance capacity (ORAC) assay

Different dilutions for EBN extract (7.8, 15.6, 31.3, 62.5, 125, 250, 500 μg/ml) and Trolox standards (3.13, 6.25, 12.5, 25, 50, 100, 200 μM) (Sigma Aldrich, USA) were prepared in phosphate buffer, immediately before measurement. Diluted extracts, Trolox standards and 125 nM fluorescein (Sigma Aldrich, USA) were added to the microplate in triplicate wells and incubated at 37°C for 30 minutes. Fluorescence was measured at 485 nm excitation and 518 nm emission every 30 seconds for 1 hour and 30 minutes using a microplate reader (Tecan Infinite 200 Pro, Switzerland). The reading from the first four cycles was used to calculate the background. Then, the oxidative reaction was triggered by adding 50 mg/ml of 2,2'-azobis (2-methylpropionamidine) dihydrochloride (AAPH) (Sigma Aldrich, USA) to the wells. The loss in fluorescence signal was expressed as the area under the curve (AUC) of the kinetic plot of extracts and Trolox standards. The AUC values were plotted against the Trolox concentrations, and a standard curve was fitted and used to interpolate the antioxidant capacity of extracts.

3.11.1.3. Dichloro-dihydro-fluorescein diacetate (DCFH-DA) assay

Intracellular ROS was measured using a DCFH-DA fluorescent probe with a protocol modified from Wolfe & Rui, 2007 (Wolfe & Rui, 2007). Briefly, cells were seeded in a 96-well plate at optimum cell density. Twenty-four hours after seeding, cells were treated with EBN extract (31.3, 62.5, 125, 250, 500 and 1000 μg/ml) or quercetin (positive control) and 50 μM DCFH-DA for 2 hours. Then, 250 μM hydrogen peroxide (Merck, USA) was added to each well. The 96-well plate was placed into a microplate reader (Tecan Infinite 200 Pro, Switzerland)

at 37°C. Fluorescence was measured at 480 nm excitation and 510 nm emission every 5 minutes for 1 hour.

3.11.2 Cell proliferation assay

The cell proliferation was evaluated using PrestoBlue Cell Viability Reagent, according to the manufacturer's protocol. Briefly, the cells were seeded in 96-well plates at optimum cell density. After 18 to 24 hours, the cells were treated with 31.3, 62.5, 125, 250, 500 and 1000 µg/ml EBN acid extract for 72 hours. Following treatment, 10 µl per well of PrestoBlue Cell Viability Reagent was added, and the cells were incubated in the dark at 37°C for 30 minutes. Fluorescence was measured at 560 nm excitation and emission at 590 nm using a microplate reader (Tecan Infinite 200 Pro, Switzerland). The percentage of viable cells was calculated using the following formula: (mean fluorescence in test wells/ mean fluorescence in control wells) x 100.

3.11.3 Autophagy detection assay

The cells were seeded in a 96-well plate at a density of 50,000 cells per well and cultured overnight. Following the overnight culture, the cells were treated for 18 hours with 10 µM chloroquine alone, 1000 µg/ml EBN acid extract alone, or a combination of 10 µM chloroquine and 1000 µg/ml EBN acid extract. An untreated well was used as the negative control. After treatment, the media were removed, and the cells were washed twice with 100 µl of 1X assay buffer. The autophagy detection assay was performed as described in section 3.9.6.

3.11.4 Assessment of mitochondrial respiration

Briefly, cells were seeded onto Seahorse Poly-D-Lysine (PDL)-coated cell culture mini plates (Agilent, USA) at a density of 125,000 cells per well and cultured overnight. Following overnight culture, the cells were treated with 1000 μg/ml EBN acid extract for 72 hours. An untreated well was used as the negative control. At the end of the treatment, the bioenergetic profiling was performed as described in section 3.9.7.1.

3.1.2 Statistical analyses

Statistical analyses were performed using GraphPad Prism software (GraphPad Software, Boston, MA, USA), and data are presented as mean ± SEM. Comparisons among multiple groups were analysed using one-way ANOVA followed by Dunnett's multiple comparison test, as experimental groups were compared against a control. Statistical significance is designated as: $p < 0.05$ (*), $p < 0.01$ (**) and $p < 0.001$ (***). Data were obtained from three independent biological experiments (n = 3), each performed with three technical replicates, unless otherwise stated.

CHAPTER 4.0

RESULTS

4.1 A strategy for low-expression *LRRK2* gene knockout using CRISPR/ Cas9

4.1.1 Double-cut and multiple gRNAs approach

Guide RNAs (gRNAs) are RNA sequences that recognise specific regions in the target genomic DNA. As the name suggests, they guide the Cas9 endonuclease to the desired target sites. To enhance editing efficiency, the double-cut approach described by Yuen *et al.* (Yuen *et al.*, 2017), in which two gRNAs are used to excise the target region instead of the conventional single gRNA method, was adopted in this study. Three gRNAs were employed to maximise the likelihood of achieving a complete knockout of the low-expression *LRRK2* gene. To attain complete abrogation of the LRRK2 protein, gRNAs targeting exon 1 and exon 2 were selected. Sequences and binding sites of gRNAs are shown in Figure 3.2 (section 3.2.1).

The double-cut approach not only improves editing efficiency but also simplifies subsequent screening. The spliced-out target region, approximately 100 bp to 400 bp in length, can be easily detected by conventional PCR. A pair of primers (pLKO_F and pLKO_R) flanking the putative target sites of gRNA 1, gRNA 2, and gRNA 3 was designed for use in PCR analysis (Figure 3.2, section 3.2.1). The amplicon length is determined by the combination of gRNAs that directs CRISPR/ Cas9 to the target site for double cutting. CRISPR/ Cas9 induces cuts 3 to 4 bp upstream of the protospacer adjacent motif (PAM) sequence, followed

by repair via non-homologous end joining (NHEJ) or homology-directed repair (HDR). The canonical PAM sequence is 5'-NGG-3', where "N" can represent any nucleotide base (A, T, G, or C), followed by two guanine (G) nucleotide bases. NHEJ is the primary pathway used to repair double-stranded breaks in DNA and typically introduces small insertions or deletions, making precise amplicon lengths difficult to predict before Sanger sequencing. The potential amplicon lengths resulting from double cuts led by either two gRNAs are summarised in Table 4.1.

Table 4.1: Estimated amplicon length resulting from double cut led by either two gRNAs

Clone	Amplicon length (bp)	gRNAs
WT	746	N/A
Mock	746	N/A
LRRK2 knockout	3xx	gRNA 2 + gRNA 3
	4xx	gRNA 1 + gRNA 2
	6xx	gRNA 1 + gRNA 3

Note:

i. N/A, not applicable
ii. "xx" indicates the approximate value (e.g. 6xx indicates approximately six hundred).

4.1.2 Optimised electroporation protocol

Delivering large plasmids into mammalian cells is widely recognised as a challenge, especially with hard-to-transfect cells like SH-SY5Y. The CRISPR/ Cas9 plasmids used in this study are particularly large, measuring 9288 bp. Since each plasmid contains a single gRNA, this study required the transfection of

three individual plasmids in a single reaction. Consequently, the initial focus was to optimise the transfection protocol. Given that chemical transfection reagents are generally less harmful to cells, Lipofectamine 3000 (Thermo Fisher Scientific, USA) and GeneJuice (Merck, USA) were first tested. However, based on our visual estimation of the percentage of GFP-expressing cells under the fluorescence microscope, neither reagent yielded a transfection efficiency greater than 1%. As a result, the electroporation method was subsequently used, despite its higher cost.

The electroporation protocol was refined meticulously, adjusting three key parameters: pulse voltage, pulse width, and pulse number (Table 3.3). Based on qualitative assessments of cell viability and GFP intensity (Figure 4.1 and Table 4.2), four promising protocols that demonstrated high GFP levels while maintaining acceptable cell viability, as seen in wells A2, A3, A4, and C3 were identified. Ultimately, the protocol that yielded the best results: 1400 V, 20 ms, and 1 pulse, which demonstrated optimal GFP expression and cell viability, was selected for use in downstream experiments.

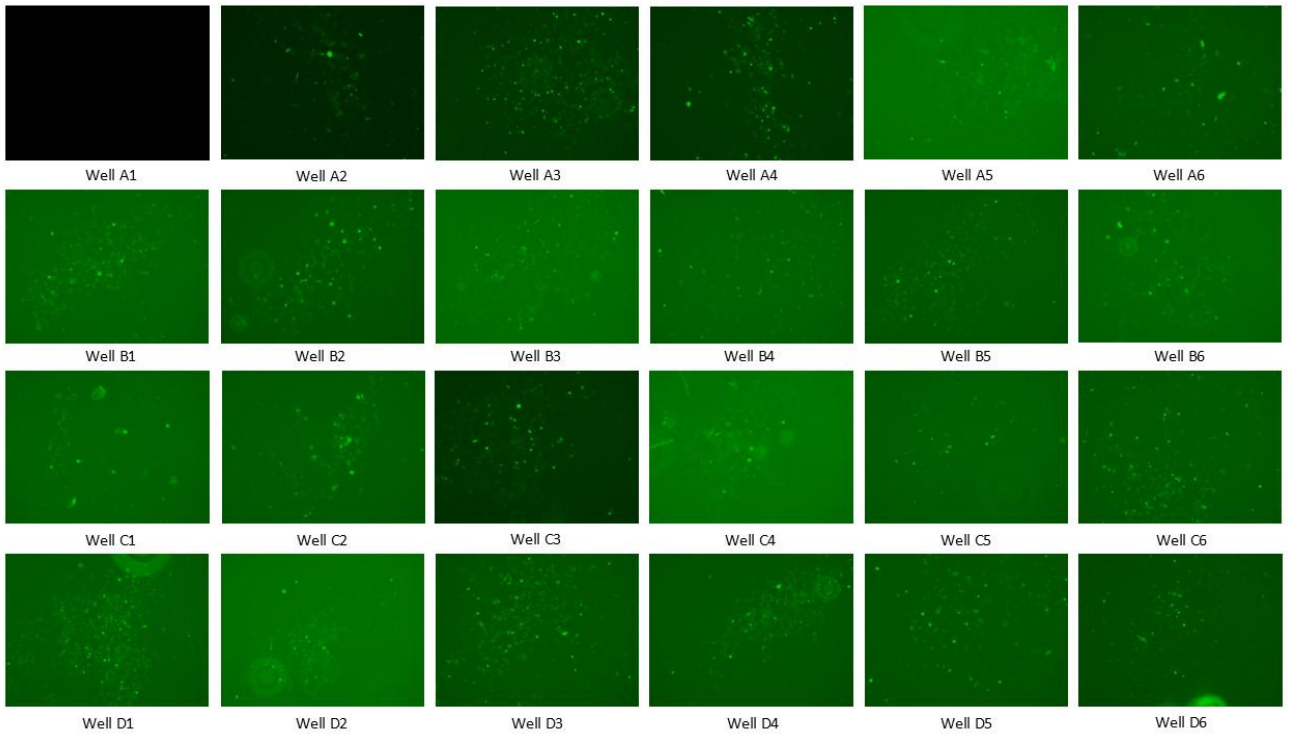

Figure 4.1: Optimisation of electroporation using the Neon Transfection System. Twenty-three different pulse voltages, widths, and numbers were tested. Images of SH-SY5Y cells with GFP signals were captured 48 hours post-electroporation (Well A2 to Well D6). Well A1 is a control without electroporation.

Table 4.2: Qualitative evaluation of cell viability and GFP intensity following electroporation, and the shortlisting of protocol

Well number	% viable cells	GFP intensity	Shortlisted protocol (Yes, Y/ No, N)
A1	High	None	N/A
A2	Medium	High	Y
A3	Medium	High	Y
A4	Medium	High	Y
A5	Low	Low	N
A6	Low	Medium	N
B1	High	Low	N
B2	High	Medium	N
B3	Medium	Low	N
B4	Low	Medium	N
B5	Medium	Medium	N
B6	Medium	Medium	N
C1	Low	Medium	N
C2	Medium	Medium	N
C3	Medium	High	Y
C4	Low	Low	N
C5	Low	Medium	N
C6	Medium	Medium	N
D1	High	Medium	N
D2	Low	Low	N
D3	High	Medium	N
D4	Medium	Medium	N
D5	Medium	Medium	N
D6	Low	Medium	N

Note: N/A, not applicable

4.1.3 Refined clonal expansion technique

Many cell lines struggle to survive as single cells *in vitro*, and SH-SY5Y cells may not be an exception, particularly after undergoing multiple stresses such as electroporation, transportation (which required the cells to be outside the CO_2 incubator for several hours, while being transported to a cell sorter facility located approximately 50 kilometres away), and cell sorting. However, to produce homogeneous knockout clones, SH-SY5Y cells must be cultured from single cells post-editing.

To address this challenge, trials of seeding single cells into each well of a 96-well plate, as well as seeding 100 to 200 cells in a 10 cm culture dish, were conducted. The trial results indicated that SH-SY5Y cells had difficulty growing into clones from single cells in the 96-well plates. Conversely, isolating clones from 10 cm culture dishes presented a challenge due to potential cross-contamination between clones.

Given these findings, both methods were pursued to maximise the success rate of obtaining homogeneous knockout clones. Ultimately, a total of 2 clones from 480 cells sorted into 96-well plates, resulting in a success rate of 0.4 %, was obtained. However, the success rate was significantly higher, i.e. 6 to 10 times greater, when the cells were sorted into 10 cm culture dishes, achieving success rates of 2.5 % (for 200 cells per dish) and 4.2 % (for 100 cells per dish) (Table 4.3). This aligns with the results from our trial run, confirming that sorting 100 cells into a 15 ml conical tube followed by transferring them to a 10 cm dish with supplemented media is the most effective approach.

Table 4.3: Success rate of the refined clonal expansion technique

Type of cell culture vessel	Number of cells sorted into the vessel (A)	Number of vessels (B)	Total number of cells (C)	Total number of clones (D)	Success rate (E)
96-well plate	1 cell per well	5	480	2	0.4 %
10 cm culture dish	100 cells per dish	5	500	21	4.2 %
10 cm culture dish	200 cells per dish	2	400	10	2.5 %

Note:

i. C = A * B
ii. E = D/C *100 %

4.1.4 Optimised protein detection protocol

Detecting low-expression proteins poses well-known challenges, so several critical steps in the Western blot protocol were optimised. This included ensuring efficient protein extraction, effective protein separation, and complete protein transfer. Primary antibodies with high specificity and a sensitive chemiluminescent substrate were employed, with image acquisition parameters carefully adjusted to achieve strong signal intensity.

The NE-PER Nuclear and Cytoplasmic Extraction Kit (Thermo Fisher Scientific, USA) allows for the separation of nuclear and cytoplasmic protein lysates, although it is not necessary for this study, as LRRK2 is expressed in both cellular compartments. To assess the kit's efficacy beyond its expiration date, the lysate obtained was compared with that extracted using fresh reagents. The protein quantification results indicated that both reagents performed equally well. The protein concentration extracted using the expired protein extraction kit is 2092 μg/ml, while the concentration from the new kit is 2334 μg/ml. Additionally, the LRRK2 protein in both the nuclear and cytoplasmic lysates was successfully detected, confirming its presence in both cellular compartments. Since LRRK2 is a low-abundance protein, the lysate was concentrated by using the minimum amount of lysis buffer and the maximum number of cells. This approach will allow the loading of more protein when running the gel, despite the limited volume that can be loaded per well.

LRRK2 is a relatively large protein (286 kDa), while GAPDH, the loading control for normalisation in Western blotting, is a smaller protein with a molecular weight of 44 kDa. To ensure effective protein separation, gradient gels were used. The gradient gels were hand-casted, and the concentration of several

ranges: 4 – 12% (w/v), 6 – 12% (w/v), 4 – 15% (w/v), and 4 – 20% (w/v), were tested. The 4 – 20% (w/v) gel yielded the best protein separation, with good resolution of proteins in the 245 kDa to 310 kDa range, as well as in the 35 kDa to 45 kDa range (Figure 4.2).

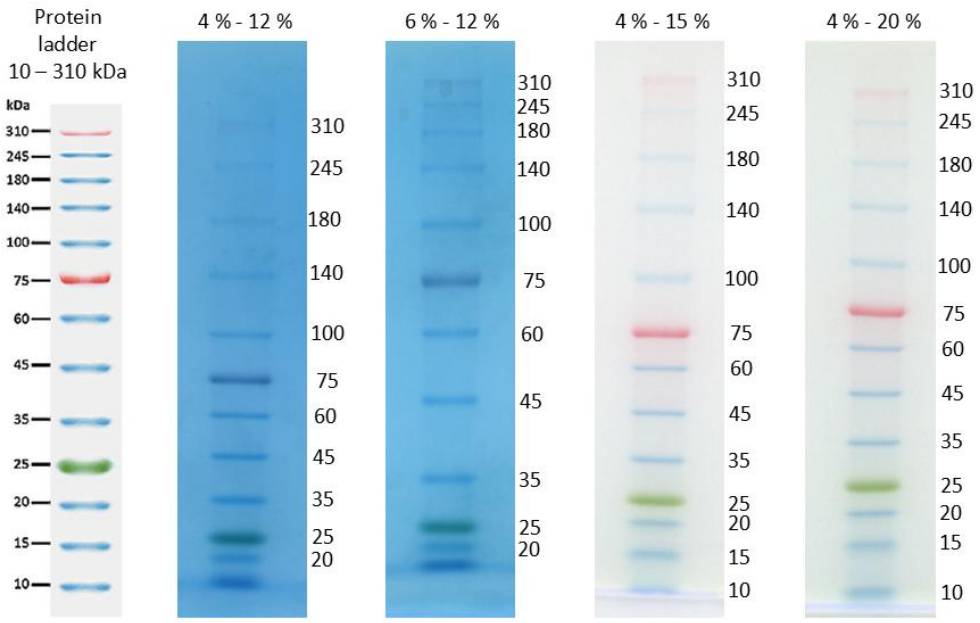

Figure 4.2: Protein separation in gradient gels of several ranges: 4 – 12% (w/v), 6 – 12% (w/v), 4 – 15% (w/v), and 4 – 20% (w/v)

To ensure the complete transfer of the large LRRK2 protein without over-transferring the small GAPDH protein, Coomassie blue staining was performed on the gel and Ponceau S staining on the membrane after overnight transfer. Coomassie Blue was used to confirm the presence of proteins in the gel, whereas Ponceau S was used to verify successful protein transfer onto the PVDF membrane. It was visually confirmed that no significant amounts of large proteins remained on the Coomassie blue-stained gel. Additionally, both large and small proteins were clearly detected on the Ponceau S-stained membrane.

The LRRK2 primary antibody used in this study was obtained from a reliable source and demonstrated high specificity (i.e. knockout-validated). The human lung cancer cell line A549, known for its high levels of LRRK2 protein, served as a positive control. To enhance detection sensitivity, a highly sensitive chemiluminescent substrate from a reputable brand capable of detecting proteins at the femtogram level was utilised.

For image acquisition, a digital imaging system with a high-resolution CCD camera was employed. Given the weak signal for low-expression LRRK2 protein, a cumulative capture mode was used, with multiple images captured at set time intervals and the signals combined to generate a final image with increased intensity.

4.2 Verification of LRRK2 knockout

4.2.1 PCR analysis

Following the cell sorting, a total of 33 clones were successfully cultivated (Table 4.3). Due to varying proliferation rates among the clones, PCR analysis was conducted on those that reached sufficient cell numbers first. Out of the 33 clones, 22 were successfully screened, while the remaining 11 did not proliferate enough to yield sufficient genomic DNA for PCR analysis. From the PCR analysis, nine clones (D3-2, D4-1, D4-3, D4-7, D4-8, D5-2, D5-4, D6-2, and D6-5) were excluded as their results indicated the presence of a 746 bp amplicon corresponding to the WT. TA cloning and Sanger sequencing were performed on the remaining 13 clones (D1-1, D1-4, D3-1, D4-2, D4-5, D5-1, D6-1, D6-3, D7-1, D7-2, D7-3, W1-1, and W2-1) for further validation of their DNA sequences (Figure 4.3A-L and Table 4.4).

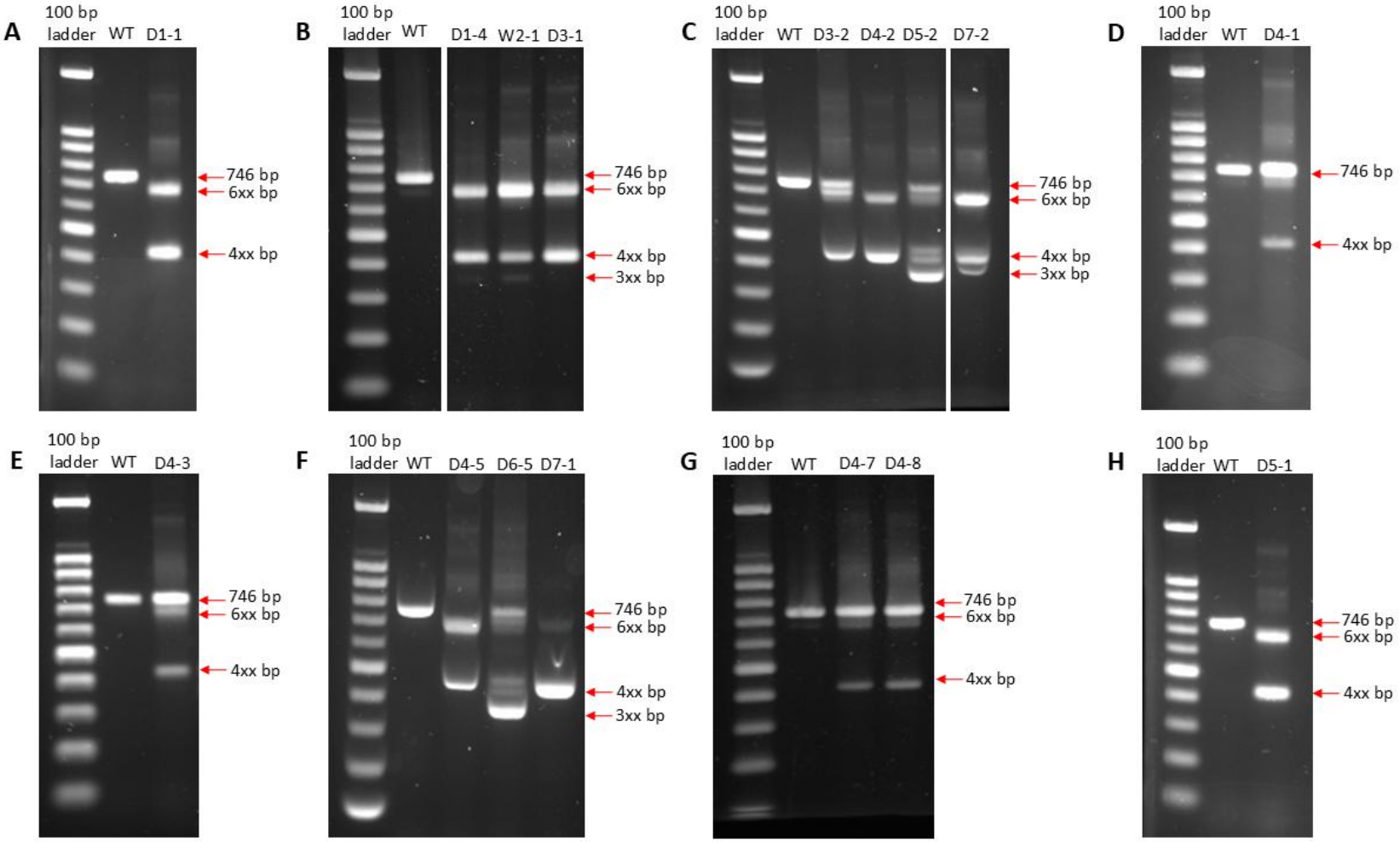
A
100 bp ladder
WT
D1-1
746 bp
6xx bp
4xx bp
B
100 bp ladder
WT
D1-4
W2-1
D3-1
746 bp
6xx bp
4xx bp
3xx bp
C
100 bp ladder
WT
D3-2
D4-2
D5-2
D7-2
746 bp
6xx bp
4xx bp
3xx bp
D
100 bp ladder
WT
D4-1
746 bp
4xx bp
E
100 bp ladder
WT
D4-3
746 bp
6xx bp
4xx bp
F
100 bp ladder
WT
D4-5
D6-5
D7-1
746 bp
6xx bp
4xx bp
3xx bp
G
100 bp ladder
WT
D4-7
D4-8
746 bp
6xx bp
4xx bp
H
100 bp ladder
WT
D5-1
746 bp
6xx bp
4xx bp

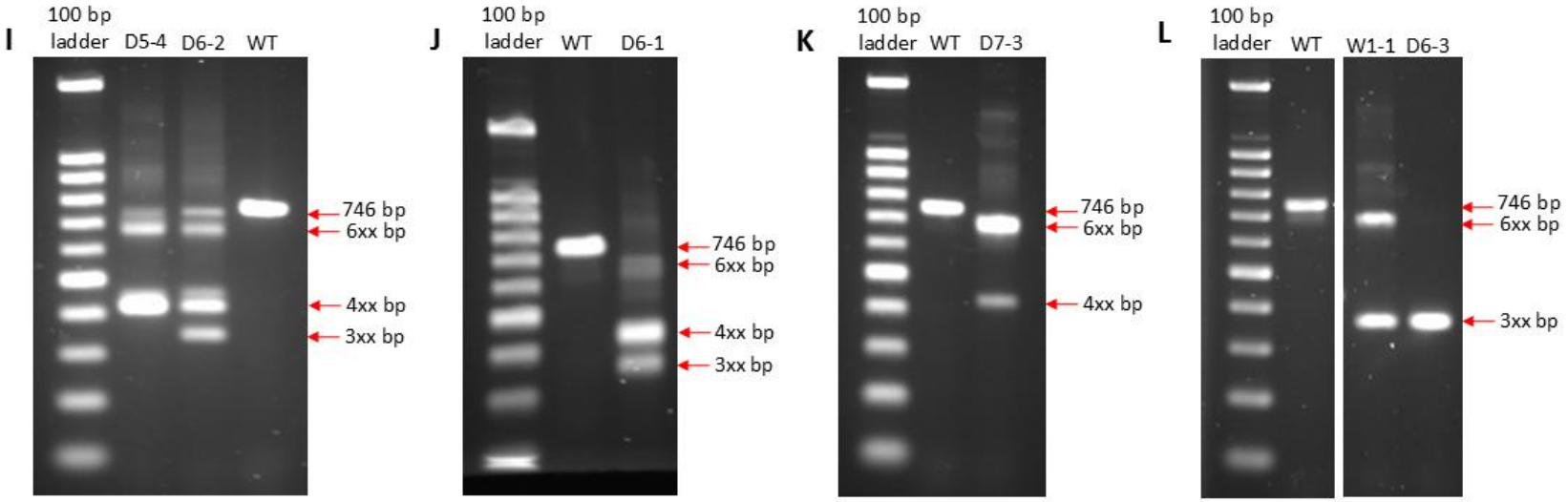

Figure 4.3: PCR screening of 22 potential clones

Table 4.4: PCR screening of 22 potential clones

No.	Clone name	Proceed with screening? (Yes, Y/ No, N)	Amplicon length (bp)				Figure no.	Proceed with TA cloning and Sanger sequencing? (Yes, Y/ No, N)
			746	6xx	4xx	3xx		
1	D1-1	Y	-	+	+	-	4.3A	Y
2	D1-2	N	N/A	N/A	N/A	N/A	N/A	N/A
3	D1-3	N	N/A	N/A	N/A	N/A	N/A	N/A
4	D1-4	Y	-	+	+	-	4.3B	Y
5	D2-1	N	N/A	N/A	N/A	N/A	N/A	N/A
6	D2-2	N	N/A	N/A	N/A	N/A	N/A	N/A
7	D3-1	Y	-	+	+	-	4.3B	Y
8	D3-2	Y	+	+	+	-	4.3C	N
9	D3-3	N	N/A	N/A	N/A	N/A	N/A	N/A
10	D4-1	Y	+	-	+	-	4.3D	N
11	D4-2	Y	-	+	+	-	4.3C	Y
12	D4-3	Y	+	+	+	-	4.3E	N

13	D4-4	N	N/A	N/A	N/A	N/A	N/A	N/A
14	D4-5	Y	-	+	+	-	4.3F	Y
15	D4-6	N	N/A	N/A	N/A	N/A	N/A	N/A
16	D4-7	Y	+	+	+	-	4.3G	N
17	D4-8	Y	+	+	+	-	4.3G	N
18	D5-1	Y	-	+	+	-	4.3H	Y
19	D5-2	Y	+	+	+	+	4.3C	N
20	D5-3	N	N/A	N/A	N/A	N/A	N/A	N/A
21	D5-4	Y	+	+	+	-	4.3I	N
22	D6-1	Y	-	+	+	+	4.3J	Y
23	D6-2	Y	+	+	+	+	4.3I	N
24	D6-3	Y	-	-	-	+	4.3L	Y
25	D6-4	N	N/A	N/A	N/A	N/A	N/A	N/A
26	D6-5	Y	+	+	+	+	4.3F	N
27	D6-6	N	N/A	N/A	N/A	N/A	N/A	N/A
28	D7-1	Y	-	+	+	-	4.3F	Y
29	D7-2	Y	-	+	+	+	4.3C	Y
30	D7-3	Y	-	+	+	-	4.3K	Y

31	D7-4	N	N/A	N/A	N/A	N/A	N/A	N/A
32	W1-1	Y	-	+	-	+	4.3L	Y
33	W2-1	Y	-	+	+	+	4.3B	Y

Note:

i. N/A = Not applicable, as this clone did not proliferate enough to yield sufficient genomic DNA for PCR analysis.

ii. "+" = Presence of PCR amplicon

iii. "-" = Absence of PCR amplicon

iv. Clone names starting with "D" indicate clones isolated from culture dishes, while those starting with "W" represent clones isolated from 96-well plates. Clones labelled D1-x to D5-x were derived from culture dishes seeded with 100 cells per dish, whereas clones labelled D6-x to D7-x were obtained from dishes seeded with 200 cells per dish. Clones labelled W1-2 and W2-1 were isolated from 96-well plates seeded with 1 cell per well.

4.2.2 TA cloning and Sanger sequencing

TA cloning was performed on each amplicon from the 13 potential clones. Ten colonies were picked from each TA cloning reaction, and plasmid DNA was extracted and sent for Sanger sequencing. However, some Sanger sequencing reactions failed due to technical issues, resulting in uninterpretable data. Due to budget constraints, failed sequencing reactions were not repeated. Despite these challenges, the available Sanger sequencing results were sufficient to identify three representative clones, i.e. D1-1, W1-1, and D6-3, for further validation and downstream assays. These clones were subsequently designated as LKO1, LKO2, and LKO3, respectively (Appendix A and Table 4.5).

In-frame mutations occur due to the deletion of base pairs in multiples of three (3n, n = …-3, -2, -1, 0, 1, 2, 3…). In contrast, frameshift mutations result from the deletion of base pairs that are not multiples of three (i.e., 3n+1 or 3n+2). Premature stop codons are generated from in-frame or frameshift mutations when indels created during NHEJ lead to the formation of one of the three stop codons: TAA, TAG, or TGA (YouRamachandra and Jin, 2020).

The sequencing results revealed that the 4xx bp amplicon in the LKO1 clone resulted from a 318 bp deletion and the formation of a premature stop codon during rejoining of the double-stranded break, while the 6xx bp amplicon arose from a 70 bp or 71 bp deletion [Figure 4.4 A (i) to (iii) and Table 4.6]. In the LKO2 clone, the 3xx bp and 6xx bp amplicons were due to deletions of 388 bp and 70 bp, respectively [Figure 4.4 B (i) to (ii) and Table 4.6]. For LKO3, there was a single amplicon, resulting from a 388 bp deletion [Figure 4.4 C (i) and Table 4.6]

Table 4.5: The mutation frequencies, types, and the number of bases deleted or inserted for each amplicon in the 13 potential clones

No.	Clone name	Mutation frequencies and types	Number of bases deleted/ inserted	Figure no.
1	D1-1 (LKO1)	4xx: 10/10 PSC 6xx: 10/10 FS	4xx: 318 bp deleted (PSC) 6xx: 70 bp or 71 bp deleted (FS)	4.4A (i) & (ii)
2	D1-4	4xx: 10/10 PSC 6xx: 8/10 FS; 2/10 IF	4xx: 318 bp deleted (PSC) 6xx: 70 bp deleted (FS); 70 bp deleted and 1 bp inserted (IF)	4.4B (i) & (ii)
3	D3-1	4xx: 10/10 PSC 6xx: 4/10 FS; 6/10 IF	4xx: 318 bp deleted (PSC) 6xx: 70 bp deleted and 3 bp insertion (FS); or 70 bp deleted (FS); or 70 bp deleted and 1 bp inserted (IF)	4.4C (i) & (ii)
4	D4-2	4xx: 10/10 PSC 6xx: 7/9 FS; 2/9 IF	4xx: 318 bp deleted (PSC) 6xx: 70 bp deleted (FS); or 70 bp deleted and 1 bp inserted (IF)	4.4D (i) & (ii)
5	D4-5	4xx: 10/10 PSC 6xx: 6/9 FS; 3/9 IF	4xx: 318 bp deleted (PSC) 6xx: 70 bp deleted (FS); or 70 bp deleted and 1 bp inserted (IF)	4.4E (i) & (ii)
6	D5-1	4xx: 9/9 PSC 6xx: 2/10 FS; 8/10 IF	4xx: 318 bp deleted (PSC) 6xx: 76 bp deleted (FS); or 70 bp deleted and 68 bp inserted (FS); or 69 bp deleted (IF)	4.4F (i) & (ii)

7	D6-1	3xx: 9/9 FS 4xx: 4/4 PSC 6xx: 6/8 FS; 2/8 IF	3xx: 388 bp deleted (FS) 4xx: 318 bp deleted (PSC) 6xx: 70 bp deleted (FS); or 70 bp deleted and 51 bp inserted (FS); or 70 bp deleted and 1 bp inserted (IF)	4.4G (i), (ii) & (iii)
8	D6-3 (LKO3)	3xx: 10/10 FS	3xx: 388 bp deleted (FS)	4.4H
9	D7-1	4xx: 8/8 PSC 6xx: 8/9 FS; 1/9 IF	4xx: 318 bp deleted (PSC) 6xx: 70 bp deleted (FS); or 69 bp deleted and 1 bp inserted (IF)	4.4I (i) & (ii)
10	D7-2	3xx:10/10 FS 4xx: 10/10 PSC 6xx: 6/10 FS; 4/10 IF	3xx: 388 bp or 395 bp deleted (FS) 4xx: 318 bp deleted (PSC) 6xx: 70 bp deleted (FS); or 70 bp deleted and 1 bp inserted (IF)	4.4J (i), (ii) & (iii)
11	D7-3	4xx: 10/10 PSC 6xx: 5/10 FS; 5/10 IF	4xx: 318 bp deleted (PSC) 6xx: 70 bp deleted (FS); or 70 bp deleted and 1 bp inserted (IF)	4.4K (i) & (ii)
12	W1-1 (LKO2)	3xx: 10/10 FS 6xx: 10/10 FS	3xx: 388 bp deleted (FS) 6xx: 70 bp deleted (FS)	4.4L (i) & (ii)
13	W2-1	3xx: 10/10 FS 4xx: 8/8 PSC 6xx: 5/10 FS; 5/10 IF	3xx: 388 bp deleted (FS) 4xx: 318 bp deleted (PSC) 6xx: 70 bp deleted (FS); or 70 bp deleted and 1 bp inserted (IF)	4.4M (i), (ii) & (iii)

Note:

i. PSC = Premature stop codon; FS = frameshift; IF = in-frame; bp = base pairs

ii. Mutation frequencies represent the proportion of colonies with a specific mutation identified through Sanger sequencing. For instance, "10/10 PSC" indicates that all 10 colonies screened (10 out of 10) were found to have a premature stop codon mutation.

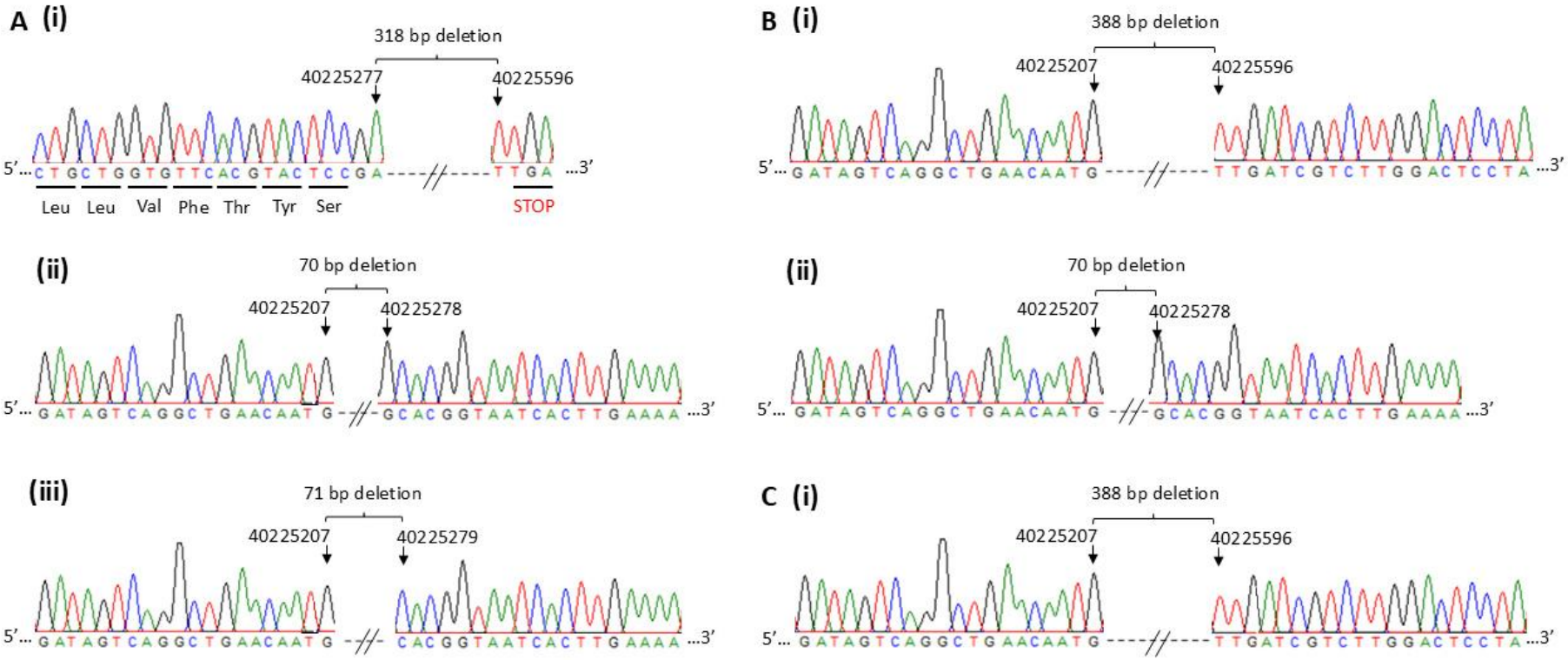

Figure 4.4: The DNA sequence of the edited *LRRK2* gene in (A) LKO1 where (i) a premature stop codon was generated, (ii) 70 bp or (iii) 71 bp were deleted, respectively; (B) LKO2 where (i) 388bp or (ii) 70 bp were deleted, respectively; (C) (i) LKO3 where 388 bp were deleted

Table 4.6: The amplicon length, combination of gRNAs involved in the genome editing, number of bases deleted, and the resulting mutation(s) in LKO1, LKO2 and LKO3

Clone	Amplicon length (bp)	gRNAs	Number of bases deleted	Mutation
WT	746	N/A	N/A	N/A
Mock	746	N/A	N/A	N/A
LKO1	428	gRNA 1 + gRNA2	318	Generation of a premature stop codon
	676 or 675	gRNA 1 + gRNA3	70 or 71	Frameshift deletion
LKO2	358	gRNA 2 + gRNA3	388	Frameshift deletion
	676	gRNA 1 + gRNA3	70	Frameshift deletion
LKO3	358	gRNA 2 + gRNA3	388	Frameshift deletion

Note: N/A, not applicable

4.2.3 Western blot analysis

To confirm the ablation of the LRRK2 protein, the Western blot analysis was performed to verify its absence. The results demonstrated a loss of LRRK2 protein in LKO1, LKO2, and LKO3 (Figure 4.5).

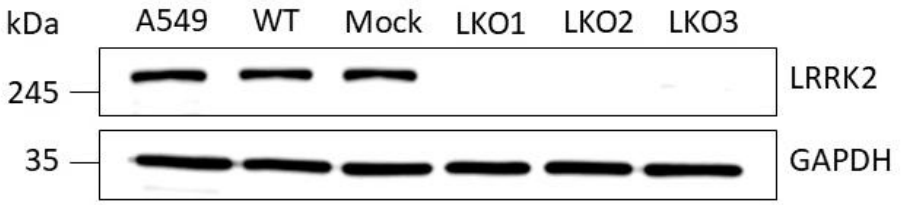

Figure 4.5: Western blot validation of LKO1, LKO2 and LKO3.

4.2.4 Off-target validation

Off-target effects are defined as unintended cleavages or genetic modifications at sites with sequences that are similar, but not identical, to the target site (Modrzejewski *et al.*, 2019). In this study, off-target prediction was performed using a web-based tool, CHOPCHOP (https://chopchop.cbu.uib.no/) (Labun *et al.*, 2019). According to CHOPCHOP, gRNA1 does not have any off-targets while gRNA2 and gRNA3 have 2 and 6 off-targets, respectively. PCR and Sanger sequencing were performed to evaluate the off-targets. Sanger sequencing results confirmed the absence of off-target effects in LKO1, LKO2, and LKO3 (Figure 4.6 A-G), as the sequences of the target regions remained unchanged in these samples compared to WT and mock controls.

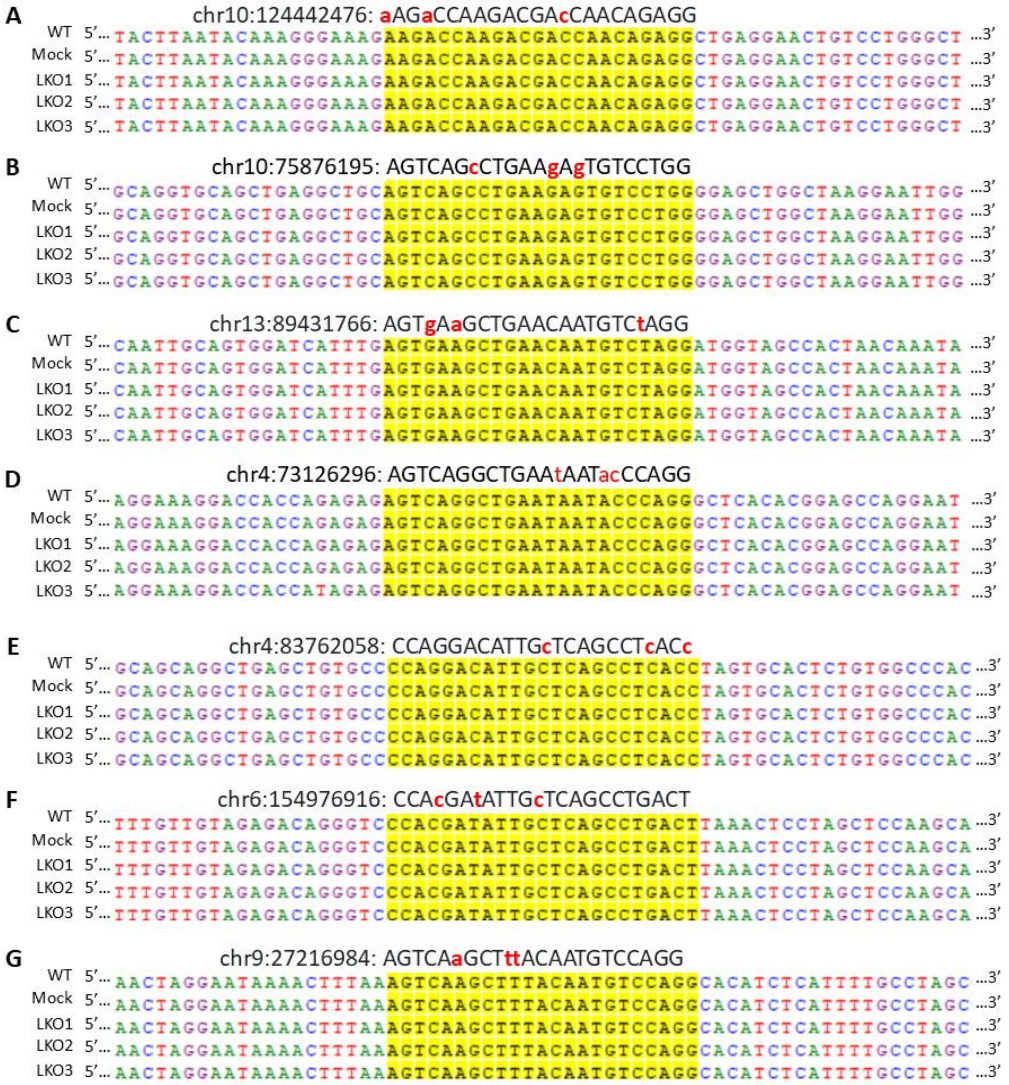

Figure 4.6: Evaluation of off-targets. DNA sequences of (A) one and (B-G) six potential off-target sites of gRNA 2 and gRNA 3, respectively, in WT, mock, LKO1, LKO2 and LKO3. gRNA 1 has no off-target site.

4.3 Phenotypic changes in LRRK2 knockout cells

4.3.1 Changes in cell morphology, size and substrate adhesion strength

Morphological alteration is a key characteristic of the senescent phenotype. Senescent cells are typically enlarged, flattened, and exhibit a "fried egg" appearance. Additionally, these cells demonstrate enhanced substrate adhesion (Kameda *et al.*, 2021, Cho *et al.*, 2004, HwangYoon and Kang, 2009). LKO cells exhibited senescence-like phenotypes, distinguishing them from WT and mock cells. While WT and mock cells exhibited multiple long, fine neurite processes, LKO cells either showed very few or completely lacked these structures (Figure 4.7). Furthermore, the LKO cells were relatively enlarged (WT and mock: 13 μm; LKO1: 16 μm; LKO2: 20 μm; LKO3: 18 μm) (Figure 4.8 A-B) and appeared more flattened compared to WT and mock cells (Figure 4.7). A qualitative evaluation of cell-substrate adhesion strength revealed that WT and mock cells had low cell-substrate adhesion, whereas LKO cells showed medium to high cell-substrate adhesion levels (Table 4.7).

As described half a century ago, substrate-adherent/ epithelial-like (S-type) and intermediate (I-type) cells may arise from the spontaneous interconversion (also known as transdifferentiation) of neuroblastic (N-type) neuroblastoma cells (RossSpengler and Biedler, 1983, Ciccarone *et al.*, 1989, Ross and Spengler, 2007). Interestingly, while LKO cells display characteristics of senescent cells, their morphology also closely resembles that of S-type or I-type neuroblastoma cells. In contrast, WT and mock cells exhibit an N-type morphology. Specifically, WT and mock cells are significantly smaller than LKO cells, featuring scant cytoplasm, loosely adherent cell bodies, multiple long and distinct neurites, and forming cell aggregates. LKO1 cells resemble I-type cells; they are larger than

WT and mock cells but smaller than LKO2 and LKO3 cells, flattened, moderately adherent, with scant cytoplasm and few short neurites. In contrast, LKO2 and LKO3 cells are enlarged and flattened, with abundant cytoplasm, lack neurites, strongly adhere to the substrate, and grow as a monolayer (Figure 4.7 & 4.9 A-B and Table 4.7).

The morphology of LKO cells was confirmed to resemble either S- or I-type cells (Robert A. Ross, personal communication, 2024; Appendix B). Consequently, it is hypothesised that the knockout of LRRK2 may have induced senescence or facilitated the conversion of WT cells (N-type) into LKO cells (S-type or I-type). To investigate these further, additional assays were conducted to confirm the senescence or conversion status of LKO cells.

Table 4.7: Qualitative evaluation of cell-substrate adhesion strength

Cell	Cell-substrate adhesion strength
WT	Low
Mock	Low
LKO1	Medium
LKO2	High
LKO3	High

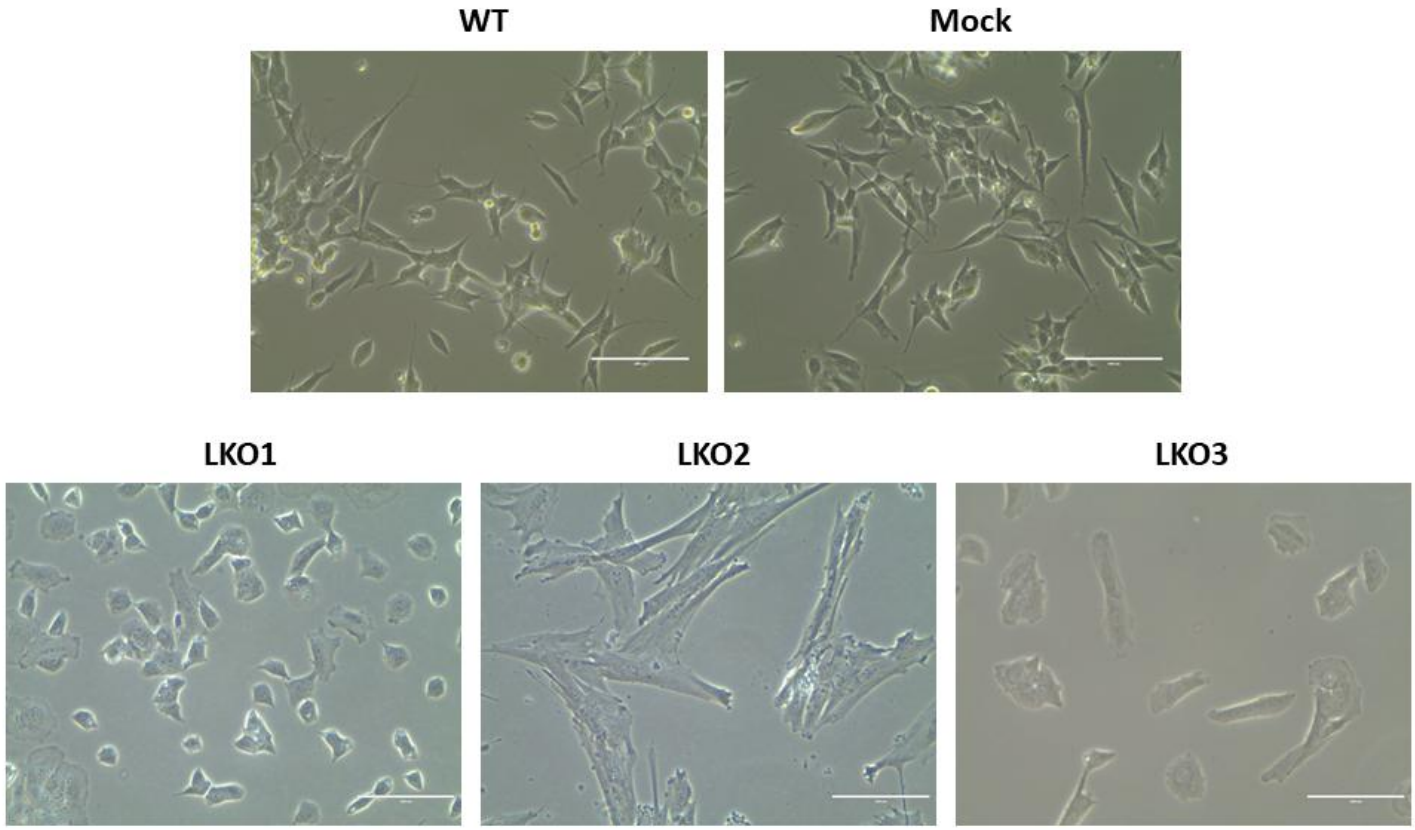

Figure 4.7: Evaluation of cell morphological changes. Representative phase-contrast images of WT, mock, LKO1, LKO2, and LKO3 cells. Scale bars = 100 μm; total magnification = 400 X

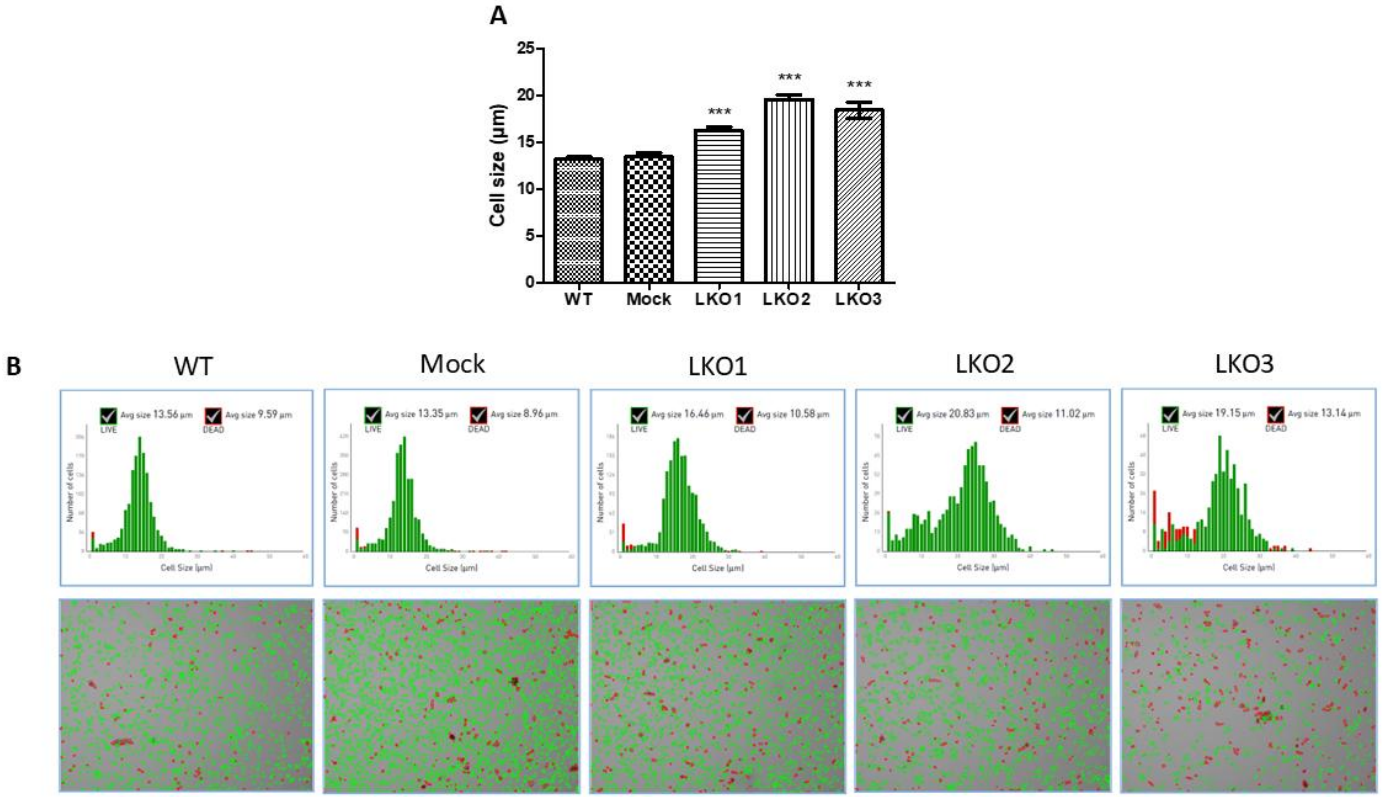

Figure 4.8: Evaluation of cell size. (A) Average cell size of WT, mock, LKO1, LKO2 and LKO3. (B) Representative images of cell size measurement performed using an automated cell counter. Data are mean ± SEM; *** P<0.001. n = 3 independent experiments, each with three technical replicates

4.3.2 Reduction or cessation of cell proliferation rate

Senescent cells enter the irreversible growth arrest phase of the cell cycle and stop proliferating, yet remain viable and metabolically active (Kumari and Jat, 2021). As LKO cells were observed to grow slower than WT and mock cells, cumulative population doubling (CPD) was recorded to evaluate the growth of the LKO cells. Cell numbers were determined at the end of each passage, and CPD was calculated based on the cell numbers from the previous passage. Continuous assessment of cell proliferation over 35 days revealed that WT and mock cells grew steadily. In contrast, LKO1 and LKO2 proliferated approximately 40 % to 60 % slower than WT and mock cells, while LKO3 cells showed minimal proliferation, as indicated by the nearly flat growth kinetic curve for LKO3. The CPD on day 35 was: WT: 13.36, mock: 13.51, LKO1: 7.80, LKO2: 5.19, LKO3: 0.67 (Figure 4.9 A-B).

Previous studies have demonstrated that N-type cells are immortal, exhibit a high proliferation rate, and show weak tumorigenicity. In contrast, I-type cells are also immortal but are highly tumorigenic. S-type cells, however, exhibit extremely slow growth after a few passages and eventually cease proliferating (Ciccarone *et al.*, 1989, Ross and Spengler, 2007). In our study, a similar growth pattern in LKO cells was observed. Specifically, WT and mock cells (both N-type) and LKO1 cells (I-type) exhibited a higher proliferation rate compared to LKO2 and LKO3 cells (S-type). LKO3 cells appeared to have halted proliferation, as indicated by their nearly flat growth curve (Figure 4.9 A-B).

During the establishment of the LKO cells, the cell sorting process was not conducted in a clean room, which introduced the potential risk of mycoplasma contamination that could have impacted cell proliferation. To rule out this

concern, mycoplasma testing was conducted. It was confirmed that LKO cells were free from contamination (Figure 4.10). This suggests that the observed decrease in proliferation rate in LKO cells is likely due to a phenotypic change associated with the loss of LRRK2, rather than a technical artefact. However, based on the morphology and growth rate alone, uncertainty remains regarding whether the LKO cells are undergoing senescence or conversion. Therefore, senescence-associated β-galactosidase (SA-β-gal) activity was assessed in these cells.

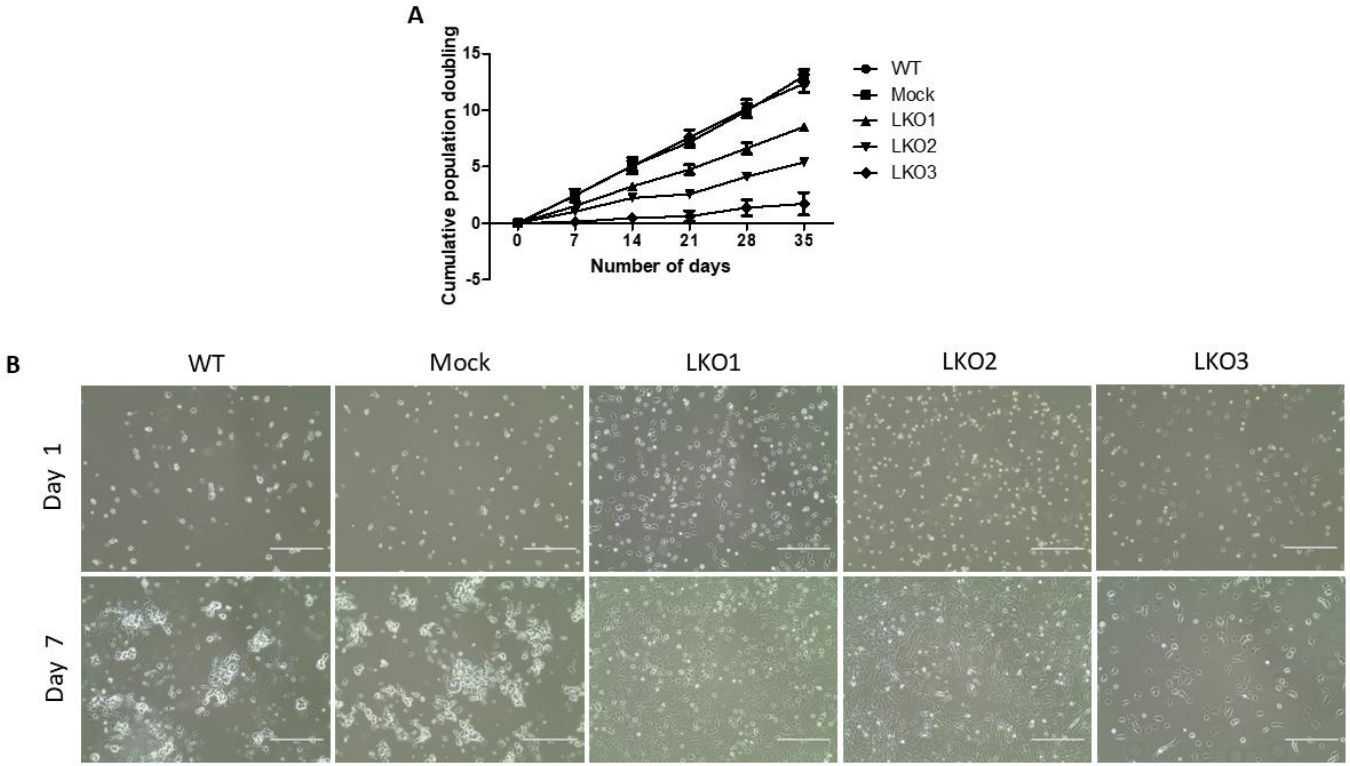

Figure 4.9: Assessment of growth kinetics. (A) The growth kinetics of WT, mock, LKO1, LKO2 and LKO3 cells. (B) Representative images depicting cell confluency on day 1 and day 7. n = 3 independent experiments, each with three technical replicates. Scale bars = 400 µm; total magnification = 100 X

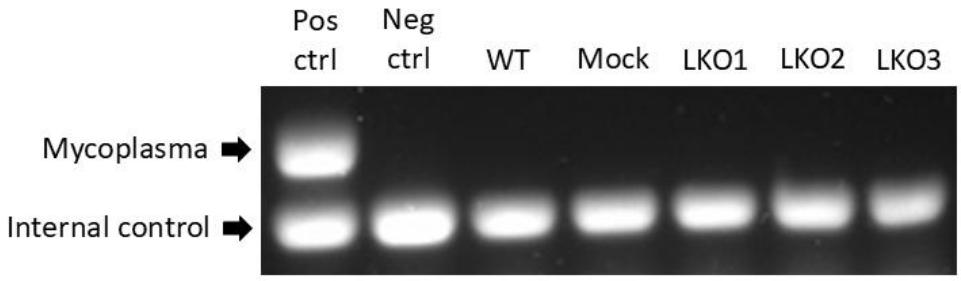

Figure 4.10: Mycoplasma detection in WT, mock, LKO1, LKO2 and LKO3 cells. Pos ctrl, positive control; Neg ctrl, negative control.

4.3.3 Increased senescence-associated β-galactosidase (SA-β-gal) activity

SA-β-gal activity has been established as a biomarker for senescence since its initial description by Dimri *et al.* in 1995 (Dimri *et al.*, 1995), and it remains the "gold standard" for identifying cellular senescence (Debacq-Chainiaux *et al.*, 2009, ItahanaCampisi and Dimri, 2007). SA-β-gal staining was performed, and a significantly higher percentage of SA-β-gal-positive cells was observed in the LKO cells: LKO1 (27 %), LKO2 (31 %), and LKO3 (98 %), compared to WT (3 %) and mock cells (0.3 %) (Figure 4.11 A-B).

Since SA-β-gal staining confirmed that LKO cells underwent senescence, the next investigation was conducted to determine whether autophagy and mitochondrial respiration were affected, two key processes that are impacted both in cellular senescence and by the loss of LRRK2. Unlike LKO2 and LKO3, which proliferated very slowly or exhibited minimal growth, LKO1 cells retained proliferative capacity despite displaying senescent characteristics. Therefore, it was hypothesised that LKO1 corresponds to the intermediate (I-type) neuroblastoma subtype, which possesses stem cell-like properties and may raise greater clinical concern, particularly in the context of tumour relapse

following chemotherapy. In contrast, the limited proliferative capacity of LKO2 and LKO3 suggests that they resemble therapy-induced senescent cells and are less likely to pose an immediate clinical risk. Hence, LKO1 was selected for subsequent analyses of autophagic vacuoles and mitochondrial respiration.

4.3.4 Reduced autophagic vacuoles

Autophagy is generally reduced in senescent cells, and previous studies have shown decreased autophagic flux in senescent neurons, both *in vitro* and *in vivo* (Suelves *et al.*, 2023, Singh *et al.*, 2020, Tai *et al.*, 2017). Given that I-type cells are clinically more concerning due to their stem cell-like properties, which enable them to escape immune surveillance and potentially trigger relapse in patients, autophagic vacuole detection was performed in LKO1 cells. Our data revealed a decrease in the percentage of autophagic vacuoles in LKO1 cells (86.7%) compared to WT (100%) and mock (87.1%), although this difference was not statistically significant (Figure 4.12).

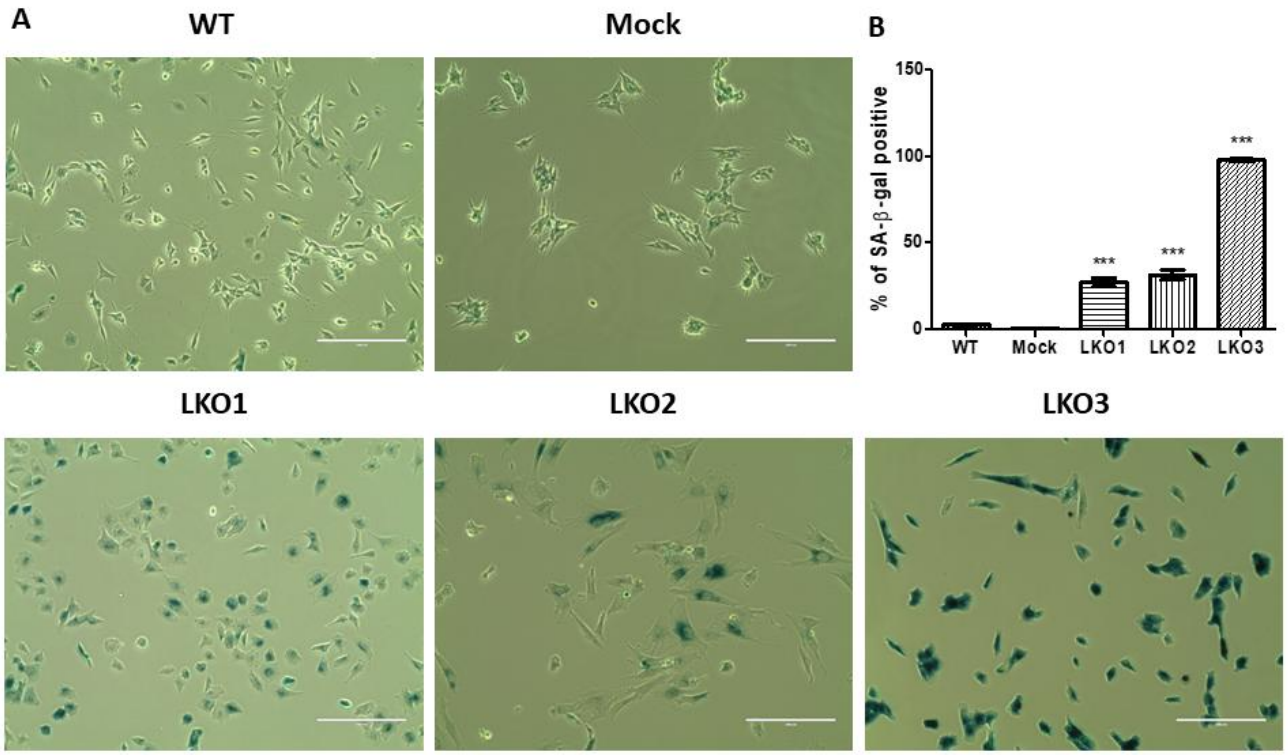

Figure 4.11: Senescence-associated β-galactosidase (SA-β-gal) staining. (A) Representative images of SA-β-gal stained WT, mock, LKO1, LKO2 and LKO3 cells. (B) The percentage of SA-β-gal positive cells. Data are mean ± SEM; *** $P<0.001$. n = 3 independent experiments, 10 microscopic fields analysed per cell type per independent experiment. Scale bars = 200 μm; total magnification = 200 X

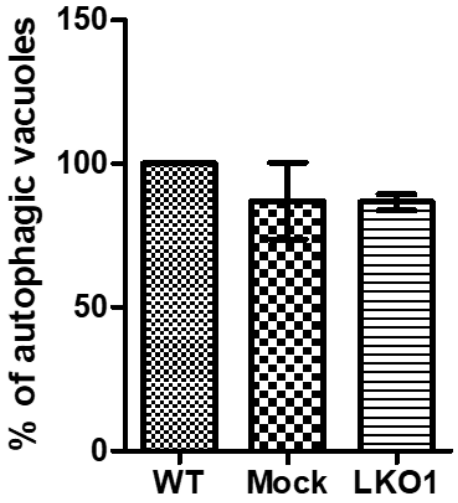

Figure 4.12: Microplate-based profiling of autophagy in WT, mock and LKO1 cells. No statistically significant differences were observed between WT and mock cells or between WT and LKO1 cells. Data are mean ± SEM. n = 3 independent experiments, each with three technical replicates.

4.3.5 Decreased mitochondrial respiration

Several studies have indicated that senescent cells accumulate dysfunctional mitochondria. A key characteristic of mitochondrial dysfunction in senescent cells is a reduction in respiratory capacity per mitochondrion. Impairments in oxidative phosphorylation (OXPHOS) have been observed across various models of senescence, establishing a direct link between senescence and OXPHOS inefficiency (Lee *et al.*, 2021b, Miwa *et al.*, 2022).

Bioenergetic profiling was conducted by measuring the oxygen consumption rate (OCR) (Figure 4.13A) and extracellular acidification rate (ECAR) (Figure 4.13I). In all other parameters measured, including spare respiratory capacity, basal respiration, maximal respiration, proton leak, non-mitochondrial oxygen

consumption, ATP production coupled respiration, and coupling efficiency, LKO1 cells showed a significant decrease (Figure 4.13B-H). Additionally, a significant decrease in ECAR was observed between WT and mock cells, as well as between WT and LKO1 cells (Figure 4.13I). The energy map indicated that LKO1 cells are less energetic and less aerobic compared to WT and mock cells (Figure 4.13J).

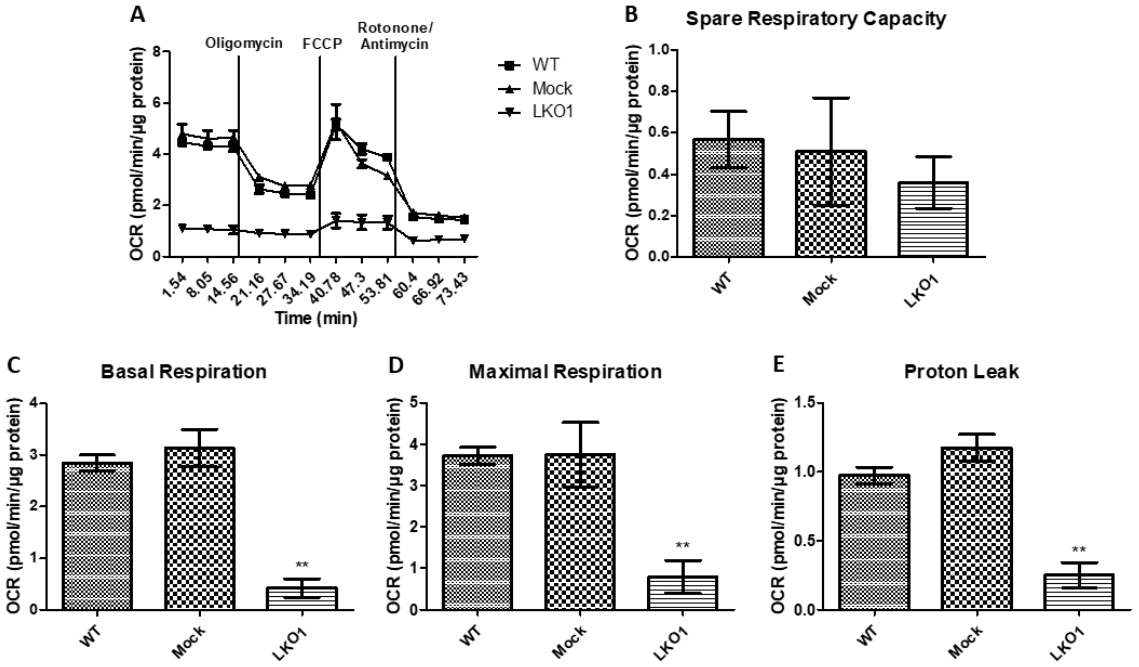
A
Oligomycin
FCCP
Rotonone/
Antimycin
WT
Mock
LKO1
OCR (pmol/min/µg protein)
Time (min)
B
Spare Respiratory Capacity
C
Basal Respiration
D
Maximal Respiration
E
Proton Leak
**

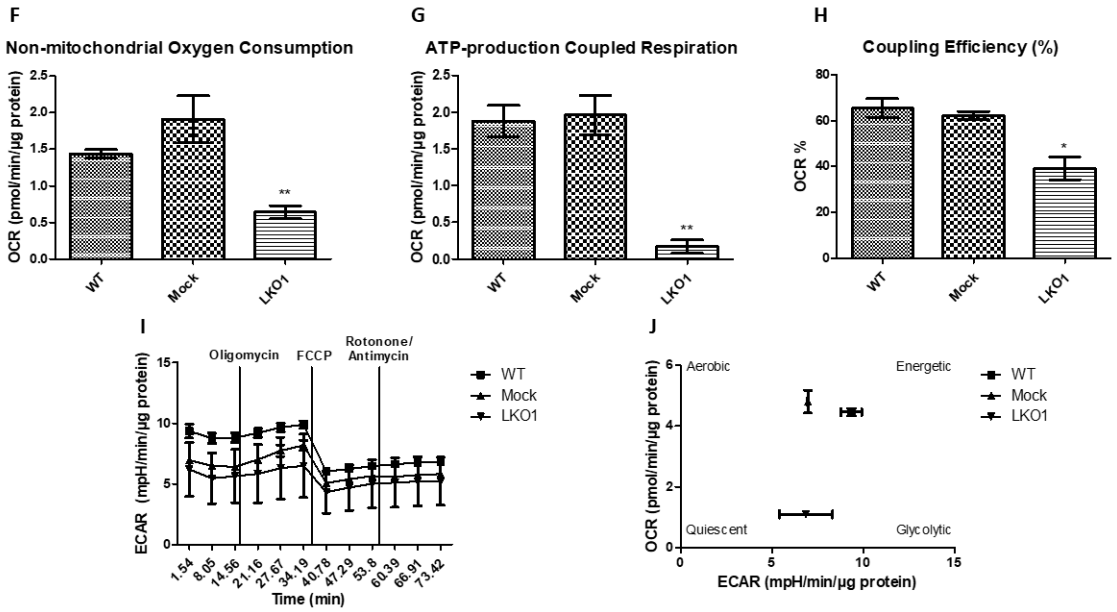

Figure 4.13: Assessment of bioenergetic profiles of WT, mock and LKO1 cells. Evaluation of (A) mitochondrial respiration, (B) spare respiratory capacity, (C) basal respiration, (D) maximal respiration, (E) proton leak, (F) non-mitochondrial oxygen consumption, (G) ATP-production coupled respiration, (H) percentage of coupling efficiency, (I) extracellular acidification rate and (J) energy map in WT, mock and LKO1 cells. Data are mean ± SEM; * P<0.05, ** P<0.01. n = 3 independent experiments, each with three technical replicates.

4.4 Effects of EBN extracts

4.4.1 Extraction yield

The EBN enzyme extract exhibited the highest yield at 92%, while the acid and aqueous extracts had significantly lower yields of 17% and 14%, respectively. The yield of EBN acid, aqueous and enzyme extracts is summarised in Table 4.8.

Table 4.8: The yield of EBN acid, aqueous and enzyme extracts

Type of EBN extract	Raw EBN (g)	Weight of EBN extract (g)	Yield (%)
Acid	2.00	0.34	17 %
Aqueous	2.00	0.28	14 %
Enzyme	2.00	1.84	92 %

Note:

i. % yield = Weight of EBN extract (g)/ raw EBN (g) *100 %

4.4.2 Antioxidant assays

Two biochemical assays [α, α-diphenyl-β-picrylhydrazyl (DPPH) free radical scavenging activity assay and oxygen radical absorbance capacity (ORAC) assay] and one cell-based assay [dichloro-dihydro-fluorescein diacetate (DCFH-DA)] were conducted to evaluate the antioxidant properties of EBN acid, aqueous, and enzyme extracts.

4.4.2.1 DPPH free radical scavenging activity assay

Quercetin, a compound well-known for its potent antioxidant activity, was used as a positive control in the DPPH assay. It demonstrated a concentration-dependent reduction in DPPH, achieving approximately 92 % inhibition at 50 μg/ml (Figure 4.14A). Neither the EBN aqueous nor the enzyme extracts showed

a significant reduction in DPPH. Conversely, the EBN acid extract exhibited a significant, concentration-dependent reduction in DPPH, with the highest inhibition reaching approximately 57 % at 2500 μg/ml (Figure 4.14B). These results suggest that the EBN acid extract possesses free radical scavenging activity, while the aqueous and enzyme extracts do not.

4.4.2.2 Oxygen radical absorbance capacity (ORAC) assay

Following the DPPH assay, the ORAC assay was conducted to assess the peroxyl radical scavenging capacity of the EBN extracts. In this assay, 2,2'-azobis(2-methylpropionamidine) dihydrochloride (AAPH) was used to generate peroxyl radicals. Trolox, a well-known antioxidant, served as the positive control. The antioxidant capacity of the EBN extracts was interpolated using a Trolox calibration curve (Figure 4.15A). All three EBN extracts (acid, aqueous, and enzyme) demonstrated significant peroxyl radical scavenging activity in a dose-dependent manner. At 500 μg/ml, each extract exhibited ORAC activity equivalent to approximately 40 μg/ml of Trolox (Figure 4.15B).

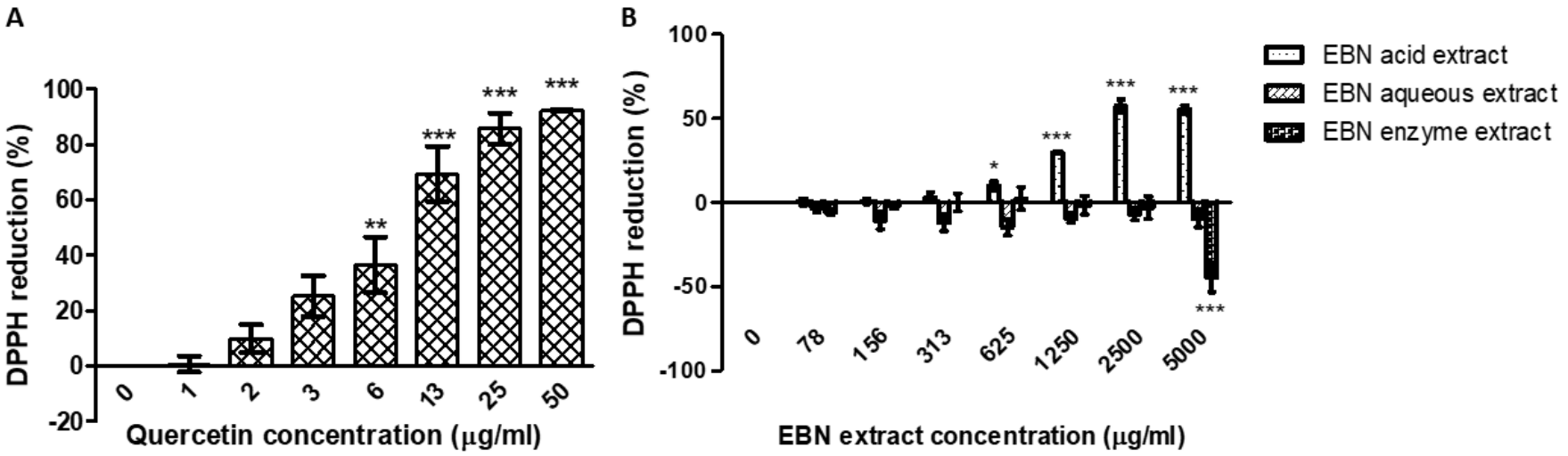

Figure 4.14: Percentage of DPPH reduction by (A) Quercetin (B) EBN acid, aqueous and enzyme extracts. Data are mean ± SEM; * $p<0.05$, ** $p<0.01$, *** $p<0.001$. n = 3 independent experiments, each with three technical replicates.

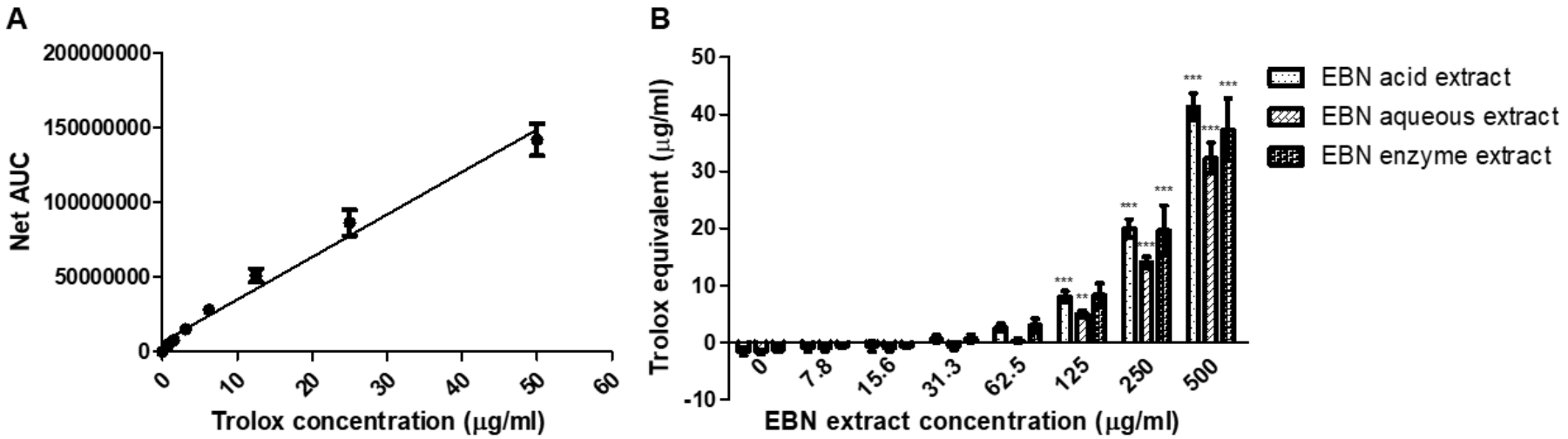

Figure 4.15: Oxygen radical absorbance capacity (ORAC) assay. (A) Trolox calibration curve, which was used to interpolate the antioxidant capacity of EBN extracts (B) Oxygen radical absorbance capacity of EBN acid, aqueous and enzyme extracts. Data are mean ± SEM; ** $p<0.01$, *** $p<0.001$. n = 3 independent experiments, each with three technical replicates.

4.4.2.3 Dichloro-dihydro-fluorescein diacetate (DCFH-DA) assay

The DCFH-DA assay is a cell-based method for detecting reactive oxygen species (ROS). Quercetin, employed as a positive control, demonstrated robust cellular antioxidant activity (CAA), ranging from 17 % to 83 % across concentrations of 0.39 µg/ml to 12.5 µg/ml (Figure 4.16A). Among the EBN extracts tested, the acid and aqueous extracts showed high CAA, with the acid extract ranging from 13 % to 52 % at concentrations of 125 µg/ml to 1000 µg/ml, and the aqueous extract ranging from 13 % to 34 % at concentrations of 250 µg/ml to 1000 µg/ml. In contrast, the enzyme extract exhibited no detectable CAA (Figure 4.16B).

Given the consistent antioxidant properties demonstrated by EBN acid extract in DPPH, ORAC, and DCFH-DA assays, its effects were further assessed in LKO1 cells. Quercetin displayed strong CAA, ranging from 17 % to 83 % at concentrations of 0.39 µg/ml to 12.5 µg/ml (Figure 4.17A). The EBN acid extract similarly exhibited significant antioxidant activity, ranging from 11 % to 75 % across concentrations of 62.5 µg/ml to 1000 µg/ml, with no significant differences in activity observed among WT, mock, and LKO1 cells (Figure 4.17B).

Building on the significant antioxidant effects demonstrated by EBN acid extract in DPPH, ORAC, and DCFH-DA assays, further functional assays were performed to evaluate its effects on LKO1 cells, which possess cancer stem cell-like properties. These assays, chosen for their relevance to potential disruptions caused by LRRK2 loss, include:

i. Cell proliferation assay
ii. Autophagy detection assay

iii. Assessment of mitochondrial respiration

LKO1 was hypothesised to possess cancer stem cell-like properties, whereas LKO2 and LKO3 resembled therapy-induced senescent cells and exhibited very slow or negligible growth. Given the unexpected shift in research direction toward evaluating the potential pro- or anti-cancer effects of EBN, LKO1 was therefore the most appropriate model, while LKO2 and LKO3 were not suitable for this purpose.

4.4.3 Cell proliferation assay

The cell proliferation assay was performed using the PrestoBlue cell viability reagent, a resazurin-based, cell-permeable solution that leverages the reducing power of viable cells to quantitatively assess cell proliferation. When added to the cells, the reagent is modified by the reducing environment of the viable cell, turns red and is highly fluorescent. In this assay, mock cells exhibited a significant, concentration-dependent increase in proliferation, reaching a maximum viability of 131 % following treatment with 1000 µg/ml EBN acid extract for 72 hours. Similarly, LKO1 cells showed a significant increase in proliferation, achieving 124 % at 500 µg/ml and 132 % at 1000 µg/ml. In contrast, WT cells demonstrated no significant increase in proliferation at any tested concentration of EBN acid extract (Figure 4.18).

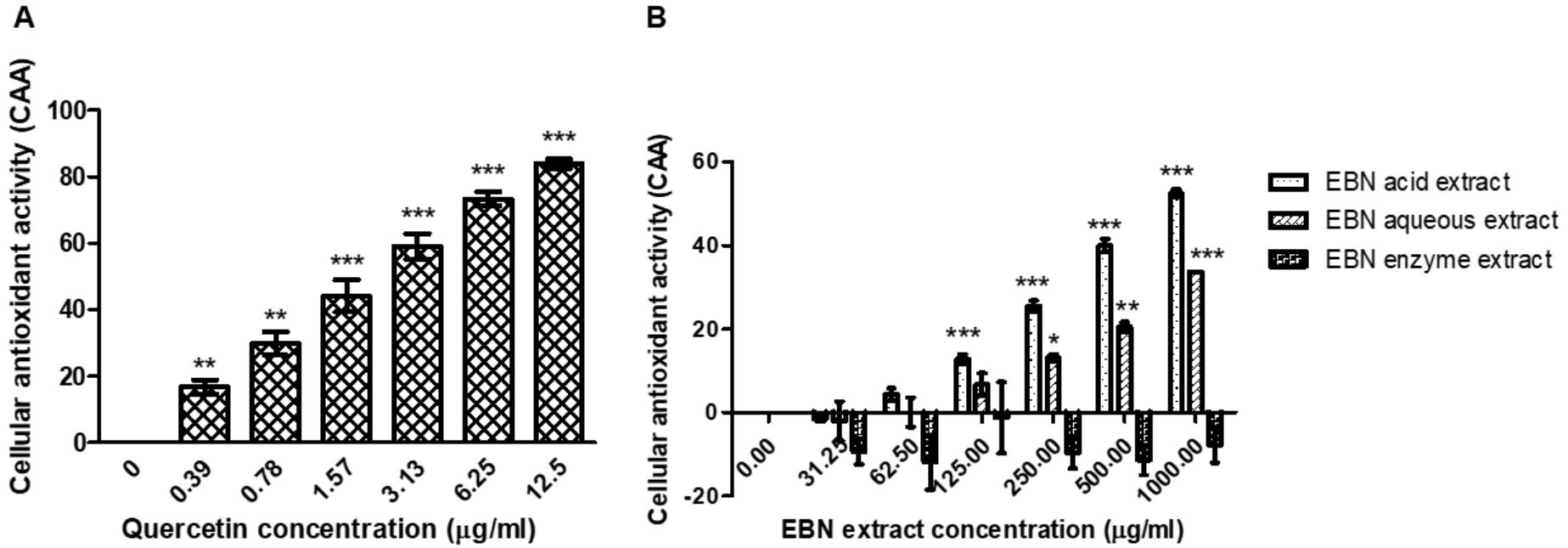

Figure 4.16: Cellular antioxidant activity of (A) quercetin and (B) EBN acid, aqueous and enzyme extracts in WT cells. Data are mean ± SEM; * P<0.05, ** P<0.01, *** P<0.001. n = 3 independent experiments, each with three technical replicates.

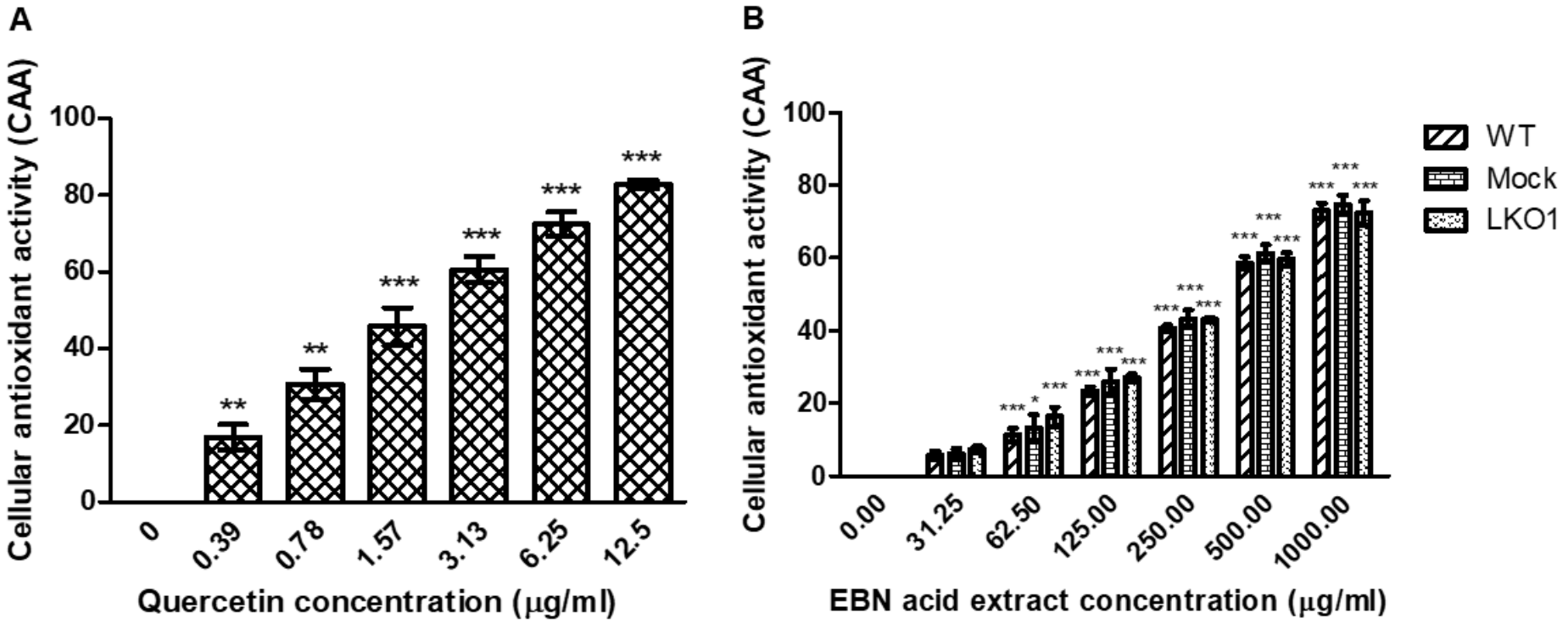

Figure 4.17: Cellular antioxidant activity of EBN acid extracts in WT, mock and LKO1 cells. Data are mean ± SEM; * P<0.05, ** P<0.01, *** P<0.001. n = 3 independent experiments, each with three technical replicates.

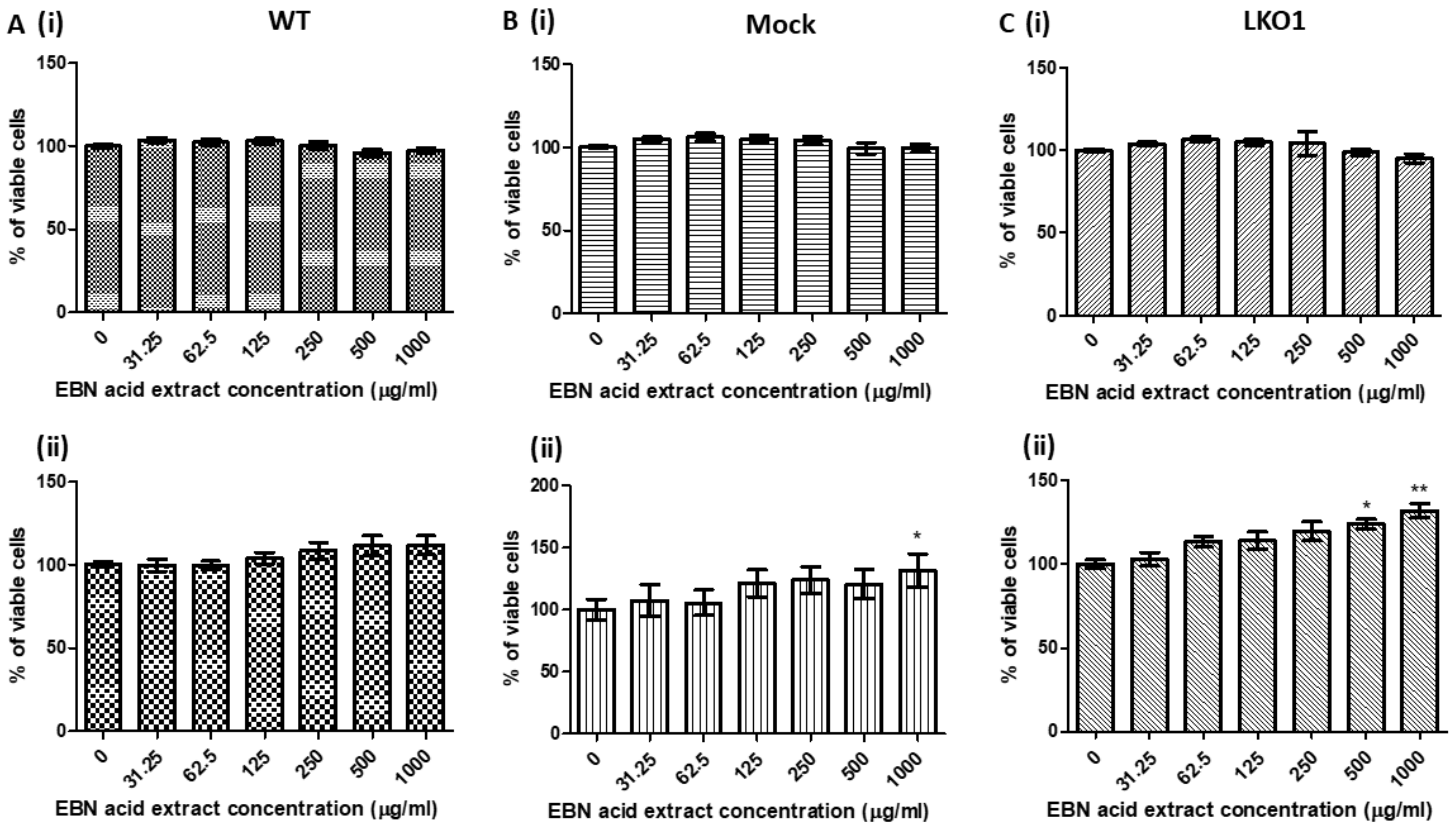

Figure 4.18: Assessment of cell proliferation in (A) WT, (B) mock and (C) LKO1 cells (i) pre- and (ii) post-EBN acid extract treatment.

Data are mean ± SEM; * P<0.05, ** P<0.01. n = 3 independent experiments, each with three technical replicates.

4.4.4 Autophagy detection assay

Autophagy is a dynamic process; thus, the accumulation of autophagosomes may indicate either increased autophagosome formation or impaired conversion to autolysosomes. Chloroquine, used as a positive control in this study, inhibits autophagosome clearance, leading to their accumulation. Treatment with 10 µM chloroquine for 18 hours significantly increased the percentage of autophagy vacuoles in mock and LKO1 cells. Similarly, a significant increase in autophagy vacuoles was observed in mock and LKO1 cells treated with 1000 µg/ml EBN acid extract alone or in combination with 10 µM chloroquine (Figure 4.19).

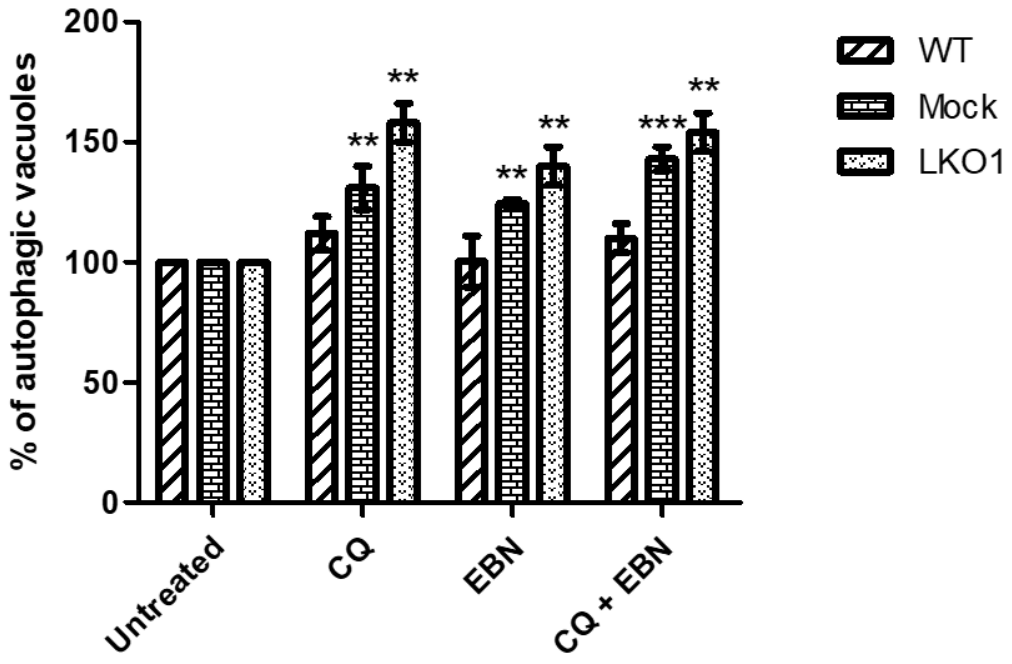

Figure 4.19: Measurement of autophagic vacuoles in WT, mock and LKO1 cells, without and with EBN acid extract treatment. Data are mean ± SEM; ** P<0.01, *** P<0.001. n = 3 independent experiments, each with three technical replicates.

4.4.5 Assessment of mitochondrial respiration

Mitochondrial respiration in untreated and 1000 μg/ml EBN acid extract-treated WT, mock, and LKO1 cells was evaluated by comparing their bioenergetic profiles, including the oxygen consumption rate (OCR) (Figure 4.20A) and extracellular acidification rate (ECAR) (Figure 4.20I). No significant differences were observed in any group, i.e. WT, mock, or LKO1, with or without 72 hours of treatment with 1000 μg/ml EBN acid extract.

Similarly, other parameters, including spare respiratory capacity, basal respiration, maximal respiration, proton leak, non-mitochondrial oxygen consumption, ATP production-coupled respiration, and coupling efficiency, showed no significant changes with or without treatment across all groups (Figures 4.21B–H). Additionally, the energy map revealed no differences between treated and untreated WT, mock, and LKO1 cells (Figure 4.20J).

Figure 4.20: Evaluation of mitochondrial function in WT, mock and LKO1 cells after EBN acid extract treatment. Assessment of (A) mitochondrial respiration, (B) spare respiratory capacity, (C) basal respiration, (D) maximal respiration, (E) proton leak, (F) non-mitochondrial oxygen consumption, (G) ATP-production coupled respiration, (H) percentage of coupling efficiency, (I) extracellular acidification rate and (J) energy map in WT, mock and LKO1 cells, with and without EBN acid extract treatment. n = 3 independent experiments, each with three technical replicates.

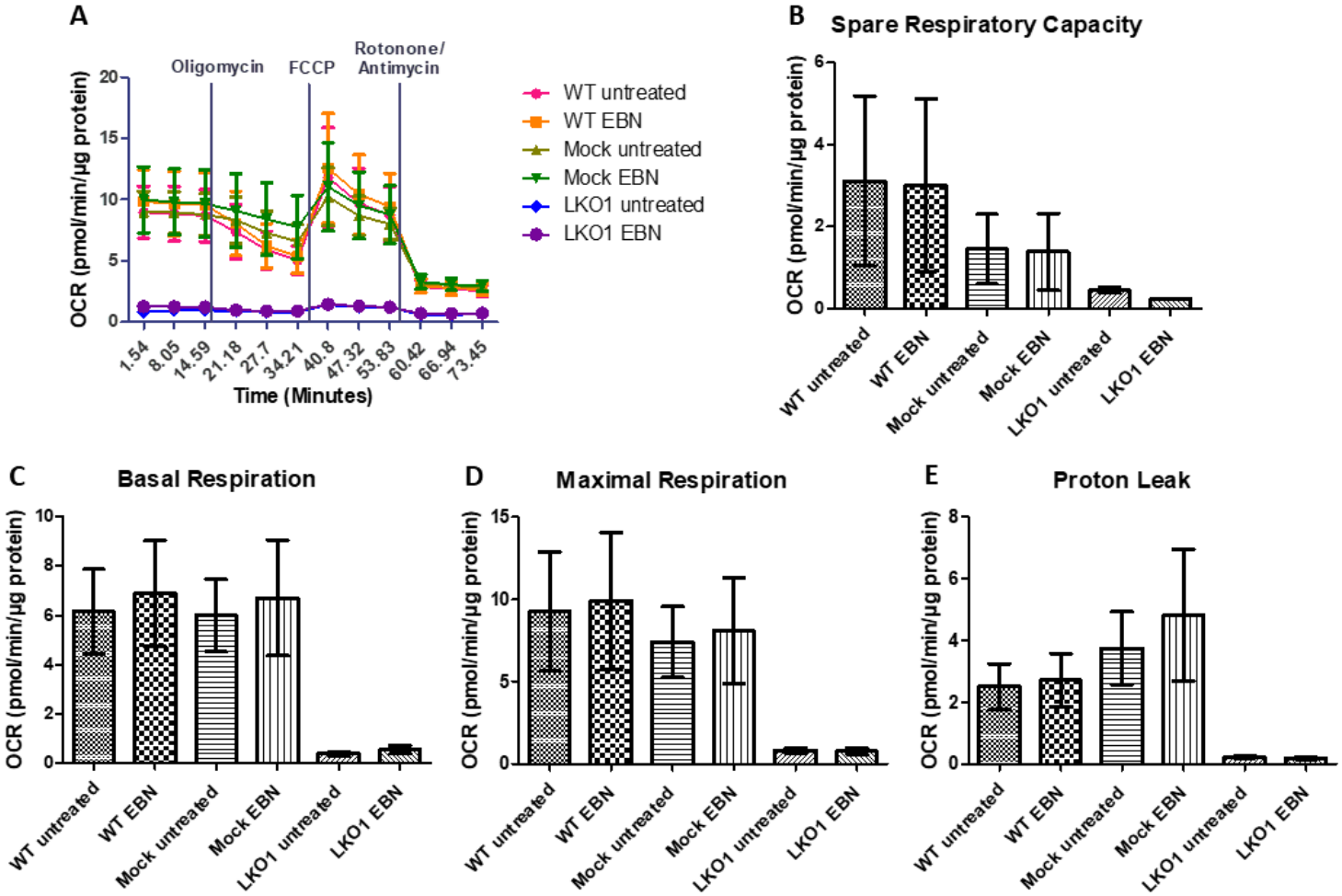
A
Oligomycin
FCCP
Rotonone/
Antimycin
OCR (pmol/min/µg protein)
Time (Minutes)
1.54
8.05
14.59
21.18
27.7
34.21
40.8
47.32
53.83
60.42
66.94
73.45
WT untreated
WT EBN
Mock untreated
Mock EBN
LKO1 untreated
LKO1 EBN
B
Spare Respiratory Capacity
C
Basal Respiration
D
Maximal Respiration
E
Proton Leak

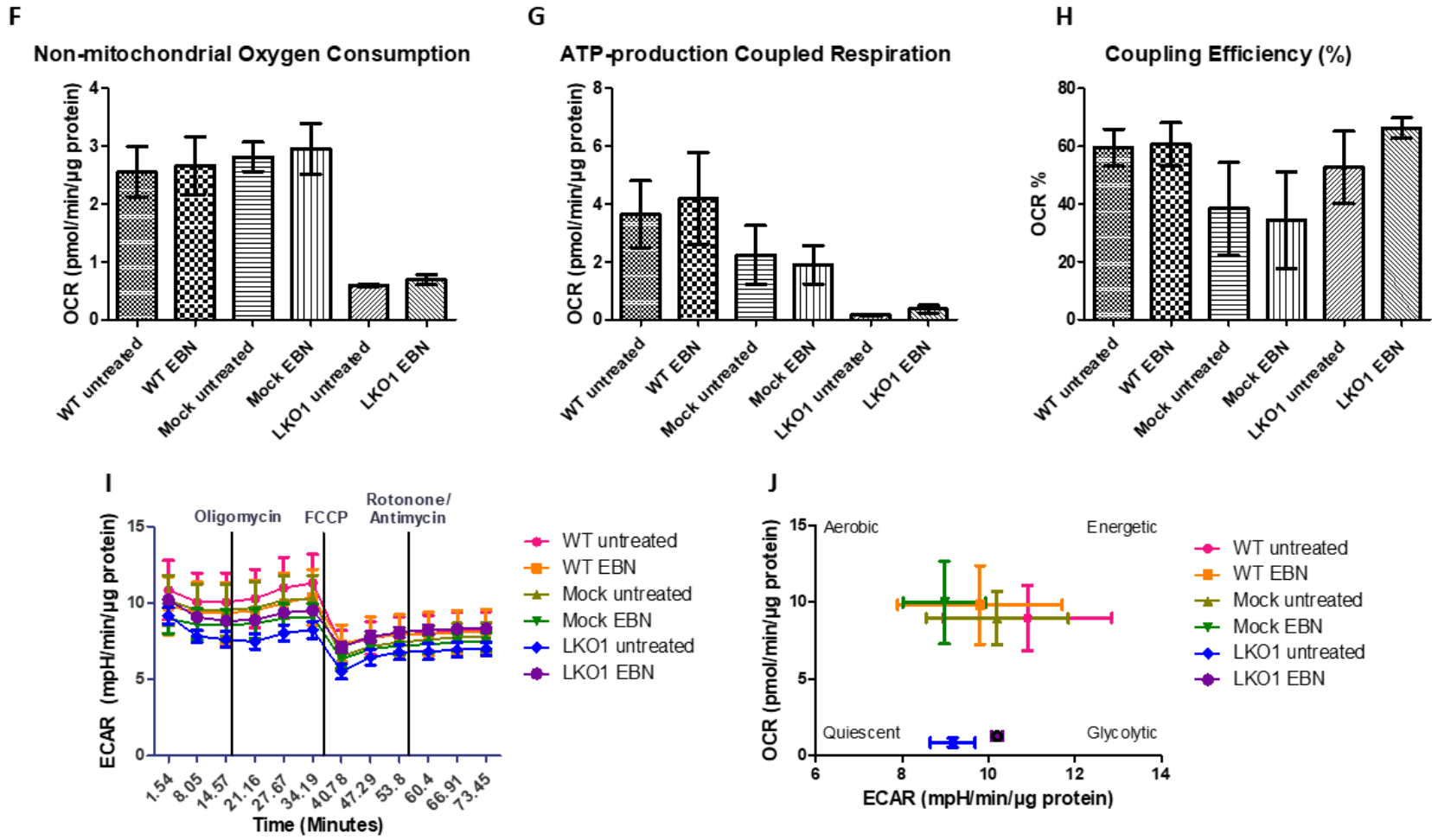
F
Non-mitochondrial Oxygen Consumption
OCR (pmol/min/µg protein)
WT untreated
WT EBN
Mock untreated
Mock EBN
LKO1 untreated
LKO1 EBN
G
ATP-production Coupled Respiration
OCR (pmol/min/µg protein)
H
Coupling Efficiency (%)
OCR %
I
Oligomycin
FCCP
Rotonone/
Antimycin
ECAR (mpH/min/µg protein)
Time (Minutes)
J
Aerobic
Energetic
Quiescent
Glycolytic
OCR (pmol/min/µg protein)
ECAR (mpH/min/µg protein)

CHAPTER 5.0

DISCUSSION

This study aimed to generate, validate, and characterise an LRRK2 knockout SH-SY5Y neuroblastoma model and to investigate the effects of edible bird's nest (EBN) extracts using this model. CRISPR/Cas9-mediated knockout of LRRK2 was successfully achieved, the model was validated, and its cellular characteristics were defined. The study outcomes were organised into three sections, each summarised by a corresponding graphical abstract (Figures 1.1-1.3).

The initial research questions focused on whether LRRK2 knockout induces deleterious cellular effects and whether EBN extracts could ameliorate these effects by exerting neuroprotective actions on dopaminergic neurons differentiated from LRRK2 knockout SH-SY5Y cells. Contrary to expectations, the LRRK2 knockout SH-SY5Y (LKO) cells exhibited pronounced and unanticipated phenotypic changes, transitioning from a neuronal (N-type) phenotype to intermediate (I-type) or substrate-adherent/Schwannian (S-type) neuroblastoma subtypes.

This phenotypic shift prompted a reassessment of the study's direction and raised concerns regarding the biological effects of EBN extracts. EBN extracts were evaluated for potential pro-proliferative effects, particularly in the context of neuroblastoma tumour relapse following chemotherapy. This concern was further supported by the possibility that the LKO1 cell line may possess stem

cell-like properties, which could enhance tumour aggressiveness or treatment resistance.

Consequently, the original hypothesis that EBN extracts would ameliorate LRRK2 knockout-associated neuronal dysfunction was revised. The findings instead support a new working hypothesis that EBN extracts may exert pro-cancer effects under certain cellular contexts, underscoring the importance of evaluating their safety and biological activity in disease-relevant cancer models.

5.1 An optimised protocol and strategy for low-expression *LRRK2* gene knockout using CRISPR/Cas9

With many countries experiencing a growing proportion of ageing populations, there is a pressing need for effective management, and, if possible, a cure, for age-related diseases, including Parkinson's disease (PD). To date, no treatment has been effective in halting or slowing the progression of PD. In 2022, Denali Therapeutics and Biogen announced the initiation of Phase 2b (LUMA study) and Phase 3 (LIGHTHOUSE study) clinical trials for DNL151, an LRRK2 kinase inhibitor (Biogen, 2022a, Biogen, 2022b, U.S. National Library of Medicine, 2024, U.S. National Library of Medicine, 2025b). Is LRRK2 kinase inhibition a viable and long-anticipated treatment for PD? The literature to date shows conflicting evidences. Numerous studies have reported detrimental effects associated with LRRK2 knockout (Gu *et al.*, 2023, Ness *et al.*, 2013, Baptista *et al.*, 2013, Tong *et al.*, 2012, Lee *et al.*, 2007, Hinkle *et al.*, 2012, Pellegrini *et al.*, 2018, Tong *et al.*, 2010). However, some studies have demonstrated that LRRK2 kinase inhibitors, such as PF-06447475, GNE-7915, PFE-360 and MLi-2, could be promising treatments for PD without adverse

pathological indications in the kidney, lung and liver (Andersen *et al.*, 2018, Baptista *et al.*, 2020a, Daher *et al.*, 2015, Ho *et al.*, 2022). The mechanisms underlying the adverse effects observed in LRRK2 knockout animals remain incompletely understood. To address this gap, the current study aims to generate an LRRK2 knockout cell line, a useful tool for elucidating the mechanisms underlying the adverse effects associated with LRRK2 loss, and to investigate its interaction with a natural product, extracts of edible bird's nest.

The present study employed an innovative genome-editing technology, CRISPR/Cas9, to generate the LRRK2 knockout model. By harnessing the cellular intrinsic double-strand break repair pathways, CRISPR/Cas9 permits precise and stable alterations to the genome (Moon *et al.*, 2019, Lander, 2016). Owing to its high specificity, efficiency, accessibility, and versatility, CRISPR/Cas9 has become a powerful tool for diverse genetic studies and applications (Moon *et al.*, 2019). CRISPR/Cas9 has proven effective in manipulating genes across varying expression levels, including those expressed at low levels (DeleuzeSoler and Andrieu-Soler, 2024). Although genes such as *LRRK2* present challenges due to their limited impact on observable cellular phenotypes, CRISPR/Cas9 provides a reliable method for achieving targeted and precise genetic modifications. However, several parameters in the protocol, including the design of gRNAs, delivery of gRNAs into the target cells and detection methods, must be meticulously optimised.

A critical step in genome editing is the design of gRNAs. Effective gRNAs warrant high specificity while maintaining robust editing efficiency. In the present study, a double-cut strategy with multiple gRNAs was adopted to achieve a successful knockout of the low-expression *LRRK2* gene (Yuen *et al.*, 2017).

Consistent with previous studies, this approach enables highly efficient gene knockout. The dual gRNAs strategy has been shown to exert synergistic effects in generating knockout clones, outperforming the conventional single gRNA method. When the two gRNAs target sequences are close, ideally within 40 to 300 base pairs, the indel frequency is significantly increased, with allele editing efficiencies reaching up to 95% in most cases. Furthermore, this approach facilitates efficient gene knockout in primary cells, such as T cells, which are typically challenging to manipulate due to their limited proliferative capacity in culture (Joberty *et al.*, 2020). The efficiency of dual gRNAs was further demonstrated in the editing of homoeologous soybean genes. Soybeans, being allotetraploid, are recognised as one of the difficult-to-transform crops. Dual gRNAs guided Cas9 to cleave two sites 1 kb apart, effectively generating double homozygous mutations in the *GMFAD2-1A* and *GmFAD2-1B* genes (Do *et al.*, 2019). In addition, the co-packaging of tandem gRNAs with single-stranded annealing-based surrogate reporter cassettes into CRISPR/Cas9 vectors was shown by Liu *et al.* to enhance gene editing efficiency by up to 6.31-fold (Liu *et al.*, 2018). To enhance editing efficiency, the current study utilised three gRNAs instead of the commonly used two, resulting in three potential double cuts. To the best of our knowledge, this approach has not been described in previous studies.

Transfection is the process of introducing foreign nucleic acids, such as DNA or RNA, into cells. Generally, there are two main types of transfection methods: chemical (cationic lipid-based reagents) and physical (electroporation). Each method has distinct advantages and disadvantages, and none is universally applicable to all cell types or experimental conditions (Fus-Kujawa *et al.*, 2021,

ChongYeap and Ho, 2021). Therefore, the choice of the most suitable transfection method should be based on the specific needs of the study. Transfection optimisation must be rigorously carried out to ensure high delivery efficiency of nucleic acids into the cells while minimising cell death. SH-SY5Y, the cell line used in the present study, is one of the recognised hard-to-transfect cell lines (Yin *et al.*, 2014). It becomes even more challenging when the CRISPR/Cas9 plasmids to be delivered into SH-SY5Y cells are large. After the failure of the attempts with chemical transfection methods, electroporation was chosen. Electroporation involves the application of high-voltage electric pulses to cells, resulting in temporary and reversible disruptions of the cell membrane. This transient increase in membrane permeability facilitates the efficient delivery of plasmids into the cells (Fus-Kujawa *et al.*, 2021). Three key parameters for electroporation, i.e. pulse voltage, pulse width and pulse number, were optimised using the Neon Transfection System. Maximising electroporation efficiency often requires compromising cell viability, and vice versa (SkruberRead and Vitriol, 2021). In the present study, electroporation efficiency was prioritised over cell viability, as the primary goal was to ensure the successful delivery of CRISPR/Cas9 plasmids into SH-SY5Y cells. High electroporation efficiency increases the likelihood that a significant proportion of SH-SY5Y cells will effectively take up the CRISPR/Cas9 plasmids, which is critical for achieving successful knockout in hard-to-transfect cells. A lower cell viability rate is an acceptable trade-off, as generating knockout clones in actively proliferating cells may only require a small number of viable cells. These viable cells are expected to proliferate post-transfection and can then undergo downstream clonal expansion and screening.

Clonal expansion is a critical and arduous step in the genome editing workflow. It starts with the isolation of a single cell from a population of edited cells, followed by its subsequent expansion to generate a homogenous cell population (Bernhard *et al.*, 2022). Commonly used methods for isolation of clones include fluorescent-activated cell sorting (FACS), limiting dilution, and clonal picking. These methods can be combined to enrich the culture with the desired cell population (Martin, 2011). Many cell lines, including SH-SY5Y cells, face challenges in surviving as single cells *in vitro*. These challenges are further compounded in the present study, where the edited SH-SY5Y cells underwent several stresses prior to clonal expansion, including electroporation, extended duration outside the CO_2 incubator, and FACS. To address these challenges, which could hinder cell proliferation during clonal expansion, both bulk and single-cell sorting methods were employed. Bulk sorting involved sorting 100 or 200 cells into a 15 ml conical tube, followed by transfer to a 10 cm dish. In contrast, single-cell sorting involved sorting individual cells into single wells of a 96-well plate. The optimised clonal expansion approach used in this study, i.e. bulk sorting of cells, followed by clonal picking in a 10 cm dish, effectively increased cell proliferation. This improvement is likely attributed to the presence of supportive signals or growth factors from surrounding cells and enhanced cell-cell interactions and communications within the bulk-sorted population, which facilitate cell attachment to the culture vessels and promote cell proliferation (Li *et al.*, 2023, Jiao *et al.*, 2017, Kovalevich and Langford, 2013a).

The detection of low-abundance proteins by Western blot is a well-known challenge. LRRK2, the protein of interest in this study, is a low-abundance protein (Uhlén *et al.*, 2015, Schapansky *et al.*, 2014, Tong *et al.*, 2010).

Nevertheless, Western blotting needs to be performed to confirm the ablation of the LRRK2 protein to verify its absence following genome editing. A previous study demonstrated that the challenge of detecting LRRK2 protein by Western blotting is compounded by the combination of a poorly expressed transcript and an unusually large, seemingly unstable protein, despite LRRK2 being highly soluble (Biskup *et al.*, 2007). Several key steps of the Western blot technique were optimised in the present study to ensure the successful detection of LRRK2 protein in SH-SY5Y cells. Sample preparation is an important yet often overlooked step in Western blotting. High-abundance proteins in whole-cell lysates can interfere with the detection of low-abundance proteins. To improve detection sensitivity, low-abundance proteins are typically enriched and used as an alternative to whole-cell lysates. Common methods for enriching low-abundance proteins include immunoprecipitation and the use of spin columns or fractionation kits (Bass *et al.*, 2017, GhoshGilda and Gomes, 2014). In the present study, the whole-cell lysate was concentrated by using the minimum amount of lysis buffer and the maximum number of cells. This approach proved effective, eliminating the need for additional enrichment methods. Furthermore, it allowed for the loading of more protein onto the gel, despite the limited volume that can be loaded per well. Another critical step in Western blotting is the separation and transfer of proteins, particularly those at both ends of the molecular weight spectrum (Bass *et al.*, 2017, SuleRivera and Gomes, 2023). In this study, LRRK2 is a relatively large protein (286 kDa) while GAPDH, the loading control for normalisation in Western blotting, is a small protein with a molecular weight of 44 kDa. The separation and transfer process becomes even more challenging when both LRRK2 and GAPDH are present on the same gel.

To overcome this, a gradient gel was employed, providing excellent separation of proteins across a broader molecular weight range (SuleRivera and Gomes, 2023). Additionally, the percentage range of the gradient gel was optimised to ensure the optimal resolution of both proteins. Following protein separation on the gel, the proteins were transferred to the PVDF membrane. To ensure complete transfer of the large LRRK2 protein without over-transferring the small GAPDH protein, Coomassie blue and Ponceau S staining were performed on the gel and membrane, respectively, after the overnight transfer. Coomassie blue is typically used to confirm the presence of proteins on the gel, while Ponceau S is employed to verify protein transfer to the PVDF membrane before proceeding to blocking and antibody incubation steps. It was confirmed that no significant amounts of large proteins remained on the Coomassie blue-stained gel. Additionally, both large and small proteins were detected on the Ponceau S-stained membrane. Therefore, the transfer was successful for both LRRK2 and GAPDH proteins. If the transfer of either protein is suboptimal, various parameters of the transfer process, such as voltage, transfer duration, and methanol percentage, may need to be further optimised (Bass *et al.*, 2017). A well-characterised or validated antibody is crucial for Western blotting to ensure the reproducibility of findings (Pillai-Kastoori *et al.*, 2020, Pauly and Hanack, 2015). The antibody used in this study was sourced from a reputable provider and is a highly specific and knockout-validated antibody widely employed by researchers in the LRRK2 research field. To confirm its reliability, the A549 cell line, known for its high LRRK2 protein levels, was used as a positive control. As expected, the A549 cell line exhibited a distinct protein band at the correct molecular weight.

Detection is the final, and one of the most important, steps in the Western blotting workflow. Chemiluminescent detection, a highly sensitive method, relies on enzymatic reactions to generate detectable signals. However, due to the dynamic nature of these reactions, signal intensity can fluctuate over time. Therefore, careful selection of an appropriate chemiluminescent substrate, along with optimisation of both reaction duration and the imaging process, is essential to ensure reliable and reproducible results (MathewsPlaisance and Kim, 2009). In the present study, to maximise signal detection for the low-abundance LRRK2 protein, a highly sensitive chemiluminescent substrate from a reputable manufacturer, capable of detecting proteins at the femtogram level, was employed. In addition, the reaction duration was optimised. The imaging system utilised was equipped with a high-resolution CCD camera, and capture parameters were refined accordingly. Specifically, the cumulative capture mode was used, enabling the integration of signals from multiple exposures to produce a final image with enhanced intensity. Following the optimisation of all the critical steps in the Western blotting protocol, the LRRK2 protein band was successfully detected with a strong and distinct signal.

5.2 Phenotypic changes in LRRK2 knockout cells

Numerous studies have emphasised that LRRK2 plays a crucial role in regulating cytoskeletal organisation and dynamics, suggesting that its disruption can affect neurite outgrowth and branching, vesicle trafficking (Civiero *et al.*, 2018, WallingsManzoni and Bandopadhyay, 2015), and neurite process morphology (MacLeod *et al.*, 2006, Chan *et al.*, 2011). Most previous studies

have shown that overexpression of wild-type LRRK2 (HeoKim and Seol, 2010, Stafa *et al.*, 2012) or expression of pathogenic variants such as G2019S (Lin *et al.*, 2020, Stormo *et al.*, 2022, Pattanayak *et al.*, 2024), R1441C (Cherra *et al.*, 2013, Verma *et al.*, 2017), R1441G (Lavalley *et al.*, 2016, Cho *et al.*, 2013) and I2020T (Maekawa *et al.*, 2012), leads to neurite process shortening. Conversely, LRRK2 knockout or inhibition is typically associated with enhanced neurite outgrowth. However, a few studies have reported the opposite. For instance, Chan *et al.* found that LRRK2 knockdown significantly reduced neurite length in differentiated SH-SY5Y neuroblastoma cells (Chan *et al.*, 2011). Similarly, Meixner *et al.* reported that LRRK2 knockdown induced morphological alterations and neurite process shortening in both embryonic mouse fibroblasts and dopaminergic midbrain primary neurons (Meixner *et al.*, 2011). Additionally, Chen *et al.* observed that LRRK2 loss caused dendritic atrophy and expedited nuclear and somatic hypertrophy in spiny projection neurons during ageing (Chen *et al.*, 2020c). The observations in my study are consistent with these less common findings. Loss of LRRK2 in SH-SY5Y neuroblastoma cells impaired neurite length: LKO1 cells displayed a few short neurites, while LKO2 and LKO3 cells lacked neurites entirely.

LKO cells exhibited slower proliferation compared to WT and mock cells. This observation is consistent with previous studies showing that downregulation of LRRK2 impairs the proliferation of various cancer cell types, including thyroid cancer (Jiang *et al.*, 2019, Looyenga *et al.*, 2011), papillary renal carcinoma (Looyenga *et al.*, 2011), lung cancer (Wu *et al.*, 2023) and clear cell renal cell carcinoma (Yang *et al.*, 2021). Post-transcriptional regulation of LRRK2 has also been shown to influence cancer cell proliferation. For example, Zhao *et al.*

demonstrated that silencing the long non-coding RNA RP11-476D10.1 inhibited the proliferation of papillary thyroid carcinoma cells through microRNA-138-5p-dependent suppression of LRRK2. In contrast, knockdown of the long non-coding RNAs LINC00707 and LINC01133 was reported to suppress LRRK2 expression while upregulating microRNA-382-5p and microRNA-205, respectively, thereby promoting the proliferation of ovarian cancer cells (ZhaoLin and Qiu, 2023, LiuShen and Wang, 2019). Beyond its role in cancer, loss of LRRK2 has also been linked to impaired neuronal cell proliferation. Tong *et al.* reported that LRRK2 deficiency induced apoptotic cell death in aged mice (Tong *et al.*, 2010), while Milosevic *et al.* observed a reduction in dopaminergic neurons due to apoptosis in LRRK2-deficient samples (Milosevic *et al.*, 2009). LRRK2 is known to participate in several signalling pathways involved in cell proliferation (WallingsManzoni and Bandopadhyay, 2015), including the mitogen-activated protein kinase (MAPK) pathway (Chen *et al.*, 2012, Gloeckner *et al.*, 2009, Hsu *et al.*, 2010), Wingless (Wnt) signalling pathway (SanchoLaw and Harvey, 2009, Berwick and Harvey, 2012, PurroGalli and Salinas, 2014) and the mesenchymal-epithelial transition (MET) signalling pathway (Looyenga *et al.*, 2011). Therefore, the reduced growth observed in LKO cells in the current study may result from LRRK2 loss, which could disrupt key proliferative signalling pathways or activate apoptotic mechanisms.

To date, no direct association has been reported between LRRK2 and cell size or cell-substrate adhesion strength. However, as previously discussed, a link between LRRK2 and cytoskeletal dynamics has been established. Interestingly, the reduced or absent neurites, enlarged and flattened morphology, along with increased cell size and adhesion strength, as well as reduced cell growth,

observed in LKO cells closely resemble characteristics typical of I-type (intermediate) and S-type (substrate-adherent or Schwannian) neuroblastoma cells.

The heterogeneity of neuroblastoma cell lines, derived from patient tumours, has been recognised since their establishment over five decades ago. In culture, neuroblastoma cells exhibit diverse morphologies, prompting the characterisation of each distinct cell type (BiedlerHelson and Spengler, 1973, RossSpengler and Biedler, 1983). Generally, three main types are identified: neuroblastic (N-type), substrate-adherent or Schwannian (S-type), and intermediate (I-type). Numerous studies have been conducted to explain the heterogeneity of neuroblastoma cell lines, and thus far, two main theories have been proposed. The first and most widely accepted theory is that of spontaneous interconversion, originally proposed by Ross *et al.* following the establishment of the SH-SY5Y cell line. This theory posits three key possibilities: 1) I-type cells, which exhibit stem cell-like properties, have the potential to differentiate into both N-type and S-type cells; 2) bidirectional conversion can occur between S-type and N-type cells; 3) I-type cells may serve as transitional intermediates during the interconversion between N-type and S-type cells (RossSpengler and Biedler, 1983, Ciccarone *et al.*, 1989). On the other hand, a second theory, proposed by Cohen *et al.* in 2003, suggests that neuroblastoma heterogeneity results from clonal expansion. In culture, N-type and S-type cells coexist, but under certain conditions, the slower-growing S-type cells may outcompete and eventually dominate the faster-proliferating N-type cells (Cohen *et al.*, 2003). Historically, neuroblastoma cells were primarily classified based on two criteria: 1) cell size, the nuclear/cytoplasmic volume ratio, and adhesiveness; and 2) the

presence, number, and length of cellular processes (Ciccarone *et al.*, 1989). However, with recent advances in technology, transcriptomic and epigenetic profiling have been employed to classify these interconverted cell types. Specifically, N-type and S-type cells are now classified as adrenergic (ADRN) and mesenchymal (MES) cells, respectively (D'Amico *et al.*, 2023, VeschiVerona and Thiele, 2019, van Groningen *et al.*, 2019, Gartlgruber *et al.*, 2021).

In this study, although direct evidence linking LRRK2 to the phenotypic shift of neuroblastoma cell types is lacking, the phenotypic similarities between LKO cells and I-type or S-type cells, such as reduced or absent neurites, enlarged and flattened morphology, increased cell size and adhesion strength, and decreased cell growth, support our postulation: LKO cells may have arisen from the conversion of N-type cells into I-type (LKO1) or S-type (LKO2 and LKO3) cells, potentially driven by transcriptional or epigenetic changes resulting from the loss of LRRK2. It is unlikely that the phenotypes observed in the LKO cells arose from adaptation during clonal expansion, stress induced by genome editing or electroporation, or clonal selection, despite these procedures being part of the LKO cells establishment process. This interpretation is supported by the observation that mock cells, which were subjected to the same genome editing, electroporation, clonal expansion, and clonal selection procedures, retained the N-type morphology characteristic of wild-type (WT) cells. The morphology of LKO cells was confirmed to resemble either S- or I-type cells (Robert A. Ross, communication, 2024; Appendix B).

The WT and mock cells in the present study exhibited characteristics typical of N-type cells. They displayed multiple long, fine neurite processes with scant

cytoplasm, had low cell-substrate adhesion, loosely adherent cell bodies, and formed cell aggregates. Moreover, these cells demonstrated a higher proliferation rate than the LKO cells. Earlier research has shown that N-type cells are characterised by long and abundant cellular processes (neurites) and exhibit neuronal marker enzyme activities, such as tyrosine hydroxylase and dopamine beta-hydroxylase. Neurofilament proteins are also detected in N-type cells. These cells are homogeneous in culture, displaying morphological uniformity, loosely adhering to the substrate, growing rapidly, and demonstrating clonogenic potential in soft agar as well as tumorigenic properties (Ciccarone *et al.*, 1989, BiedlerHelson and Spengler, 1973, RossSpengler and Biedler, 1983, La Quaglia and Manchester, 1996, Walton *et al.*, 2004).

The LKO1 cells displayed characteristics resembling those of I-type cells. Previous studies have shown that I-type cells are heterogeneous, varying in the presence and length of cellular processes. For example, SH-IN cells lack processes, while some clones, such as BE (2)-C, may exhibit occasional long processes, and others, like LA1-22n/i, display numerous long processes. These cells are typically flattened with scant cytoplasm, moderately adhere to the substrate, and are immortal (Ciccarone *et al.*, 1989, BiedlerHelson and Spengler, 1973, RossSpengler and Biedler, 1983, La Quaglia and Manchester, 1996, Walton *et al.*, 2004). Consistent with the morphology described in these studies, the LKO1 cells are flattened, have few short neurites, and exhibit moderate adhesion.

On the other hand, earlier research has shown that S-type cells are heterogeneous, exhibiting significant differences between clones. Their morphology can range from epithelial-like, with no distinct directional orientation, to fibroblast-like,

with cells growing in swirling patterns. S-type cells are slow or extremely slow growers, with some clones ceasing to proliferate. They adhere tightly to the substrate, lack cellular processes, appear flattened with abundant cytoplasm, and display a sail-like shape. Furthermore, S-type cells exhibit characteristics commonly associated with Schwann cells or melanocytes, such as tyrosinase activity and the expression of fibronectin, vimentin, and type IV collagen (Ciccarone *et al.*, 1989, BiedlerHelson and Spengler, 1973, RossSpengler and Biedler, 1983, La Quaglia and Manchester, 1996, Walton *et al.*, 2004). The expression of fibronectin, vimentin, and collagen likely contributes to the enhanced adhesion strength of S-type cells. Both LKO2 and LKO3 displayed features resembling those of S-type cells, including enlargement, flattening, abundant cytoplasm, lack of neurites, strong substrate adhesion, and growth as a monolayer. Additionally, LKO2 proliferated very slowly, while LKO3 nearly ceased proliferation.

Cellular senescence is a phenomenon in which cells undergo irreversible growth arrest in response to various intrinsic and extrinsic stresses, including telomere shortening, oxidative stress, oncogene activation, mitochondrial dysfunction, impaired autophagy and epigenetic alterations. The accumulation of senescent cells leads to various detrimental effects, such as chronic inflammation, tissue dysfunction, and loss of homeostasis, which in turn accelerate the ageing process (MaErb and Moore, 2025, Mylonas and O'Loghlen, 2022). Although it was postulated that LKO cells may have undergone conversion into I- or S-type cells, the observed phenotypic changes, such as enlarged and flattened morphology, increased cell size and cell-substrate adhesion strength, and reduced growth rate, also closely resembled features of cellular senescence. This raised uncertainty as

to whether conversion had occurred prior to the onset of senescence. To address this, senescence-associated β-galactosidase (SA-β-gal) staining, the gold standard for detecting cellular senescence, was performed. The results confirmed that senescence had indeed occurred in the LKO cells. A previous study by Cimmino *et al.* demonstrated that long-term treatment with all-*trans* retinoic acid, in combination with hypoxia-inducible factors HIF1-α (*HIF1A* gene) and HIF2-α (*EPAS1* gene) silencing, induced transdifferentiation of neuroblastoma cells from N-type to S-type and triggered senescence (Cimmino *et al.*, 2015). Consistent with Cimmino *et al.*'s findings, it was observed that LKO2 and LKO3 cells (S-type) displayed a significantly higher percentage of SA-β-gal-positive cells compared to WT and mock cells (N-type). Additionally, Yang *et al.* reported that LRRK2 may regulate the *HIF1A* gene and influence the survival of patients with clear cell renal cell carcinoma (ccRCC). Specifically, knockdown of *LRRK2* reduced the proliferation of ccRCC tumour cell lines (Yang *et al.*, 2021). This observation aligns with the findings in this study, where LKO cells exhibited reduced or minimal proliferative capacity, a hallmark of cellular senescence.

Based on these findings, it is suggested that the knockout of LRRK2 may have triggered an initial conversion of N-type cells into I-type (LKO1) or S-type (LKO2 and LKO3), followed by entry into a senescent state. Given that senescence was confirmed by SA-β-gal staining, autophagy and mitochondrial respiration, two cellular processes known to be affected both by LRRK2 loss and during senescence, were subsequently assessed.

Several studies have reported that LRRK2 is involved in the regulation of autophagy (AlbaneseNovello and Morari, 2019). Literature has presented conflicting evidence on the role of LRRK2 in autophagy regulation. Treatment

of LRRK2 kinase inhibitors in H4 and SH-SY5Y cells was shown to stimulate autophagy (Manzoni *et al.*, 2013, Saez-Atienzar *et al.*, 2014). In addition, LRRK2 knockout mice showed progressive or biphasic enhancement of autophagic activity (Hinkle *et al.*, 2012, Tong *et al.*, 2012) and proteomic analysis revealed that LRRK2 deficiency resulted in the enrichment of proteins involved in lysosomal degradation (Pellegrini *et al.*, 2018). As opposed to the aforementioned findings, previous studies also demonstrated that loss of LRRK2 caused impairment of the autophagy-lysosomal pathway in aged LRRK2 knockout mice (Tong *et al.*, 2010) and silencing of LRRK2 kinase activity resulted in early glucocerebrosidase deregulation as well as late impairment of autophagy *in vivo* (Albanese *et al.*, 2021). It has been observed that autophagy is typically decreased in senescent cells. Previous studies have shown reduced autophagic flux in senescent neurons both *in vitro* and *in vivo* (Suelves *et al.*, 2023, Singh *et al.*, 2020, Tai *et al.*, 2017). The data from this study revealed a reduction in the number of autophagic vacuoles in LKO cells, consistent with previous reports showing impaired autophagy in the context of LRRK2 deficiency or cellular senescence. Interestingly, a comparable decrease was also observed in mock cells, although the underlying cause remains unclear. In the absence of autophagic flux assessment in the current study, the observed reduction in autophagic vacuoles represents an alteration in autophagy but does not allow discrimination between reduced autophagic vacuoles formation and enhanced autophagic vacuoles clearance. Therefore, future studies assessing autophagic flux will be required to clarify current findings. This could be achieved through the combined use of rapamycin, a mechanistic target of rapamycin complex 1 (mTORC1) inhibitor that induces autophagy, and

chloroquine, a lysosomal inhibitor that blocks autophagic vacuoles degradation. Together, these agents allow discrimination between altered autophagic vacuoles formation and defective degradation, enabling assessment of dynamic autophagic flux rather than static autophagic vacuoles levels.

Numerous lines of evidence demonstrate that LRRK2 plays a crucial role in the regulation of mitochondrial functions through its role in mitochondrial dynamics (Wang *et al.*, 2012, SinghZhi and Zhang, 2019, Su and Qi, 2013), quality control mechanisms (Williamson *et al.*, 2023, Singh and Ganley, 2021, Singh *et al.*, 2021), energy production (Papkovskaia *et al.*, 2012) and oxidative stress response (Niu *et al.*, 2012, Ilieva *et al.*, 2024). In the present study, LKO cells showed a significant reduction in ATP-production coupled respiration and coupling efficiency, which suggests impaired oxidative phosphorylation (OXPHOS) in LKO cells. This finding is in line with a previous study that reported that loss of LRRK2 leads to mitochondrial fragmentation and reduced OXPHOS activity (Mazaki *et al.*, 2023). Furthermore, Weindel *et al.* found that LRRK2 knockout macrophages exhibited defects in both OXPHOS and glycolysis (Weindel *et al.*, 2020). Additionally, the bioenergetic profile of LKO cells in this study concurs with findings from a previous study using telomere-ablated cells (an ageing model of SH-SY5Y), which revealed significant reductions in mitochondrial basal respiration, maximum respiration, and spare respiratory capacity (Kim *et al.*, 2017). This further corroborates the postulation that LKO cells may have entered a senescent state following the loss of LRRK2. In opposition to findings in other studies where senescent cells typically rely on glycolysis as an energy source due to impaired OXPHOS (Lee *et al.*, 2021b, Korolchuk *et al.*, 2017), glycolysis did not significantly increase in LKO cells as

compared to WT and mock. This suggests that LKO cells rely minimally, or not at all, on either OXPHOS or glycolysis for energy production. Future investigations could explore the alternative energy sources utilised by LKO cells.

While the initial goal of this study was to establish LKO cells as a valuable tool for elucidating the mechanisms underlying the detrimental effects of LRRK2 loss (Jong *et al.*, 2025), the LKO2 and LKO3 cells (S-type) characterised in this study may no longer be suitable for this purpose. This is due to the loss of neuronal characteristics in S-type cells, which compromises their capacity to differentiate into dopaminergic neurons. To date, no studies have reported the use of differentiation agents to induce the conversion of S-type cells into N-type cells. While S-type cells can undergo spontaneous differentiation into N-type cells, the efficiency of this process has not been quantitatively assessed or documented. In contrast, LKO1 cells (I-type) remain suitable for achieving the initial goal, as they retain the capacity to differentiate into N-type cells, which exhibit neuronal characteristics, as previously reported (Walton *et al.*, 2004, Ross *et al.*, 2015). Furthermore, N-type cells can be further directed to differentiate into dopaminergic neurons using differentiation agents such as retinoic acid, 12-O-tetradecanoylphorbol-13-acetate (TPA) or phorbol-12-myristate-13-acetate (PMA) (IoghenCeafalan and Popescu, 2023, Avola *et al.*, 2018).

However, following the establishment of the LKO cell lines, subsequent works were guided by the availability of institutional resources and facilities. Given that LKO1 cells (I-type) are actively proliferating, unlike LKO2 and LKO3, which are not, downstream experiments were conducted using LKO1 cells. Within the time frame and practical considerations of this study, LKO1 cells

were utilised as a model of cancer stem cells, as I-type cells are known to exhibit stem cell-like properties.

In contrast to the findings of the current study, which demonstrate that LRRK2 knockout induces senescence, previous studies have reported that LRRK2 activation, particularly in pathogenic/ risk variants such as G2019S (HoSeol and Son, 2019) and R1627P (Yang *et al.*, 2024), promotes senescence in neuronal cells. Ho *et al.* showed that activation of the p53-p21 pathway triggered senescence in differentiated SH-SY5Y cells, leading to impaired protein degradation and increased accumulation of α-synuclein aggregates (HoSeol and Son, 2019). More recently, they also demonstrated that MLi-2 reduced senescence and α-synuclein secretion in rotenone-treated human dopaminergic progenitor cells (Ho *et al.*, 2025). Consistent with these findings, Yang *et al.* found that the R1627P mutation accelerated senescence in rats by disrupting the Golgi-lysosome signalling pathway (Yang *et al.*, 2024). As reduced cell proliferation is a hallmark of senescence, it is noteworthy that while LRRK2 pathogenic/ risk variants induce senescence and LRRK2 inhibition can attenuate it in neuronal cells, other studies have shown that LRRK2 knockout suppresses proliferation in various cancer cell types, including thyroid cancer (Jiang *et al.*, 2019, Looyenga *et al.*, 2011), papillary renal carcinoma (Looyenga *et al.*, 2011), lung cancer (Wu *et al.*, 2023), and clear cell renal cell carcinoma (Yang *et al.*, 2021). However, suppression of proliferation in neuroblastoma cells following LRRK2 knockout has not been previously reported. Therefore, the current finding that LRRK2 knockout induces senescence in SH-SY5Y neuroblastoma cells is both novel and represents the first report of its kind.

Cellular senescence has long been described as a tumour-suppressor mechanism and has been harnessed for cancer treatment (SchmittWang and Demaria, 2022, WangLankhorst and Bernards, 2022). Therapy-induced senescence-based treatments, including the use of low doses of hydroxyurea, tumour necrosis factor-alpha, interferon-gamma, and metronomic topotecan, have been studied in neuroblastoma (Narath *et al.*, 2007, Harmuth *et al.*, 2019, Taschner-Mandl *et al.*, 2015). A previous study identified a unique mechanism of cell cycle arrest that governs the decision between differentiation and senescence in neuroblastoma cells. It was shown that rapid inhibition of cyclin D-dependent kinases by retinoic acid in neuroblastoma cells leads to early cell cycle arrest, impedes neuronal differentiation, and induces a senescence-like state (WainwrightLasorella and Iavarone, 2001). Therefore, understanding the mechanisms that regulate the differentiation and senescence of neuroblastoma cells is crucial. Such insights are important for developing targeted treatments aimed at manipulating differentiation or senescence to slow tumour progression and improve treatment outcomes for neuroblastoma patients (ZeineldinPatel and Dyer, 2022).

Although LKO2 and LKO3 cells (both are converted to S-type) are not suitable to be utilised as cell models for neurodegeneration or PD research, their conversion provides valuable insights for neuroblastoma studies. Given that S-type cells are slow-growing, with some clones even ceasing proliferation and exhibiting non-tumorigenic properties, these findings suggest that LRRK2 knockout could potentially serve as a maintenance strategy to reduce the risk of relapse in highly aggressive neuroblastoma. However, as demonstrated in this study, LRRK2 knockout may not result in a complete conversion of N-type cells

into S-type; rather, some cells may convert into I-type, which are likely to evade immune surveillance and may exhibit enhanced malignancy. Further investigation is warranted to elucidate the mechanisms governing the conversion of N-type cells into I- or S-type phenotypes following LRRK2 loss.

5.3 Effects of EBN extracts

Edible bird's nest (EBN) is one of the most expensive animal products consumed by humans, particularly within the Chinese community across various countries, including China, Malaysia, Singapore, Taiwan and North America. Its popularity has also spread to the Middle East, Korea and Japan recently. China stands as the largest importer of EBN, while Indonesia, Malaysia, and Thailand are the top three exporters in Southeast Asia (Zulkefle *et al.*, 2024, Daud *et al.*, 2021). Numerous studies have highlighted the health benefits of EBN, leading to extensive scientific investigations into the key components responsible for these benefits. Proximate analysis revealed that the main constituents of EBN include proteins, carbohydrates, minerals, lipids, and ash. Notably, glycoproteins, particularly sialic acid, have been recognised for their neuroprotective properties, garnering significant attention (Unal *et al.*, 2024, Lee *et al.*, 2021a, Unal *et al.*, 2022, Ling *et al.*, 2022).

To investigate the beneficial effects of EBN, the choice of EBN extraction method is crucial, as each method offers distinct advantages and disadvantages in terms of efficiency, yield, extraction duration, metabolite content, and cost (Unal *et al.*, 2024, Ling *et al.*, 2022). Several methods for preparing EBN extracts have been reported, including heat extraction, solvent extraction, acid

or alkaline extraction, enzymatic hydrolysis, and microwave- or ultrasound-assisted extraction methods (Daud *et al.*, 2021, Tong *et al.*, 2020, Mohamad Nasir *et al.*, 2021). The extraction methods used in the present study aim to simulate the preparation or digestion of EBN as it occurs in the human body, thereby accurately reflecting the bioactive metabolites available upon consumption.

The acid extract was prepared using sulphuric acid to simulate the denaturation of glycoproteins in EBN by hydrochloric acid in the stomach. This method was adapted from Oda *et al.*, who used it to extract neutral monosaccharides from EBN (Oda, 1983). Extraction of EBN with hydrochloric acid necessitates neutralisation with sodium hydroxide to obtain a neutral pH extract suitable for downstream assays. However, neutralising with sodium hydroxide results in the formation of sodium chloride, which is water-soluble and would remain in the extract, potentially interfering with downstream assays. In contrast, neutralising sulphuric acid with barium hydroxide forms barium sulphate, which is insoluble in water and can be separated from the extract by centrifugation, while also being non-toxic. Therefore, sulphuric acid and barium hydroxide were selected in this study as alternatives to the commonly used hydrochloric acid (Kong *et al.*, 1987, VimalaHussain and Nazaimoon, 2012, NorhayatiAzman and Nazaimoon, 2010) and sodium hydroxide (Aswir and Wan Nazaimoon, 2011). This acid extraction method is more cost-effective than enzymatic hydrolysis, as acids and alkalis are cheaper than enzymes. However, it is more time-consuming than aqueous extraction methods due to the additional neutralisation and centrifugation steps. This method was anticipated to yield significantly more than the aqueous extraction method. However, the yield in the present study was relatively low,

likely due to insufficient acid concentration and inadequate incubation time. In this study, 0.4 M sulphuric acid was used with a 4-hour incubation period. In contrast, previous studies employed 4 M hydrochloric acid or acetic acid with a 4-hour incubation time, accompanied by shaking the reaction mixture at 50 rpm for EBN extraction (Napavichayanun *et al.*, 2021). Another study used 2 M acetic acid and a 4-hour incubation period for extracting sialic acid from red meats, including beef, pork, lamb, and rabbit (Ling *et al.*, 2022). To date, no report has focused on optimising sulphuric acid for the EBN extraction protocol to obtain the best yield, along with comprehensive bioactive metabolite profiles and functional validation of their beneficial activities. This represents a significant research gap that warrants further investigation.

The aqueous extract was prepared by heating in a water bath, simulating the traditional double-boiling method used to prepare EBN for consumption (Marcone, 2005, Daud *et al.*, 2021). The slow and gentle heating process effectively loosened the glycoprotein structure in the EBN. The selection of optimal temperature for the heating process is crucial, as high temperature may destroy the metabolites in the EBN. Conversely, lower temperatures could not effectively uncoil the glycoprotein in EBN (Unal *et al.*, 2024). As indicated in previous studies, the commonly used heating temperature ranges from 80 to 100 °C (Kong HangKinWong KaHing and ChunLap, 2016, Daud *et al.*, 2021, Zainal Abidin *et al.*, 2011, Unal *et al.*, 2024). Consistent with these studies, EBN was heated at 80 °C in the present study. This aqueous extraction method is relatively simple, with a shorter extraction duration, and is cost-effective, but its efficiency and yield are low.

The enzyme extract was prepared using pancreatin to simulate the digestion of EBN by pancreatic enzymes in the human body. The enzymatic activity breaks down long glycoprotein chains, releasing shorter peptides with lower molecular weights, which exhibit enhanced solubility and absorption, thereby improving bioactivity. Various enzymes, including alcalase, bromelain, pancreatin, papain, and pepsin, have been used for EBN extraction. Among these, pancreatin is the most commonly used, likely due to its composition of amylase, lipase, and protease, which together provide more efficient digestion of glycoproteins in EBN (RamachandranBabji and Sani, 2018, MuhammadBabji and Ayub, 2015, Yew *et al.*, 2014, Yew *et al.*, 2018, Haghani *et al.*, 2017, Haghani *et al.*, 2016, Guo *et al.*, 2006). Therefore, pancreatin was chosen for the present study. This enzyme hydrolysis method is the most efficient of the three tested, yielding the highest output. However, it is also more expensive (due to the cost of the enzyme) and time-consuming.

Complementary and alternative medicine (CAM) refers to healthcare systems, practices, or products that are not typically part of conventional medical treatment. Common forms of CAM include traditional Chinese medicine, dietary supplements, specialised diets, traditional Malay medicine, and Ayurvedic medicine. Many cancer patients use CAM to enhance their immunity, alleviate pain, and reduce complications caused by the disease or its treatment side effects. Additionally, some cancer patients use CAM alongside conventional treatments to adopt a more holistic approach to managing their disease, while others turn to CAM for its potential anti-cancer effects (ShihChiang and Chan, 2009, National Cancer Institute USA, 2024).

EBN, traditionally used to boost immunity and surrounded by controversy regarding its anti-cancer benefits, has become one of the popular CAMs among cancer patients (Wong *et al.*, 2010, ShihChiang and Chan, 2009, Lim *et al.*, 2006). Recent scientific findings support the traditional use of EBN to enhance immunity (Dobutr *et al.*, 2022, Zeng *et al.*, 2022, Dobutr *et al.*, 2023, Fan *et al.*, 2021b) and its application as adjuvant therapy to reduce the side effects of chemotherapy (Zhao *et al.*, 2016). However, EBN has also been reported to promote cell growth in various cell types (Roh *et al.*, 2012, Zainal Abidin *et al.*, 2011, Chua *et al.*, 2013, Albishtue *et al.*, 2018b). This raises the question: Given the potential risk that EBN may promote cancer cell growth, is it appropriate to consider EBN as a CAM for cancer patients, despite its potential immunity-boosting benefits? To explore this, the present study evaluates the effects of EBN extracts on LKO1 cells, which exhibit cancer stem cell-like properties.

Building on previous studies that had consistently demonstrated the antioxidant properties of EBN extracts (MuhammadBabji and Ayub, 2015, Quek *et al.*, 2018b, Ali *et al.*, 2019, Yew *et al.*, 2014, Yida *et al.*, 2015a, Murugan *et al.*, 2020, Yew *et al.*, 2018, Careena *et al.*, 2018, Napavichayanun *et al.*, 2021), this study first investigated the antioxidant properties of EBN acid, aqueous, and enzyme extracts before exploring their other potential beneficial effects. A variety of chemical-based methods have been employed to evaluate the antioxidant properties of natural products or compounds, which can be categorised into two main types: 1) assays based on hydrogen atom transfer (HAT), such as the ORAC (oxygen radical absorbance capacity) assay, and 2) assays based on electron transfer (ET), including the DPPH (2,2-diphenyl-1-picrylhydrazyl) free radical scavenging assay, the ABTS (2,2′-azino-bis (3-ethylbenzothiazoline-6-sulphonic

acid)) assay, and the FRAP (ferric reducing antioxidant power) assay. No single method is sufficient on its own, as antioxidants may act through various mechanisms. Therefore, a combination of methods is typically employed to comprehensively assess the antioxidant properties of natural products or compounds (Danet, 2021, Dudonne *et al.*, 2009).

In the present study, three antioxidant assays were conducted: 1) the DPPH assay (ET assay), 2) the ORAC assay (HAT assay), and 3) the DCFH-DA assay (cell-based assay). Unlike the previously described chemical-based assays, the DCFH-DA assay offers the advantage of reflecting antioxidant activity within cells by simulating cellular processes such as uptake, distribution, and metabolism (Zhang *et al.*, 2020). In the DPPH assay, the EBN acid extract exhibited free radical scavenging activity, while the aqueous and enzyme extracts did not. Interestingly, all three EBN extracts (acid, aqueous, and enzyme) demonstrated significant peroxyl radical scavenging activity in the ORAC assay. Unlike the DPPH assay, the ORAC assay accounts for the kinetic action of antioxidants, which may explain the discrepancy between the results obtained from the two assays.

In a preliminary study using the DCFH-DA assay, both the acid and aqueous extracts exhibited high cellular antioxidant activity (CAA) in WT cells, while the enzyme extract showed no detectable CAA. Given that the EBN acid extract consistently demonstrated antioxidant activity across all three assays (DPPH, ORAC, and DCFH-DA), its effects were further tested in both mock and LKO1 cells, where a similarly high CAA was observed. Although both the ORAC and DCFH-DA assays consider the kinetic action of antioxidants, the DCFH-DA assay also reflects biological processes within cells, but not the ORAC assay.

This distinction likely explains the differences observed between the results of the ORAC and DCFH-DA assays. A previous study has shown that LRRK2 knockout HEK293 cells exhibit resistance to oxidative stress, mitochondrial damage and apoptosis induced by rotenone (Quintero-Espinosa *et al.*, 2023). In this study, no significant differences in antioxidant activity were observed among WT, mock, and LKO1 cells, as assessed by the DCFH-DA assay. This may be attributed to the relatively subtle effects of EBN acid extracts in the absence of pre-induced cellular stress (e.g., rotenone treatment). Future studies could explore the use of oxidants or other stressors prior to EBN acid extract treatment to better assess potential antioxidant responses.

As EBN acid extract demonstrated consistent and significant antioxidant effects, functional assays were conducted to evaluate its impact on LKO1 cells, which exhibit cancer stem cell-like properties. The functional assays were chosen for their relevance to potential disruptions caused by LRRK2 loss, including the cell proliferation assay, the autophagy detection assay and the assessment of mitochondrial respiration.

Previous studies have demonstrated that EBN enhances the proliferation of various normal cells, including human-derived adipose stem cells (Roh *et al.*, 2012), rabbit corneal keratocytes (Zainal Abidin *et al.*, 2011), human chondrocytes (Chua *et al.*, 2013), B- and T-lymphocytes (Dobutr *et al.*, 2022, Zhao *et al.*, 2016), mouse fibroblast (L929) (Napavichayanun *et al.*, 2021), human keratinocytes (Wang *et al.*, 2024a, Terazawa and Shimoda, 2020), human fibroblasts (Terazawa and Shimoda, 2020) as well as cancer cells such as human colorectal adenocarcinoma cells (Caco2) (Aswir Abd Rashed and Wan Nazaimoon, 2010), human neuroblastoma cells (SH-SY5Y and SK-N-MC) and

rat pheochromocytoma (PC-12) (Rashed *et al.*, 2021). While cancer cells typically serve as cell models for specific diseases in EBN research, such as SH-SY5Y and SK-N-MC as neuronal cell models, and Caco2 as a model for the intestinal system, the increased proliferation observed in these cells might indicate that EBN could potentiate similar effects in cancer cells in patients. Conversely, the enhancement of normal cell proliferation by EBN suggests beneficial effects in many aspects, such as wound healing (e.g. skin), tissue regeneration (e.g., eye and bone) and immune system boosting.

In line with previous studies, the EBN acid extract in the present study stimulated the proliferation of both mock and LKO1 cells, but not WT cells. The significant increase in cell proliferation may be attributed to the presence of mitogenic or growth-stimulating factors in EBN acid extract, including sialic acid (Rashed *et al.*, 2021, Aswir and Wan Nazaimoon, 2011), epidermal growth factor (EGF) (Zainal Abidin *et al.*, 2011, Terazawa and Shimoda, 2020), and vascular endothelial growth factor (VEGF) (Roh *et al.*, 2012, Albishtue *et al.*, 2018a, Albishtue *et al.*, 2018b). Sialic acid is the most abundant glycoprotein in edible bird's nests (EBN) and is well-recognised for its essential role in brain function and development (Liu *et al.*, 2023a, Ling *et al.*, 2022). In addition to promoting cell proliferation, recent studies on EBN have highlighted many therapeutic benefits of sialic acid, including its antiviral, neuroprotective, antihypertensive, antioxidant, anti-inflammatory, and prebiotic properties (Unal *et al.*, 2024, Ling *et al.*, 2022). As a result, the quantification of sialic acid content has become a crucial criterion for EBN authentication, as well as for evaluating its quality and grading (Ling *et al.*, 2022, Chan *et al.*, 2013, Zulkefle *et al.*, 2024). EGF, another key growth-stimulating factor found in EBN, is a well-known mitogenic agent.

It is recognised for its ability to stimulate the proliferation, differentiation and migration of various cell types, particularly epithelial cells and fibroblasts (Wong and Guillaud, 2004, Bai *et al.*, 2023). VEGF was initially described as a vascular endothelial cell-specific mitogen. However, studies indicated that its growth-promoting ability is not limited to endothelial cells, but extended to other non-endothelial cells such as keratinocytes, macrophages and renal mesangial cells (DuffyBouchier-Hayes and Harmey, 2000 - 2013). Despite numerous studies reporting the proliferative effects of EBN, two studies suggest that EBN does not stimulate cell proliferation in cancer cells. Tan *et al.* and Roh *et al.* postulated that this may be due to several factors: 1) the protein and EGF extraction from EBN may be insufficient to release all relevant bioactive substances, 2) the relatively low levels of EGF in EBN, 3) there is only 36% amino acid sequence similarity between human EGF and avian EGF (Tan *et al.*, 2020), and 4) the proliferative effects of EBN may be limited to normal cells, rather than cancer cell lines such as MCF7 and Hep2B (Roh *et al.*, 2012).

To date, only a limited number of studies have explored the effects of EBN on autophagy. To the best of our knowledge, only one study has reported that EBN inhibits intracellular autophagy during the influenza virus A life cycle. The enzyme extract of EBN was shown to reduce LC3-II levels, thereby enhancing lysosomal degradation (Haghani *et al.*, 2017). For the first time, this study demonstrates that EBN promotes autophagy in cancer cells, specifically in LKO1 cells, a neuroblastoma cell line exhibiting cancer stem cell-like properties following LRRK2 knockout. LKO1 cells, which were postulated to undergo senescence, showed a reduction in autophagy. However, treatment with EBN acid extracts resulted in enhanced autophagy in these cells. This observation

suggests that EBN may facilitate LKO1 cells, possessing cancer stem cell-like properties, to escape senescence and progress as more aggressive cancer cells, as evidenced by increased cell proliferation and autophagy. These results align with previous studies showing enhanced autophagy flux in breast and lung cancer cells that escaped chemotherapy-induced senescence (Bojko *et al.*, 2020, Evangelou *et al.*, 2023, Olszewska *et al.*, 2022, Dudkowska *et al.*, 2021). Autophagy was enhanced to degrade and recycle damaged organelles, misfolded proteins and cellular debris, thereby meeting the heightened metabolic demands of aggressive cancer cells that had escaped senescence (ErenpreisaSalmina and Cragg, 2017). Furthermore, the use of a pharmacological autophagy inhibitor was shown to block this escape (Olszewska *et al.*, 2022). In line with these findings, the present study suggests that LKO1 cells, exhibiting cancer stem cell-like properties, may undergo metabolic shifts, converting to a more aggressive phenotype following EBN treatment.

Thus far, there is a limited study on the effects of EBN on mitochondrial function. A previous study by Yew *et al.* found that EBN extracts did not improve mitochondrial membrane potential in SH-SY5Y cells challenged with the neurotoxin 6-hydroxydopamine (6-OHDA) (Yew *et al.*, 2014). Consistent with this, our study also showed no significant increase in mitochondrial respiration following EBN treatment. In contrast, a separate study by Rashed *et al.* reported that sialic acid extracted from EBN enhanced the number of active mitochondria in SH-SY5Y cells (Rashed *et al.*, 2021). This discrepancy may be attributed to the difference in the type of EBN extract used, i.e. our study employed a crude extract, whereas sialic acid was specifically extracted in their study. A previous study by Wong *et al.* indicated that sialic acid constitutes only about 10% of the

total dried weight of EBN (Wong *et al.*, 2018). As a result, the effects of the crude EBN extract in our study are likely less pronounced compared to the sialic acid extract used in the study by Rashed *et al.* In the current study, despite the upregulation of proliferation and autophagy (potentially including mitochondrial degradation through autophagy) following EBN treatment, mitochondrial respiration did not increase significantly. This is likely due to impaired mitochondrial turnover. Specifically, mitochondrial biogenesis may be compromised, leading to a reduced number of functional mitochondria (Li *et al.*, 2022, Liu *et al.*, 2023b). Mitochondrial turnover encompasses both the removal of damaged mitochondria through autophagy and the replenishment of new, functional mitochondria via mitochondrial biogenesis. A reduction in mitochondrial respiration may indicate that the remaining mitochondria are not functioning properly, possibly due to an insufficient or delayed replacement of dysfunctional mitochondria. Essentially, while damaged mitochondria are being cleared through autophagy, the replacement mitochondria may not be produced efficiently, resulting in overall reduced mitochondrial respiration, as reflected by the unchanged mitochondrial respiration observed in LKO1 cells following EBN treatment.

CHAPTER 6.0

CONCLUSION

6.1 Conclusions

Knocking out a gene with low endogenous expression is achievable, but it requires meticulous planning, as well as consideration of potential compensatory mechanisms and detection challenges. Recent advancements in genome-editing technologies and detection methods have made it increasingly feasible to study such difficult genes. The protocol established in this study offers a robust strategy for effectively knocking out the low-expression *LRRK2* gene in the hard-to-transfect neuroblastoma SH-SY5Y cells (Figure 6.1). Additionally, this approach can be easily adapted to target other low-expression genes in various challenging cell lines.

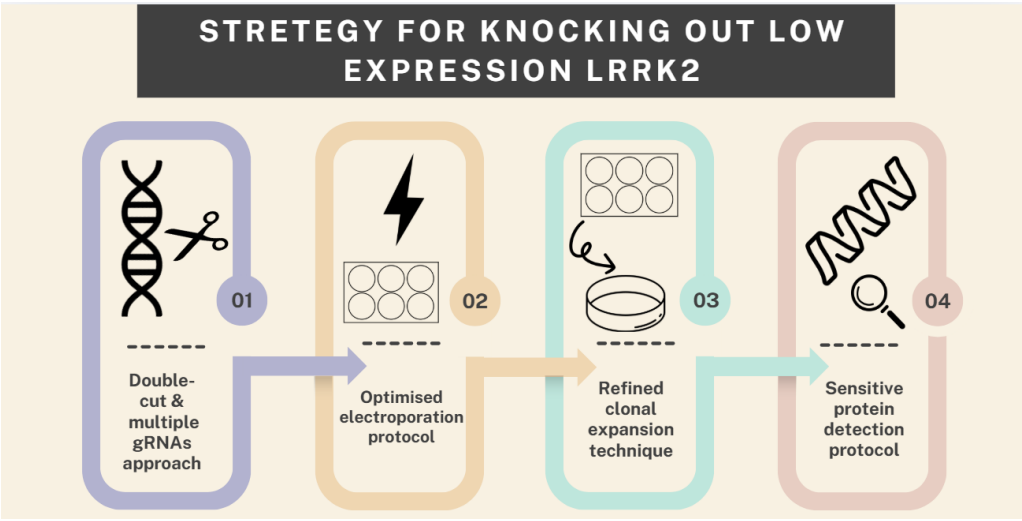

Figure 6.1: Schematic illustration of a strategy for knocking out low-expression LRRK2 in hard-to-transfect neuroblastoma SH-SY5Y cells

The loss of LRRK2 may drive the phenotypic transition from N-type to I- or S-type and induce senescence (Figure 6.2). Consequently, future studies using the SH-SY5Y neuroblastoma cell line as a model for PD should take this possibility into account. The findings of this study provide a novel perspective on the role of LRRK2 in the phenotypic shift of SH-SY5Y neuroblastoma cells and the induction of cellular senescence.

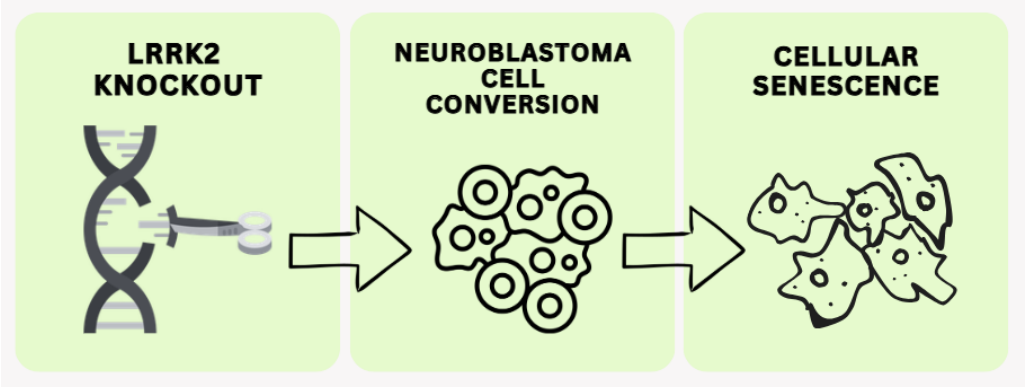

Figure 6.2: Schematic illustration of the effects of loss of LRRK2, which may promote phenotypic transitions from N-type neuroblastoma cells to I- or S-type cells, accompanied by the induction of cellular senescence

Among all the extracts tested, EBN acid extract demonstrated the highest and most consistent antioxidant effects. Treatment with EBN acid extract may allow LKO1 cells, which possess cancer stem cell-like properties, to evade senescence and progress into more aggressive cancer cells, as evidenced by increased cell proliferation and autophagy. Therefore, despite its antioxidant potential, EBN may not be an ideal choice for complementary and alternative medicine for cancer patients (Figure 6.3).

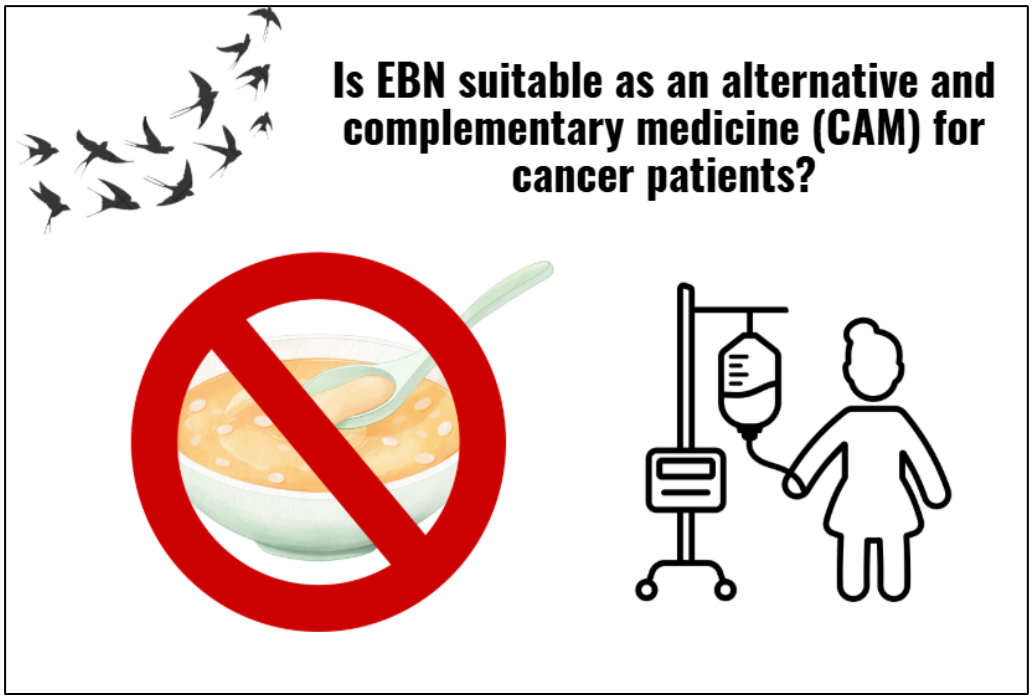

Figure 6.3: Diagrammatic model of the suitability of EBN as a complementary and alternative medicine for cancer patients

6.2 Limitations of the current study

The scope of the present study was limited by institutional facilities and resources, as well as funding and time constraints.

Although Sanger sequencing confirmed the absence of off-target mutations at the predicted off-target sites, whole-genome sequencing was not performed to comprehensively evaluate potential off-target effects of CRISPR/Cas9 genome editing. In addition, the potential compensatory effects of LRRK1 in LRRK2 knockout clones were not assessed.

Furthermore, rescue experiments were not conducted to determine whether the observed phenotypic changes were directly attributable to the loss of LRRK2. The LKO1 (I-type) and LKO2 and LKO3 (S-type) clones were also not validated

using previously reported subtype-specific markers, and the differentiation potential of LRRK2 knockout cells was not examined. With respect to cellular senescence, senescence in LRRK2 knockout cells was not characterised using a comprehensive panel of established senescence markers.

Pertaining to the EBN-related investigations, a more extensive analysis was not performed to complement the proliferation and autophagy findings of the present study in order to further elucidate the potential pro-cancer effects of EBN. In addition, metabolomic profiling of EBN extracts was not carried out to identify the bioactive compounds responsible for the observed pro-proliferative effects.

6.3 Future work

In future investigations, whole-genome sequencing could be performed to comprehensively assess potential off-target effects of CRISPR/Cas9 genome editing. In addition, potential compensatory effects of LRRK1 in LRRK2 knockout cells could be evaluated by quantifying LRRK1 mRNA expression using quantitative PCR or assessing protein levels by Western blotting with a well-validated LRRK1-specific antibody. These approaches would help determine whether LRRK1 functionally compensates for the loss of LRRK2.

Future research should also investigate transcriptional and epigenetic alterations following LRRK2 loss to gain deeper insight into its regulatory roles. Given the unexpected phenotypic changes observed after LRRK2 knockout, this study opens two promising avenues for further investigation. First, elucidating the role of LRRK2 in neuroblastoma phenotypic transitions and cellular senescence may improve understanding of neuroblastoma plasticity and identify potential therapeutic strategies, such as senescence induction to suppress tumour growth.

Second, exploring the role of LRRK2 in Parkinson's disease, particularly the potential adverse consequences of LRRK2 loss, represents another important direction. However, this will require prior validation of the LRRK2 knockout model through differentiation of LKO1 (I-type) cells into N-type cells and subsequently into dopaminergic neurons.

In the present study, rescue experiments were not performed. Future studies should include forced re-expression of LRRK2 in LKO cells to determine whether the observed phenotypic changes are directly attributable to LRRK2 loss. This approach would also help exclude the possibility that the observed effects arise from clonal variation rather than specific gene disruption. As an alternative strategy, pharmacological inhibition of LRRK2 kinase activity in wild-type cells using a selective inhibitor such as MLi-2 could be employed to assess whether similar phenotypic changes are induced. Inclusion of a kinase-dead LRRK2 variant would provide an important control, enabling discrimination between effects due to loss of kinase activity and those resulting from complete protein depletion.

In addition, LKO1 (I-type) and LKO2 and LKO3 (S-type) cells were not validated using previously reported subtype-specific markers. Future studies could confirm subtype identity by examining the expression of characteristic markers, such as stem cell-associated markers (e.g. CD133 and c-KIT) in LKO1 (I-type) cells, non-neuronal markers (e.g. fibronectin and tyrosinase) in LKO2 and LKO3 (S-type) cells, and neuronal markers (e.g. neurofilaments and dopamine β-hydroxylase) in wild-type (N-type) cells.

Moreover, the differentiation potential of LRRK2 knockout cells was not validated in the present study. Future work could assess the differentiation of I-type cells into N-type cells using retinoic acid, followed by further differentiation into dopaminergic neurons using agents such as 12-O-tetradecanoylphorbol-13-acetate (TPA) or phorbol-12-myristate-13-acetate (PMA).

Cellular senescence in LRRK2 knockout cells could also be further characterised using a panel of established senescence markers. As telomere attrition is a key hallmark of senescence, telomere length or telomerase activity could be assessed. To evaluate proliferative status, cell cycle analysis could be performed to confirm arrest in the G0/G1 phase. Alternatively, proliferation assays measuring Ki-67 expression or BrdU incorporation could be used. In addition, senescence-associated secretory phenotype (SASP) factors could be examined by quantifying pro-inflammatory cytokines in conditioned media.

Further studies are also required to elucidate the potential pro-cancer effects of EBN. More comprehensive analyses could complement the proliferation and autophagy findings of the present study, including cell cycle analysis, assessment of proliferation markers (e.g. Ki-67 and BrdU), and evaluation of autophagic flux with detection of autophagy-related markers such as LC3-II and p62. The senescence status of LRRK2 knockout cells following EBN treatment should also be assessed using established senescence assays to determine whether EBN promotes senescence evasion.

Finally, metabolomic profiling of EBN extracts could be performed to identify bioactive compounds responsible for the observed pro-proliferative effects.

Functional validation of these compounds, either individually or in combination, would provide mechanistic insight into how EBN supports cancer cell growth. Collectively, these investigations would be essential for determining the safety and suitability of EBN as a complementary and alternative medicine in oncology settings.

REFERENCES

Abdalla-Carvalho, C. B., Santos-Rebouças, C. B., Guimarães, B. C., Campos, M., Pereira, J. S., De Rosso, A. L., Nicaretta, D. H., Marinho E Silva, M., Dos Santos, M. J. and Pimentel, M. M. (2010) 'Genetic analysis of LRRK2 functional domains in Brazilian patients with Parkinson's disease', *Eur J Neurol.* 17**,** pp. 1479-81.

Agalliu, I., Ortega, R. A., Luciano, M. S., Mirelman, A., Pont-Sunyer, C., Brockmann, K., Vilas, D., Tolosa, E., Berg, D., Warø, B., Glickman, A., Raymond, D., Inzelberg, R., Ruiz-Martinez, J., Mondragon, E., Friedman, E., Hassin-Baer, S., Alcalay, R. N., Mejia-Santana, H., Aasly, J., Foroud, T., Marder, K., Giladi, N., Bressman, S. and Saunders-Pullman, R. (2019) 'Cancer outcomes among Parkinson's disease patients with leucine rich repeat kinase 2 mutations, idiopathic Parkinson's disease patients, and nonaffected controls', *Mov Disord.* 34**,** pp. 1392-1398.

Agalliu, I., San Luciano, M., Mirelman, A., Giladi, N., Waro, B., Aasly, J., Inzelberg, R., Hassin-Baer, S., Friedman, E., Ruiz-Martinez, J., Marti-Masso, J. F., Orr-Urtreger, A., Bressman, S. and Saunders-Pullman, R. (2015) 'Higher Frequency of Certain Cancers in LRRK2 G2019S Mutation Carriers With Parkinson Disease: A Pooled Analysis', *JAMA Neurology.* 72**,** pp. 58-65.

Ahmad, M. H., Fatima, M., Ali, M., Rizvi, M. A. and Mondal, A. C. (2021) 'Naringenin alleviates paraquat-induced dopaminergic neuronal loss in SH-SY5Y cells and a rat model of Parkinson's disease', *Neuropharmacology.* 201**,** pp. 108831.

Ahmadi Rastegar, D., Hughes, L. P., Perera, G., Keshiya, S., Zhong, S., Gao, J., Halliday, G. M., Schüle, B. and Dzamko, N. (2022) 'Effect of LRRK2 protein and activity on stimulated cytokines in human monocytes and macrophages', *npj Parkinson's Disease.* 8**,** pp. 34.

Albanese, F., Mercatelli, D., Finetti, L., Lamonaca, G., Pizzi, S., Shimshek, D. R., Bernacchia, G. and Morari, M. (2021) 'Constitutive silencing of LRRK2 kinase activity leads to early glucocerebrosidase deregulation and late impairment of autophagy in vivo', *Neurobiology of Disease.* 159**,** pp. 105487.

Albanese, F., Novello, S. and Morari, M. (2019) 'Autophagy and LRRK2 in the Aging Brain', *Frontiers in Neuroscience.* 13**,** pp. 1352-1352.

Albishtue, A. A., Yimer, N., Zakaria, M. Z. A., Haron, A. W., Babji, A. S., Abubakar, A. A., Baiee, F. H., Almhanna, H. K. and Almhanawi, B. H. (2019) 'The role of edible bird’s nest and mechanism of averting lead acetate toxicity effect on rat uterus', *Veterinary World.* 12**,** pp. 1013.

Albishtue, A. A., Yimer, N., Zakaria, M. Z. A., Haron, A. W., Yusoff, R. and Almhanawi, B. H. (2018a) 'Ameliorating effect of edible bird's nest against lead acetate toxicity on the rat hypothalamic–pituitary–ovarian axis and expressions of epidermal growth factor and vascular endothelial growth factor in ovaries', *Comparative Clinical Pathology.* 27**,** pp. 1257-1267.

Albishtue, A. A., Yimer, N., Zakaria, M. Z. A., Yusoff, R., Assi, M. A. and Almhanawi, B. H. (2018b) 'Edible bird's nest impact on rats' uterine histomorphology, expressions of genes of growth factors and proliferating cell nuclear antigen, and oxidative stress level', *Veterinary world.* 11**,** pp. 71.

Ali, A. a. M., Noor, H. S. M., Chong, P. K., Babji, A. S. and Lim, S. J. (2019) 'Comparison of amino acids profile and antioxidant activities between edible bird nest and chicken egg', *Malaysian Applied Biology.* 48**,** pp. 63-69.

Allegra, R., Tunesi, S., Cilia, R., Pezzoli, G. and Goldwurm, S. (2014) 'LRRK2-G2019S mutation is not associated with an increased cancer risk: A kin-cohort study', *Movement Disorders.* 29**,** pp. 1325-1326.

Almudimeegh, S. 2022. *Modulation of LRRK2 mediated signaling in immune cells.* UCL (University College London).

American Type Culture Collection, A. (2023) *LRRK2 KO RAW 264.7 (ATCC SC-6004)*. Available at: https://www.atcc.org/products/sc-6004#required-products (Accessed: 31 March 2025).

An, J., Yang, H., Park, S. M., Chwae, Y. J. and Joe, E. H. (2024) 'The LRRK2-G2019S mutation attenuates repair of brain injury partially by reducing the release of osteopontin-containing monocytic exosome-like vesicles', *Neurobiol Dis.* 197**,** pp. 106528.

Anandan, A., Ak, M. U., Saika, S., Shibu, M. A. and Viswanadha, V. P. (2025) 'Shikonin Ameliorates Rotenone-Induced Neurotoxicity Through Inhibition of Apoptosis via IGF-1R/PI3K/AKT Pathway in a Parkinson's Disease-Associated SH-SY5Y Cell Model', *Mol Neurobiol.*

Anantha, J., Goulding, S. R., Tuboly, E., O'mahony, A. G., Moloney, G. M., Lomansey, G., Mccarthy, C. M., Collins, L. M., Sullivan, A. M. and O'keeffe, G. W. (2022) 'NME1 Protects Against Neurotoxin-, α-Synuclein- and LRRK2-Induced Neurite Degeneration in Cell Models of Parkinson's Disease', *Mol Neurobiol.* 59**,** pp. 61-76.

Andersen, M. A., Wegener, K. M., Larsen, S., Badolo, L., Smith, G. P., Jeggo, R., Jensen, P. H., Sotty, F., Christensen, K. V. and Thougaard, A. (2018) 'PFE-360-induced LRRK2 inhibition induces reversible, non-adverse renal changes in rats', *Toxicology.* 395**,** pp. 15-22.

Andres-Mateos, E., Mejias, R., Sasaki, M., Li, X., Lin, B. M., Biskup, S., Zhang, L., Banerjee, R., Thomas, B., Yang, L., Liu, G., Beal, M. F., Huso, D. L., Dawson, T. M. and Dawson, V. L. (2009) 'Unexpected lack of hypersensitivity in LRRK2 knock-out mice to MPTP (1-methyl-4-phenyl-1,2,3,6-tetrahydropyridine)', *J Neurosci.* 29**,** pp. 15846-50.

Aswir, A. and Wan Nazaimoon, W. (2011) 'Effect of edible bird's nest on cell proliferation and tumor necrosis factor-alpha (TNF-α) release in vitro', *International Food Research Journal.* 18.

Aswir Abd Rashed, A. a. R. and Wan Nazaimoon, W. (2010) 'Effect of edible bird's nest on Caco-2 cell proliferation'.

Avola, R., Graziano, A. C. E., Pannuzzo, G., Albouchi, F. and Cardile, V. (2018) 'New insights on Parkinson's disease from differentiation of SH-SY5Y into dopaminergic neurons: An involvement of aquaporin4 and 9', *Mol Cell Neurosci.* 88**,** pp. 212-221.

Azeggagh, S. and Berwick, D. C. (2022) 'The development of inhibitors of leucine-rich repeat kinase 2 (LRRK2) as a therapeutic strategy for Parkinson's disease: the current state of play', *British journal of pharmacology.* 179**,** pp. 1478-1495.

Bahnassawy, L. A., Nicklas, S., Palm, T., Menzl, I., Birzele, F., Gillardon, F. and Schwamborn, J. C. (2013) 'The Parkinson's disease-associated LRRK2 mutation R1441G inhibits neuronal differentiation of neural stem cells', *Stem cells and development.* 22**,** pp. 2487-2496.

Bai, W., Deng, F., Liu, X., Yin, X., Qiu, X., Yang, J., Yang, W., Zhang, X., Lian, J., Fan, Q. and Guo, B. (2024) 'Edible bird's nest peptide (EBNP) with high whitening activity: Sequences analysis, whitening activity characterization and molecular docking study', *Journal of Functional Foods.* 123**,** pp. 106617.

Bai, W., Deng, F., Zhang, X., Han, Y., Xiao, Y. E., Wang, N., Liu, X., Fan, Q. and Guo, B. (2023) 'The determination of epidermal growth factor in Edible bird's nest by enzyme-linked immunosorbent assay', *Applied Biological Chemistry.* 66**,** pp. 36.

Baptista, M. A., Dave, K. D., Frasier, M. A., Sherer, T. B., Greeley, M., Beck, M. J., Varsho, J. S., Parker, G. A., Moore, C. and Churchill, M. J. (2013) 'Loss of

leucine-rich repeat kinase 2 (LRRK2) in rats leads to progressive abnormal phenotypes in peripheral organs', *PloS one.* 8**,** pp. e80705.

Baptista, M. A., Merchant, K., Barrett, T., Bhargava, S., Bryce, D. K., Ellis, J. M., Estrada, A. A., Fell, M. J., Fiske, B. K. and Fuji, R. N. (2020a) 'LRRK2 inhibitors induce reversible changes in nonhuman primate lungs without measurable pulmonary deficits', *Science translational medicine.* 12**,** pp. eaav0820.

Baptista, M. a. S., Merchant, K., Barrett, T., Bhargava, S., Bryce, D. K., Ellis, J. M., Estrada, A. A., Fell, M. J., Fiske, B. K., Fuji, R. N., Galatsis, P., Henry, A. G., Hill, S., Hirst, W., Houle, C., Kennedy, M. E., Liu, X., Maddess, M. L., Markgraf, C., Mei, H., Meier, W. A., Needle, E., Ploch, S., Royer, C., Rudolph, K., Sharma, A. K., Stepan, A., Steyn, S., Trost, C., Yin, Z., Yu, H., Wang, X. and Sherer, T. B. (2020b) 'LRRK2 inhibitors induce reversible changes in nonhuman primate lungs without measurable pulmonary deficits', *Science Translational Medicine.* 12**,** pp. eaav0820.

Barbuti, P., Antony, P., Santos, B., Massart, F., Cruciani, G., Dording, C., Arias, J., Schwamborn, J. and Krüger, R. (2020) 'Using high-content screening to generate single-cell gene-corrected patient-derived iPS clones reveals excess alpha-synuclein with familial Parkinson's disease point mutation A30P', *Cells.* 9**,** pp. 2065.

Barrangou, R., Fremaux, C., Deveau, H., Richards, M., Boyaval, P., Moineau, S., Romero, D. A. and Horvath, P. (2007) 'CRISPR Provides Acquired Resistance Against Viruses in Prokaryotes', *Science.* 315**,** pp. 1709-1712.

Bass, J. J., Wilkinson, D. J., Rankin, D., Phillips, B. E., Szewczyk, N. J., Smith, K. and Atherton, P. J. (2017) 'An overview of technical considerations for Western blotting applications to physiological research', *Scandinavian journal of medicine & science in sports.* 27**,** pp. 4-25.

Beal, M. F. (2005) 'Mitochondria take center stage in aging and neurodegeneration', *Annals of Neurology: Official Journal of the American Neurological Association and the Child Neurology Society.* 58**,** pp. 495-505.

Bernhard, P., Feilen, T., Rogg, M., Fröhlich, K., Cosenza-Contreras, M., Hause, F., Schell, C. and Schilling, O. (2022) 'Proteome alterations during clonal isolation of established human pancreatic cancer cell lines', *Cellular and Molecular Life Sciences.* 79**,** pp. 561.

Berwick, D. C. and Harvey, K. (2012) 'LRRK2 functions as a Wnt signaling scaffold, bridging cytosolic proteins and membrane-localized LRP6', *Human molecular genetics.* 21**,** pp. 4966-4979.

Beylina, A., Langston, R. G., Rosen, D., Reed, X. and Cookson, M. R. (2021) 'Generation of fourteen isogenic cell lines for Parkinson's disease-associated leucine-rich repeat kinase (LRRK2)', *Stem Cell Research.* 53**,** pp. 102354.

Biedler, J. L., Helson, L. and Spengler, B. A. (1973) 'Morphology and growth, tumorigenicity, and cytogenetics of human neuroblastoma cells in continuous culture', *Cancer research.* 33**,** pp. 2643-2652.

Biedler, J. L., Roffler-Tarlov, S., Schachner, M. and Freedman, L. S. (1978) 'Multiple neurotransmitter synthesis by human neuroblastoma cell lines and clones', *Cancer research.* 38**,** pp. 3751-3757.

Biogen (2020) *Biogen and Denali to Collaborate on LRRK2 Program for Parkinson's Disease and Certain TV Platform-Enabled Programs for Neurodegenerative Diseases*. Available at: https://investors.biogen.com/news-releases/news-release-details/biogen-and-denali-collaborate-lrrk2-program-parkinsons-disease (Accessed: 26 March 2025).

Biogen (2022a) *Biogen and Denali Therapeutics Announce Initiation of the Phase 3 LIGHTHOUSE Study in Parkinson's Disease Associated with LRRK2 Pathogenic Mutations*. Available at: https://investors.biogen.com/news-releases/news-release-details/biogen-and-denali-therapeutics-announce-initiation-phase-3 (Accessed: 27 Jan 2025).

Biogen (2022b) *Denali Therapeutics and Biogen Announce Initiation of Phase 2b Study of LRRK2 Inhibitor in Parkinson's Disease*. Available at: https://investors.biogen.com/news-releases/news-release-details/denali-therapeutics-and-biogen-announce-initiation-phase-2b (Accessed: 27 Jan 2025).

Biskup, S., Moore, D. J., Rea, A., Lorenz-Deperieux, B., Coombes, C. E., Dawson, V. L., Dawson, T. M. and West, A. B. (2007) 'Dynamic and redundant regulation of LRRK2 and LRRK1 expression', *BMC neuroscience.* 8**,** pp. 1-11.

Boecker, C. A., Goldsmith, J., Dou, D., Cajka, G. G. and Holzbaur, E. L. (2021) 'Increased LRRK2 kinase activity alters neuronal autophagy by disrupting the axonal transport of autophagosomes', *Current Biology.* 31**,** pp. 2140-2154. e6.

Bojko, A., Staniak, K., Czarnecka-Herok, J., Sunderland, P., Dudkowska, M., Śliwińska, M. A., Salmina, K. and Sikora, E. (2020) 'Improved autophagic flux in escapers from doxorubicin-induced senescence/polyploidy of breast cancer cells', *International journal of molecular sciences.* 21**,** pp. 6084.

Bosgraaf, L. and Van Haastert, P. J. M. (2003) 'Roc, a Ras/GTPase domain in complex proteins', *Biochimica et Biophysica Acta (BBA) - Molecular Cell Research.* 1643**,** pp. 5-10.

Bryce, D. K., Ware, C. M., Woodhouse, J. D., Ciaccio, P. J., Ellis, J. M., Hegde, L. G., Kuruvilla, S., Maddess, M. L., Markgraf, C. G., Otte, K. M., Poulet, F. M., Timmins, L. M., Kennedy, M. E. and Fell, M. J. (2021) 'Characterization of the Onset, Progression, and Reversibility of Morphological Changes in Mouse Lung after Pharmacological Inhibition of Leucine-Rich Kinase 2 Kinase Activity', *The Journal of Pharmacology and Experimental Therapeutics.* 377**,** pp. 11-19.

Bu, M., Follett, J., Deng, I., Tatarnikov, I., Wall, S., Guenther, D., Maczis, M., Wimsatt, G., Milnerwood, A. and Moehle, M. S. (2023) 'Inhibition of LRRK2 kinase activity rescues deficits in striatal dopamine physiology in VPS35 p. D620N knock-in mice', *npj Parkinson's Disease.* 9**,** pp. 167.

Cabezudo, D., Tsafaras, G., Van Acker, E., Van Den Haute, C. and Baekelandt, V. (2023) 'Mutant LRRK2 exacerbates immune response and neurodegeneration in a chronic model of experimental colitis', *Acta Neuropathol.* 146**,** pp. 245-261.

Caesar, M., Felk, S., Aasly, J. and Gillardon, F. (2015) 'Changes in actin dynamics and F-actin structure both in synaptoneurosomes of LRRK2 (R1441G) mutant mice and in primary human fibroblasts of LRRK2 (G2019S) mutation carriers', *Neuroscience.* 284**,** pp. 311-324.

Caesar, M., Felk, S., Zach, S., Brønstad, G., Aasly, J. O., Gasser, T. and Gillardon, F. (2014) 'Changes in matrix metalloprotease activity and progranulin levels may contribute to the pathophysiological function of mutant leucine-rich repeat kinase 2', *Glia.* 62**,** pp. 1075-92.

Cao, J., Xiong, N., Zhang, Y., Dai, Y., Wang, Y., Lu, L. and Jiang, L. (2022) 'Using RSM for Optimum of Optimum Production of Peptides from Edible Bird's Nest By-Product and Characterization of Its Antioxidant's Properties', *Foods.* 11.

Careena, S., Sani, D., Tan, S., Lim, C., Hassan, S., Norhafizah, M., Kirby, B. P., Ideris, A., Stanslas, J. and Bin Basri, H. (2018) 'Effect of Edible Bird's Nest Extract on Lipopolysaccharide-Induced Impairment of Learning and Memory in Wistar Rats', *Evidence-Based Complementary and Alternative Medicine.* 2018**,** pp. 9318789.

Carneiro, P., Ferreira, M., Marisa Costa, V., Carvalho, F. and Capela, J. P. (2024) 'Protective effects of amphetamine and methylphenidate against dopaminergic neurotoxicants in SH-SY5Y cells', *Curr Res Toxicol.* 6**,** pp. 100165.

Ceccarini, M. R., Alunni Cardinali, M., Malaspina, R., Libera, V., Scattini, G., Codini, M., Chiesa, I., De Maria, C., Comez, L., Paciaroni, A., Sassi, P. and Valentini, L. (2025) 'Protective effects of silk fibroin against 6-OHDA in SH-

SY5Y human neuroblastoma cells and comparative study with its release from gelatin films', *Int J Biol Macromol.* 303**,** pp. 140697.

Chan, D., Citro, A., Cordy, J. M., Shen, G. C. and Wolozin, B. (2011) 'Rac1 protein rescues neurite retraction caused by G2019S leucine-rich repeat kinase 2 (LRRK2)', *Journal of Biological Chemistry.* 286**,** pp. 16140-16149.

Chan, G., Zheng, K., Zhu, K. Y., Dong, T. and Tsim, K. (2013) 'Determination of free N-acetylneuraminic acid in edible bird nest: a development of chemical marker for quality control', *Journal of Ethnobiology and Traditional Medicine.* 120**,** pp. 620-628.

Chan, G. K. L., Wong, Z. C. F., Lam, K. Y. C., Cheng, L. K. W., Zhang, L. M., Lin, H., Dong, T. T. and Tsim, K. W. K. (2015) 'Edible bird's nest, an Asian health food supplement, possesses skin lightening activities: identification of N-acetylneuraminic acid as active ingredient', *Journal of Cosmetics, Dermatological Sciences and Applications.* 5**,** pp. 262.

Chang, M.-Y., Oh, B., Rhee, Y.-H. and Lee, S.-H. (2015) 'Doxycycline supplementation allows for the culture of human ESCs/iPSCs with media changes at 3-day intervals', *Stem Cell Research.* 15**,** pp. 608-613.

Chantakun, K. and Benjakul, S. (2022) 'Effect of ultrasound-assisted pretreatment in combination with heating on characteristics and antioxidant activities of protein hydrolysate from edible bird's nest co-product', *J Food Sci Technol.* 59**,** pp. 3908-3917.

Chen, C., Soto, G., Dumrongprechachan, V., Bannon, N., Kang, S., Kozorovitskiy, Y. and Parisiadou, L. (2020a) 'Pathway-specific dysregulation of striatal excitatory synapses by LRRK2 mutations', *Elife.* 9**,** pp. e58997.

Chen, C., Weng, Y. H., Chien, K. Y., Lin, K., Yeh, T., Cheng, Y., Lu, C. and Wang, H. (2012) '(G2019S) LRRK2 activates MKK4-JNK pathway and causes degeneration of SN dopaminergic neurons in a transgenic mouse model of PD', *Cell Death & Differentiation.* 19**,** pp. 1623-1633.

Chen, M.-L. and Wu, R.-M. (2018) 'LRRK 2 gene mutations in the pathophysiology of the ROCO domain and therapeutic targets for Parkinson's disease: a review', *Journal of Biomedical Science.* 25**,** pp. 1-11.

Chen, S., Luo, Z., Ward, C., Ibañez, D. P., Liu, H., Zhong, X., Sharma, N. K., Qin, B., Fan, W. and Wang, D. (2020b) 'Generation of two LRRK2 homozygous knockout human induced pluripotent stem cell lines using CRISPR/Cas9', *Stem Cell Research.* 45**,** pp. 101804.

Chen, X., Xie, C., Tian, W., Sun, L., Zheng, W., Hawes, S., Chang, L., Kung, J., Ding, J. and Chen, S. (2020c) 'Parkinson's disease-related Leucine-rich repeat kinase 2 modulates nuclear morphology and genomic stability in striatal projection neurons during aging', *Molecular neurodegeneration.* 15**,** pp. 1-19.

Cheng, Y. S., Xu, M., Chen, G., Beers, J., Chen, C. Z., Liu, C., Zou, J. and Zheng, W. (2023) 'A protocol for culture and characterization of human induced pluripotent stem cells after induction', *Current protocols.* 3**,** pp. e866.

Cherra Iii, S. J., Steer, E., Gusdon, A. M., Kiselyov, K. and Chu, C. T. (2013) 'Mutant LRRK2 elicits calcium imbalance and depletion of dendritic mitochondria in neurons', *The American journal of pathology.* 182**,** pp. 474-484.

Cherra, S. J., 3rd, Steer, E., Gusdon, A. M., Kiselyov, K. and Chu, C. T. (2013) 'Mutant LRRK2 elicits calcium imbalance and depletion of dendritic mitochondria in neurons', *Am J Pathol.* 182**,** pp. 474-84.

Cho, H. J., Liu, G., Jin, S. M., Parisiadou, L., Xie, C., Yu, J., Sun, L., Ma, B., Ding, J., Vancraenenbroeck, R., Lobbestael, E., Baekelandt, V., Taymans, J. M., He, P., Troncoso, J. C., Shen, Y. and Cai, H. (2013) 'MicroRNA-205 regulates the expression of Parkinson's disease-related leucine-rich repeat kinase 2 protein', *Hum Mol Genet.* 22**,** pp. 608-20.

Cho, K. A., Ryu, S. J., Oh, Y. S., Park, J. H., Lee, J. W., Kim, H.-P., Kim, K. T., Jang, I. S. and Park, S. C. (2004) 'Morphological adjustment of senescent cells by modulating caveolin-1 status', *Journal of Biological Chemistry.* 279**,** pp. 42270-42278.

Choi, I., Kim, B., Byun, J.-W., Baik, S. H., Huh, Y. H., Kim, J.-H., Mook-Jung, I., Song, W. K., Shin, J.-H., Seo, H., Suh, Y. H., Jou, I., Park, S. M., Kang, H. C. and Joe, E.-H. (2015) 'LRRK2 G2019S mutation attenuates microglial motility by inhibiting focal adhesion kinase', *Nature Communications.* 6**,** pp. 8255.

Chong, Z. X., Yeap, S. K. and Ho, W. Y. (2021) 'Transfection types, methods and strategies: a technical review', *PeerJ.* 9**,** pp. e11165.

Choy, K. W., Zain, Z. M., Murugan, D. D., Giribabu, N., Zamakshshari, N. H., Lim, Y. M. and Mustafa, M. R. (2021) 'Effect of hydrolyzed bird's nest on β-cell function and insulin signaling in type 2 diabetic mice', *Frontiers in Pharmacology.* 12**,** pp. 632169.

Chua, K.-H., Lee, T.-H., Nagandran, K., Md Yahaya, N. H., Lee, C.-T., Tjih, E. T. T. and Abdul Aziz, R. (2013) 'Edible Bird's nest extract as a chondro-protective agent for human chondrocytes isolated from osteoarthritic knee: in vitro study', *BMC complementary and alternative medicine.* 13**,** pp. 1-9.

Ciccarone, V., Spengler, B. A., Meyers, M. B., Biedler, J. L. and Ross, R. A. (1989) 'Phenotypic diversification in human neuroblastoma cells: expression of distinct neural crest lineages', *Cancer research.* 49**,** pp. 219-225.

Cimmino, F., Pezone, L., Avitabile, M., Acierno, G., Andolfo, I., Capasso, M. and Iolascon, A. (2015) 'Inhibition of hypoxia inducible factors combined with all-trans retinoic acid treatment enhances glial transdifferentiation of neuroblastoma cells', *Scientific reports.* 5**,** pp. 11158.

Çınar, R. and Yıldızhan, K. (2025) 'Curcumin protects against MPP(+)-induced neurotoxicity in SH-SY5Y cells by modulating the TRPV4 channel', *Mol Biol Rep.* 52**,** pp. 255.

Cirmi, S., Maugeri, A., Lombardo, G. E., Russo, C., Musumeci, L., Gangemi, S., Calapai, G., Barreca, D. and Navarra, M. (2021) 'A Flavonoid-Rich Extract of Mandarin Juice Counteracts 6-OHDA-Induced Oxidative Stress in SH-SY5Y Cells and Modulates Parkinson-Related Genes', *Antioxidants (Basel).* 10.

Civiero, L., Cogo, S., Biosa, A. and Greggio, E. (2018) 'The role of LRRK2 in cytoskeletal dynamics', *Biochemical Society Transactions.* 46**,** pp. 1653-1663.

Cohen, N., Betts, D. R., Rechavi, G., Amariglio, N. and Trakhtenbrot, L. (2003) 'Clonal expansion and not cell interconversion is the basis for the neuroblast and nonneuronal types of the SK-N-SH neuroblastoma cell line', *Cancer genetics and cytogenetics.* 143**,** pp. 80-84.

Coku, I., Mutez, E., Eddarkaoui, S., Carrier, S., Marchand, A., Deldycke, C., Goveas, L., Baille, G., Tir, M. and Magnez, R. (2022) 'Functional Analyses of Two Novel LRRK2 Pathogenic Variants in Familial Parkinson′ s Disease', *Movement Disorders.* 37**,** pp. 1761-1767.

Cong, L., Ran, F. A., Cox, D., Lin, S., Barretto, R., Habib, N., Hsu, P. D., Wu, X., Jiang, W. and Marraffini, L. A. (2013) 'Multiplex genome engineering using CRISPR/Cas systems', *Science.* 339**,** pp. 819-823.

Connolly, C. (2016) '‘A place for everything’: Moral landscapes of ‘swiftlet farming’ in George Town, Malaysia', *Geoforum.* 77**,** pp. 182-191.

Cook, D., Kannarkat, G., Cintron, A., Butkovich, L. M., Fraser, K. B., Chang, J., Grigoryan, N., Factor, S., West, A. B. and Boss, J. (2017) 'LRRK2 levels in immune cells are increased in Parkinson’s disease', *NPJ Parkinson's disease.* 3**,** pp. 11.

Cookson, M. R. (2010) 'The role of leucine-rich repeat kinase 2 (LRRK2) in Parkinson's disease', *Nat Rev Neurosci.* 11**,** pp. 791-7.

Covy, J. P. and Giasson, B. I. (2009) 'Identification of compounds that inhibit the kinase activity of leucine-rich repeat kinase 2', *Biochem Biophys Res Commun.* 378**,** pp. 473-7.

Cristofalo, V. J., Volker, C. and Allen, R. G. 2000. Use of the fibroblast model in the study of cellular senescence. *In:* YVONNE A. BARNETT, C. R. B. (ed.) *Aging methods and protocols.*

Cuny, G. D. (2009) 'Kinase inhibitors as potential therapeutics for acute and chronic neurodegenerative conditions', *Curr Pharm Des.* 15**,** pp. 3919-39.

D'amico, S., Tempora, P., Gragera, P., Król, K., Melaiu, O., De Ioris, M. A., Locatelli, F. and Fruci, D. (2023) 'Two bullets in the gun: combining immunotherapy with chemotherapy to defeat neuroblastoma by targeting adrenergic-mesenchymal plasticity', *Frontiers in Immunology.* 14**,** pp. 1268645.

Dächsel, J. C., Behrouz, B., Yue, M., Beevers, J. E., Melrose, H. L. and Farrer, M. J. (2010) 'A comparative study of Lrrk2 function in primary neuronal cultures', *Parkinsonism & related disorders.* 16**,** pp. 650-655.

Daher, J. P., Abdelmotilib, H. A., Hu, X., Volpicelli-Daley, L. A., Moehle, M. S., Fraser, K. B., Needle, E., Chen, Y., Steyn, S. J. and Galatsis, P. (2015) 'Leucine-rich repeat kinase 2 (LRRK2) pharmacological inhibition abates α-synuclein gene-induced neurodegeneration', *Journal of Biological Chemistry.* 290**,** pp. 19433-19444.

Dallmann-Sauer, M., Xu, Y. Z., Da Costa, A. L. F., Tao, S., Gomes, T. A., Prata, R., Correa-Macedo, W., Manry, J., Alcaïs, A., Abel, L., Cobat, A., Fava, V. M., Pinheiro, R. O., Lara, F. A., Probst, C. M., Mira, M. T. and Schurr, E. (2023) 'Allele-dependent interaction of LRRK2 and NOD2 in leprosy', *PLoS Pathog.* 19**,** pp. e1011260.

Danet, A. F. 2021. *Recent advances in antioxidant capacity assays*, IntechOpen.

Daud, N. A., Mohamad Yusop, S., Babji, A. S., Lim, S. J., Sarbini, S. R. and Hui Yan, T. (2021) 'Edible bird's nest: physicochemical properties, production, and application of bioactive extracts and glycopeptides', *Food Reviews International.* 37**,** pp. 177-196.

Debacq-Chainiaux, F., Erusalimsky, J. D., Campisi, J. and Toussaint, O. (2009) 'Protocols to detect senescence-associated beta-galactosidase (SA-βgal) activity,

a biomarker of senescent cells in culture and in vivo', *Nature protocols.* 4**,** pp. 1798-1806.

Deleuze, V., Soler, E. and Andrieu-Soler, C. (2024) 'Protocol for efficient CRISPR-Cas9-mediated fluorescent tag knockin in hard-to-transfect erythroid cell lines', *STAR protocols.* 5**,** pp. 103016.

Deng, X., Dzamko, N., Prescott, A., Davies, P., Liu, Q., Yang, Q., Lee, J.-D., Patricelli, M. P., Nomanbhoy, T. K. and Alessi, D. R. (2011) 'Characterization of a selective inhibitor of the Parkinson's disease kinase LRRK2', *Nature chemical biology.* 7**,** pp. 203-205.

Dimri, G. P., Lee, X., Basile, G., Acosta, M., Scott, G., Roskelley, C., Medrano, E. E., Linskens, M., Rubelj, I. and Pereira-Smith, O. (1995) 'A biomarker that identifies senescent human cells in culture and in aging skin in vivo', *Proceedings of the National Academy of Sciences, USA.* 92**,** pp. 9363-9367.

Do, P. T., Nguyen, C. X., Bui, H. T., Tran, L. T., Stacey, G., Gillman, J. D., Zhang, Z. J. and Stacey, M. G. (2019) 'Demonstration of highly efficient dual gRNA CRISPR/Cas9 editing of the homeologous GmFAD2–1A and GmFAD2–1B genes to yield a high oleic, low linoleic and α-linolenic acid phenotype in soybean', *BMC plant biology.* 19**,** pp. 1-14.

Dobutr, T., Jangpromma, N., Patramanon, R., Daduang, J., Klaynongsruang, S., Poopornchai, S., Yabe, T. and Daduang, S. (2023) 'The effect of edible bird's nests on the expression of MHC-II and costimulatory molecules of C57BL/6 mouse splenocytes', *Biochemistry and Biophysics Reports.* 35**,** pp. 101534.

Dobutr, T., Kantamala, W., Phimwapi, S., Jangpromma, N., Tippayawat, P., Boonlue, S., Daduang, J., Klaynongsruang, S., Poopornchai, S. and Daduang, S. (2022) 'The effects of edible bird’s nest on T-lymphocyte proliferation, secondary lymphoid organs, and interleukin-2 production', *Journal of Functional Foods.* 90**,** pp. 104977.

Dou, D., Aiken, J. and Holzbaur, E. L. (2024) 'RAB3 phosphorylation by pathogenic LRRK2 impairs trafficking of synaptic vesicle precursors', *Journal of Cell Biology.* 223.

Doudna, J. A. and Charpentier, E. (2014) 'The new frontier of genome engineering with CRISPR-Cas9', *Science.* 346**,** pp. 1258096.

Dudkowska, M., Staniak, K., Bojko, A. and Sikora, E. (2021) 'The role of autophagy in escaping therapy-induced polyploidy/senescence', *Advances in Cancer Research.* 150**,** pp. 209-247.

Dudonne, S., Vitrac, X., Coutiere, P., Woillez, M. and Mérillon, J.-M. (2009) 'Comparative study of antioxidant properties and total phenolic content of 30 plant extracts of industrial interest using DPPH, ABTS, FRAP, SOD, and ORAC assays', *Journal of agricultural and food chemistry.* 57**,** pp. 1768-1774.

Duffy, A., Bouchier-Hayes, D. and Harmey, J. (2000 - 2013) *Vascular Endothelial Growth Factor (VEGF) and Its Role in Non-Endothelial Cells: Autocrine Signalling by VEGF*. Landes Bioscience. Available at: https://www.ncbi.nlm.nih.gov/books/NBK6482/ (Accessed: 22 Jan 2025).

Dzamko, N., Deak, M., Hentati, F., Reith, A. D., Prescott, A. R., Alessi, D. R. and Nichols, R. J. (2010) 'Inhibition of LRRK2 kinase activity leads to dephosphorylation of Ser(910)/Ser(935), disruption of 14-3-3 binding and altered cytoplasmic localization', *Biochem J.* 430**,** pp. 405-13.

Erenpreisa, J., Salmina, K. and Cragg, M. S. (2017) 'Accelerated senescence of cancer stem cells: A failure to thrive or a route to survival', *Senescence Physiology or Pathology; Dorszewska, J., Kozubsk, W., Eds.* pp. 45-62.

Esteves, A. R. and Cardoso, S. M. (2017) 'LRRK2 at the crossroad between autophagy and microtubule trafficking: insights into Parkinson's disease', *The Neuroscientist.* 23**,** pp. 16-26.

Evangelou, K., Belogiannis, K., Papaspyropoulos, A., Petty, R. and Gorgoulis, V. G. (2023) 'Escape from senescence: molecular basis and therapeutic ramifications', *The Journal of Pathology.* 260**,** pp. 649-665.

Fan, Q., Lian, J., Liu, X., Zou, F., Wang, X. and Chen, M. (2021a) 'A Study on the Skin Whitening Activity of Digesta from Edible Bird's Nest: A Mucin Glycoprotein', *Gels.* 8.

Fan, Y., Fan, Y., Liu, K., Lonan, P., Liao, F., Huo, Y., Zhong, X., Liang, Y., Wang, Y. and Hou, S. (2021b) 'Edible bird's nest ameliorates dextran sulfate sodium-induced ulcerative colitis in C57BL/6J mice by restoring the Th17/Treg cell balance', *Frontiers in Pharmacology.* 12**,** pp. 632602.

Fell, M. J., Mirescu, C., Basu, K., Cheewatrakoolpong, B., Demong, D. E., Ellis, J. M., Hyde, L. A., Lin, Y., Markgraf, C. G., Mei, H., Miller, M., Poulet, F. M., Scott, J. D., Smith, M. D., Yin, Z., Zhou, X., Parker, E. M., Kennedy, M. E. and Morrow, J. A. (2015) 'MLi-2, a Potent, Selective, and Centrally Active Compound for Exploring the Therapeutic Potential and Safety of LRRK2 Kinase Inhibition', *The Journal of Pharmacology and Experimental Therapeutics.* 355**,** pp. 397-409.

Feng, L., Lo, H., Hong, Z., Zheng, J., Yan, Y., Ye, Z., Chen, X. and Pan, X. (2023) 'Microglial LRRK2-mediated NFATc1 attenuates α-synuclein immunotoxicity in association with CX3CR1-induced migration and the lysosome-initiated degradation', *Glia.* 71**,** pp. 2266-2284.

Fenicsbio (2025) *Human LRRK2 Knockout HEK293T cell line*. Available at: https://fenicsbio.com/human-lrrk2-knockout-hek293t-cell-line/ (Accessed: 31 March 2025).

Fernández, B., Chittoor-Vinod, V. G., Kluss, J. H., Kelly, K., Bryant, N., Nguyen, A. P. T., Bukhari, S. A., Smith, N., Lara Ordóñez, A. J. and Fdez, E. (2022) 'Evaluation of current methods to detect cellular leucine-rich repeat kinase 2 (LRRK2) kinase activity', *Journal of Parkinson's disease.* 12**,** pp. 1423-1447.

Filippone, A., Mannino, D., Cucinotta, L., Calapai, F., Crupi, L., Paterniti, I. and Esposito, E. (2024) 'Rebalance of mitophagy by inhibiting LRRK2 improves colon alterations in an MPTP in vivo model', *iScience.* 27.

Fuji, R. N., Flagella, M., Baca, M., Baptista, M. A., Brodbeck, J., Chan, B. K., Fiske, B. K., Honigberg, L., Jubb, A. M., Katavolos, P., Lee, D. W., Lewin-Koh, S. C., Lin, T., Liu, X., Liu, S., Lyssikatos, J. P., O'mahony, J., Reichelt, M., Roose-Girma, M., Sheng, Z., Sherer, T., Smith, A., Solon, M., Sweeney, Z. K., Tarrant, J., Urkowitz, A., Warming, S., Yaylaoglu, M., Zhang, S., Zhu, H., Estrada, A. A. and Watts, R. J. (2015) 'Effect of selective LRRK2 kinase inhibition on nonhuman primate lung', *Sci Transl Med.* 7**,** pp. 273ra15.

Funayama, M., Hasegawa, K., Kowa, H., Saito, M., Tsuji, S. and Obata, F. (2002) 'A new locus for Parkinson's disease (PARK8) maps to chromosome 12p11. 2–q13. 1', *Annals of Neurology: Official Journal of the American Neurological Association and the Child Neurology Society.* 51**,** pp. 296-301.

Fus-Kujawa, A., Prus, P., Bajdak-Rusinek, K., Teper, P., Gawron, K., Kowalczuk, A. and Sieron, A. L. (2021) 'An overview of methods and tools for transfection of eukaryotic cells in vitro', *Frontiers in bioengineering and biotechnology.* 9**,** pp. 701031.

Gandhi, P. N., Wang, X., Zhu, X., Chen, S. G. and Wilson-Delfosse, A. L. (2008) 'The Roc domain of leucine-rich repeat kinase 2 is sufficient for interaction with microtubules', *Journal of neuroscience research.* 86**,** pp. 1711-1720.

Gao, C., Jiang, J., Tan, Y. and Chen, S. (2023) 'Microglia in neurodegenerative diseases: mechanism and potential therapeutic targets', *Signal transduction and targeted therapy.* 8**,** pp. 359.

Gartlgruber, M., Sharma, A. K., Quintero, A., Dreidax, D., Jansky, S., Park, Y.-G., Kreth, S., Meder, J., Doncevic, D. and Saary, P. (2021) 'Super enhancers define regulatory subtypes and cell identity in neuroblastoma', *Nature Cancer.* 2**,** pp. 114-128.

Ghaedi, M. and Niklason, L. E. 2016. Human pluripotent stem cells (iPSC) generation, culture, and differentiation to lung progenitor cells. *Organoids: Stem Cells, Structure, and Function.* Springer.

Ghassem, M., Arihara, K., Mohammadi, S., Sani, N. A. and Babji, A. S. (2017) 'Identification of two novel antioxidant peptides from edible bird's nest (Aerodramus fuciphagus) protein hydrolysates', *Food & function.* 8**,** pp. 2046-2052.

Ghosh, R., Gilda, J. E. and Gomes, A. V. (2014) 'The necessity of and strategies for improving confidence in the accuracy of Western blots', *Expert review of proteomics.* 11**,** pp. 549-560.

Giaime, E., Tong, Y., Wagner, L. K., Yuan, Y., Huang, G. and Shen, J. (2017) 'Age-dependent dopaminergic neurodegeneration and impairment of the autophagy-lysosomal pathway in LRRK-deficient mice', *Neuron.* 96**,** pp. 796-807. e6.

Gillardon, F. (2009) 'Leucine-rich repeat kinase 2 phosphorylates brain tubulin-beta isoforms and modulates microtubule stability–a point of convergence in parkinsonian neurodegeneration?', *Journal of neurochemistry.* 110**,** pp. 1514-1522.

Gillardon, F., Schmid, R. and Draheim, H. (2012) 'Parkinson's disease-linked leucine-rich repeat kinase 2(R1441G) mutation increases proinflammatory cytokine release from activated primary microglial cells and resultant neurotoxicity', *Neuroscience.* 208**,** pp. 41-8.

Gilsbach, B. K. and Kortholt, A. (2014) 'Structural biology of the LRRK2 GTPase and kinase domains: implications for regulation', *Frontiers in molecular neuroscience.* 7**,** pp. 32.

Gloeckner, C. J., Boldt, K., Von Zweydorf, F., Helm, S., Wiesent, L., Sarioglu, H. and Ueffing, M. (2010) 'Phosphopeptide analysis reveals two discrete clusters of phosphorylation in the N-terminus and the Roc domain of the Parkinson-disease associated protein kinase LRRK2', *J Proteome Res.* 9**,** pp. 1738-45.

Gloeckner, C. J., Kinkl, N., Schumacher, A., Braun, R. J., O'neill, E., Meitinger, T., Kolch, W., Prokisch, H. and Ueffing, M. (2006) 'The Parkinson disease

causing LRRK2 mutation I2020T is associated with increased kinase activity', *Hum Mol Genet.* 15**,** pp. 223-32.

Gloeckner, C. J., Schumacher, A., Boldt, K. and Ueffing, M. (2009) 'The Parkinson disease-associated protein kinase LRRK2 exhibits MAPKKK activity and phosphorylates MKK3/6 and MKK4/7, in vitro', *Journal of neurochemistry.* 109**,** pp. 959-968.

Godena, V. K., Brookes-Hocking, N., Moller, A., Shaw, G., Oswald, M., Sancho, R. M., Miller, C. C., Whitworth, A. J. and De Vos, K. J. (2014) 'Increasing microtubule acetylation rescues axonal transport and locomotor deficits caused by LRRK2 Roc-COR domain mutations', *Nature communications.* 5**,** pp. 5245.

Goh, D. L., Chew, F.-T., Chua, K.-Y., Chay, O.-M. and Lee, B.-W. (2000) 'Edible "bird's nest"–induced anaphylaxis: An under-recognized entity?', *The Journal of pediatrics.* 137**,** pp. 277-279.

Goh, D. L. M., Chua, K. Y., Chew, F. T., Liang, R. C. M. Y., Seow, T. K., Ou, K. L., Yi, F. C. and Lee, B. W. (2001) 'Immunochemical characterization of edible bird's nest allergens', *Journal of allergy and clinical immunology.* 107**,** pp. 1082-1088.

Gómez-Virgilio, L., Silva-Lucero, M.-D.-C., Flores-Morelos, D.-S., Gallardo-Nieto, J., Lopez-Toledo, G., Abarca-Fernandez, A.-M., Zacapala-Gómez, A.-E., Luna-Muñoz, J., Montiel-Sosa, F. and Soto-Rojas, L. O. (2022) 'Autophagy: a key regulator of homeostasis and disease: an overview of molecular mechanisms and modulators', *Cells.* 11**,** pp. 2262.

Gopalai, A. A., Lim, J. L., Li, H. H., Zhao, Y., Lim, T. T., Eow, G. B., Puvanarajah, S., Viswanathan, S., Norlinah, M. I. and Abdul Aziz, Z. (2019) 'LRRK2 N551K and R1398H variants are protective in Malays and Chinese in Malaysia: A case–control association study for Parkinson's disease', *Molecular Genetics & Genomic Medicine.* 7**,** pp. e604.

Gopalai, A. A., Lim, S.-Y., Chua, J. Y., Tey, S., Lim, T. T., Mohamed Ibrahim, N., Tan, A. H., Eow, G. B., Abdul Aziz, Z. and Puvanarajah, S. D. (2014) 'LRRK2 G2385R and R1628P mutations are associated with an increased risk of Parkinson's disease in the Malaysian population', *BioMed research international.* 2014**,** pp. 867321.

Gopar-Cuevas, Y., Saucedo-Cardenas, O., Loera-Arias, M. J., Montes-De-Oca-Luna, R., Rodriguez-Rocha, H. and Garcia-Garcia, A. (2023) 'Metformin and Trehalose-Modulated Autophagy Exerts a Neurotherapeutic Effect on Parkinson's Disease', *Mol Neurobiol.* 60**,** pp. 7253-7273.

Greggio, E., Jain, S., Kingsbury, A., Bandopadhyay, R., Lewis, P., Kaganovich, A., Van Der Brug, M. P., Beilina, A., Blackinton, J., Thomas, K. J., Ahmad, R., Miller, D. W., Kesavapany, S., Singleton, A., Lees, A., Harvey, R. J., Harvey, K. and Cookson, M. R. (2006) 'Kinase activity is required for the toxic effects of mutant LRRK2/dardarin', *Neurobiol Dis.* 23**,** pp. 329-41.

Greggio, E., Taymans, J. M., Zhen, E. Y., Ryder, J., Vancraenenbroeck, R., Beilina, A., Sun, P., Deng, J., Jaffe, H., Baekelandt, V., Merchant, K. and Cookson, M. R. (2009) 'The Parkinson's disease kinase LRRK2 autophosphorylates its GTPase domain at multiple sites', *Biochem Biophys Res Commun.* 389**,** pp. 449-54.

Gu, Y.-Z., Vlasakova, K., Miller, G., Gatto, N. T., Ciaccio, P. J., Kuruvilla, S., Besteman, E. G., Smith, R., Reynolds, S. J. and Amin, R. P. (2023) 'Early-onset albuminuria and associated renal pathology in leucine-rich repeat kinase 2 knockout rats', *Toxicologic Pathology.* 51**,** pp. 15-26.

Guevara, C. A., Matikainen-Ankney, B. A., Kezunovic, N., Leclair, K., Conway, A. P., Menard, C., Flanigan, M. E., Pfau, M., Russo, S. J. and Benson, D. L. (2020) 'LRRK2 mutation alters behavioral, synaptic, and nonsynaptic adaptations to acute social stress', *Journal of neurophysiology.* 123**,** pp. 2382-2389.

Guo, C.-T., Takahashi, T., Bukawa, W., Takahashi, N., Yagi, H., Kato, K., Hidari, K. I. P. J., Miyamoto, D., Suzuki, T. and Suzuki, Y. (2006) 'Edible bird's nest extract inhibits influenza virus infection', *Antiviral Research.* 70**,** pp. 140-146.

Guo, L., Wu, Y., Liu, M., Wang, B., Ge, Y. and Chen, Y. (2017) 'Determination of edible bird's nests by FTIR and SDS-PAGE coupled with multivariate analysis', *Food Control.* 80**,** pp. 259-266.

Gupta, S., Jash, M., Khan, J., Garg, S., Roy, R., Arshi, M. U., Nayak, P. and Ghosh, S. (2025) 'Discovery of potential Leonurine-based therapeutic lead MJ210 attenuates Parkinson's disease pathogenesis via NF-κB and MAPK pathways: Mechanistic insights from in vitro and in vivo rotenone models', *Eur J Med Chem.* 289**,** pp. 117471.

Haghani, A., Mehrbod, P., Safi, N., Aminuddin, N. A., Bahadoran, A., Omar, A. R. and Ideris, A. (2016) '*In vitro* and i*n vivo* mechanism of immunomodulatory and antiviral activity of Edible Bird's Nest (EBN) against influenza A virus (IAV) infection', *Journal of ethnopharmacology.* 185**,** pp. 327-340.

Haghani, A., Mehrbod, P., Safi, N., Kadir, F. a. I. A., Omar, A. R. and Ideris, A. (2017) 'Edible bird's nest modulate intracellular molecular pathways of influenza A virus infected cells', *BMC complementary and alternative medicine.* 17**,** pp. 1-13.

Haque, M. E., Akther, M., Azam, S., Choi, D. K. and Kim, I. S. (2020) 'GPR4 Knockout Improves the Neurotoxin-Induced, Caspase-Dependent Mitochondrial Apoptosis of the Dopaminergic Neuronal Cell', *Int J Mol Sci.* 21.

Harmuth, T., Heubach, F., Wieder, T., Handgretinger, R. and Lang, P. Cytokine-induced senescence in neuroblastoma cell lines: Therapeutic option or idle wish? Cancer Immunol. Res., 2019 New York, NY. Philadelphia (PA). AACR, A080.

Härtlova, A., Herbst, S., Peltier, J., Rodgers, A., Bilkei-Gorzo, O., Fearns, A., Dill, B. D., Lee, H., Flynn, R. and Cowley, S. A. (2018) 'LRRK2 is a negative regulator of Mycobacterium tuberculosis phagosome maturation in macrophages', *The EMBO journal.* 37**,** pp. e98694.

Heo, H. Y., Kim, K. S. and Seol, W. (2010) 'Coordinate Regulation of Neurite Outgrowth by LRRK2 and Its Interactor, Rab5', *Exp Neurobiol.* 19**,** pp. 97-105.

Hernandez-Baltazar, D., Zavala-Flores, L. M. and Villanueva-Olivo, A. (2017) 'The 6-hydroxydopamine model and parkinsonian pathophysiology: Novel findings in an older model', *Neurología (English Edition).* 32**,** pp. 533-539.

Herrick, M. K. and Tansey, M. G. (2021) 'Is LRRK2 the missing link between inflammatory bowel disease and Parkinson's disease?', *NPJ Parkinsons Dis.* 7**,** pp. 26.

Hinkle, K. M., Yue, M., Behrouz, B., Dächsel, J. C., Lincoln, S. J., Bowles, E. E., Beevers, J. E., Dugger, B., Winner, B. and Prots, I. (2012) 'LRRK2 knockout mice have an intact dopaminergic system but display alterations in exploratory and motor co-ordination behaviors', *Molecular neurodegeneration.* 7**,** pp. 1-17.

Hipp, J. A., Hipp, J. D., Atala, A. and Soker, S. (2010) 'Functional genomics: new insights into the 'function' of low levels of gene expression in stem cells', *Curr Genomics.* 11**,** pp. 354-8.

Ho, D. H., Je, A. R., Lee, H., Son, I., Kweon, H.-S., Kim, H.-G. and Seol, W. (2018) 'LRRK2 kinase activity induces mitochondrial fission in microglia via Drp1 and modulates neuroinflammation', *Experimental Neurobiology.* 27**,** pp. 171.

Ho, D. H., Kim, H., Nam, D., Seo, M. K., Park, S. W. and Son, I. (2024) 'Expression of G2019S LRRK2 in Rat Primary Astrocytes Mediates Neurotoxicity and Alters the Dopamine Synthesis Pathway in N27 Cells via Astrocytic Proinflammatory Cytokines and Neurotrophic Factors', *Curr Issues Mol Biol.* 46**,** pp. 4324-4336.

Ho, D. H., Lee, H., Son, I. and Seol, W. (2019) 'G2019S LRRK2 promotes mitochondrial fission and increases TNFα-mediated neuroinflammation responses', *Animal Cells and Systems.* 23**,** pp. 106-111.

Ho, D. H., Lee, M., Nam, D., Kim, H., Kim, J., Seo, M. K., Park, S. W. and Son, I. (2025) 'Exacerbated Cellular Senescence in Human Dopaminergic Neurons along with an Increase in LRRK2 Kinase Activity', *Biocell.* 49.

Ho, D. H., Seol, W. and Son, I. (2019) 'Upregulation of the p53-p21 pathway by G2019S LRRK2 contributes to the cellular senescence and accumulation of α-synuclein', *Cell Cycle.* 18**,** pp. 467-475.

Ho, P. W., Chang, E. E., Leung, C. T., Liu, H., Malki, Y., Pang, S. Y., Choi, Z. Y., Liang, Y., Lai, W. S., Ruan, Y., Leung, K. M., Yung, S., Mak, J. C., Kung, M. H., Ramsden, D. B. and Ho, S. L. (2022) 'Long-term inhibition of mutant LRRK2 hyper-kinase activity reduced mouse brain α-synuclein oligomers without adverse effects', *NPJ Parkinsons Dis.* 8**,** pp. 115.

Hoffmann, L. F., Martins, A., Majolo, F., Contini, V., Laufer, S. and Goettert, M. I. (2023) 'Neural regeneration research model to be explored: SH-SY5Y human neuroblastoma cells', *Neural Regeneration Research.* 18**,** pp. 1265-1266.

Hou, Z., He, P., Imam, M. U., Qi, J., Tang, S., Song, C. and Ismail, M. (2017) 'Edible Bird's Nest Prevents Menopause-Related Memory and Cognitive Decline in Rats via Increased Hippocampal Sirtuin-1 Expression', *Oxidative Medicine and Cellular Longevity.* 2017**,** pp. 7205082.

Hou, Z., Imam, M. U., Ismail, M., Azmi, N. H., Ismail, N., Ideris, A. and Mahmud, R. (2015a) 'Lactoferrin and ovotransferrin contribute toward antioxidative effects of Edible Bird's Nest against hydrogen peroxide-induced oxidative stress in human SH-SY5Y cells', *Bioscience, Biotechnology, and Biochemistry.* 79**,** pp. 1570-1578.

Hou, Z., Imam, M. U., Ismail, M., Ooi, D. J., Ideris, A. and Mahmud, R. (2015b) 'Nutrigenomic effects of edible bird's nest on insulin signaling in ovariectomized rats', *Drug design, development and therapy.* pp. 4115-4125.

Hsieh, C.-H., Shaltouki, A., Gonzalez, A. E., Da Cruz, A. B., Burbulla, L. F., Lawrence, E. S., Schüle, B., Krainc, D., Palmer, T. D. and Wang, X. (2016) 'Functional impairment in miro degradation and mitophagy is a shared feature in familial and sporadic Parkinson's disease', *Cell stem cell.* 19**,** pp. 709-724.

Hsu, C. H., Chan, D., Greggio, E., Saha, S., Guillily, M. D., Ferree, A., Raghavan, K., Shen, G. C., Segal, L. and Ryu, H. (2010) 'MKK6 binds and regulates expression of Parkinson's disease-related protein LRRK2', *Journal of neurochemistry.* 112**,** pp. 1593-1604.

Huda, M. N., Zuki, A., Azhar, K., Goh, Y., Suhaimi, H., Hazmi, A. A. and Zairi, M. (2008) 'Proximate, elemental and fatty acid analysis of pre-processed edible birds' nest (Aerodramus fuciphagus): a comparison between regions and type of nest'.

Hun, L. T., Wani, W. A., Tjih, E. T. T., Adnan, N. A., Le Ling, Y. and Aziz, R. A. (2015) 'Investigations into the physicochemical, biochemical and antibacterial properties of edible bird's nest', *J. Chem. Pharm. Res.* 7**,** pp. 228-247.

Hung, C. (2021) 'Importance of retrograde axonal transport in mitochondrial health and distribution', *Cell Death Discovery.* 7**,** pp. 106.

Hwang, E. S., Yoon, G. and Kang, H. T. (2009) 'A comparative analysis of the cell biology of senescence and aging', *Cellular and Molecular Life Sciences.* 66**,** pp. 2503-2524.

Hwang, G.-H., Song, B. and Bae, S. (2021) 'Current widely-used web-based tools for CRISPR nucleases, base editors, and prime editors', *Gene and Genome Editing.* 1**,** pp. 100004.

Ilieva, N. M., Hoffman, E. K., Ghalib, M. A., Greenamyre, J. T. and De Miranda, B. R. (2024) 'LRRK2 kinase inhibition protects against Parkinson's disease-associated environmental toxicants', *Neurobiology of Disease.* 196**,** pp. 106522.

Inoue, S., Nishimura, K., Gima, S., Nakano, M. and Takata, K. (2023) 'CRISPR-Cas9-edited SNCA knockout human induced pluripotent stem cell-derived dopaminergic neurons and their vulnerability to neurotoxicity', *Biological and Pharmaceutical Bulletin.* 46**,** pp. 517-522.

Ioghen, O. C., Ceafalan, L. C. and Popescu, B. O. (2023) 'SH-SY5Y cell line in vitro models for Parkinson disease research—old practice for new trends', *Journal of Integrative Neuroscience.* 22**,** pp. 20.

Ishino, Y., Shinagawa, H., Makino, K., Amemura, M. and Nakata, A. (1987) 'Nucleotide sequence of the iap gene, responsible for alkaline phosphatase isozyme conversion in Escherichia coli, and identification of the gene product', *J Bacteriol.* 169**,** pp. 5429-33.

Itahana, K., Campisi, J. and Dimri, G. P. 2007. Methods to detect biomarkers of cellular senescence: the senescence-associated β-galactosidase assay. *In:* TOLLEFSBOL, T. O. (ed.) *Biological aging: methods and protocols.*

Ito, G. and Utsunomiya-Tate, N. (2023) 'Overview of the Impact of Pathogenic LRRK2 Mutations in Parkinson's Disease', *Biomolecules.* 13.

Jaffar, F. H. F., Osman, K., Hui, C. K., Zulkefli, A. F. and Ibrahim, S. F. (2021) 'Edible Bird's Nest Supplementation Improves Male Reproductive Parameters of Sprague Dawley Rat', *Front Pharmacol.* 12**,** pp. 631402.

Jamal, M., Khan, F. A., Da, L., Habib, Z., Dai, J. and Cao, G. (2016) 'Keeping CRISPR/Cas on-target', *Current Issues in Molecular Biology.* 20**,** pp. 1-12.

Jiang, Z.-C., Chen, X.-J., Zhou, Q., Gong, X.-H., Chen, X. and Wu, W.-J. (2019) 'Downregulated LRRK2 gene expression inhibits proliferation and migration while promoting the apoptosis of thyroid cancer cells by inhibiting activation of the JNK signaling pathway', *International journal of oncology.* 55**,** pp. 21-34.

Jiang, Z., Huang, Y., Zhang, P., Han, C., Lu, Y., Mo, Z., Zhang, Z., Li, X., Zhao, S. and Cai, F. (2020) 'Characterization of a pathogenic variant in GBA for Parkinson's disease with mild cognitive impairment patients', *Molecular brain.* 13**,** pp. 1-10.

Jiao, Q., Li, X., An, J., Zhang, Z., Chen, X., Tan, J., Zhang, P., Lu, H. and Liu, Y. (2017) 'Cell-cell connection enhances proliferation and neuronal differentiation of rat embryonic neural stem/progenitor cells', *Frontiers in cellular neuroscience.* 11**,** pp. 200.

Jinek, M., Chylinski, K., Fonfara, I., Hauer, M., Doudna, J. A. and Charpentier, E. (2012) 'A Programmable Dual-RNA–Guided DNA Endonuclease in Adaptive Bacterial Immunity', *Science.* 337**,** pp. 816-821.

Joberty, G., Fälth-Savitski, M., Paulmann, M., Bösche, M., Doce, C., Cheng, A. T., Drewes, G. and Grandi, P. (2020) 'A tandem guide RNA-based strategy for efficient CRISPR gene editing of cell populations with low heterogeneity of edited alleles', *The CRISPR journal.* 3**,** pp. 123-134.

Jong, H.-L., Yuen, K.-S., Jin, D.-Y., Hoe, S. L. L., Ideris, A., Tan, C.-H., Lam, S.-K., Lim, Y.-M. and Cheong, S.-K. (2025) 'Generation of Leucine-Rich Repeat Kinase 2 (LRRK2) Knockout Neuroblastoma Cells SH-SY5Y by CRISPR/Cas9-Mediated Genome Editing', *Biochemical Genetics.*

Juan, C. A., Pérez De La Lastra, J. M., Plou, F. J. and Pérez-Lebeña, E. (2021) 'The chemistry of reactive oxygen species (ROS) revisited: outlining their role in biological macromolecules (DNA, lipids and proteins) and induced pathologies', *International journal of molecular sciences.* 22**,** pp. 4642.

Juárez-Flores, D. L., González-Casacuberta, I., Ezquerra, M., Bañó, M., Carmona-Pontaque, F., Catalán-García, M., Guitart-Mampel, M., Rivero, J. J., Tobias, E. and Milisenda, J. C. (2018) 'Exhaustion of mitochondrial and autophagic reserve may contribute to the development of LRRK2 G2019S-Parkinson's disease', *Journal of translational medicine.* 16**,** pp. 1-13.

Jung, K., Choi, J.-S., Koo, B.-M., Kim, Y. J., Song, J.-Y., Sung, M., Chang, E. S., Noh, K.-W., An, S., Lee, M.-S., Song, K., Lee, H., Kim, R. N., Shin, Y. K., Oh, D.-Y. and Choi, Y.-L. (2021) 'TM4SF4 and LRRK2 Are Potential Therapeutic Targets in Lung and Breast Cancers through Outlier Analysis', *Cancer Res Treat.* 53**,** pp. 9-24.

Kadgien, C. A., Kamesh, A. and Milnerwood, A. J. (2021) 'Endosomal traffic and glutamate synapse activity are increased in VPS35 D620N mutant knock-in mouse neurons, and resistant to LRRK2 kinase inhibition', *Molecular brain.* 14**,** pp. 143.

Kalogeropulou, A. F., Purlyte, E., Tonelli, F., Lange, S. M., Wightman, M., Prescott, A. R., Padmanabhan, S., Sammler, E. and Alessi, D. R. (2022) 'Impact of 100 LRRK2 variants linked to Parkinson's disease on kinase activity and microtubule binding', *Biochem J.* 479**,** pp. 1759-1783.

Kameda, M., Mikawa, T., Yokode, M., Inagaki, N. and Kondoh, H. (2021) 'Senescence research from historical theory to future clinical application', *Geriatrics & Gerontology International.* 21**,** pp. 125-130.

Kamikawaji, S., Ito, G. and Iwatsubo, T. (2009) 'Identification of the autophosphorylation sites of LRRK2', *Biochemistry.* 48**,** pp. 10963-75.

Kantor, B., Tagliafierro, L., Gu, J., Zamora, M. E., Ilich, E., Grenier, C., Huang, Z. Y., Murphy, S. and Chiba-Falek, O. (2018) 'Downregulation of SNCA expression by targeted editing of DNA methylation: a potential strategy for precision therapy in PD', *Molecular therapy.* 26**,** pp. 2638-2649.

Kim, H., Ham, S., Jo, M., Lee, G. H., Lee, Y.-S., Shin, J.-H. and Lee, Y. (2017) 'CRISPR-Cas9 mediated telomere removal leads to mitochondrial stress and protein aggregation', *International journal of molecular sciences.* 18**,** pp. 2093.

Kim, H. M., Lee, Y. M., Kim, E. H., Eun, S. W., Sung, H. K., Ko, H., Youn, S. J., Choi, Y., Yamada, W. and Shin, S. M. (2022) 'Anti-wrinkle efficacy of edible

bird’s nest extract: A randomized, double-blind, placebo-controlled, comparative study', *Frontiers in Pharmacology.* 13**,** pp. 843469.

Kim, J., Pajarillo, E., Rizor, A., Son, D.-S., Lee, J., Aschner, M. and Lee, E. (2019) 'LRRK2 kinase plays a critical role in manganese-induced inflammation and apoptosis in microglia', *PloS one.* 14**,** pp. e0210248.

Kim, K. S., Marcogliese, P. C., Yang, J., Callaghan, S. M., Resende, V., Abdel-Messih, E., Marras, C., Visanji, N. P., Huang, J. and Schlossmacher, M. G. (2018a) 'Regulation of myeloid cell phagocytosis by LRRK2 via WAVE2 complex stabilization is altered in Parkinson’s disease', *Proceedings of the National Academy of Sciences.* 115**,** pp. E5164-E5173.

Kim, O. K., Kim, D., Lee, M., Park, S. H., Yamada, W., Eun, S. and Lee, J. (2021a) 'Standardized Edible Bird's Nest Extract Prevents UVB Irradiation-Mediated Oxidative Stress and Photoaging in the Skin', *Antioxidants (Basel).* 10.

Kim, S., Yun, S. P., Lee, S., Umanah, G. E., Bandaru, V. V. R., Yin, X., Rhee, P., Karuppagounder, S. S., Kwon, S. H., Lee, H., Mao, X., Kim, D., Pandey, A., Lee, G., Dawson, V. L., Dawson, T. M. and Ko, H. S. (2018b) 'GBA1 deficiency negatively affects physiological α-synuclein tetramers and related multimers', *Proc Natl Acad Sci U S A.* 115**,** pp. 798-803.

Kim, Y. J., Goh, Y. S., Cheung, W., Kim, Y. S., Lee, H., Kim, Y. J., Goh, Y. S., Cheung, W., Kim, Y. S. and Lee, H. (2021b) 'Whitening and moisturizing effects of hydrolyzed swiftlet nest extracts', *Asian Journal of Beauty and Cosmetology.* 19**,** pp. 639-649.

Klein, C. L., Rovelli, G., Springer, W., Schall, C., Gasser, T. and Kahle, P. J. (2009) 'Homo- and heterodimerization of ROCO kinases: LRRK2 kinase inhibition by the LRRK2 ROCO fragment', *J Neurochem.* 111**,** pp. 703-15.

Kong Hangkin, K. H., Wong Kahing, W. K. and Chunlap, L. (2016) 'Identification of peptides released from hot water insoluble fraction of edible bird's nest under simulated gastro-intestinal conditions'.

Kong, Y., Keung, W., Yip, T., Ko, K., Tsao, S. and Ng, M. (1987) 'Evidence that epidermal growth factor is present in swiftlet's (Collocalia) nest', *Comparative biochemistry and physiology. B, Comparative biochemistry.* 87**,** pp. 221-226.

Koon, L. C. and Cranbrook, E. O. 2002. *Swiftlets of Borneo – Builders of edible nests,* Sabah, Malaysia, Natural History Publication (Borneo) Sdn. Bhd. .

Korolchuk, V. I., Miwa, S., Carroll, B. and Von Zglinicki, T. (2017) 'Mitochondria in cell senescence: is mitophagy the weakest link?', *EBioMedicine.* 21**,** pp. 7-13.

Kovalevich, J. and Langford, D. (2013a) 'Considerations for the use of SH-SY5Y neuroblastoma cells in neurobiology', *Neuronal cell culture: methods and protocols.* pp. 9-21.

Kovalevich, J. and Langford, D. (2013b) 'Considerations for the use of SH-SY5Y neuroblastoma cells in neurobiology', *Methods in Molecular Biology.* 1078**,** pp. 9-21.

Krüger, C., Lim, S.-Y., Buhrmann, A., Fahrig, F. L., Gabbert, C., Bahr, N., Madoev, H., Marras, C., Klein, C. and Lohmann, K. (2025) 'Updated MDSGene review on the clinical and genetic spectrum of LRRK2 variants in Parkinson´ s disease', *npj Parkinson's Disease.* 11**,** pp. 30.

Kuhlmann, N. and Milnerwood, A. J. (2020) 'A critical LRRK at the synapse? The neurobiological function and pathophysiological dysfunction of LRRK2', *Frontiers in molecular neuroscience.* 13**,** pp. 153.

Kumari, R. and Jat, P. (2021) 'Mechanisms of cellular senescence: cell cycle arrest and senescence associated secretory phenotype', *Frontiers in cell and developmental biology.* 9**,** pp. 645593.

Kurz, D. J., Decary, S., Hong, Y., Trivier, E., Akhmedov, A. and Erusalimsky, J. D. (2004) 'Chronic oxidative stress compromises telomere integrity and accelerates the onset of senescence in human endothelial cells', *Journal of cell science.* 117**,** pp. 2417-2426.

La Quaglia, M. P. and Manchester, K. M. (1996) 'A comparative analysis of neuroblastic and substrate-adherent human neuroblastoma cell lines', *Journal of pediatric surgery.* 31**,** pp. 315-318.

Labun, K., Montague, T. G., Krause, M., Torres Cleuren, Y. N., Tjeldnes, H. and Valen, E. (2019) 'CHOPCHOP v3: expanding the CRISPR web toolbox beyond genome editing', *Nucleic acids research.* 47**,** pp. W171-W174.

Lamonaca, G. and Volta, M. (2020) 'Alpha-synuclein and LRRK2 in synaptic autophagy: linking early dysfunction to late-stage pathology in Parkinson's disease', *Cells.* 9**,** pp. 1115.

Lander, E. S. (2016) 'The heroes of CRISPR', *Cell.* 164**,** pp. 18-28.

Larsen, S., Hanss, Z. and Krüger, R. (2018) 'The genetic architecture of mitochondrial dysfunction in Parkinson's disease', *Cell and tissue research.* 373**,** pp. 21-37.

Lavalley, N. J., Slone, S. R., Ding, H., West, A. B. and Yacoubian, T. A. (2016) '14-3-3 Proteins regulate mutant LRRK2 kinase activity and neurite shortening', *Hum Mol Genet.* 25**,** pp. 109-22.

Lawana, V. and Cannon, J. R. 2020. Chapter Five - Rotenone neurotoxicity: Relevance to Parkinson's disease. *In:* ASCHNER, M. & COSTA, L. G. (eds.) *Advances in Neurotoxicology.* Academic Press.

Lebovitz, C., Wretham, N., Osooly, M., Milne, K., Dash, T., Thornton, S., Tessier-Cloutier, B., Sathiyaseelan, P., Bortnik, S., Go, N. E., Halvorsen, E., Cederberg, R. A., Chow, N., Dos Santos, N., Bennewith, K. L., Nelson, B. H., Bally, M. B., Lam, W. L. and Gorski, S. M. (2021) 'Loss of Parkinson's susceptibility gene LRRK2 promotes carcinogen-induced lung tumorigenesis', *Sci Rep.* 11**,** pp. 2097.

Ledford, H. and Callaway, E. (2020) 'Pioneers of revolutionary CRISPR gene editing win chemistry Nobel', *Nature.* 586**,** pp. 346-347.

Lee, B. D., Shin, J. H., Vankampen, J., Petrucelli, L., West, A. B., Ko, H. S., Lee, Y. I., Maguire-Zeiss, K. A., Bowers, W. J., Federoff, H. J., Dawson, V. L. and Dawson, T. M. (2010) 'Inhibitors of leucine-rich repeat kinase-2 protect against models of Parkinson's disease', *Nat Med.* 16**,** pp. 998-1000.

Lee, C. H., Hamdan, N., Nyakuma, B. B., Wong, S. L., Wong, K. Y., Tan, H., Jamaluddin, H. and Lee, T. H. (2024) 'Purification, identification and molecular docking studies of antioxidant and anti-inflammatory peptides from Edible Bird's Nest', *Food Chemistry.* 454**,** pp. 139797.

Lee, S. B., Kim, W., Lee, S. and Chung, J. (2007) 'Loss of LRRK2/PARK8 induces degeneration of dopaminergic neurons in Drosophila', *Biochemical and biophysical research communications.* 358**,** pp. 534-539.

Lee, T. H., Wani, W. A., Lee, C. H., Cheng, K. K., Shreaz, S., Wong, S., Hamdan, N. and Azmi, N. A. (2021a) 'Edible bird's nest: The functional values of the prized animal-based bioproduct from Southeast Asia–A review', *Frontiers in pharmacology.* 12**,** pp. 626233.

Lee, Y. H., Park, J. Y., Lee, H., Song, E. S., Kuk, M. U., Joo, J., Oh, S., Kwon, H. W., Park, J. T. and Park, S. C. (2021b) 'Targeting mitochondrial metabolism as a strategy to treat senescence', *Cells.* 10**,** pp. 3003.

Lesage, S., Janin, S., Lohmann, E., Leutenegger, A. L., Leclere, L., Viallet, F., Pollak, P., Durif, F., Thobois, S., Layet, V., Vidailhet, M., Agid, Y., Dürr, A., Brice, A., Bonnet, A. M., Borg, M., Broussolle, E., Damier, P., Destée, A., Martinez, M., Penet, C., Rasco, O., Tison, F., Tranchan, C. and Vérin, M. (2007) 'LRRK2 exon 41 mutations in sporadic Parkinson disease in Europeans', *Arch Neurol.* 64**,** pp. 425-30.

Li, A., Gao, M., Liu, B., Qin, Y., Chen, L., Liu, H., Wu, H. and Gong, G. (2022) 'Mitochondrial autophagy: molecular mechanisms and implications for cardiovascular disease', *Cell death & disease.* 13**,** pp. 444.

Li, L., Su, H., Ji, Y., Zhu, F., Deng, J., Bai, X., Li, H., Liu, X., Luo, Y. and Lin, B. (2023) 'Deciphering Cell–Cell Interactions with Integrative Single-Cell Secretion Profiling', *Advanced Science.* 10**,** pp. 2301018.

Li, S., Zhao, S., Sinson, J. C., Bajic, A., Rosenfeld, J. A., Neeley, M. B., Pena, M., Worley, K. C., Burrage, L. C., Weisz-Hubshman, M., Ketkar, S., Craigen, W. J., Clark, G. D., Lalani, S., Bacino, C. A., Machol, K., Chao, H. T., Potocki, L., Emrick, L., Sheppard, J., Nguyen, M. T. T., Khoramnia, A., Hernandez, P. P., Nagamani, S. C., Liu, Z., Eng, C. M., Lee, B. and Liu, P. (2024a) 'The clinical utility and diagnostic implementation of human subject cell transdifferentiation followed by RNA sequencing', *Am J Hum Genet.* 111**,** pp. 841-862.

Li, X., Moore, D. J., Xiong, Y., Dawson, T. M. and Dawson, V. L. (2010) 'Reevaluation of phosphorylation sites in the Parkinson disease-associated leucine-rich repeat kinase 2', *J Biol Chem.* 285**,** pp. 29569-76.

Li, X. L., Lian, J. M., Chen, X. L., Fan, Q. Y., Yan, Y. and Cui, F. J. (2024b) 'A Novel Bacillus amyloliquefaciens Specifically Improving the Solubility and Antioxidant Activities of Edible Bird's Nest', *Curr Microbiol.* 81**,** pp. 164.

Lim, J., Wong, M., Chan, M. Y., Tan, A. M., Rajalingam, V., Lim, L., Lou, J. and Tan, C. L. (2006) 'Use of complementary and alternative medicine in paediatric oncology patients in Singapore', *Annals-Academy of Medicine Singapore.* 35**,** pp. 753.

Lin, C. H., Lin, H. Y., Fang, J. M. and Chen, C. C. (2020) 'A dual inhibitor targeting HMG-CoA reductase and histone deacetylase mitigates neurite degeneration in LRRK2-G2019S parkinsonism', *Aging (Albany NY).* 12**,** pp. 25581-25598.

Ling, A. J. W., Chang, L. S., Babji, A. S., Latip, J., Koketsu, M. and Lim, S. J. (2022) 'Review of sialic acid's biochemistry, sources, extraction and functions with special reference to edible bird's nest', *Food Chemistry.* 367**,** pp. 130755.

Ling, J. W. A., Chang, L. S., Babji, A. S. and Lim, S. J. (2020) 'Recovery of value-added glycopeptides from edible bird's nest (EBN) co-products: enzymatic hydrolysis, physicochemical characteristics and bioactivity', *Journal of the Science of Food and Agriculture.* 100**,** pp. 4714-4722.

Liu, C., Li, X., Chen, M., Liu, Y., Li, K., Wang, D., Yang, Z., Guo, Y., Zhao, Y., Zhao, H. and Zhang, C. (2025) 'Characterization and neurotherapeutic evaluation of venom polypeptides identified from Vespa magnifica: The role of Mastoparan-M in Parkinson's disease intervention', *J Ethnopharmacol.* 343**,** pp. 119481.

Liu, F., Simpson, A. B., D'costa, E., Bunn, F. S. and Van Leeuwen, S. S. (2023a) 'Sialic acid, the secret gift for the brain', *Critical Reviews in Food Science and Nutrition.* 63**,** pp. 9875-9894.

Liu, L., Li, Y., Chen, G. and Chen, Q. (2023b) 'Crosstalk between mitochondrial biogenesis and mitophagy to maintain mitochondrial homeostasis', *Journal of Biomedical Science.* 30**,** pp. 86.

Liu, M., Dobson, B., Glicksman, M. A., Yue, Z. and Stein, R. L. (2010a) 'Kinetic mechanistic studies of wild-type leucine-rich repeat kinase 2: characterization of the kinase and GTPase activities', *Biochemistry.* 49**,** pp. 2008-17.

Liu, M., Poulose, S., Schuman, E., Zaitsev, A. D., Dobson, B., Auerbach, K., Seyb, K., Cuny, G. D., Glicksman, M. A., Stein, R. L. and Yue, Z. (2010b) 'Development of a mechanism-based high-throughput screen assay for leucine-rich repeat kinase 2--discovery of LRRK2 inhibitors', *Anal Biochem.* 404**,** pp. 186-92.

Liu, M., Rehman, S., Tang, X., Gu, K., Fan, Q., Chen, D. and Ma, W. (2019) 'Methodologies for improving HDR efficiency', *Frontiers in genetics.* 9**,** pp. 691.

Liu, M., Shen, C. and Wang, C. (2019) 'Long Noncoding RNA LINC01133 Confers Tumor-Suppressive Functions in Ovarian Cancer by Regulating Leucine-Rich Repeat Kinase 2 as an miR-205 Sponge', *Am J Pathol.* 189**,** pp. 2323-2339.

Liu, W., Li, S., Zhang, Y., Li, J. and Li, Y. (2018) 'Efficient CRISPR-based genome editing using tandem guide RNA s and editable surrogate reporters', *FEBS Open Bio.* 8**,** pp. 1167-1175.

Liu, W., Liu, X., Li, Y., Zhao, J., Liu, Z., Hu, Z., Wang, Y., Yao, Y., Miller, A. W., Su, B., Cookson, M. R., Li, X. and Kang, Z. (2017) 'LRRK2 promotes the activation of NLRC4 inflammasome during Salmonella Typhimurium infection', *J Exp Med.* 214**,** pp. 3051-3066.

Liu, Y. J., Mcintyre, R. L., Janssens, G. E. and Houtkooper, R. H. (2020) 'Mitochondrial fission and fusion: A dynamic role in aging and potential target for age-related disease', *Mechanisms of ageing and development.* 186**,** pp. 111212.

Lobbestael, E., Van Den Haute, C., Macchi, F., Taymans, J.-M. and Baekelandt, V. (2020) 'Pathogenic LRRK2 requires secondary factors to induce cellular toxicity', *Bioscience Reports.* 40**,** pp. BSR20202225.

Loeffler, D. A., Klaver, A. C., Coffey, M. P., Aasly, J. O. and Lewitt, P. A. (2017) 'Increased oxidative stress markers in cerebrospinal fluid from healthy subjects with Parkinson's disease-associated LRRK2 gene mutations', *Frontiers in Aging Neuroscience.* 9**,** pp. 89.

Looi, Q. H. and Omar, A. R. (2016) 'Swiftlets and edible bird's nest industry in Asia', *Pertanika Journal of Scholarly Research Reviews.* 2.

Looyenga, B. D., Furge, K. A., Dykema, K. J., Koeman, J., Swiatek, P. J., Giordano, T. J., West, A. B., Resau, J. H., Teh, B. T. and Mackeigan, J. P. (2011) 'Chromosomal amplification of leucine-rich repeat kinase-2 (LRRK2) is required for oncogenic MET signaling in papillary renal and thyroid carcinomas', *Proc Natl Acad Sci U S A.* 108**,** pp. 1439-44.

Lopez, G., Lazzeri, G., Rappa, A., Isimbaldi, G., Cribiù, F. M., Guerini-Rocco, E., Ferrero, S., Vaira, V. and Di Fonzo, A. (2020) 'Comprehensive Genomic Analysis Reveals the Prognostic Role of LRRK2 Copy-Number Variations in Human Malignancies', *Genes (Basel).* 11.

Ludtmann, M. H., Kostic, M., Horne, A., Gandhi, S., Sekler, I. and Abramov, A. Y. (2019) 'LRRK2 deficiency induced mitochondrial Ca2+ efflux inhibition can be rescued by Na+/Ca2+/Li+ exchanger upregulation', *Cell death & disease.* 10**,** pp. 265.

Luerman, G. C., Nguyen, C., Samaroo, H., Loos, P., Xi, H., Hurtado-Lorenzo, A., Needle, E., Stephen Noell, G., Galatsis, P., Dunlop, J., Geoghegan, K. F. and Hirst, W. D. (2014) 'Phosphoproteomic evaluation of pharmacological inhibition of leucine-rich repeat kinase 2 reveals significant off-target effects of LRRK-2-IN-1', *J Neurochem.* 128**,** pp. 561-76.

Luo, J., Sun, T., Liu, Z., Liu, Y., Liu, J., Wang, S., Shi, X. and Zhou, H. (2025) 'Persistent accumulation of therapy-induced senescent cells: an obstacle to long-term cancer treatment efficacy', *International Journal of Oral Science.* 17**,** pp. 59.

Luo, Y. and Sakamoto, K. (2023) 'Ethyl pyruvate protects SHSY5Y cells against 6-hydroxydopamine-induced neurotoxicity by upregulating autophagy', *PLoS One.* 18**,** pp. e0281957.

Ma, B., Xu, L., Pan, X., Sun, L., Ding, J., Xie, C., Koliatsos, V. E. and Cai, H. (2016) 'LRRK2 modulates microglial activity through regulation of chemokine (C–X3–C) receptor 1 –mediated signalling pathways', *Human Molecular Genetics.* 25**,** pp. 3515-3523.

Ma, F., Liu, D.-C. and Dai, M.-X. (2012) 'The effects of the edible bird's nest on sexual function of male castrated rats', *Afr. J. Pharm. Pharmacol.* 6**,** pp. 2875-2879.

Ma, Y., Erb, M. L. and Moore, D. J. (2025) 'Aging, cellular senescence and Parkinson's disease', *Journal of Parkinson's Disease.* pp. 1877718X251316552.

Macleod, D., Dowman, J., Hammond, R., Leete, T., Inoue, K. and Abeliovich, A. (2006) 'The familial Parkinsonism gene LRRK2 regulates neurite process morphology', *Neuron.* 52**,** pp. 587-593.

Maday, S., Twelvetrees, A. E., Moughamian, A. J. and Holzbaur, E. L. (2014) 'Axonal transport: cargo-specific mechanisms of motility and regulation', *Neuron.* 84**,** pp. 292-309.

Madureira, M., Connor-Robson, N. and Wade-Martins, R. (2020) 'LRRK2: autophagy and lysosomal activity', *Frontiers in neuroscience.* 14**,** pp. 498.

Maekawa, T., Mori, S., Sasaki, Y., Miyajima, T., Azuma, S., Ohta, E. and Obata, F. (2012) 'The I2020T Leucine-rich repeat kinase 2 transgenic mouse exhibits impaired locomotive ability accompanied by dopaminergic neuron abnormalities', *Mol Neurodegener.* 7**,** pp. 15.

Maekawa, T., Sasaoka, T., Azuma, S., Ichikawa, T., Melrose, H. L., Farrer, M. J. and Obata, F. (2016) 'Leucine-rich repeat kinase 2 (LRRK2) regulates α-synuclein clearance in microglia', *BMC Neuroscience.* 17**,** pp. 77.

Maimun, A., Hana, N. and Choon, Y. K. (2024) 'Swiftlet Farming Industry--A White Gold in the Malaysian Housing Market?', *Pertanika Journal of Social Sciences & Humanities.* 32.

Mancini, A., Mazzocchetti, P., Sciaccaluga, M., Megaro, A., Bellingacci, L., Beccano-Kelly, D. A., Di Filippo, M., Tozzi, A. and Calabresi, P. (2020) 'From synaptic dysfunction to neuroprotective strategies in genetic Parkinson's disease: lessons from LRRK2', *Frontiers in cellular neuroscience.* 14**,** pp. 158.

Manzoni, C., Mamais, A., Dihanich, S., Abeti, R., Soutar, M. P. M., Plun-Favreau, H., Giunti, P., Tooze, S. A., Bandopadhyay, R. and Lewis, P. A. (2013) 'Inhibition of LRRK2 kinase activity stimulates macroautophagy', *Biochimica et Biophysica Acta.* 1833**,** pp. 2900-2900.

Marcone, M. F. (2005) 'Characterization of the edible bird's nest the "Caviar of the East"', *Food research international.* 38**,** pp. 1125-1134.

Martin, B. M. 2011. Clonal Isolation and Plating Efficiency. *In:* JOHN WILEY & SONS, L. (ed.) *eLS.*

Mata, I. F., Wedemeyer, W. J., Farrer, M. J., Taylor, J. P. and Gallo, K. A. (2006) 'LRRK2 in Parkinson's disease: protein domains and functional insights', *Trends in Neurosciences.* 29**,** pp. 286-293.

Mathews, S. T., Plaisance, E. P. and Kim, T. (2009) 'Imaging Systems for Westerns: Chemiluminescence vs. Infrared Detection', *Protein blotting and detection: methods and protocols.* pp. 499-513.

Matsukawa, N., Matsumoto, M., Bukawa, W., Chiji, H., Nakayama, K., Hara, H. and Tsukahara, T. (2011) 'Improvement of bone strength and dermal thickness due to dietary edible bird's nest extract in ovariectomized rats', *Biosci Biotechnol Biochem.* 75**,** pp. 590-2.

Mazaki, Y., Handa, H., Fumoto, Y., Horinouchi, T. and Onodera, Y. (2023) 'LRRK2 is involved in the chemotaxis of neutrophils and differentiated HL-60 cells, and the inhibition of LRRK2 kinase activity increases f MLP-induced chemotactic activity', *Cell Communication and Signaling.* 21**,** pp. 300.

Meixner, A., Boldt, K., Van Troys, M., Askenazi, M., Gloeckner, C. J., Bauer, M., Marto, J. A., Ampe, C., Kinkl, N. and Ueffing, M. (2011) 'A QUICK screen for Lrrk2 interaction partners–leucine-rich repeat kinase 2 is involved in actin cytoskeleton dynamics', *Molecular & Cellular Proteomics.* 10.

Milosevic, J., Schwarz, S. C., Ogunlade, V., Meyer, A. K., Storch, A. and Schwarz, J. (2009) 'Emerging role of LRRK2 in human neural progenitor cell cycle progression, survival and differentiation', *Molecular Neurodegeneration.* 4**,** pp. 1-9.

Miwa, S., Kashyap, S., Chini, E. and Von Zglinicki, T. (2022) 'Mitochondrial dysfunction in cell senescence and aging', *The Journal of clinical investigation.* 132.

Modrzejewski, D., Hartung, F., Sprink, T., Krause, D., Kohl, C. and Wilhelm, R. (2019) 'What is the available evidence for the range of applications of genome-editing as a new tool for plant trait modification and the potential occurrence of associated off-target effects: a systematic map', *Environmental Evidence.* 8**,** pp. 1-33.

Moehle, M. S., Daher, J. P. L., Hull, T. D., Boddu, R., Abdelmotilib, H. A., Mobley, J., Kannarkat, G. T., Tansey, M. G. and West, A. B. (2015) 'The G2019S LRRK2 mutation increases myeloid cell chemotactic responses and enhances LRRK2 binding to actin-regulatory proteins', *Human Molecular Genetics.* 24**,** pp. 4250-4267.

Moehle, M. S., Webber, P. J., Tse, T., Sukar, N., Standaert, D. G., Desilva, T. M., Cowell, R. M. and West, A. B. (2012) 'LRRK2 inhibition attenuates microglial inflammatory responses', *Journal of Neuroscience.* 32**,** pp. 1602-1611.

Mohamad Nasir, N. N., Mohamad Ibrahim, R., Abu Bakar, M. Z., Mahmud, R. and Ab Razak, N. A. (2021) 'Characterization and extraction influence protein profiling of edible bird's nest', *Foods.* 10**,** pp. 2248.

Mohamad Nasir, N. N., Mohamad Ibrahim, R., Mahmud, R., Ab Razak, N. A., Ismail, N., Chan, K. W. and Abu Bakar, M. Z. (2023) 'Edible Bird's Nest Effectively Attenuates Atherosclerosis through Modulation of Cholesterol Metabolism via Activation of PPARγ/LXRα Signaling Pathway In Vivo', *Journal of Food Biochemistry.* 2023**,** pp. 7861265.

Mojica, F. J., Díez-Villaseñor, C., Soria, E. and Juez, G. (2000) 'Biological significance of a family of regularly spaced repeats in the genomes of Archaea, Bacteria and mitochondria', *Mol Microbiol.* 36**,** pp. 244-6.

Moon, S. B., Kim, D. Y., Ko, J.-H. and Kim, Y.-S. (2019) 'Recent advances in the CRISPR genome editing tool set', *Experimental and Molecular Medicine.* 51**,** pp. 1-11.

Muhammad, N. N., Babji, A. S. and Ayub, M. K. Antioxidative activities of hydrolysates from edible birds nest using enzymatic hydrolysis. AIP Conference Proceedings, 2015. AIP Publishing.

Mun, S. L., Ter, Z. Y., Ariff, R. M., Rahman, N. F. A., Chang, L. S., Latip, J., Babji, A. S. and Lim, S. J. (2024) 'Fractionation and characterisation of sialylated-mucin glycoprotein from edible birds' nest hydrolysates through anion exchange chromatography', *Int J Biol Macromol.* 269**,** pp. 132022.

Murugan, D. D., Md Zain, Z., Choy, K. W., Zamakshshari, N. H., Choong, M. J., Lim, Y. M. and Mustafa, M. R. (2020) 'Edible bird's nest protects against

hyperglycemia-induced oxidative stress and endothelial dysfunction', *Frontiers in Pharmacology.* 10**,** pp. 1624.

Mylonas, A. and O'loghlen, A. (2022) 'Cellular senescence and ageing: mechanisms and interventions', *Frontiers in Aging.* 3**,** pp. 866718.

Napavichayanun, S., Yamdech, R., Reddy, N. and Aramwit, P. (2021) 'Edible Aerodramus fuciphagus bird nest for wound healing: in search of the best extraction method to increase sialic acid and its relationship with collagen production', *Agriculture and Natural Resources.* 55**,** pp. 301–310-301–310.

Narath, R., Ambros, I., Kowalska, A., Bozsaky, E., Boukamp, P. and Ambros, P. F. (2007) 'Induction of senescence in MYCN amplified neuroblastoma cell lines by hydroxyurea', *Genes, Chromosomes and Cancer.* 46**,** pp. 130-142.

Narváez-Pérez, L. F., Paz-Bermúdez, F., Avalos-Fuentes, J. A., Campos-Romo, A., Florán-Garduño, B. and Segovia, J. (2024) 'CRISPR/sgRNA-directed synergistic activation mediator (SAM) as a therapeutic tool for Parkinson´ s disease', *Gene Therapy.* 31**,** pp. 31-44.

National Cancer Institute USA (2024) *Complementary and Alternative Medicine*. Available at: https://www.cancer.gov/about-cancer/treatment/cam (Accessed: 5 January 2025).

Ness, D., Ren, Z., Gardai, S., Sharpnack, D., Johnson, V. J., Brennan, R. J., Brigham, E. F. and Olaharski, A. J. (2013) 'Leucine-rich repeat kinase 2 (LRRK2)-deficient rats exhibit renal tubule injury and perturbations in metabolic and immunological homeostasis', *PLoS One.* 8**,** pp. e66164.

Nguyen, A. P. and Moore, D. J. (2017) 'Understanding the GTPase Activity of LRRK2: Regulation, Function, and Neurotoxicity', *Adv Neurobiol.* 14**,** pp. 71-88.

Nguyen, T.-P., Le, Q. T., Bui, C. C., Ta, K. N. and Nguyen, K. T. (2024) 'Employing fruit juices to hydrolyze edible bird's nest and enhance the antioxidant, anti-tyrosinase, and wound-healing activities of the hydrolysates', *Heliyon.* 10.

Nichols, R. J., Dzamko, N., Hutti, J. E., Cantley, L. C., Deak, M., Moran, J., Bamborough, P., Reith, A. D. and Alessi, D. R. (2009) 'Substrate specificity and inhibitors of LRRK2, a protein kinase mutated in Parkinson's disease', *Biochem J.* 424**,** pp. 47-60.

Niu, J., Yu, M., Wang, C. and Xu, Z. (2012) 'Leucine-rich repeat kinase 2 disturbs mitochondrial dynamics via Dynamin-like protein', *Journal of neurochemistry.* 122**,** pp. 650-658.

Nixon-Abell, J., Berwick, D. C., Grannó, S., Spain, V. A., Blackstone, C. and Harvey, K. (2016) 'Protective LRRK2 R1398H variant enhances GTPase and Wnt signaling activity', *Frontiers in molecular neuroscience.* 9**,** pp. 18.

Norhayati, M., Azman, O. and Nazaimoon, W. (2010) 'Preliminary Study of the Nutritional Content of Malaysian Edible Bird's Nest', *Malaysian journal of nutrition.* 16.

Nur Ain, A., Abdul Rahman, O. and Aini, I. (2017) 'Preliminary Studies of Edible Bird Nest (EBN) Extract Reduced H1N1 Virus Induced Apoptosis on Cultured Cells-*In Vitro*', *Journal of Infectious Diseases and Epidemiology.* 3.

Nuytemans, K., Rademakers, R., Theuns, J., Pals, P., Engelborghs, S., Pickut, B., De Pooter, T., Peeters, K., Mattheijssens, M., Van Den Broeck, M., Cras, P., De Deyn, P. P. and Van Broeckhoven, C. (2008) 'Founder mutation p.R1441C in the leucine-rich repeat kinase 2 gene in Belgian Parkinson's disease patients', *European Journal of Human Genetics.* 16**,** pp. 471-479.

O'mahony, A. G., Mazzocchi, M., Morris, A., Morales-Prieto, N., Guinane, C., Wyatt, S. L., Collins, L. M., Sullivan, A. M. and O'keeffe, G. W. (2025) 'The class-IIa HDAC inhibitor TMP269 promotes BMP-Smad signalling and is neuroprotective in in vitro and in vivo 6-hydroxydopamine models of Parkinson's disease', *Neuropharmacology.* 268**,** pp. 110319.

Obergasteiger, J., Frapporti, G., Lamonaca, G., Pizzi, S., Picard, A., Lavdas, A. A., Pischedda, F., Piccoli, G., Hilfiker, S. and Lobbestael, E. (2020) 'Kinase inhibition of G2019S-LRRK2 enhances autolysosome formation and function to reduce endogenous alpha-synuclein intracellular inclusions', *Cell death discovery.* 6**,** pp. 45.

Oda, M. (1983) 'Saccharides and amino acids of the mucoid in an edible bird's nest', *Nippon Shokuhin Kogyo Gakkaishi.* 30**,** pp. 221-227.

Ohtonen, S., Giudice, L., Jäntti, H., Fazaludeen, M. F., Shakirzyanova, A., Gómez-Budia, M., Välimäki, N. N., Niskanen, J., Korvenlaita, N., Fagerlund, I., Koistinaho, J., Amiry-Moghaddam, M., Savchenko, E., Roybon, L., Lehtonen, Š., Korhonen, P. and Malm, T. (2023) 'Human iPSC-derived microglia carrying the LRRK2-G2019S mutation show a Parkinson's disease related transcriptional profile and function', *Sci Rep.* 13**,** pp. 22118.

Olszewska, A., Borkowska, A., Granica, M., Karolczak, J., Zglinicki, B., Kieda, C. and Was, H. (2022) 'Escape from cisplatin-induced senescence of hypoxic lung cancer cells can be overcome by hydroxychloroquine', *Frontiers in Oncology.* 11**,** pp. 738385.

Østergaard, F. G. (2024) 'Knocking out the LRRK2 gene increases sensitivity to wavelength information in rats', *Scientific Reports.* 14**,** pp. 4984.

Pacelli, C., Giguère, N., Bourque, M.-J., Lévesque, M., Slack, R. S. and Trudeau, L.-É. (2015) 'Elevated mitochondrial bioenergetics and axonal arborization size are key contributors to the vulnerability of dopamine neurons', *Current Biology.* 25**,** pp. 2349-2360.

Paisán-RuíZ, C., Jain, S., Evans, E. W., Gilks, W. P., Simón, J., Van Der Brug, M., De Munain, A. L., Aparicio, S., Gil, A. M. N. and Khan, N. (2004) 'Cloning of the gene containing mutations that cause PARK8-linked Parkinson's disease', *Neuron.* 44**,** pp. 595-600.

Palese, F., Pontis, S., Realini, N. and Piomelli, D. (2021) 'NAPE-specific phospholipase D regulates LRRK2 association with neuronal membranes', *Adv Pharmacol.* 90**,** pp. 217-238.

Panagiotakopoulou, V., Ivanyuk, D., De Cicco, S., Haq, W., Arsić, A., Yu, C., Messelodi, D., Oldrati, M., Schöndorf, D. C., Perez, M. J., Cassatella, R. P., Jakobi, M., Schneiderhan-Marra, N., Gasser, T., Nikić-Spiegel, I. and Deleidi, M. (2020) 'Interferon-γ signaling synergizes with LRRK2 in neurons and microglia derived from human induced pluripotent stem cells', *Nat Commun.* 11**,** pp. 5163.

Pang, S. Y.-Y., Lo, R. C. N., Ho, P. W.-L., Liu, H.-F., Chang, E. E. S., Leung, C.-T., Malki, Y., Choi, Z. Y.-K., Wong, W. Y. and Kung, M. H.-W. (2022) 'LRRK2, GBA and their interaction in the regulation of autophagy: implications on therapeutics in Parkinson's disease', *Translational Neurodegeneration.* 11**,** pp. 5.

Papkovskaia, T. D., Chau, K.-Y., Inesta-Vaquera, F., Papkovsky, D. B., Healy, D. G., Nishio, K., Staddon, J., Duchen, M. R., Hardy, J. and Schapira, A. H. (2012) 'G2019S leucine-rich repeat kinase 2 causes uncoupling protein-mediated mitochondrial depolarization', *Human molecular genetics.* 21**,** pp. 4201-4213.

Parrilla Castellar, E. R., Plichta, J. K., Davis, R., Gonzalez-Hunt, C. and Sanders, L. H. (2020) 'Somatic Mutations in LRRK2 Identify a Subset of Invasive Mammary Carcinomas Associated with High Mutation Burden', *Am J Pathol.* 190**,** pp. 2478-2482.

Pattanayak, R., Ekkatine, R., Petit, C. M. and Yacoubian, T. A. (2024) '14-3-3 phosphorylation inhibits 14-3-3θ's ability to regulate LRRK2 kinase activity and toxicity', *Hum Mol Genet.* 33**,** pp. 2071-2083.

Pauly, D. and Hanack, K. (2015) 'How to avoid pitfalls in antibody use', *F1000Research.* 4.

Pedro, L., Padrós, J., Beaudet, L., Schubert, H. D., Gillardon, F. and Dahan, S. (2010) 'Development of a high-throughput AlphaScreen assay measuring full-length LRRK2(G2019S) kinase activity using moesin protein substrate', *Anal Biochem.* 404**,** pp. 45-51.

Pellegrini, L., Hauser, D. N., Li, Y., Mamais, A., Beilina, A., Kumaran, R., Wetzel, A., Nixon-Abell, J., Heaton, G. and Rudenko, I. (2018) 'Proteomic analysis reveals co-ordinated alterations in protein synthesis and degradation pathways in LRRK2 knockout mice', *Human molecular genetics.* 27**,** pp. 3257-3271.

Pereira, C., Martins, L. M. and Saraiva, L. (2014) 'LRRK2, but not pathogenic mutants, protects against H2O2 stress depending on mitochondrial function and endocytosis in a yeast model', *Biochimica et Biophysica Acta (BBA)-General Subjects.* 1840**,** pp. 2025-2031.

Perez Carrion M, P. F., Biosa a, Russo I, Straniero L, Civiero L, Guida M, Gloeckner Cj, Ticozzi N, Tiloca C, Mariani C, Pezzoli G, Duga S, Pichler I, Pan L, Landers Je, Greggio E, Hess Mw, Goldwurm S, Piccoli G. (2018) 'The LRRK2 Variant E193K Prevents Mitochondrial Fission Upon MPP+ Treatment by Altering LRRK2 Binding to DRP1', *Front Mol Neurosci.* 11.

Pillai-Kastoori, L., Heaton, S., Shiflett, S. D., Roberts, A. C., Solache, A. and Schutz-Geschwender, A. R. (2020) 'Antibody validation for Western blot: By the user, for the user', *Journal of Biological Chemistry.* 295**,** pp. 926-939.

Pinjala, P., Tryphena, K. P., Prasad, R., Khatri, D. K., Sun, W., Singh, S. B., Gugulothu, D., Srivastava, S. and Vora, L. (2023) 'CRISPR/Cas9 assisted stem cell therapy in Parkinson's disease', *Biomaterials Research.* 27**,** pp. 46.

Pischedda, F. and Piccoli, G. (2021) 'LRRK2 at the pre-synaptic site: A 16-years perspective', *Journal of neurochemistry.* 157**,** pp. 297-311.

Pizzino, G., Irrera, N., Cucinotta, M., Pallio, G., Mannino, F., Arcoraci, V., Squadrito, F., Altavilla, D. and Bitto, A. (2017) 'Oxidative Stress: Harms and Benefits for Human Health', *Oxid Med Cell Longev.* 2017**,** pp. 8416763.

Plowey, E. D., Cherra Iii, S. J., Liu, Y. J. and Chu, C. T. (2008) 'Role of autophagy in G2019S-LRRK2-associated neurite shortening in differentiated SH-SY5Y cells', *Journal of neurochemistry.* 105**,** pp. 1048-1056.

Potdar, C., Jagtap, S., Singh, K., Yadav, R., Pal, P. K. and Datta, I. (2024) 'Impaired Sonic Hedgehog Responsiveness of Induced Pluripotent Stem Cell-Derived Floor Plate Cells Carrying the LRRK2-I1371V Mutation Contributes to the Ontogenic Origin of Lower Dopaminergic Neuron Yield', *Stem Cells Dev.* 33**,** pp. 306-320.

Pozsgay, V., Jennings, H. and Kasper, D. L. (1987) '4,8-anhydro-N-acetylneuraminic acid. Isolation from edible bird's nest and structure determination', *Eur J Biochem.* 162**,** pp. 445-50.

Przedborski, S., Jackson-Lewis, V., Djaldetti, R., Liberatore, G., Vila, M., Vukosavic, S. and Almer, G. (2000) 'The parkinsonian toxin MPTP: action and mechanism', *Restor Neurol Neurosci.* 16**,** pp. 135-142.

Pungaliya, P. P., Bai, Y., Lipinski, K., Anand, V. S., Sen, S., Brown, E. L., Bates, B., Reinhart, P. H., West, A. B., Hirst, W. D. and Braithwaite, S. P. (2010) 'Identification and characterization of a leucine-rich repeat kinase 2 (LRRK2) consensus phosphorylation motif', *PLoS One.* 5**,** pp. e13672.

Purro, S. A., Galli, S. and Salinas, P. C. (2014) 'Dysfunction of Wnt signaling and synaptic disassembly in neurodegenerative diseases', *Journal of molecular cell biology.* 6**,** pp. 75-80.

Qian, N., Zhang, C. X., Fang, G. D., Qiu, S., Song, Y., Yuan, M., Wang, D. L. and Cheng, X. R. (2025) 'Interventional Effects of Edible Bird's Nest and Free Sialic Acids on LPS-Induced Brain Inflammation in Mice', *Nutrients.* 17.

Qing, X., Walter, J., Jarazo, J., Arias-Fuenzalida, J., Hillje, A.-L. and Schwamborn, J. C. (2017) 'CRISPR/Cas9 and piggyBac-mediated footprint-free LRRK2-G2019S knock-in reveals neuronal complexity phenotypes and α-Synuclein modulation in dopaminergic neurons', *Stem Cell Research.* 24**,** pp. 44-50.

Quddus, A., Yimer, N., Jesse, F. F. A., Basit, M. A., Amir, M. and Islam, M. S. (2021) 'Edible bird's nest protects histomorphology of rat's uterus against cadmium (Cd) toxicity through a reduction of Cd deposition and enhanced antioxidant activity', *Saudi J Biol Sci.* 28**,** pp. 7068-7076.

Quek, M. C., Chin, N. L., Tan, S. W., Yusof, Y. A. and Law, C. L. (2018a) 'Molecular identification of species and production origins of edible bird's nest

using FINS and SYBR green I based real-time PCR', *Food Control.* 84**,** pp. 118-127.

Quek, M. C., Chin, N. L., Yusof, Y. A., Law, C. L. and Tan, S. W. (2018b) 'Characterization of edible bird's nest of different production, species and geographical origins using nutritional composition, physicochemical properties and antioxidant activities', *Food Research International.* 109**,** pp. 35-43.

Quintero-Espinosa, D. A., Sanchez-Hernandez, S., Velez-Pardo, C., Martin, F. and Jimenez-Del-Rio, M. (2023) 'LRRK2 Knockout Confers Resistance in HEK-293 Cells to Rotenone-Induced Oxidative Stress, Mitochondrial Damage, and Apoptosis', *Int J Mol Sci.* 24.

Rahman, M. U., Bilal, M., Shah, J. A., Kaushik, A., Teissedre, P. L. and Kujawska, M. (2022) 'CRISPR-Cas9-Based Technology and Its Relevance to Gene Editing in Parkinson's Disease', *Pharmaceutics.* 14.

Rakotoarisoa, M., Angelov, B., Garamus, V. M. and Angelova, A. (2019) 'Curcumin-and fish oil-loaded spongosome and cubosome nanoparticles with neuroprotective potential against H2O2-induced oxidative stress in differentiated human SH-SY5Y cells', *ACS Omega.* 4**,** pp. 3061-3073.

Ramachandran, R., Babji, A. S. and Sani, N. A. Antihypertensive potential of bioactive hydrolysate from edible bird’s nest. AIP Conference Proceedings, 2018. AIP Publishing.

Ramalingam, M., Huh, Y.-J. and Lee, Y.-I. (2019) 'The impairments of α-synuclein and mechanistic target of rapamycin in rotenone-induced SH-SY5Y cells and mice model of Parkinson’s disease', *Frontiers in neuroscience.* 13**,** pp. 1028.

Ramonet, D., Daher, J. P. L., Lin, B. M., Stafa, K., Kim, J., Banerjee, R., Westerlund, M., Pletnikova, O., Glauser, L. and Yang, L. (2011) 'Dopaminergic neuronal loss, reduced neurite complexity and autophagic abnormalities in transgenic mice expressing G2019S mutant LRRK2', *PloS one.* 6**,** pp. e18568.

Ran, F. A., Hsu, P. D., Wright, J., Agarwala, V., Scott, D. A. and Zhang, F. (2013) 'Genome engineering using the CRISPR-Cas9 system', *Nature Protocols.* 8**,** pp. 2281-2308.

Rashed, A. A., Ahmad, H., Abdul Khalid, S. K. and Rathi, D.-N. G. (2021) 'The potential use of sialic acid from edible bird’s nest to attenuate mitochondrial dysfunction by in vitro study', *Frontiers in Pharmacology.* 12**,** pp. 633303.

Rodríguez-Losada, N., De La Rosa, J., Larriva, M., Wendelbo, R., Aguirre, J. A., Castresana, J. S. and Ballaz, S. J. (2020) 'Overexpression of alpha-synuclein promotes both cell proliferation and cell toxicity in human SH-SY5Y neuroblastoma cells', *Journal of Advanced Research.* 23**,** pp. 37-45.

Roh, K.-B., Lee, J., Kim, Y.-S., Park, J., Kim, J.-H., Lee, J. and Park, D. (2012) 'Mechanisms of Edible Bird′ s Nest Extract-Induced Proliferation of Human Adipose-Derived Stem Cells', *Evidence-based Complementary and Alternative Medicine.* 2012**,** pp. 797520.

Ross, O. A., Soto-Ortolaza, A. I., Heckman, M. G., Aasly, J. O., Abahuni, N., Annesi, G., Bacon, J. A., Bardien, S., Bozi, M. and Brice, A. (2011) 'Association of LRRK2 exonic variants with susceptibility to Parkinson's disease: a case–control study', *The Lancet Neurology.* 10**,** pp. 898-908.

Ross, R. A. and Spengler, B. A. Human neuroblastoma stem cells. Seminars in cancer biology, 2007. Elsevier, 241-247.

Ross, R. A., Spengler, B. A. and Biedler, J. L. (1983) 'Coordinate morphological and biochemical interconversion of human neuroblastoma cells', *Journal of the National Cancer Institute.* 71**,** pp. 741-747.

Ross, R. A., Walton, J. D., Han, D., Guo, H. F. and Cheung, N. K. (2015) 'A distinct gene expression signature characterizes human neuroblastoma cancer stem cells', *Stem Cell Res.* 15**,** pp. 419-26.

Rudyk, C., Dwyer, Z. and Hayley, S. (2019) 'Leucine-rich repeat kinase-2 (LRRK2) modulates paraquat-induced inflammatory sickness and stress phenotype', *J Neuroinflammation.* 16**,** pp. 120.

Russo, I., Bubacco, L. and Greggio, E. (2022) 'LRRK2 as a target for modulating immune system responses', *Neurobiology of Disease.* 169**,** pp. 105724.

Russo, I., Kaganovich, A., Ding, J., Landeck, N., Mamais, A., Varanita, T., Biosa, A., Tessari, I., Bubacco, L. and Greggio, E. (2019) 'Transcriptome analysis of LRRK2 knock-out microglia cells reveals alterations of inflammatory-and oxidative stress-related pathways upon treatment with α-synuclein fibrils', *Neurobiology of disease.* 129**,** pp. 67-78.

Saengkrajang, W., Matan, N. and Matan, N. (2013) 'Nutritional composition of the farmed edible bird's nest (Collocalia fuciphaga) in Thailand', *Journal of food composition and analysis.* 31**,** pp. 41-45.

Saez-Atienzar, S., Bonet-Ponce, L., Blesa, J., Romero, F. J., Murphy, M., Jordan, J. and Galindo, M. (2014) 'The LRRK2 inhibitor GSK2578215A induces protective autophagy in SH-SY5Y cells: involvement of Drp-1-mediated mitochondrial fission and mitochondrial-derived ROS signaling', *Cell death & disease.* 5**,** pp. e1368-e1368.

Sancho, R. M., Law, B. M. and Harvey, K. (2009) 'Mutations in the LRRK2 Roc-COR tandem domain link Parkinson's disease to Wnt signalling pathways', *Human molecular genetics.* 18**,** pp. 3955-3968.

Sanders, L. H., Laganière, J., Cooper, O., Mak, S. K., Vu, B. J., Huang, Y. A., Paschon, D. E., Vangipuram, M., Sundararajan, R. and Urnov, F. D. (2014) 'LRRK2 mutations cause mitochondrial DNA damage in iPSC-derived neural cells from Parkinson's disease patients: reversal by gene correction', *Neurobiology of disease.* 62**,** pp. 381-386.

Sastre, D., Zafar, F., Torres, C. a. M., Piper, D., Kirik, D., Sanders, L. H., Qi, L. S. and Schüle, B. (2023) 'Inactive S. aureus Cas9 downregulates alpha-synuclein and reduces mtDNA damage and oxidative stress levels in human stem cell model of Parkinson's disease', *Scientific Reports.* 13**,** pp. 17796.

Satake, W., Nakabayashi, Y., Mizuta, I., Hirota, Y., Ito, C., Kubo, M., Kawaguchi, T., Tsunoda, T., Watanabe, M., Takeda, A., Tomiyama, H., Nakashima, K., Hasegawa, K., Obata, F., Yoshikawa, T., Kawakami, H., Sakoda, S., Yamamoto, M., Hattori, N., Murata, M., Nakamura, Y. and Toda, T. (2009) 'Genome-wide association study identifies common variants at four loci as genetic risk factors for Parkinson's disease', *Nat Genet.* 41**,** pp. 1303-7.

Schapansky, J., Nardozzi, J. D., Felizia, F. and Lavoie, M. J. (2014) 'Membrane recruitment of endogenous LRRK2 precedes its potent regulation of autophagy', *Human Molecular Genetics.* 23**,** pp. 4201-4214.

Schmitt, C. A., Wang, B. and Demaria, M. (2022) 'Senescence and cancer—role and therapeutic opportunities', *Nature reviews Clinical oncology.* 19**,** pp. 619-636.

Schwab, A. J., Sison, S. L., Meade, M. R., Broniowska, K. A., Corbett, J. A. and Ebert, A. D. (2017) 'Decreased sirtuin deacetylase activity in LRRK2 G2019S iPSC-derived dopaminergic neurons', *Stem cell reports.* 9**,** pp. 1839-1852.

Seol, W., Nam, D. and Son, I. (2019) 'Rab GTPases as physiological substrates of LRRK2 kinase', *Experimental neurobiology.* 28**,** pp. 134.

Seow, E.-K., Ibrahim, B., Muhammad, S. A., Lee, L. H. and Cheng, L.-H. (2016) 'Differentiation between house and cave edible bird's nests by chemometric analysis of amino acid composition data', *Lwt.* 65**,** pp. 428-435.

Shih, V., Chiang, J. and Chan, A. (2009) 'Complementary and alternative medicine (CAM) usage in Singaporean adult cancer patients', *Annals of Oncology.* 20**,** pp. 752-757.

Shutinoski, B., Hakimi, M., Harmsen, I. E., Lunn, M., Rocha, J., Lengacher, N., Zhou, Y. Y., Khan, J., Nguyen, A., Hake-Volling, Q., El-Kodsi, D., Li, J., Alikashani, A., Beauchamp, C., Majithia, J., Coombs, K., Shimshek, D., Marcogliese, P. C., Park, D. S., Rioux, J. D., Philpott, D. J., Woulfe, J. M., Hayley, S., Sad, S., Tomlinson, J. J., Brown, E. G. and Schlossmacher, M. G. (2019) 'Lrrk2 alleles modulate inflammation during microbial infection of mice in a sex-dependent manner', *Sci Transl Med.* 11.

Simpson, C., Vinikoor-Imler, L., Nassan, F. L., Shirvan, J., Lally, C., Dam, T. and Maserejian, N. (2022) 'Prevalence of ten LRRK2 variants in Parkinson's disease: A comprehensive review', *Parkinsonism & Related Disorders.* 98**,** pp. 103-113.

Singh, A., Zhi, L. and Zhang, H. (2019) 'LRRK2 and mitochondria: recent advances and current views', *Brain research.* 1702**,** pp. 96-104.

Singh, B. K., Tripathi, M., Sandireddy, R., Tikno, K., Zhou, J. and Yen, P. M. (2020) 'Decreased autophagy and fuel switching occur in a senescent hepatic cell model system', *Aging (Albany NY).* 12**,** pp. 13958.

Singh, F. and Ganley, I. G. (2021) 'Parkinson's disease and mitophagy: an emerging role for LRRK2', *Biochemical Society Transactions.* 49**,** pp. 551-562.

Singh, F., Prescott, A. R., Rosewell, P., Ball, G., Reith, A. D. and Ganley, I. G. (2021) 'Pharmacological rescue of impaired mitophagy in Parkinson's disease-related LRRK2 G2019S knock-in mice', *elife.* 10**,** pp. e67604.

Sirinupong, N., Chansuwan, W. and Kaewkaen, P. (2024) 'Effect of Edible Bird's Nest on Protecting against Cognitive Deficit and Ameliorating Beta-Amyloid in Hippocampal Rats' Model of Cerebral Ischemia', *Journal of Food Biochemistry.* 2024**,** pp. 7367894.

Skiteva, O., Yao, N., Sitzia, G. and Chergui, K. (2022) 'LRRK2-G2019S mice display alterations in glutamatergic synaptic transmission in midbrain dopamine neurons', *Journal of Neurochemistry.* 161**,** pp. 158-172.

Skruber, K., Read, T.-A. and Vitriol, E. A. (2021) 'Delivering defined amounts of purified protein with high precision into living cells', *STAR protocols.* 2**,** pp. 100272.

Smith, W. W., Pei, Z., Jiang, H., Dawson, V. L., Dawson, T. M. and Ross, C. A. (2006) 'Kinase activity of mutant LRRK2 mediates neuronal toxicity', *Nat Neurosci.* 9**,** pp. 1231-3.

Snoderly-Foster, L. J. and Olivas, W. M. (2022) 'Regulation of Parkinson's disease-associated genes by Pumilio proteins and microRNAs in SH-SY5Y neuronal cells', *PLoS One.* 17**,** pp. e0275235.

Soni, D., Garg, Y., Upadhayay, S., Bhatia, A., Basir, B., Singh, S. K., Dua, K. and Kumar, P. (2025) 'Auranofin-loaded chitosan-lipid hybrid nanoparticle protects against rotenone model of Parkinson's disease via modulation of GSK-3β/ Nrf2/HO-1 signaling', *Eur J Pharmacol.* 998**,** pp. 177523.

Sriwilaijaroen, N., Hanamatsu, H., Yokota, I., Nishikaze, T., Ijichi, T., Takahashi, T., Sakoda, Y., Furukawa, J.-I. and Suzuki, Y. (2024) 'Edible bird's nest: N- and O-glycan analysis and synergistic anti-avian influenza virus activity with neuraminidase inhibitors', *Antiviral Research.* 232**,** pp. 106040.

Stafa, K., Trancikova, A., Webber, P. J., Glauser, L., West, A. B. and Moore, D. J. (2012) 'GTPase Activity and Neuronal Toxicity of Parkinson's Disease–Associated LRRK2 Is Regulated by ArfGAP1', *PLoS genetics.* 8**,** pp. e1002526.

Steger, M., Tonelli, F., Ito, G., Davies, P., Trost, M., Vetter, M., Wachter, S., Lorentzen, E., Duddy, G. and Wilson, S. (2016) 'Phosphoproteomics reveals that Parkinson's disease kinase LRRK2 regulates a subset of Rab GTPases', *elife.* 5**,** pp. e12813.

Sternberg, S. H., Redding, S., Jinek, M., Greene, E. C. and Doudna, J. A. (2014) 'DNA interrogation by the CRISPR RNA-guided endonuclease Cas9', *Nature.* 507**,** pp. 62-67.

Stormo, A. E. D., Shavarebi, F., Fitzgibbon, M., Earley, E. M., Ahrendt, H., Lum, L. S., Verschueren, E., Swaney, D. L., Skibinski, G., Ravisankar, A., Van Haren, J., Davis, E. J., Johnson, J. R., Von Dollen, J., Balen, C., Porath, J., Crosio, C., Mirescu, C., Iaccarino, C., Dauer, W. T., Nichols, R. J., Wittmann, T., Cox, T. C., Finkbeiner, S., Krogan, N. J., Oakes, S. A. and Hiniker, A. (2022) 'The E3 ligase TRIM1 ubiquitinates LRRK2 and controls its localization, degradation, and toxicity', *J Cell Biol.* 221.

Streubel-Gallasch, L., Giusti, V., Sandre, M., Tessari, I., Plotegher, N., Giusto, E., Masato, A., Iovino, L., Battisti, I. and Arrigoni, G. (2021) 'Parkinson’s

disease–associated LRRK2 interferes with astrocyte-mediated alpha-synuclein clearance', *Molecular Neurobiology.* 58**,** pp. 3119-3140.

Su, Y.-C., Guo, X. and Qi, X. (2015) 'Threonine 56 phosphorylation of Bcl-2 is required for LRRK2 G2019S-induced mitochondrial depolarization and autophagy', *Biochimica et Biophysica Acta (BBA)-Molecular Basis of Disease.* 1852**,** pp. 12-21.

Su, Y.-C. and Qi, X. (2013) 'Inhibition of excessive mitochondrial fission reduced aberrant autophagy and neuronal damage caused by LRRK2 G2019S mutation', *Human molecular genetics.* 22**,** pp. 4545-4561.

Suda, Y., Kuzumaki, N., Sone, T., Narita, M., Tanaka, K., Hamada, Y., Iwasawa, C., Shibasaki, M., Maekawa, A. and Matsuo, M. (2018) 'Down-regulation of ghrelin receptors on dopaminergic neurons in the substantia nigra contributes to Parkinson's disease-like motor dysfunction', *Molecular brain.* 11**,** pp. 1-9.

Suelves, N., Saleki, S., Ibrahim, T., Palomares, D., Moonen, S., Koper, M. J., Vrancx, C., Vadukul, D. M., Papadopoulos, N. and Viceconte, N. (2023) 'Senescence-related impairment of autophagy induces toxic intraneuronal amyloid-β accumulation in a mouse model of amyloid pathology', *Acta neuropathologica communications.* 11**,** pp. 82.

Sulaiman, S. Z. S., Umran, N. S. S., Mohamed, S., Abu, J., Ng, A. M. H., Lau, B. Y. C., Lai, K. S., Ilias, N., Lau, S. F. and Ajat, M. (2024) 'Proteomic and Morphological Analysis of Bone and Articular Cartilage Changes in Osteoarthritic Rabbits Supplemented with Edible Bird's Nest (EBN)', *Malaysian Journal of Fundamental and Applied Sciences.* 20**,** pp. 1274-1287.

Sule, R., Rivera, G. and Gomes, A. V. (2023) 'Western blotting (immunoblotting): history, theory, uses, protocol and problems', *Biotechniques.* 75**,** pp. 99-114.

Sun, S., Hodel, M., Wang, X., De Vicente, J., Haritunians, T., Debebe, A., Hung, C.-T., Ma, C., Malique, A. and Nguyen, H. N. (2024) 'Macrophage LRRK2 hyperactivity impairs autophagy and induces Paneth cell dysfunction', *Science immunology.* 9**,** pp. eadi7907.

Tai, H., Wang, Z., Gong, H., Han, X., Zhou, J., Wang, X., Wei, X., Ding, Y., Huang, N. and Qin, J. (2017) 'Autophagy impairment with lysosomal and mitochondrial dysfunction is an important characteristic of oxidative stress-induced senescence', *Autophagy.* 13**,** pp. 99-113.

Tan, S. N., Sani, D., Lim, C. W., Ideris, A., Stanslas, J. and Lim, C. T. S. (2020) 'Proximate analysis and safety profile of farmed edible bird's nest in Malaysia

and its effect on cancer cells', *Evidence-Based Complementary and Alternative Medicine.* 2020**,** pp. 8068797.

Tang, P. L., Goh, H. S. and Sia, S. S. (2021) 'Combined enzymatic hydrolysis and herbal extracts fortification to boost in vitro antioxidant activity of edible bird's nest solution', *Chinese Herbal Medicines.* 13**,** pp. 549-555.

Taschner-Mandl, S., Schwarz, M., Blaha, J., Kauer, M., Kromp, F., Frank, N., Rifatbegovic, F., Weiss, T., Ladenstein, R. and Hohenegger, M. (2015) 'Metronomic topotecan impedes tumor growth of MYCN-amplified neuroblastoma cells in vitro and in vivo by therapy induced senescence', *Oncotarget.* 7**,** pp. 3571.

Taymans, J.-M., Fell, M., Greenamyre, T., Hirst, W. D., Mamais, A., Padmanabhan, S., Peter, I., Rideout, H. and Thaler, A. (2023) 'Perspective on the current state of the LRRK2 field', *npj Parkinson's Disease.* 9**,** pp. 104.

Ter, Z. Y., Chang, L. S., Zaini, N. a. M., Fazry, S., Babji, A. S., Koketsu, M., Takashima, S., Kamal, N. and Lim, S. J. (2024) 'Untargeted metabolomics profiling for revealing water-soluble bioactive components and biological activities in edible bird's nest', *Food Res Int.* 198**,** pp. 115289.

Terazawa, S. and Shimoda, H. (2020) 'Keratinocyte proliferative and wound healing effects of edible bird's nest extract on human skin', *Int. J. Biomed. Sci.* 16**,** pp. 43-51.

Thavamanithevi, S., Sarifah, R., Lim, C., Theanmalar, M., Aidawati, M., Devi, M. D. and Saleha, A. Characterization and standardization of edible birds Nest (EBN)-determination of sialic acid. Proceedings of the Edible Bird Nest Industry Conference, 2014. 25-26.

The Human Protein Atlas (no date) *Human Protein Atlas proteinatlas.org*. Available at: https://www.proteinatlas.org/ENSG00000188906-LRRK2/tissue (Accessed: 24 April 2025).

Thomas, J. M., Li, T., Yang, W., Xue, F., Fishman, P. S. and Smith, W. W. (2017) '68 and FX2149 attenuate mutant LRRK2-R1441C-induced neural transport impairment', *Frontiers in aging neuroscience.* 8**,** pp. 337.

Toh, J., Chua, L. L., Ho, P., Sandanaraj, E., Tang, C., Wang, H. and Tan, E. K. (2021) 'Identification of targets from LRRK2 rescue phenotypes', *Cells.* 10**,** pp. 76.

Tolosa, E., Vila, M., Klein, C. and Rascol, O. (2020) 'LRRK2 in Parkinson disease: challenges of clinical trials', *Nature Reviews Neurology.* 16**,** pp. 97-107.

Tombesi, G., Kompella, S., Favetta, G., Chen, C., Zhao, Y., Sevegnani, M., Marte, A., Battisti, I., Morosin, E. and Ornaghi, M. (2024) 'LRRK2 regulates synaptic function through BDNF signaling and actin cytoskeleton', *eLife.* pp. 2022.10. 31.514622.

Tong, S.-R., Lee, T.-H., Cheong, S.-K. and Lim, Y.-M. (2020) 'Untargeted metabolite profiling on the water-soluble metabolites of edible bird's nest through liquid chromatography-mass spectrometry', *Veterinary World.* 13**,** pp. 304.

Tong, T., Duan, W., Xu, Y., Hong, H., Xu, J., Fu, G., Wang, X., Yang, L., Deng, P., Zhang, J., He, H., Mao, G., Lu, Y., Lin, X., Yu, Z., Pi, H., Cheng, Y., Xu, S. and Zhou, Z. (2022) 'Paraquat exposure induces Parkinsonism by altering lipid profile and evoking neuroinflammation in the midbrain', *Environ Int.* 169**,** pp. 107512.

Tong, Y., Giaime, E., Yamaguchi, H., Ichimura, T., Liu, Y., Si, H., Cai, H., Bonventre, J. V. and Shen, J. (2012) 'Loss of leucine-rich repeat kinase 2 causes age-dependent bi-phasic alterations of the autophagy pathway', *Molecular neurodegeneration.* 7**,** pp. 1-16.

Tong, Y., Yamaguchi, H., Giaime, E., Boyle, S., Kopan, R., Kelleher Iii, R. J. and Shen, J. (2010) 'Loss of leucine-rich repeat kinase 2 causes impairment of protein degradation pathways, accumulation of α-synuclein, and apoptotic cell death in aged mice', *Proceedings of the National Academy of Sciences.* 107**,** pp. 9879-9884.

U.S. National Library of Medicine (2020) *A Study to Evaluate the Safety, Tolerability, Pharmacokinetics, and Pharmacodynamics of DNL201 in Healthy Volunteers*. Available at: https://clinicaltrials.gov/study/NCT04551534?term=DNL201&rank=2 (Accessed: 26 March 2025).

U.S. National Library of Medicine (2024) *A Study to Assess if BIIB122 Tablets Are Safe and Can Slow Worsening of Early-Stage Parkinson's Disease in Participants With Specific LRRK2 Genetic Variants Between the Ages of 30 and 80 Using the Movement Disorder Society-Unified Parkinson's Disease Rating Scale (LIGHTHOUSE)*. Available at: https://clinicaltrials.gov/study/NCT05418673 (Accessed: 27 Jan 2025).

U.S. National Library of Medicine (2025a) *Safety and Pharmacodynamic Effects of BIIB122 in Participants With LRRK2-Associated Parkinson's Disease (LRRK2-PD)*. Available at:

https://clinicaltrials.gov/study/NCT06602193?term=DNL151&aggFilters=phase:2&rank=1 (Accessed: 26 March 2025).

U.S. National Library of Medicine (2025b) *A Study to Assess the Safety of BIIB122 Tablets and if it Can Slow the Worsening of Early-Stage Parkinson's Disease in Participants Between the Ages of 30 and 80 (LUMA)*. Available at: https://clinicaltrials.gov/study/NCT05348785 (Accessed: 27 Jan 2025).

U.S. National Library of Medicine (2025c) *A Study to Evaluate the Safety, Tolerability, and Pharmacokinetics of BIIB094 in Adults With Parkinson's Disease (REASON)* Available at: https://clinicaltrials.gov/study/NCT03976349 (Accessed: 26 March 2025).

U.S. National Library of Medicine (2025d) *A Study to Learn About the Safety of BIIB122 Tablets and Whether They Can Slow the Worsening of Early-Stage Parkinson's Disease in Adults Between the Ages of 30 and 80 (LUMA)*. Available at: https://clinicaltrials.gov/study/NCT05348785?term=DNL151&aggFilters=phase:2&rank=2 (Accessed: 26 March 2025).

Uhlén, M., Fagerberg, L., Hallström, B. M., Lindskog, C., Oksvold, P., Mardinoglu, A., Sivertsson, Å., Kampf, C., Sjöstedt, E., Asplund, A., Olsson, I., Edlund, K., Lundberg, E., Navani, S., Szigyarto, C. a.-K., Odeberg, J., Djureinovic, D., Takanen, J. O., Hober, S., Alm, T., Edqvist, P.-H., Berling, H., Tegel, H., Mulder, J., Rockberg, J., Nilsson, P., Schwenk, J. M., Hamsten, M., Von Feilitzen, K., Forsberg, M., Persson, L., Johansson, F., Zwahlen, M., Von Heijne, G., Nielsen, J. and Pontén, F. (2015) 'Tissue-based map of the human proteome', *Science.* 347**,** pp. 1260419.

Unal, K. I., Chang, L., Mustapha, W. a. W., Razali, N. S. M., Babji, A. S. and Lim, S. J. (2022) 'Edible bird's nest, a valuable glycoprotein source: Current research prospects and challenges in Malaysia', *Sains Malaysiana.* 51**,** pp. 2829-2842.

Unal, K. I., Chang, L. S., Mustapha, W. a. W., Razali, N. S. M., Babji, A. S. and Lim, S. J. (2024) 'Extraction, structural analysis and biological activities of edible bird's nest sialylated mucin (siamuc) glycoproteins: a review', *Food Bioscience.* pp. 104791.

Van Groningen, T., Akogul, N., Westerhout, E. M., Chan, A., Hasselt, N. E., Zwijnenburg, D. A., Broekmans, M., Stroeken, P., Haneveld, F. and Hooijer, G. K. (2019) 'A NOTCH feed-forward loop drives reprogramming from adrenergic to mesenchymal state in neuroblastoma', *Nature communications.* 10**,** pp. 1530.

Verma, M., Callio, J., Otero, P. A., Sekler, I., Wills, Z. P. and Chu, C. T. (2017) 'Mitochondrial Calcium Dysregulation Contributes to Dendrite Degeneration

Mediated by PD/LBD-Associated LRRK2 Mutants', *J Neurosci.* 37**,** pp. 11151-11165.

Vermilyea, S. C., Babinski, A., Tran, N., To, S., Guthrie, S., Kluss, J. H., Schmidt, J. K., Wiepz, G. J., Meyer, M. G. and Murphy, M. E. (2020) 'In vitro CRISPR/Cas9-directed gene editing to model LRRK2 G2019S Parkinson's disease in common marmosets', *Scientific reports.* 10**,** pp. 3447.

Veschi, V., Verona, F. and Thiele, C. J. (2019) 'Cancer stem cells and neuroblastoma: characteristics and therapeutic targeting options', *Frontiers in endocrinology.* 10**,** pp. 782.

Vimala, B., Hussain, H. and Nazaimoon, W. W. (2012) 'Effects of edible bird's nest on tumour necrosis factor-alpha secretion, nitric oxide production and cell viability of lipopolysaccharide-stimulated RAW 264.7 macrophages', *Food and agricultural immunology.* 23**,** pp. 303-314.

Wainwright, L. J., Lasorella, A. and Iavarone, A. (2001) 'Distinct mechanisms of cell cycle arrest control the decision between differentiation and senescence in human neuroblastoma cells', *Proceedings of the National Academy of Sciences, USA.* 98**,** pp. 9396-9400.

Wallings, R., Manzoni, C. and Bandopadhyay, R. (2015) 'Cellular processes associated with LRRK 2 function and dysfunction', *The FEBS journal.* 282**,** pp. 2806-2826.

Wallings, R. L., Herrick, M. K. and Tansey, M. G. (2020) 'LRRK2 at the interface between peripheral and central immune function in Parkinson's', *Frontiers in Neuroscience.* 14**,** pp. 443.

Wallings, R. L. and Tansey, M. G. (2019) 'LRRK2 regulation of immune-pathways and inflammatory disease', *Biochem Soc Trans.* 47**,** pp. 1581-1595.

Walton, J. D., Kattan, D. R., Thomas, S. K., Spengler, B. A., Guo, H.-F., Biedler, J. L., Cheung, N.-K. V. and Ross, R. A. (2004) 'Characteristics of stem cells from human neuroblastoma cell lines and in tumors', *Neoplasia.* 6**,** pp. 838-845.

Wang, B. (2009) 'Sialic acid is an essential nutrient for brain development and cognition', *Annu Rev Nutr.* 29**,** pp. 177-222.

Wang, B. and Brand-Miller, J. (2003) 'The role and potential of sialic acid in human nutrition', *European journal of clinical nutrition.* 57**,** pp. 1351-1369.

Wang, D., Shimamura, N., Mochizuki, M., Nakahara, T., Sunada, K. and Xiao, L. (2023a) 'Enzyme-Digested Edible Bird's Nest (EBND) Prevents UV and Arid Environment-Induced Cellular Oxidative Stress, Cell Death and DNA Damage in Human Skin Keratinocytes and Three-Dimensional Epithelium Equivalents', *Antioxidants (Basel).* 12.

Wang, L., Lankhorst, L. and Bernards, R. (2022) 'Exploiting senescence for the treatment of cancer', *Nature Reviews Cancer.* 22**,** pp. 340-355.

Wang, M., Qing, Y., Fan, Q., Li, S., Yan, T., Amakye, W. K., Xu, Y., Liu, X. and Ren, J. (2024a) 'Identification of the Wound Healing Activity Peptidome of Edible Bird's Nest Protein Hydrolysate and the In Silico Evaluation of Its Transport and Absorption Potential in Skin', *Journal of Agricultural and Food Chemistry.*

Wang, S., Long, H., Hou, L., Feng, B., Ma, Z., Wu, Y., Zeng, Y., Cai, J., Zhang, D.-W. and Zhao, G. (2023b) 'The mitophagy pathway and its implications in human diseases', *Signal transduction and targeted therapy.* 8**,** pp. 304.

Wang, S., Zhang, X., Guo, Y., Rong, H. and Liu, T. (2017) 'The long noncoding RNA HOTAIR promotes Parkinson's disease by upregulating LRRK2 expression', *Oncotarget.* 8**,** pp. 24449-24456.

Wang, X., Yan, M. H., Fujioka, H., Liu, J., Wilson-Delfosse, A., Chen, S. G., Perry, G., Casadesus, G. and Zhu, X. (2012) 'LRRK2 regulates mitochondrial dynamics and function through direct interaction with DLP1', *Human molecular genetics.* 21**,** pp. 1931-1944.

Wang, Y., Gao, J. Z., Sakaguchi, T., Maretzky, T., Gurung, P., Narayanan, N. S., Short, S., Xiong, Y. and Kang, Z. (2024b) 'LRRK2 G2019S Promotes Colon Cancer Potentially via LRRK2–GSDMD Axis-Mediated Gut Inflammation', *Cells.* 13**,** pp. 565.

Wauters, F., Cornelissen, T., Imberechts, D., Martin, S., Koentjoro, B., Sue, C., Vangheluwe, P. and Vandenberghe, W. (2020) 'LRRK2 mutations impair depolarization-induced mitophagy through inhibition of mitochondrial accumulation of RAB10', *Autophagy.* 16**,** pp. 203-222.

Weindel, C. G., Bell, S. L., Vail, K. J., West, K. O., Patrick, K. L. and Watson, R. O. (2020) 'LRRK2 maintains mitochondrial homeostasis and regulates innate immune responses to Mycobacterium tuberculosis', *Elife.* 9.

West, A. B., Moore, D. J., Biskup, S., Bugayenko, A., Smith, W. W., Ross, C. A., Dawson, V. L. and Dawson, T. M. (2005) 'Parkinson's disease-associated

mutations in leucine-rich repeat kinase 2 augment kinase activity', *Proc Natl Acad Sci U S A.* 102**,** pp. 16842-7.

Williamson, M. G., Madureira, M., Mcguinness, W., Heon-Roberts, R., Mock, E. D., Naidoo, K., Cramb, K. M., Caiazza, M.-C., Malpartida, A. B. and Lavelle, M. (2023) 'Mitochondrial dysfunction and mitophagy defects in LRRK2-R1441C Parkinson's disease models', *Human Molecular Genetics.* 32**,** pp. 2808-2821.

Winner, B., Melrose, H., Zhao, C., Hinkle, K., Yue, M., Kent, C., Braithwaite, A., Ogholikhan, S., Aigner, R. and Winkler, J. (2011) 'Adult neurogenesis and neurite outgrowth are impaired in LRRK2 G2019S mice', *Neurobiology of disease.* 41**,** pp. 706-716.

Wolfe, K. L. and Liu, R. H. (2007) 'Cellular Antioxidant Activity (CAA) Assay for Assessing Antioxidants, Foods, and Dietary Supplements', *Journal of Agricultural and Food Chemistry.* 55**,** pp. 8896-8907.

Wong, L. C., Chan, E., Tay, S., Lee, K. M. and Back, M. (2010) 'Complementary and alternative medicine practices among Asian radiotherapy patients', *Asia-Pacific Journal of Clinical Oncology.* 6**,** pp. 357-363.

Wong, R. W. C. and Guillaud, L. (2004) 'The role of epidermal growth factor and its receptors in mammalian CNS', *Cytokine & growth factor reviews.* 15**,** pp. 147-156.

Wong, Z. C., Chan, G. K., Wu, K. Q., Poon, K. K., Chen, Y., Dong, T. T. and Tsim, K. W. (2018) 'Complete digestion of edible bird's nest releases free N-acetylneuraminic acid and small peptides: an efficient method to improve functional properties', *Food & function.* 9**,** pp. 5139-5149.

Wu, J., Yang, S., Wu, H., Huang, Y. and Miao, Y. (2023) 'Knockdown of LRRK2 inhibits the progression of lung cancer by regulating TLR4/NF-κB pathways and NLRP3 inflammasome', *J Clin Biochem Nutr.* 73**,** pp. 178-184.

Xie, Y., Zeng, H., Huang, Z., Xu, H., Fan, Q., Zhang, Y. and Zheng, B. (2018) 'Effect of maternal administration of edible bird's nest on the learning and memory abilities of suckling offspring in mice', *Neural Plasticity.* 2018**,** pp. 7697261.

Xu, Y. and Li, Z. (2020) 'CRISPR-Cas systems: Overview, innovations and applications in human disease research and gene therapy', *Comput Struct Biotechnol J.* 18**,** pp. 2401-2415.

Xu, Z., Yang, D., Huang, X. and Huang, H. (2021) 'Astragaloside IV protects 6-hydroxydopamine-induced SH-SY5Y cell model of Parkinson's disease via activating the JAK2/STAT3 pathway', *Frontiers in neuroscience.* 15**,** pp. 631501.

Yadavalli, N. and Ferguson, S. M. (2023) 'LRRK2 suppresses lysosome degradative activity in macrophages and microglia through MiT-TFE transcription factor inhibition', *Proceedings of the National Academy of Sciences.* 120**,** pp. e2303789120.

Yan, R. and Liu, Z. (2017) 'LRRK2 enhances Nod1/2-mediated inflammatory cytokine production by promoting Rip2 phosphorylation', *Protein Cell.* 8**,** pp. 55-66.

Yang, C., Pang, J., Xu, J., Pan, H., Li, Y., Zhang, H., Liu, H. and Xiao, S. Y. (2021) 'LRRK2 is a candidate prognostic biomarker for clear cell renal cell carcinoma', *Cancer Cell Int.* 21**,** pp. 343.

Yang, M., Cheung, S.-H., Li, S. C. and Cheung, H.-Y. (2014) 'Establishment of a holistic and scientific protocol for the authentication and quality assurance of edible bird's nest', *Food Chemistry.* 151**,** pp. 271-278.

Yang, Q., Pang, S., Zhao, C., Wang, Y., Lu, J., Yue, Z. and Chan, P. (2024) 'Impairment of the trans-Golgi-Lysosomal Pathway Accelerates Dopaminergic Neuronal Senescence in LRRK2R1627P Rats', *Aging and Disease.* 16**,** pp. 3089.

Yew, M. Y., Koh, R. Y., Chye, S. M., Othman, I. and Ng, K. Y. (2014) 'Edible bird's nest ameliorates oxidative stress-induced apoptosis in SH-SY5Y human neuroblastoma cells', *BMC complementary and alternative medicine.* 14**,** pp. 1-12.

Yew, M. Y., Koh, R. Y., Chye, S. M., Othman, I., Soga, T., Parhar, I. and Ng, K. Y. (2018) 'Edible bird's nest improves motor behavior and protects dopaminergic neuron against oxidative and nitrosative stress in Parkinson's disease mouse model', *Journal of Functional Foods.* 48**,** pp. 576-585.

Yi, H., Piao, M., Chen, Q., He, Z. and Chen, T. (2023) 'Fractionation of simulated digestive products of bird's nest in vitro: skin whitening activity of fractions', *Journal of Food Biochemistry.* 2023**,** pp. 3211692.

Yida, Z., Imam, M. U. and Ismail, M. (2014) 'In vitro bioaccessibility and antioxidant properties of edible bird's nest following simulated human gastro-intestinal digestion', *BMC complementary and alternative medicine.* 14**,** pp. 1-7.

Yida, Z., Imam, M. U., Ismail, M., Hou, Z., Abdullah, M. A., Ideris, A. and Ismail, N. (2015a) 'Edible Bird's Nest attenuates high fat diet-induced oxidative stress and inflammation via regulation of hepatic antioxidant and inflammatory genes', *BMC Complementary and Alternative Medicine.* 15**,** pp. 1-7.

Yida, Z., Imam, M. U., Ismail, M., Ismail, N. and Hou, Z. (2015b) 'Edible bird's nest attenuates procoagulation effects of high-fat diet in rats', *Drug Design, Development and Therapy.* pp. 3951-3959.

Yida, Z., Imam, M. U., Ismail, M., Ooi, D.-J., Sarega, N., Azmi, N. H., Ismail, N., Chan, K. W., Hou, Z. and Yusuf, N. B. (2015c) 'Edible Bird's Nest Prevents High Fat Diet-Induced Insulin Resistance in Rats', *Journal of diabetes research.* 2015**,** pp. 760535.

Yin, D., Wells, J., Clinton, J., Volpe, L.-A., Grady, K. and Curley, J. Development of lipid-based transfection reagents for efficient expression of transgenes in hard-to-transfect cell types. Cancer Research, 2014. AMER ASSOC CANCER RESEARCH 615 CHESTNUT ST, 17TH FLOOR, PHILADELPHIA, PA ….

You, Y., Ramachandra, S. G. and Jin, T. (2020) 'A CRISPR-based method for testing the essentiality of a gene', *Scientific Reports.* 10**,** pp. 14779.

Yuen, K.-S., Chan, C.-P., Kok, K.-H. and Jin, D.-Y. 2017. Mutagenesis and Genome Engineering of Epstein–Barr Virus in Cultured Human Cells by CRISPR/Cas9. *In:* REEVES, A. (ed.) *In Vitro Mutagenesis: Methods and Protocols.* New York, NY: Springer New York.

Zainal Abidin, F., Hui, C. K., Luan, N. S., Mohd Ramli, E. S., Hun, L. T. and Abd Ghafar, N. (2011) 'Effects of edible bird's nest (EBN) on cultured rabbit corneal keratocytes', *BMC complementary and alternative medicine.* 11**,** pp. 1-10.

Zeineldin, M., Patel, A. G. and Dyer, M. A. (2022) 'Neuroblastoma: When differentiation goes awry', *Neuron.* 110**,** pp. 2916-2928.

Zeng, H., Jian, Y., Xie, Y., Fan, Q., Chang, Q., Zheng, B. and Zhang, Y. (2022) 'Edible bird's nest inhibits the inflammation and regulates the immunological balance of lung injury mice by SO2', *Food Frontiers.* 3**,** pp. 773-784.

Zhang, J., Li, K., Wang, X., Smith, A. M., Ning, B., Liu, Z., Liu, C., Ross, C. A. and Smith, W. W. (2021) 'Curcumin Reduced H(2)O(2)- and G2385R-LRRK2-Induced Neurodegeneration', *Front Aging Neurosci.* 13**,** pp. 754956.

Zhang, M., Yao, C., Cai, J., Liu, S., Liu, X. N., Chen, Y., Wang, S., Ji, P., Pan, M., Kang, Z. and Wang, Y. (2019) 'LRRK2 is involved in the pathogenesis of system lupus erythematosus through promoting pathogenic antibody production', *J Transl Med.* 17**,** pp. 37.

Zhang, M., Yi, F., Wu, J. and Tang, Y. (2022a) 'The efficient generation of knockout microglia cells using a dual-sgRNA strategy by CRISPR/Cas9', *Frontiers in Molecular Neuroscience.* 15**,** pp. 1008827.

Zhang, Q., Cheng, X., Wu, W., Yang, S., You, H., Ye, Z., Liu, N., Chen, X. and Pan, X. (2022b) 'Age-related LRRK2 G2019S mutation impacts microglial dopaminergic fiber refinement and synaptic pruning involved in abnormal behaviors', *Journal of Molecular Neuroscience.* pp. 1-17.

Zhang, Q., Yang, W., Liu, J., Liu, H., Lv, Z., Zhang, C., Chen, D. and Jiao, Z. (2020) 'Identification of Six Flavonoids as Novel Cellular Antioxidants and Their Structure-Activity Relationship', *Oxidative medicine and cellular longevity.* 2020**,** pp. 4150897.

Zhang, Y. M., Zhou, X. J., Cheng, F. J., Qi, Y. Y., Hou, P., Zhao, M. H. and Zhang, H. (2017) 'Autophagy-related gene LRRK2 is likely a susceptibility gene for systemic lupus erythematosus in northern Han Chinese', *Oncotarget.* 8**,** pp. 13754-13761.

Zhao, J., Geng, L., Chen, Y. and Wu, C. (2020) 'SNHG1 promotes MPP+-induced cytotoxicity by regulating PTEN/AKT/mTOR signaling pathway in SH-SY5Y cells via sponging miR-153-3p', *Biological Research.* 53**,** pp. 1-11.

Zhao, M. W., Lin, C. J. and Qiu, J. P. (2023) 'LINC00707 promotes multidrug resistance of ovarian cancer cells by targeting the miR-382-5p/LRRK2 axis', *Acta Biochim Pol.* 70**,** pp. 799-806.

Zhao, R., Li, G., Kong, X.-J., Huang, X.-Y., Li, W., Zeng, Y.-Y. and Lai, X.-P. (2016) 'The improvement effects of edible bird’s nest on proliferation and activation of B lymphocyte and its antagonistic effects on immunosuppression induced by cyclophosphamide', *Drug design, development and therapy.* pp. 371-381.

Zhiping, H., Imam, M. U., Ismail, M., Ismail, N., Yida, Z., Ideris, A., Sarega, N. and Mahmud, R. (2015) 'Effects of edible bird's nest on hippocampal and cortical neurodegeneration in ovariectomized rats', *Food & function.* 6**,** pp. 1701-1711.

Zhu, H., Sydor, A. M., Yan, B. R., Li, R., Boniecki, M. T., Lyons, C., Cygler, M., Muise, A. M., Maxson, M. E., Grinstein, S., Raught, B. and Brumell, J. H. (2025)

'Salmonella exploits LRRK2-dependent plasma membrane dynamics to invade host cells', *Nat Commun.* 16**,** pp. 2329.

Zimprich, A., Biskup, S., Leitner, P., Lichtner, P., Farrer, M., Lincoln, S., Kachergus, J., Hulihan, M., Uitti, R. J. and Calne, D. B. (2004) 'Mutations in LRRK2 cause autosomal-dominant parkinsonism with pleomorphic pathology', *Neuron.* 44**,** pp. 601-607.

Zou, J., Mali, P., Huang, X., Dowey, S. N. and Cheng, L. (2011) 'Site-specific gene correction of a point mutation in human iPS cells derived from an adult patient with sickle cell disease', *Blood.* 118**,** pp. 4599-4608.

Zulkefle, N. N., Ibrahim, M. A., Azuan, N. F., Ch'ng, S. E., Ismail, N., Abu Bakar, M. Z. and Chan, K. W. (2024) 'A Review on the Edible Bird's Nest Quality and Manufacturing Standards of the Three Largest Exporting Countries in the World', *Journal of Food Quality.* 2024**,** pp. 5608357.

Zulkifli, A. S., Babji, A. S., Lim, S. J., Teh, A. H., Daud, N. M. and Rahman, H. A. (2019) 'Effect of different hydrolysis time and enzymes on chemical properties, antioxidant and antihyperglycemic activities of edible bird nest hydrolysate', *Malaysian applied biology.* 48**,** pp. 149-156.

APPENDIX A

DNA sequence of the edited *LRRK2* gene in 13 potential clones i.e. (A) D1-1, (B) D1-4, (C) D3-1, (D) D4-2, (E) D4-5, (F) D5-1, (G) D6-1, (H) D6-3, (I) D7-1, (J) D7-2, (K) D7-3, (L) W1-1 and (M) W2-1.

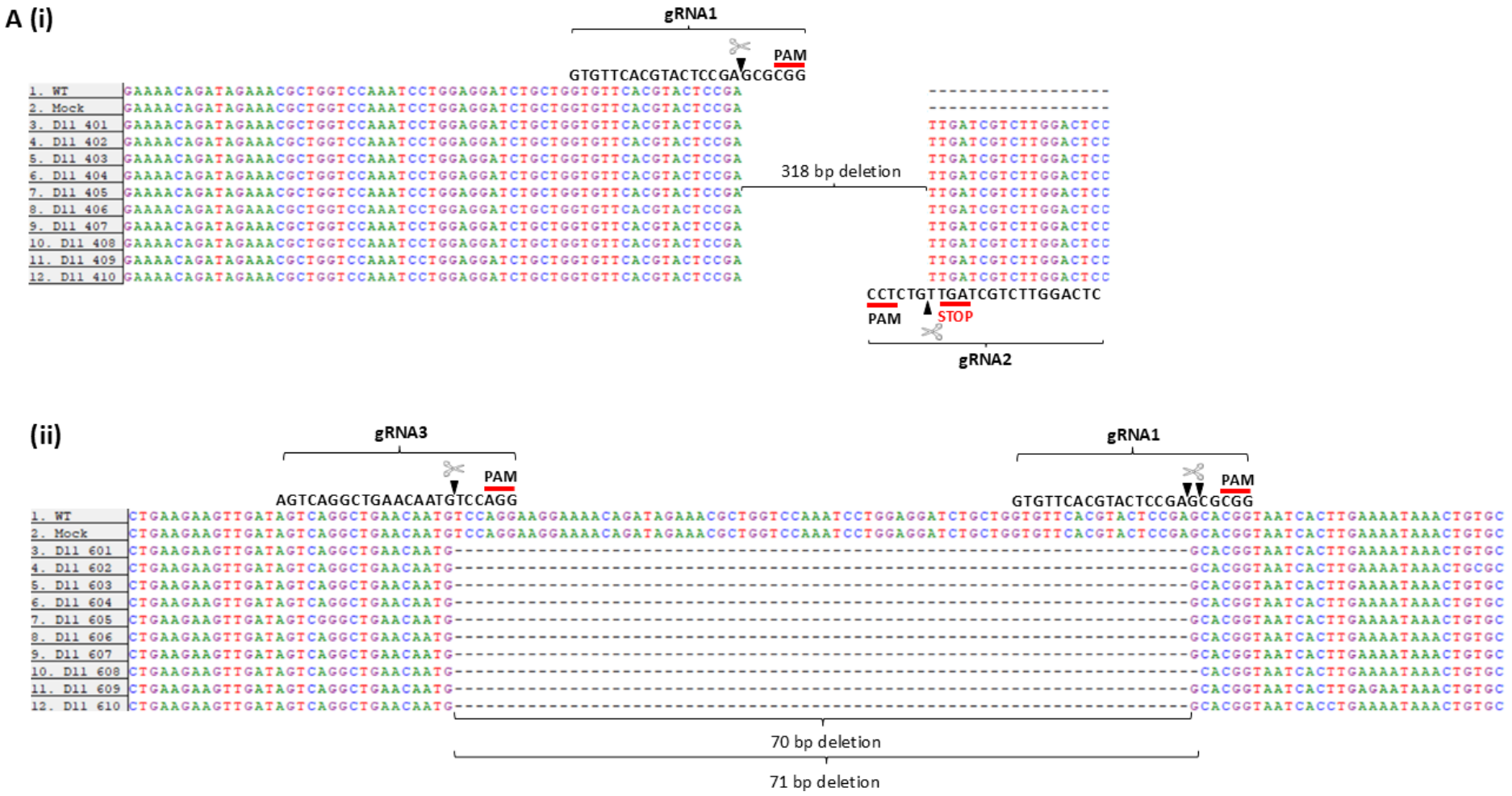
A (i)
gRNA1
PAM
GTGTTCACGTACTCCGAGCGCGG
1. WT
2. Mock
3. D11 401
4. D11 402
5. D11 403
6. D11 404
7. D11 405
8. D11 406
9. D11 407
10. D11 408
11. D11 409
12. D11 410
318 bp deletion
CCTCTGTTGATCGTCTTGGACTC
PAM
STOP
gRNA2
(ii)
gRNA3
PAM
AGTCAGGCTGAACAATGTCCAGG
gRNA1
PAM
GTGTTCACGTACTCCGAGCGCGG
70 bp deletion
71 bp deletion

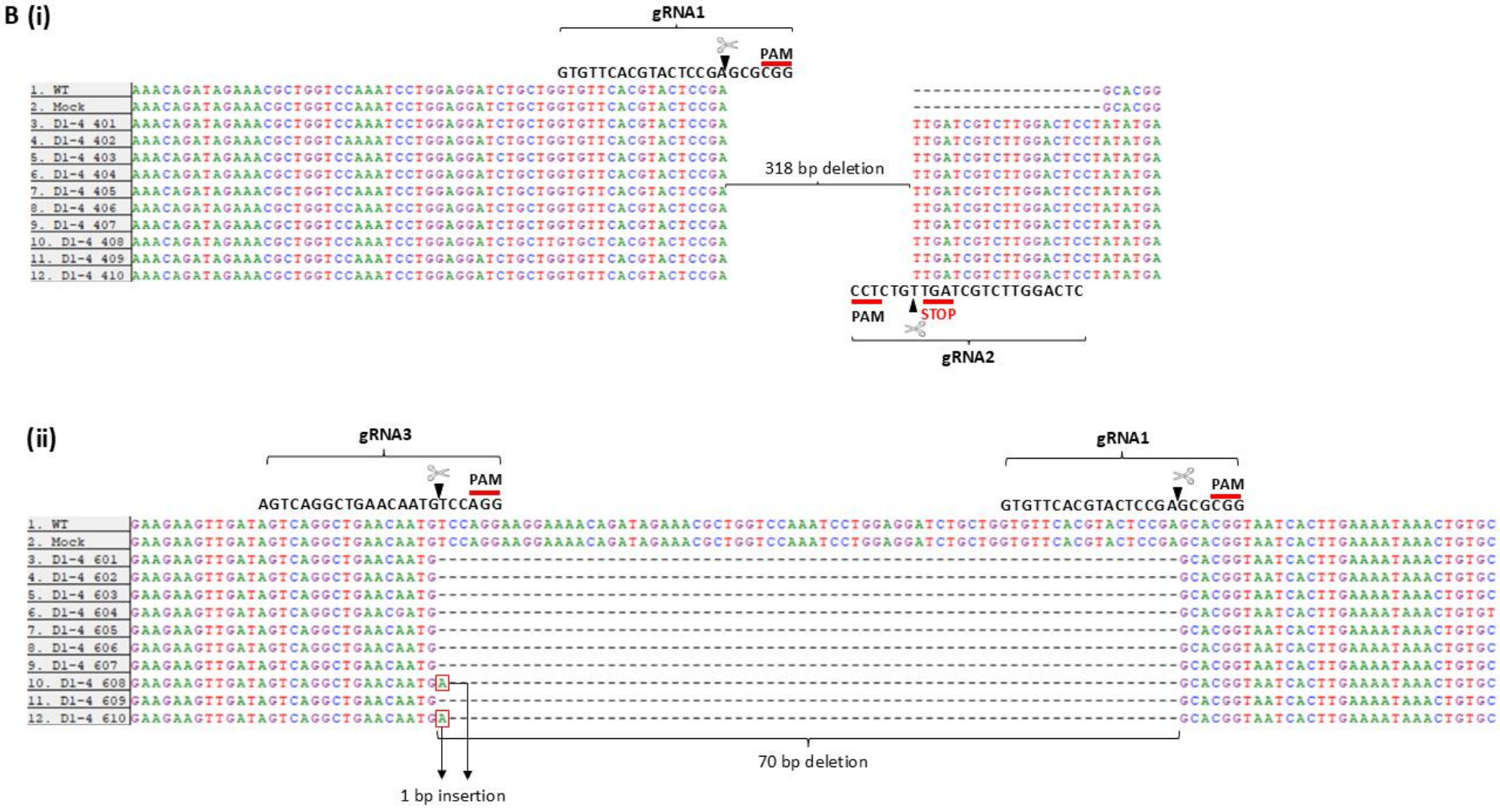
B (i)
gRNA1
PAM
GTGTTCACGTACTCCGAGCGCGG
1. WT
2. Mock
3. D1-4 401
4. D1-4 402
5. D1-4 403
6. D1-4 404
7. D1-4 405
8. D1-4 406
9. D1-4 407
10. D1-4 408
11. D1-4 409
12. D1-4 410
318 bp deletion
CCTCTGTTGATCGTCTTGGACTC
PAM
STOP
gRNA2
(ii)
gRNA3
PAM
AGTCAGGCTGAACAATGTCCAGG
gRNA1
PAM
GTGTTCACGTACTCCGAGCGCGG
1. WT
2. Mock
3. D1-4 601
4. D1-4 602
5. D1-4 603
6. D1-4 604
7. D1-4 605
8. D1-4 606
9. D1-4 607
10. D1-4 608
11. D1-4 609
12. D1-4 610
70 bp deletion
1 bp insertion

C (i)

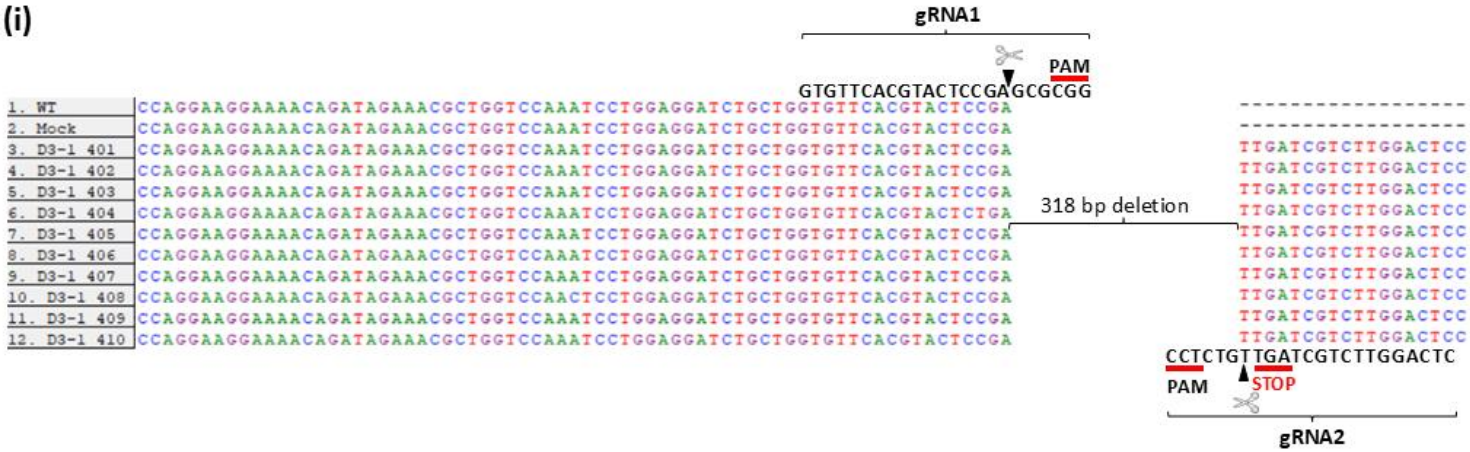
gRNA1
PAM
GTGTTCACGTACTCCGAGCGCGG
1. WT
2. Mock
3. D3-1 401
4. D3-1 402
5. D3-1 403
6. D3-1 404
7. D3-1 405
8. D3-1 406
9. D3-1 407
10. D3-1 408
11. D3-1 409
12. D3-1 410
318 bp deletion
CCTCTGTTGATCGTCTTGGACTC
PAM
STOP
gRNA2

(ii)

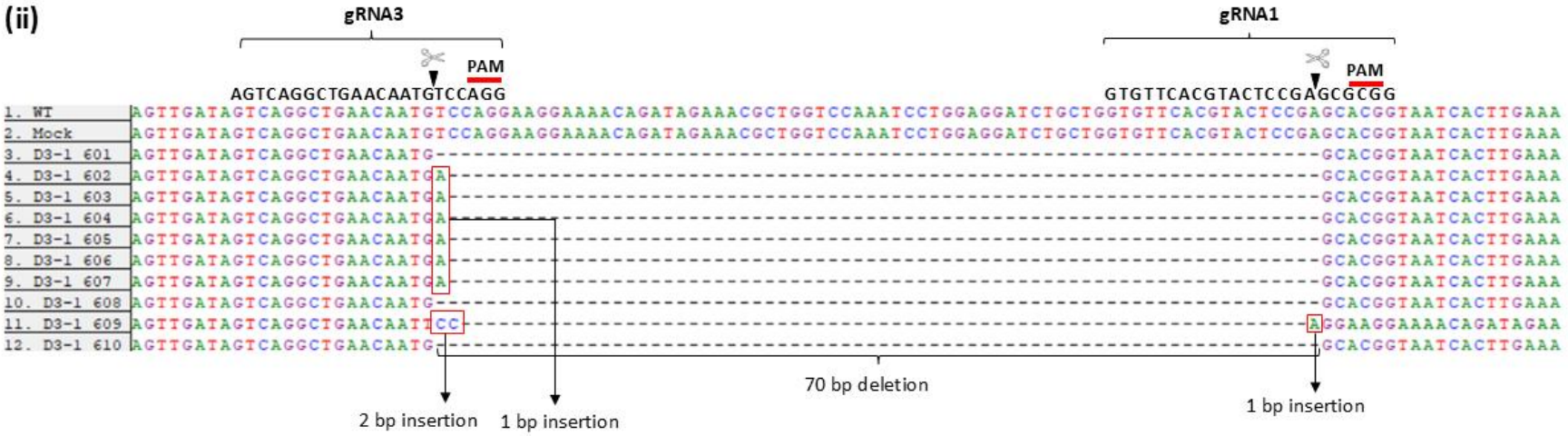
gRNA3
PAM
AGTCAGGCTGAACAATGTCCAGG
gRNA1
PAM
GTGTTCACGTACTCCGAGCGCGG
1. WT
2. Mock
3. D3-1 601
4. D3-1 602
5. D3-1 603
6. D3-1 604
7. D3-1 605
8. D3-1 606
9. D3-1 607
10. D3-1 608
11. D3-1 609
12. D3-1 610
2 bp insertion
1 bp insertion
70 bp deletion
1 bp insertion

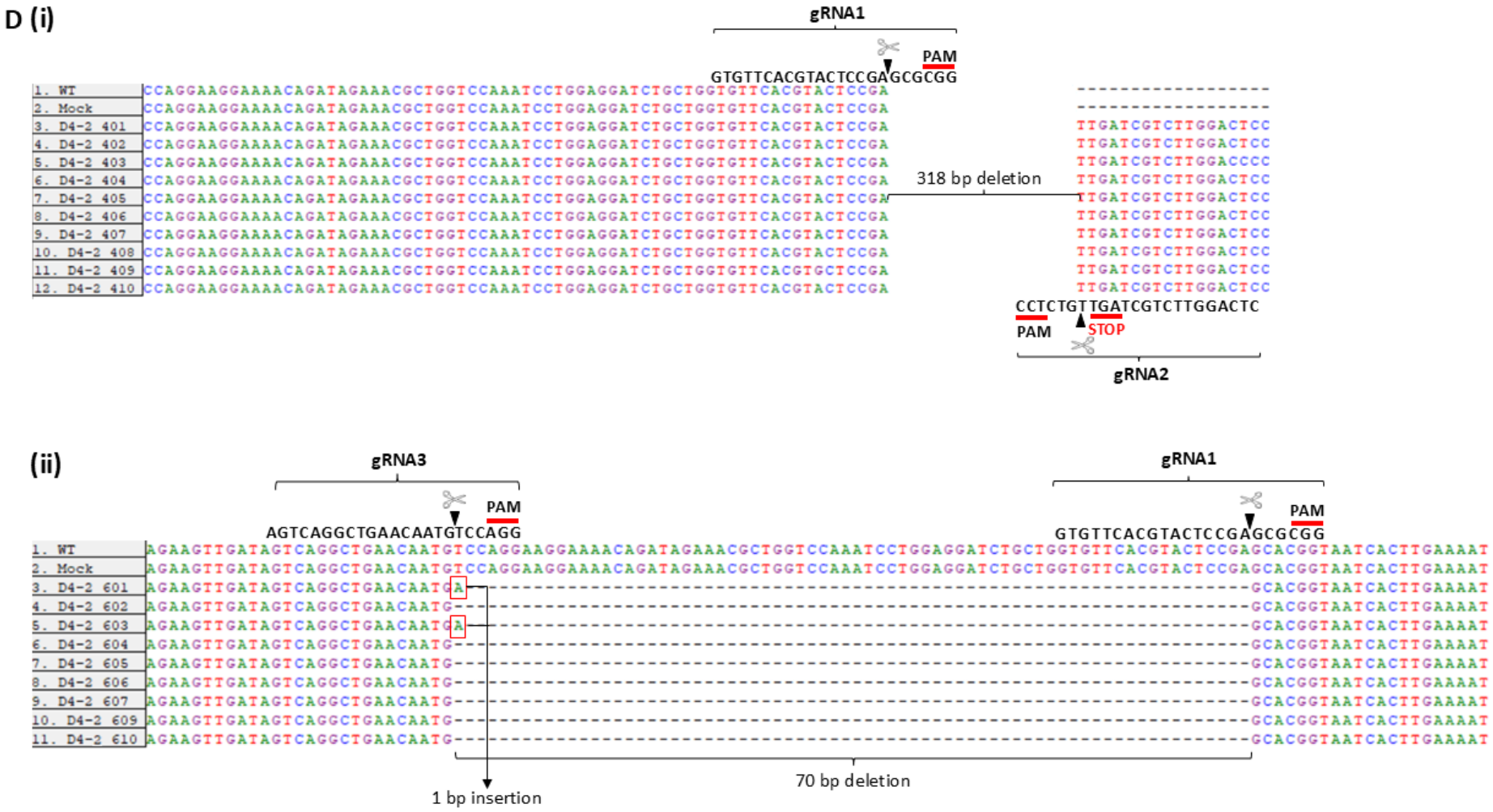
D (i)
gRNA1
PAM
GTGTTCACGTACTCCGAGCGCGG
1. WT
2. Mock
3. D4-2 401
4. D4-2 402
5. D4-2 403
6. D4-2 404
7. D4-2 405
8. D4-2 406
9. D4-2 407
10. D4-2 408
11. D4-2 409
12. D4-2 410
318 bp deletion
CCTCTGTTGATCGTCTTGGACTC
PAM
STOP
gRNA2
(ii)
gRNA3
PAM
AGTCAGGCTGAACAATGTCCAGG
gRNA1
PAM
GTGTTCACGTACTCCGAGCGCGG
1 bp insertion
70 bp deletion

E (i)

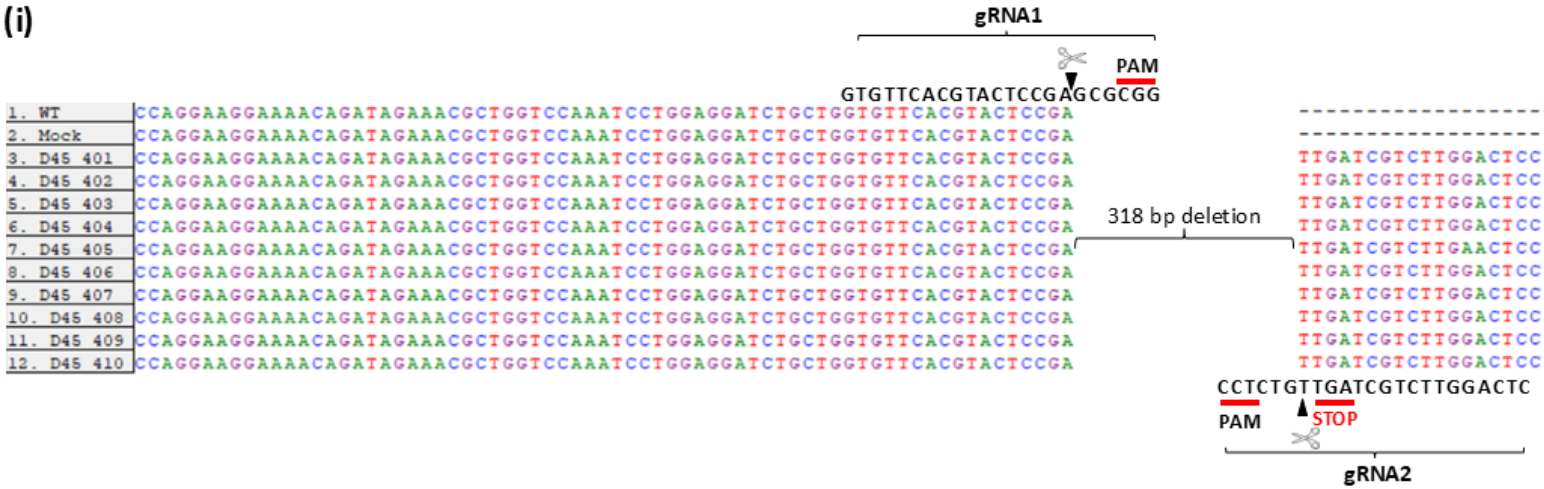
gRNA1
PAM
GTGTTCACGTACTCCGAGCGCGG
1. WT
2. Mock
3. D45 401
4. D45 402
5. D45 403
6. D45 404
7. D45 405
8. D45 406
9. D45 407
10. D45 408
11. D45 409
12. D45 410
CCAGGAAGGAAAACAGATAGAAACGCTGGTCCAAATCCTGGAGGATCTGCTGGTGTTCACGTACTCCGA
318 bp deletion
TTGATCGTCTTGGACTCC
TTGATCGTCTTGAACTCC
CCTCTGTTGATCGTCTTGGACTC
PAM
STOP
gRNA2

(ii)

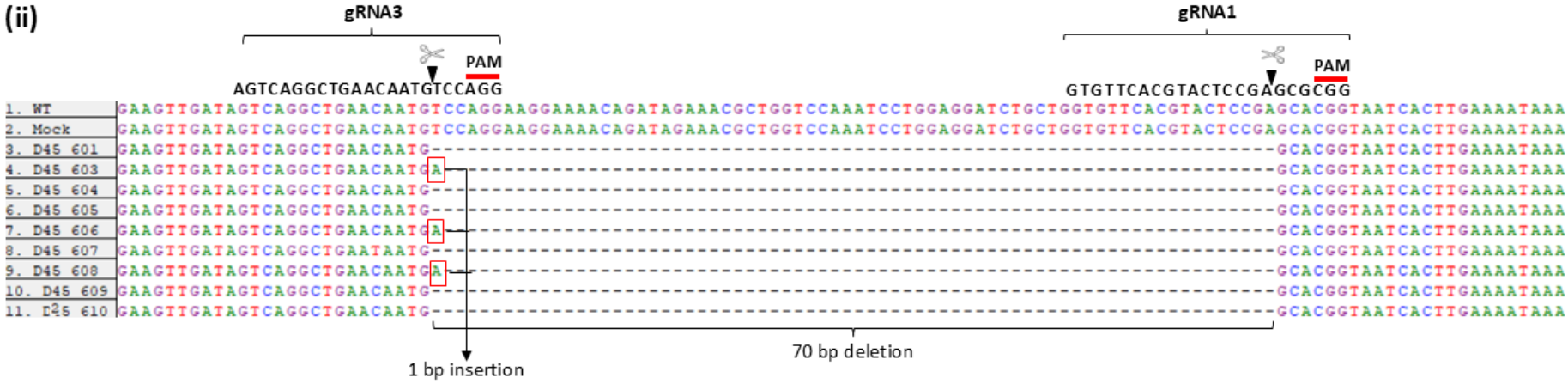
gRNA3
PAM
AGTCAGGCTGAACAATGTCCAGG
gRNA1
PAM
GTGTTCACGTACTCCGAGCGCGG
1. WT
2. Mock
3. D45 601
4. D45 603
5. D45 604
6. D45 605
7. D45 606
8. D45 607
9. D45 608
10. D45 609
11. D45 610
GAAGTTGATAGTCAGGCTGAACAATG
GAAGTTGATAGTCAGGCTGAATAATG
GCACGGTAATCACTTGAAAATAAA
1 bp insertion
70 bp deletion

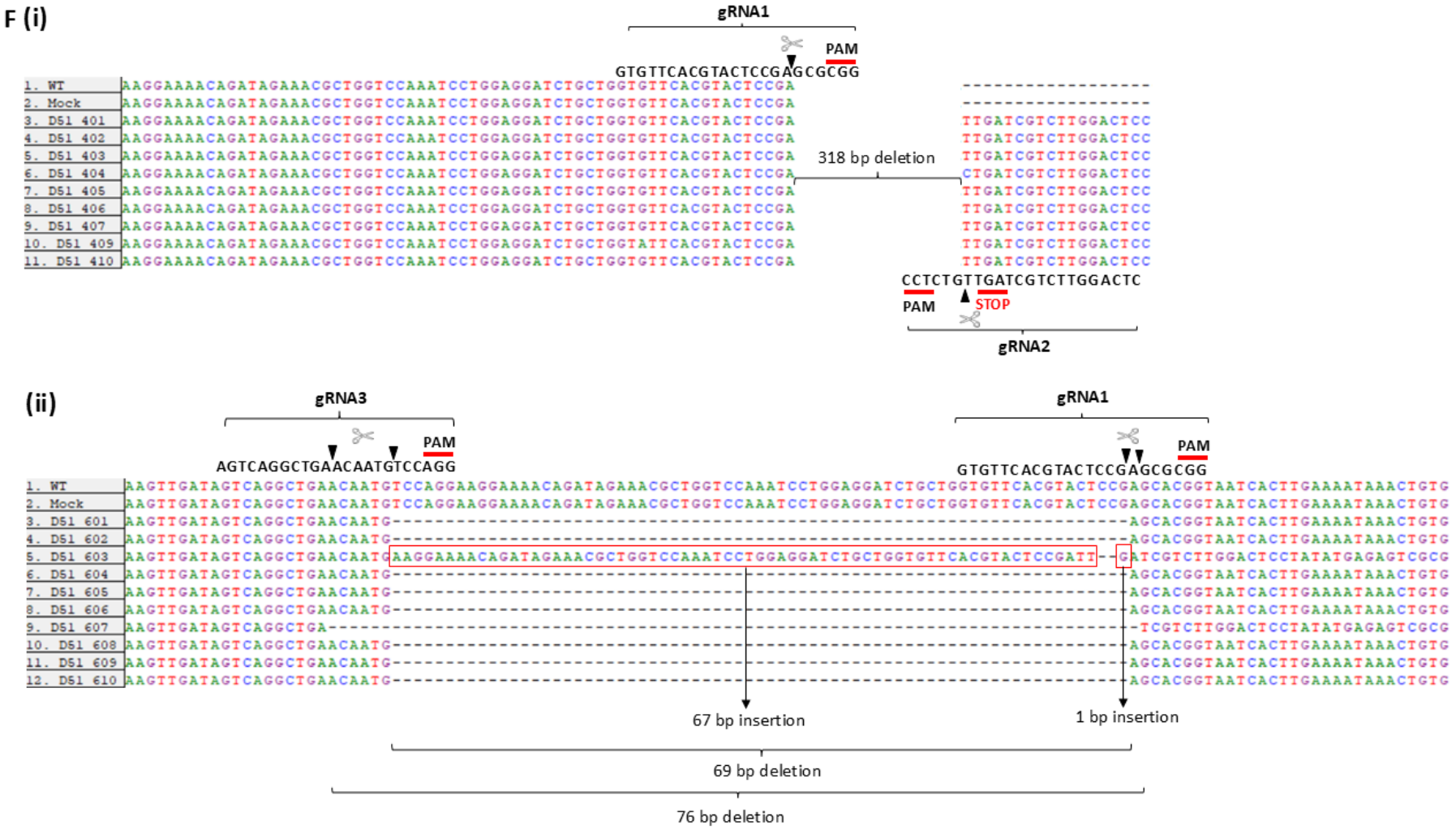
F (i)
gRNA1
PAM
GTGTTCACGTACTCCGAGCGCGG
1. WT
2. Mock
3. D51 401
4. D51 402
5. D51 403
6. D51 404
7. D51 405
8. D51 406
9. D51 407
10. D51 409
11. D51 410
318 bp deletion
CCTCTGTTGATCGTCTTGGACTC
PAM
STOP
gRNA2
(ii)
gRNA3
PAM
AGTCAGGCTGAACAATGTCCAGG
gRNA1
PAM
GTGTTCACGTACTCCGAGCGCGG
1. WT
2. Mock
3. D51 601
4. D51 602
5. D51 603
6. D51 604
7. D51 605
8. D51 606
9. D51 607
10. D51 608
11. D51 609
12. D51 610
67 bp insertion
1 bp insertion
69 bp deletion
76 bp deletion

G (i)


gRNA3
PAM
AGTCAGGCTGAACAATGTCCAGG
1. WT GCTGTCAGGGGTGCGAAGAGGACGAGGAAACTCTGAAGAAGTTGATAGTCAGGCTGAACAATG TCCAGGAAGGAAAAC---
2. Mock GCTGTCAGGGGTGCGAAGAGGACGAGGAAACTCTGAAGAAGTTGATAGTCAGGCTGAACAATG TCCAGGAAGGAAAAC---
3. D61 301 GCTGTCAGGGGTGCGAAGAGGACGAGGAAACTCTGAAGAAGTTGATAGTCAGGCTGAACAATG TTGATCGTCTTGGACTCC
4. D61 302 GCTGTCAGGGGTGCGAAGAGGACGAGGAAACTCTGAAGAAGTTGATAGTCAGGCTGAACAATG TTGGTCGTCTTGGACTCC
5. D61 303 GCTGTCAGGGGTGCGAAGAGGACGAGGAAACTCTGAAGAAGTTGATAGTCAGGCTGAACAATG TTGATCGTCTTGGACTCC
388 bp deletion
6. D61 304 GCTGTCAGGGGTGCGAAGAGGACGAGGAAACTCTGAAGAAGTTGATAGTCAGGCTGAACAATG TTGATCGTCTTGGACTCC
7. D61 305 GCTGTCAGGGGTGCGAAGAGGACGAGGAAACTCTGAAGAAGTTGATAGTCAGGCTGAACAATG TTGATCGTCTTGGACTCC
8. D61 306 GCTGTCAGGGGTGCGAAGAGGACGAGGAAACTCTGAAGAAGTTGATAGTCAGGCTGAACAATG TTGATCGTCTTGGACTCC
9. D61 308 GCTGTCAGGGGTGCGAAGAGGACGAGGAAACTCTGAAGAAGTTGATAGTCAGGCTGAACAATG TTGATCGTCTTGGACTCC
10. D61 309 GCTGTCAGGGGTGCGAAGAGGACGAGGAAACTCTGAAGAAGTTGATAGTCAGGCTGAACAATG TTGATCGTCTTGGACTCC
11. D61 310 GCTGTCAGGGGTGCGAAGAGGACGAGGAAACTCTGAAGAAGTTGATAGTCAGGCTGAACAATG TTGATCGTCTTGGACTCC
CCTCTGTTGATCGTCTTGGACTC
PAM
gRNA2

(ii)

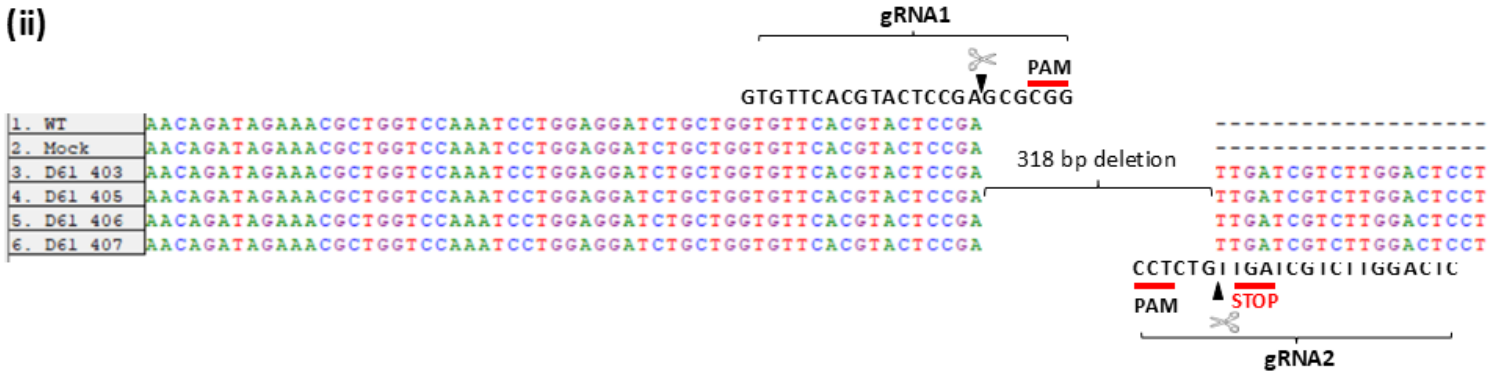
gRNA1
PAM
GTGTTCACGTACTCCGAGCGCGG
1. WT AACAGATAGAAACGCTGGTCCAAATCCTGGAGGATCTGCTGGTGTTCACGTACTCCGA ----------
2. Mock AACAGATAGAAACGCTGGTCCAAATCCTGGAGGATCTGCTGGTGTTCACGTACTCCGA ----------
3. D61 403 AACAGATAGAAACGCTGGTCCAAATCCTGGAGGATCTGCTGGTGTTCACGTACTCCGA TTGATCGTCTTGGACTCCT
318 bp deletion
4. D61 405 AACAGATAGAAACGCTGGTCCAAATCCTGGAGGATCTGCTGGTGTTCACGTACTCCGA TTGATCGTCTTGGACTCCT
5. D61 406 AACAGATAGAAACGCTGGTCCAAATCCTGGAGGATCTGCTGGTGTTCACGTACTCCGA TTGATCGTCTTGGACTCCT
6. D61 407 AACAGATAGAAACGCTGGTCCAAATCCTGGAGGATCTGCTGGTGTTCACGTACTCCGA TTGATCGTCTTGGACTCCT
CCTCTGTTGATCGTCTTGGACTC
PAM
STOP
gRNA2

(iii)

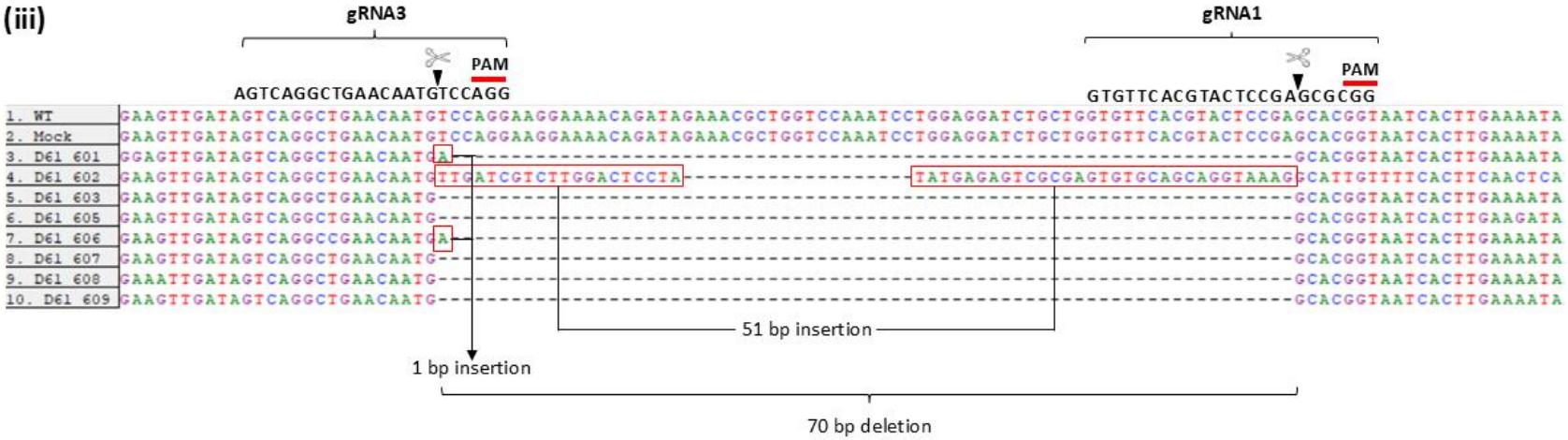
gRNA3
PAM
AGTCAGGCTGAACAATGTCCAGG
gRNA1
PAM
GTGTTCACGTACTCCGAGCGCGG
1. WT
2. Mock
3. D61 601
4. D61 602
5. D61 603
6. D61 605
7. D61 606
8. D61 607
9. D61 608
10. D61 609
51 bp insertion
1 bp insertion
70 bp deletion

H

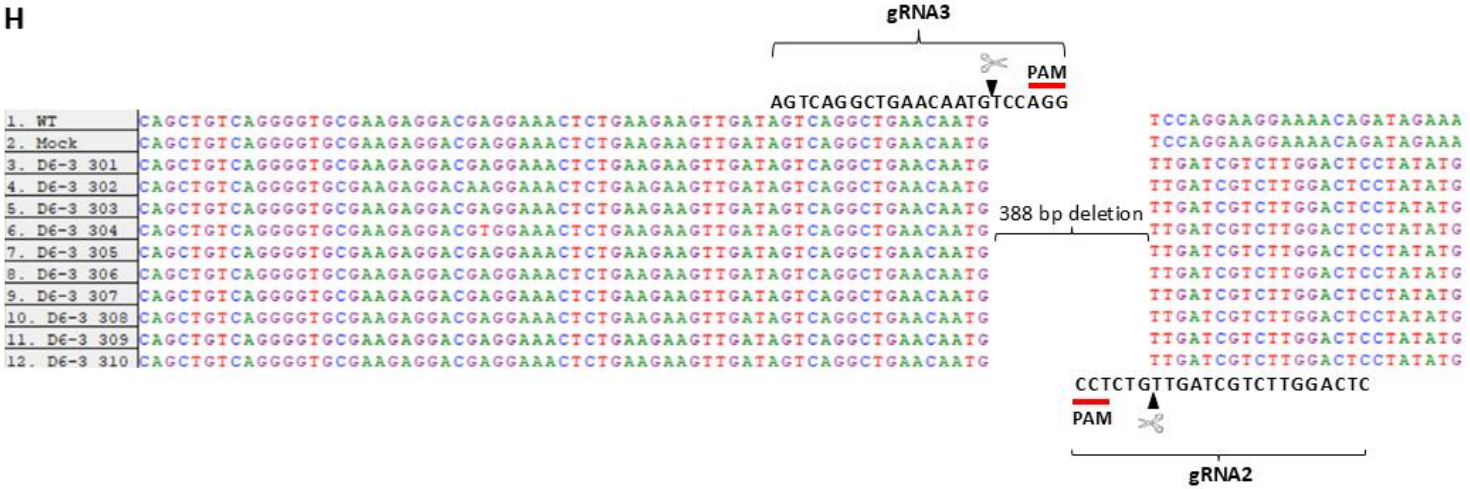
gRNA3
PAM
AGTCAGGCTGAACAATGTCCAGG
1. WT
2. Mock
3. D6-3 301
4. D6-3 302
5. D6-3 303
6. D6-3 304
7. D6-3 305
8. D6-3 306
9. D6-3 307
10. D6-3 308
11. D6-3 309
12. D6-3 310
388 bp deletion
CCTCTGTTGATCGTCTTGGACTC
PAM
gRNA2

I (i)


gRNA1
PAM
GTGTTCACGTACTCCGAGCGCGG
1. WT
2. Mock
3. D71 401
4. D71 402
5. D71 403
6. D71 404
7. D71 406
8. D71 407
9. D71 408
10. D71 409
318 bp deletion
CCTCTGTTGATCGTCTTGGACTC
PAM
STOP
gRNA2

(ii)

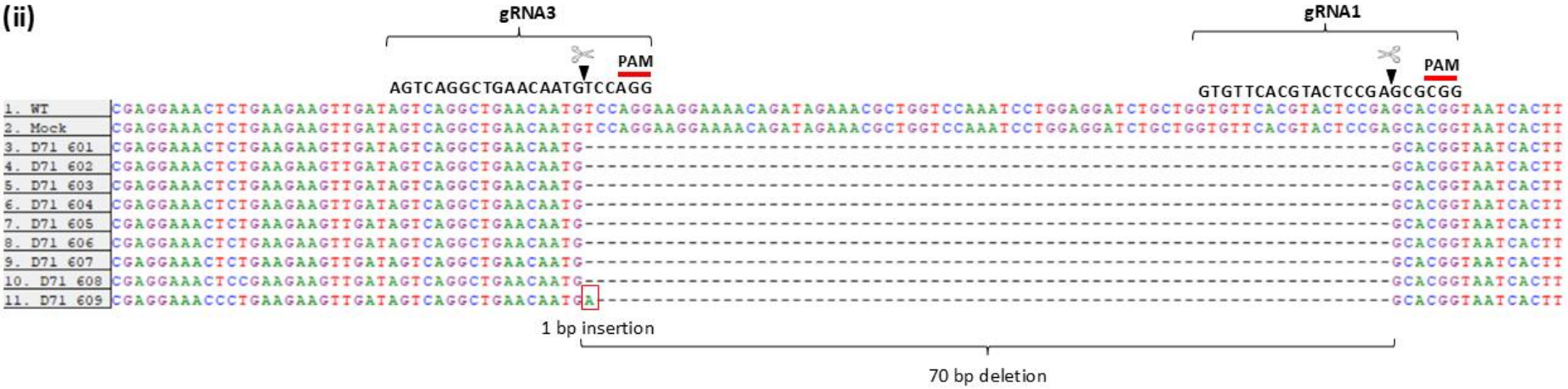
gRNA3
PAM
AGTCAGGCTGAACAATGTCCAGG
gRNA1
PAM
GTGTTCACGTACTCCGAGCGCGG
1. WT
2. Mock
3. D71 601
4. D71 602
5. D71 603
6. D71 604
7. D71 605
8. D71 606
9. D71 607
10. D71 608
11. D71 609
1 bp insertion
70 bp deletion

J (i)

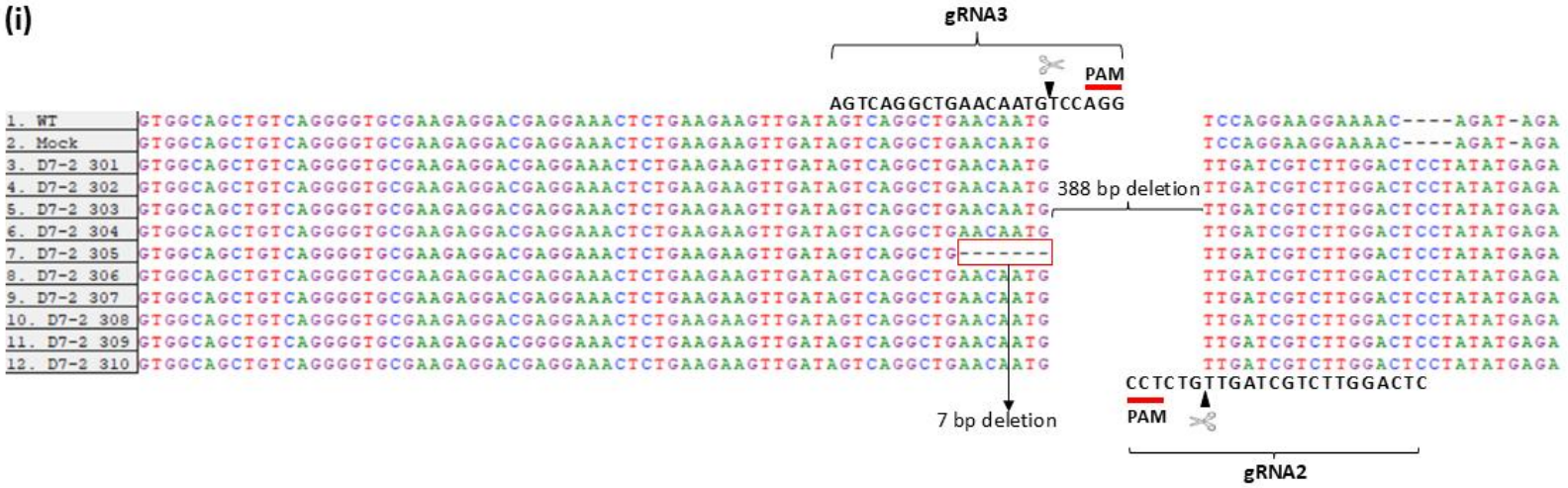
gRNA3
PAM
AGTCAGGCTGAACAATGTCCAGG
1. WT GTGGCAGCTGTCAGGGGTGCGAAGAGGACGAGGAAACTCTGAAGAAGTTGATAGTCAGGCTGAACAATG TCCAGGAAGGAAAAC----AGAT-AGA
2. Mock GTGGCAGCTGTCAGGGGTGCGAAGAGGACGAGGAAACTCTGAAGAAGTTGATAGTCAGGCTGAACAATG TCCAGGAAGGAAAAC----AGAT-AGA
3. D7-2 301 GTGGCAGCTGTCAGGGGTGCGAAGAGGACGAGGAAACTCTGAAGAAGTTGATAGTCAGGCTGAACAATG TTGATCGTCTTGGACTCCTATATGAGA
4. D7-2 302 GTGGCAGCTGTCAGGGGTGCGAAGAGGACGAGGAAACTCTGAAGAAGTTGATAGTCAGGCTGAACAATG 388 bp deletion TTGATCGTCTTGGACTCCTATATGAGA
5. D7-2 303 GTGGCAGCTGTCAGGGGTGCGAAGAGGACGAGGAAACTCTGAAGAAGTTGATAGTCAGGCTGAACAATG TTGATCGTCTTGGACTCCTATATGAGA
6. D7-2 304 GTGGCAGCTGTCAGGGGTGCGAAGAGGACGAGGAAACTCTGAAGAAGTTGATAGTCAGGCTGAACAATG TTGATCGTCTTGGACTCCTATATGAGA
7. D7-2 305 GTGGCAGCTGTCAGGGGTGCGAAGAGGACGAGGAAACTCTGAAGAAGTTGATAGTCAGGCTG------- TTGATCGTCTTGGACTCCTATATGAGA
8. D7-2 306 GTGGCAGCTGTCAGGGGTGCGAAGAGGACGAGGAAACTCTGAAGAAGTTGATAGTCAGGCTGAACAATG TTGATCGTCTTGGACTCCTATATGAGA
9. D7-2 307 GTGGCAGCTGTCAGGGGTGCGAAGAGGACGAGGAAACTCTGAAGAAGTTGATAGTCAGGCTGAACAATG TTGATCGTCTTGGACTCCTATATGAGA
10. D7-2 308 GTGGCAGCTGTCAGGGGTGCGAAGAGGACGAGGAAACTCTGAAGAAGTTGATAGTCAGGCTGAACAATG TTGATCGTCTTGGACTCCTATATGAGA
11. D7-2 309 GTGGCAGCTGTCAGGGGTGCGAAGAGGACGGGGAAACTCTGAAGAAGTTGATAGTCAGGCTGAACAATG TTGATCGTCTTGGACTCCTATATGAGA
12. D7-2 310 GTGGCAGCTGTCAGGGGTGCGAAGAGGACGAGGAAACTCTGAAGAAGTTGATAGTCAGGCTGAACAATG TTGATCGTCTTGGACTCCTATATGAGA
7 bp deletion
CCTCTGTTGATCGTCTTGGACTC
PAM
gRNA2

(ii)


gRNA1
PAM
GTGTTCACGTACTCCGAGCGCGG
1. WT CCAGGAAGGAAAACAGATAGAAACGCTGGTCCAAATCCTGGAGGATCTGCTGGTGTTCACGTACTCCGA ----------
2. Mock CCAGGAAGGAAAACAGATAGAAACGCTGGTCCAAATCCTGGAGGATCTGCTGGTGTTCACGTACTCCGA ----------
3. D7-2 401 CCAGGAAGGAAAACAGATAGAAACGCTGGTCCAAATCCTGGAGGATCTGCTGGTGTTCACGTACTCCGA TTGATCGTCTTGGACTCCT
4. D7-2 402 CCAGGAAGGAAAACAGATAGAAACGCTGGTCCAAATCCTGGAGGATCTGCTGGTGTTCACGTACTCCGA TTGATCGTCTTGGACTCCT
5. D7-2 403 CCAGGAAGGAAAACAGATAGAAACGCTGGTCCAAATCCTGGAGGATCTGCTGGTGTTCACGTACTCCGA 318 bp deletion TTGATCGTCTTGGACTCCT
6. D7-2 404 CCAGGAAGGAAAACAGATAGAAACGCTGGTCAAAATCCTGGAGGATCTGCTGGTGTTCACGTACTCCGA TTGATCGTCTTGGACTCCT
7. D7-2 405 CCAGGAAGGAAAACAGATAGAAACGCTGGTCCAAATCCTGGAGGATCTGCTGGTGTTCACGTACTCCGA TTGATCGTCTTGGACTCCT
8. D7-2 406 ----GAAGGAAAACAGATAGAAACGCTGGTCCAAATCCTGGAGGATCTGCTGGTGTTCACGTACTCCGA TTGATCGCCTTGGACTCCT
9. D7-2 407 CCAGGAAGGAAAACAAATAGAAACGCTGGTCAAAATCCTGGAGGATCTGCTGGTGTTCACGTACTCCGA TTGATCGTCTTGGACTCCT
10. D7-2 408 CCAGGAAGGAAAACAGATAGAAACGCTGGTCCAGATCCTGGAGGATCTGCTGGTGTTCACGTACTCCGA TTGATCGTCTTGGACTCCT
11. D7-2 409 CCAGGAAGGAAAACAGATAGAAACGCTGGTCCAAATCCTGGAGGATCTGCTGGTGTTCACGTACTCCGA TTGATCGTCTTGGACTCCT
12. D7-2 410 CCAGGAAGGAAAACAGATAGAAACGCTGGTCCAAATCCTGGAGGATCTGCTGGTGTTCACGTACTCCGA TTGATCGTCTTGGACTCCT
CCTCTGTTGATCGTCTTGGACTC
PAM
STOP
gRNA2

(iii)

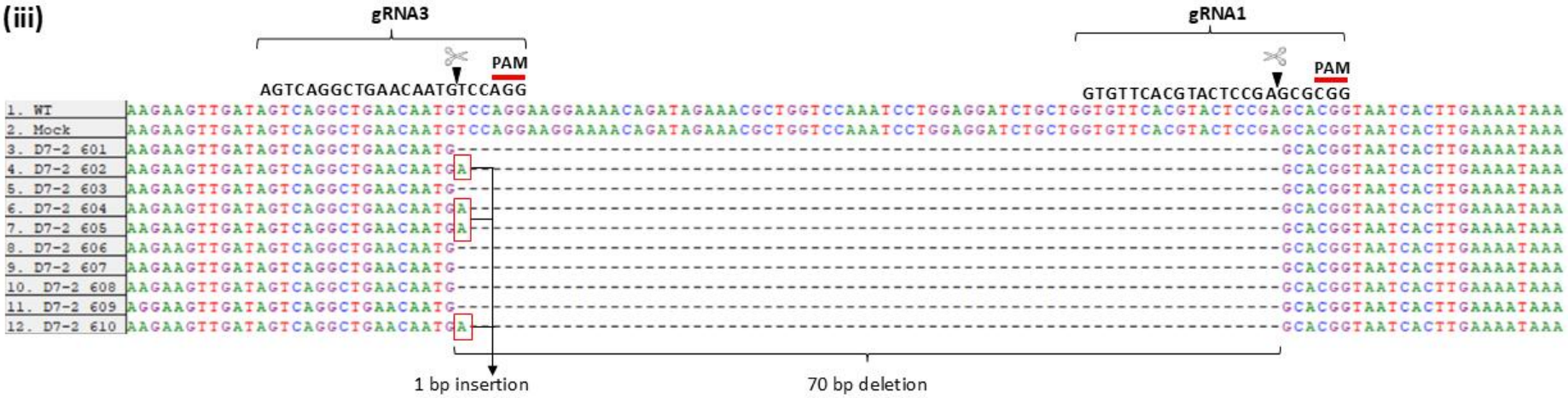
gRNA3
PAM
AGTCAGGCTGAACAATGTCCAGG
gRNA1
PAM
GTGTTCACGTACTCCGAGCGCGG
1. WT AAGAAGTTGATAGTCAGGCTGAACAATGTCCAGGAAGGAAAACAGATAGAAACGCTGGTCCAAATCCTGGAGGATCTGCTGGTGTTCACGTACTCCGAGCACGGTAATCACTTGAAAATAAA
2. Mock AAGAAGTTGATAGTCAGGCTGAACAATGTCCAGGAAGGAAAACAGATAGAAACGCTGGTCCAAATCCTGGAGGATCTGCTGGTGTTCACGTACTCCGAGCACGGTAATCACTTGAAAATAAA
3. D7-2 601 AAGAAGTTGATAGTCAGGCTGAACAATG----------GCACGGTAATCACTTGAAAATAAA
4. D7-2 602 AAGAAGTTGATAGTCAGGCTGAACAATGA---------GCACGGTAATCACTTGAAAATAAA
5. D7-2 603 AAGAAGTTGATAGTCAGGCTGAACAATG----------GCACGGTAATCACTTGAAAATAAA
6. D7-2 604 AAGAAGTTGATAGTCAGGCTGAACAATGA---------GCACGGTAATCACTTGAAAATAAA
7. D7-2 605 AAGAAGTTGATAGTCAGGCTGAACAATGA---------GCACGGTAATCACTTGAAAATAAA
8. D7-2 606 AAGAAGTTGATAGTCAGGCTGAACAATG----------GCACGGTAATCACTTGAAAATAAA
9. D7-2 607 AAGAAGTTGATAGTCAGGCTGAACAATG----------GCACGGTAATCACTTGAAAATAAA
10. D7-2 608 AAGAAGTTGATAGTCAGGCTGAACAATG----------GCACGGTAATCACTTGAAAATAAA
11. D7-2 609 AGGAAGTTGATAGTCAGGCTGAACAATG----------GCACGGTAATCACTTGAAAATAAA
12. D7-2 610 AAGAAGTTGATAGTCAGGCTGAACAATGA---------GCACGGTAATCACTTGAAAATAAA
1 bp insertion
70 bp deletion

K (i)

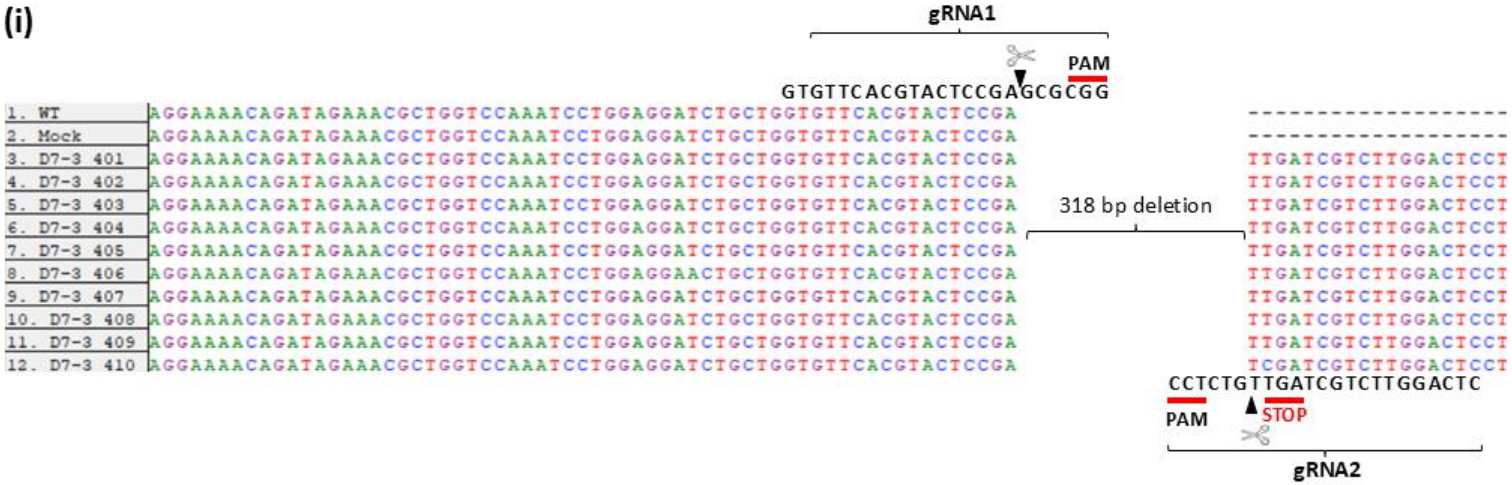
gRNA1
PAM
GTGTTCACGTACTCCGAGCGCGG
1. WT AGGAAAACAGATAGAAACGCTGGTCCAAATCCTGGAGGATCTGCTGGTGTTCACGTACTCCGA----------
2. Mock AGGAAAACAGATAGAAACGCTGGTCCAAATCCTGGAGGATCTGCTGGTGTTCACGTACTCCGA----------
3. D7-3 401 AGGAAAACAGATAGAAACGCTGGTCCAAATCCTGGAGGATCTGCTGGTGTTCACGTACTCCGATTGATCGTCTTGGACTCCT
4. D7-3 402 AGGAAAACAGATAGAAACGCTGGTCCAAATCCTGGAGGATCTGCTGGTGTTCACGTACTCCGATTGATCGTCTTGGACTCCT
5. D7-3 403 AGGAAAACAGATAGAAACGCTGGTCCAAATCCTGGAGGATCTGCTGGTGTTCACGTACTCCGATTGATCGTCTTGGACTCCT
6. D7-3 404 AGGAAAACAGATAGAAACGCTGGTCCAAATCCTGGAGGATCTGCTGGTGTTCACGTACTCCGATTGATCGTCTTGGACTCCT
7. D7-3 405 AGGAAAACAGATAGAAACGCTGGTCCAAATCCTGGAGGATCTGCTGGTGTTCACGTACTCCGATTGATCGTCTTGGACTCCT
8. D7-3 406 AGGAAAACAGATAGAAACGCTGGTCCAAATCCTGGAGGAACTGCTGGTGTTCACGTACTCCGATTGATCGTCTTGGACTCCT
9. D7-3 407 AGGAAAACAGATAGAAACGCTGGTCCAAATCCTGGAGGATCTGCTGGTGTTCACGTACTCCGATTGATCGTCTTGGACTCCT
10. D7-3 408 AGGAAAACAGATAGAAACGCTGGTCCAAATCCTGGAGGATCTGCTGGTGTTCACGTACTCCGATTGATCGTCTTGGACTCCT
11. D7-3 409 AGGAAAACAGATAGAAACGCTGGTCCAAATCCTGGAGGATCTGCTGGTGTTCACGTACTCCGATTGATCGTCTTGGACTCCT
12. D7-3 410 AGGAAAACAGATAGAAACGCTGGTCCAAATCCTGGAGGATCTGCTGGTGTTCACGTACTCCGATCGATCGTCTTGGACTCCT
318 bp deletion
CCTCTGTTGATCGTCTTGGACTC
PAM
STOP
gRNA2

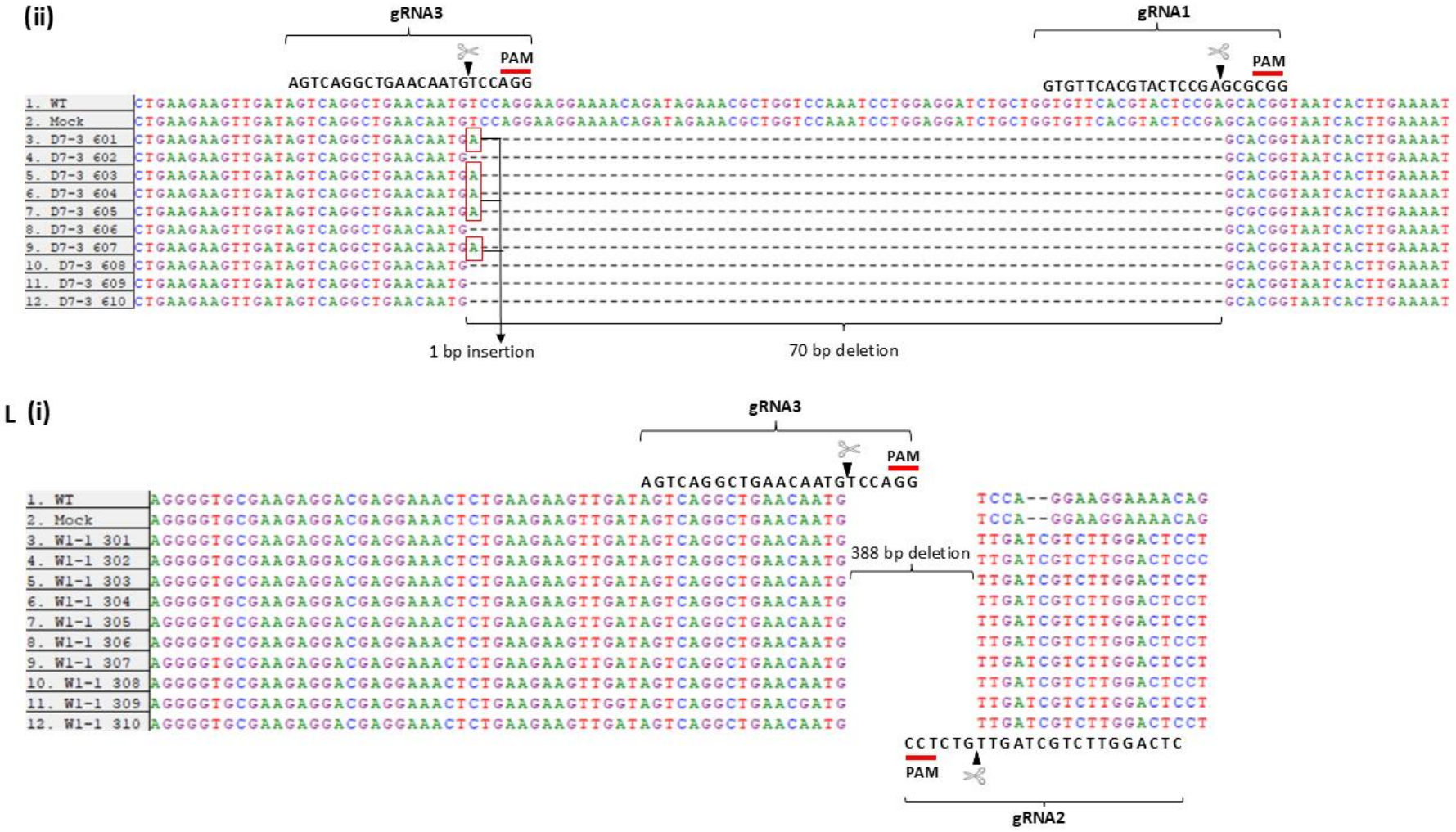
(ii)
gRNA3
PAM
AGTCAGGCTGAACAATGTCCAGG
gRNA1
PAM
GTGTTCACGTACTCCGAGCGCGG
1. WT
2. Mock
3. D7-3 601
4. D7-3 602
5. D7-3 603
6. D7-3 604
7. D7-3 605
8. D7-3 606
9. D7-3 607
10. D7-3 608
11. D7-3 609
12. D7-3 610
1 bp insertion
70 bp deletion
L (i)
gRNA3
PAM
AGTCAGGCTGAACAATGTCCAGG
1. WT
2. Mock
3. W1-1 301
4. W1-1 302
5. W1-1 303
6. W1-1 304
7. W1-1 305
8. W1-1 306
9. W1-1 307
10. W1-1 308
11. W1-1 309
12. W1-1 310
388 bp deletion
CCTCTGTTGATCGTCTTGGACTC
PAM
gRNA2

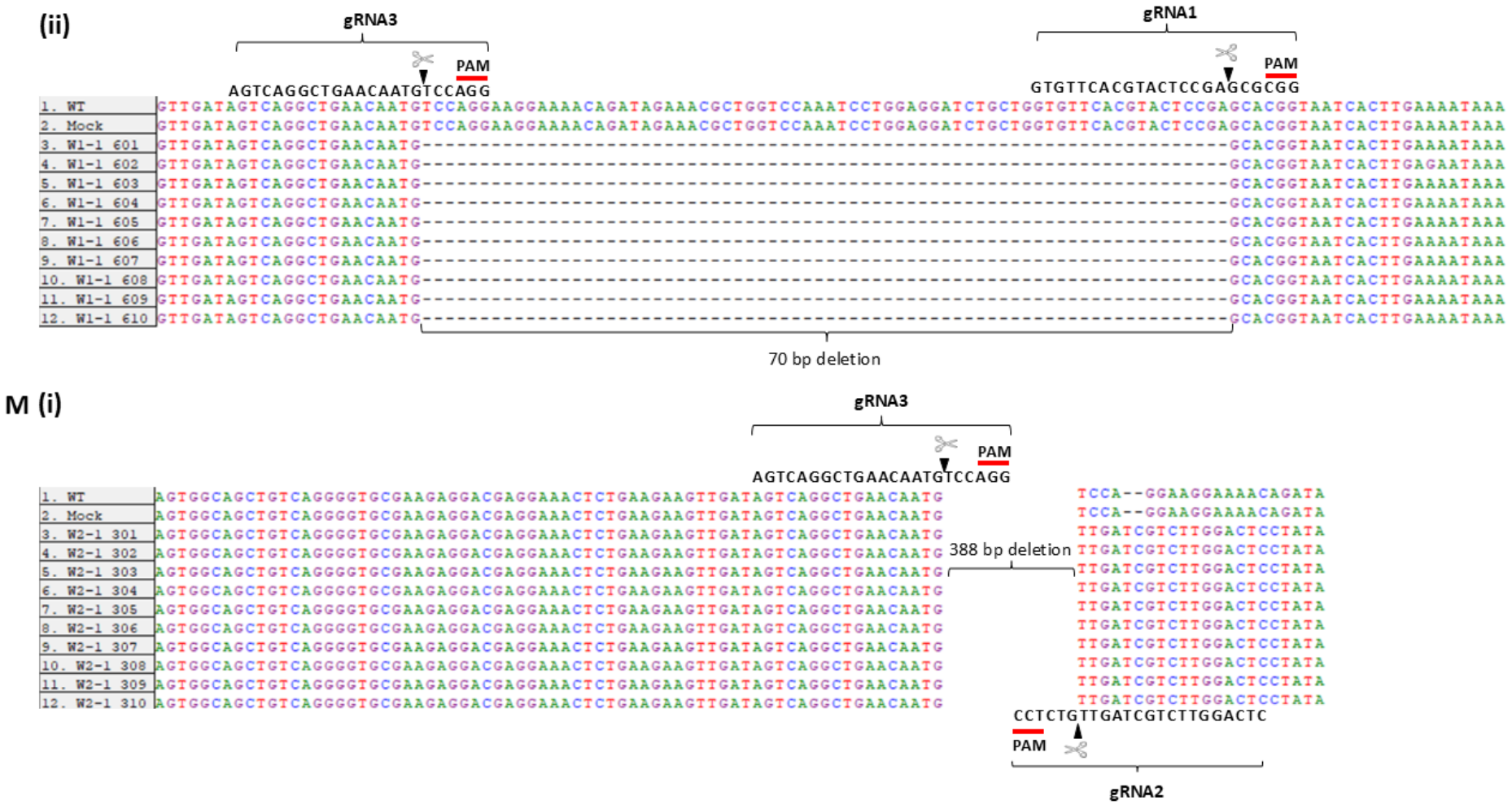
(ii)
gRNA3
PAM
AGTCAGGCTGAACAATGTCCAGG
gRNA1
PAM
GTGTTCACGTACTCCGAGCGCGG
1. WT GTTGATAGTCAGGCTGAACAATGTCCAGGAAGGAAAACAGATAGAAACGCTGGTCCAAATCCTGGAGGATCTGCTGGTGTTCACGTACTCCGAGCACGGTAATCACTTGAAAATAAA
2. Mock GTTGATAGTCAGGCTGAACAATGTCCAGGAAGGAAAACAGATAGAAACGCTGGTCCAAATCCTGGAGGATCTGCTGGTGTTCACGTACTCCGAGCACGGTAATCACTTGAAAATAAA
3. W1-1 601 GTTGATAGTCAGGCTGAACAATG----------GCACGGTAATCACTTGAAAATAAA
4. W1-1 602 GTTGATAGTCAGGCTGAACAATG----------GCACGGTAATCACTTGAGAATAAA
5. W1-1 603 GTTGATAGTCAGGCTGAACAATG----------GCACGGTAATCACTTGAAAATAAA
6. W1-1 604 GTTGATAGTCAGGCTGAACAATG----------GCACGGTAATCACTTGAAAATAAA
7. W1-1 605 GTTGATAGTCAGGCTGAACAATG----------GCACGGTAATCACTTGAAAATAAA
8. W1-1 606 GTTGATAGTCAGGCTGAACAATG----------GCACGGTAATCACTTGAAAATAAA
9. W1-1 607 GTTGATAGTCAGGCTGAACAATG----------GCACGGTAATCACTTGAAAATAAA
10. W1-1 608 GTTGATAGTCAGGCTGAACAATG----------GCACGGTAATCACTTGAAAATAAA
11. W1-1 609 GTTGATAGTCAGGCTGAACAATG----------GCACGGTAATCACTTGAAAATAAA
12. W1-1 610 GTTGATAGTCAGGCTGAACAATG----------GCACGGTAATCACTTGAAAATAAA
70 bp deletion
M (i)
gRNA3
PAM
AGTCAGGCTGAACAATGTCCAGG
1. WT AGTGGCAGCTGTCAGGGGTGCGAAGAGGACGAGGAAACTCTGAAGAAGTTGATAGTCAGGCTGAACAATG TCCA--GGAAGGAAAACAGATA
2. Mock AGTGGCAGCTGTCAGGGGTGCGAAGAGGACGAGGAAACTCTGAAGAAGTTGATAGTCAGGCTGAACAATG TCCA--GGAAGGAAAACAGATA
3. W2-1 301 AGTGGCAGCTGTCAGGGGTGCGAAGAGGACGAGGAAACTCTGAAGAAGTTGATAGTCAGGCTGAACAATG TTGATCGTCTTGGACTCCTATA
4. W2-1 302 AGTGGCAGCTGTCAGGGGTGCGAAGAGGACGAGGAAACTCTGAAGAAGTTGATAGTCAGGCTGAACAATG 388 bp deletion TTGATCGTCTTGGACTCCTATA
5. W2-1 303 AGTGGCAGCTGTCAGGGGTGCGAAGAGGACGAGGAAACTCTGAAGAAGTTGATAGTCAGGCTGAACAATG TTGATCGTCTTGGACTCCTATA
6. W2-1 304 AGTGGCAGCTGTCAGGGGTGCGAAGAGGACGAGGAAACTCTGAAGAAGTTGATAGTCAGGCTGAACAATG TTGATCGTCTTGGACTCCTATA
7. W2-1 305 AGTGGCAGCTGTCAGGGGTGCGAAGAGGACGAGGAAACTCTGAAGAAGTTGATAGTCAGGCTGAACAATG TTGATCGTCTTGGACTCCTATA
8. W2-1 306 AGTGGCAGCTGTCAGGGGTGCGAAGAGGACGAGGAAACTCTGAAGAAGTTGATAGTCAGGCTGAACAATG TTGATCGTCTTGGACTCCTATA
9. W2-1 307 AGTGGCAGCTGTCAGGGGTGCGAAGAGGACGAGGAAACTCTGAAGAAGTTGATAGTCAGGCTGAACAATG TTGATCGTCTTGGACTCCTATA
10. W2-1 308 AGTGGCAGCTGTCAGGGGTGCGAAGAGGACGAGGAAACTCTGAAGAAGTTGATAGTCAGGCTGAACAATG TTGATCGTCTTGGACTCCTATA
11. W2-1 309 AGTGGCAGCTGTCAGGGGTGCGAAGAGGACGAGGAAACTCTGAAGAAGTTGATAGTCAGGCTGAACAATG TTGATCGTCTTGGACTCCTATA
12. W2-1 310 AGTGGCAGCTGTCAGGGGTGCGAAGAGGACGAGGAAACTCTGAAGAAGTTGATAGTCAGGCTGAACAATG TTGATCGTCTTGGACTCCTATA
CCTCTGTTGATCGTCTTGGACTC
PAM
gRNA2

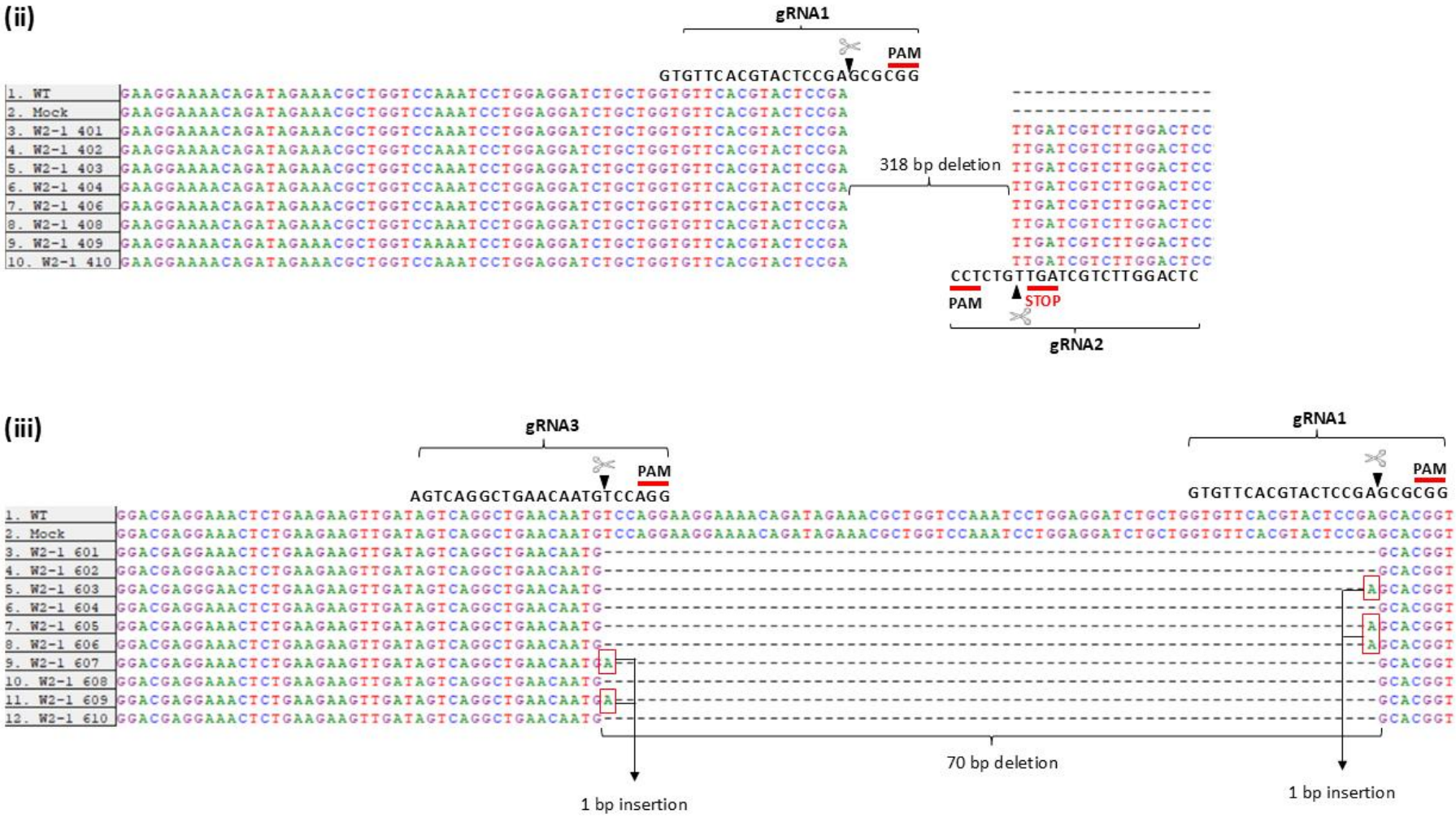
(ii)
gRNA1
PAM
GTGTTCACGTACTCCGAGCGCGG
1. WT
2. Mock
3. W2-1 401
4. W2-1 402
5. W2-1 403
6. W2-1 404
7. W2-1 406
8. W2-1 408
9. W2-1 409
10. W2-1 410
318 bp deletion
CCTCTGTTGATCGTCTTGGACTC
PAM
STOP
gRNA2
(iii)
gRNA3
PAM
AGTCAGGCTGAACAATGTCCAGG
gRNA1
PAM
GTGTTCACGTACTCCGAGCGCGG
1. WT
2. Mock
3. W2-1 601
4. W2-1 602
5. W2-1 603
6. W2-1 604
7. W2-1 605
8. W2-1 606
9. W2-1 607
10. W2-1 608
11. W2-1 609
12. W2-1 610
70 bp deletion
1 bp insertion
1 bp insertion

APPENDIX B

E-MAIL CORRESPONDENCE WITH PROFESSOR ROBERT ROSS IN FORDHAM UNIVERSITY, NEW YORK, USA

Note: Professor Robert Ross is the pioneer in the study of neuroblastoma interconversion

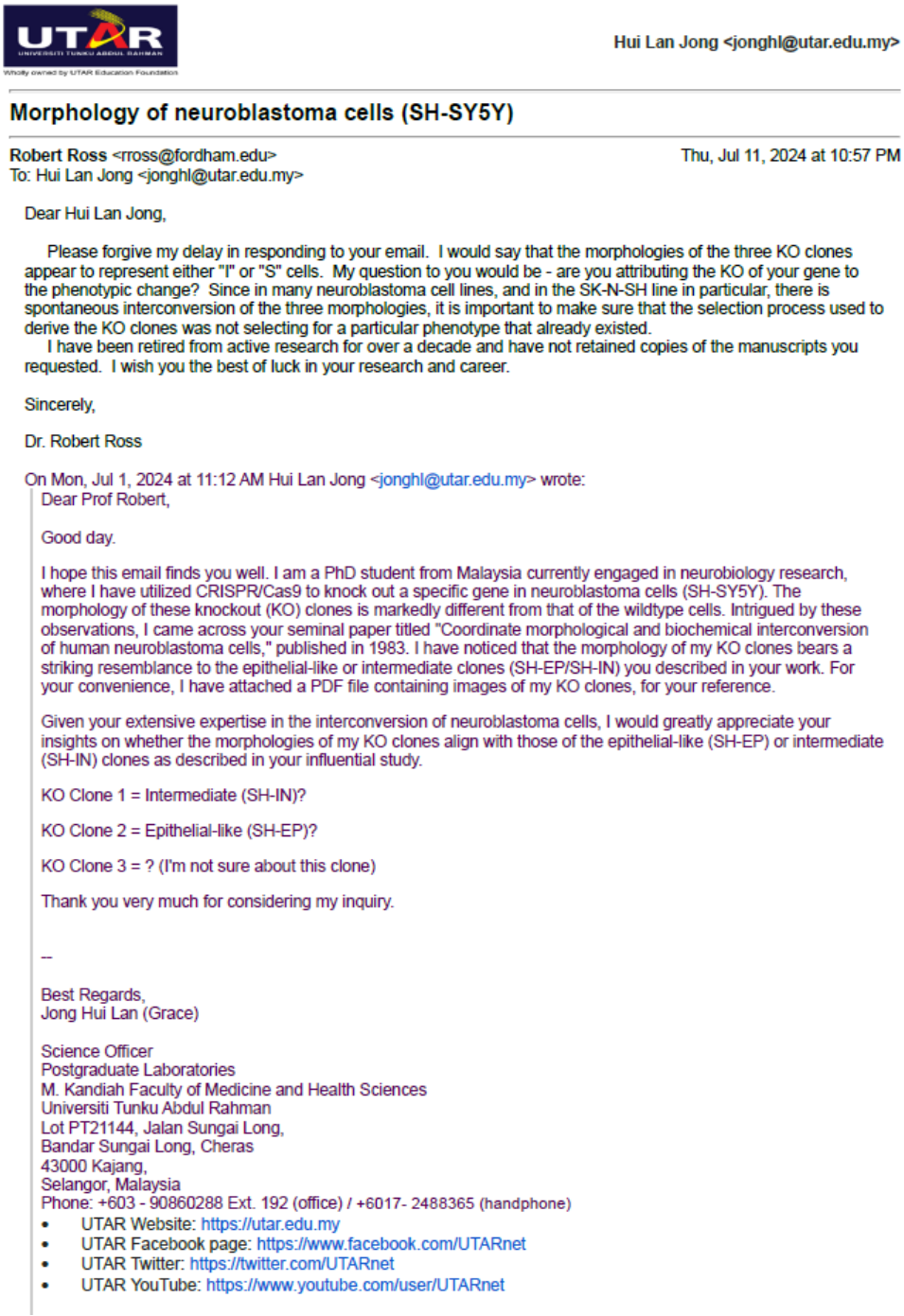

Hui Lan Jong <jonghl@utar.edu.my>

Morphology of neuroblastoma cells (SH-SY5Y)

Robert Ross <rross@fordham.edu> Thu, Jul 11, 2024 at 10:57 PM
To: Hui Lan Jong <jonghl@utar.edu.my>

Dear Hui Lan Jong,

Please forgive my delay in responding to your email. I would say that the morphologies of the three KO clones appear to represent either "I" or "S" cells. My question to you would be - are you attributing the KO of your gene to the phenotypic change? Since in many neuroblastoma cell lines, and in the SK-N-SH line in particular, there is spontaneous interconversion of the three morphologies, it is important to make sure that the selection process used to derive the KO clones was not selecting for a particular phenotype that already existed.

I have been retired from active research for over a decade and have not retained copies of the manuscripts you requested. I wish you the best of luck in your research and career.

Sincerely,

Dr. Robert Ross

On Mon, Jul 1, 2024 at 11:12 AM Hui Lan Jong <jonghl@utar.edu.my> wrote:

> Dear Prof Robert,
>
> Good day.
>
> I hope this email finds you well. I am a PhD student from Malaysia currently engaged in neurobiology research, where I have utilized CRISPR/Cas9 to knock out a specific gene in neuroblastoma cells (SH-SY5Y). The morphology of these knockout (KO) clones is markedly different from that of the wildtype cells. Intrigued by these observations, I came across your seminal paper titled "Coordinate morphological and biochemical interconversion of human neuroblastoma cells," published in 1983. I have noticed that the morphology of my KO clones bears a striking resemblance to the epithelial-like or intermediate clones (SH-EP/SH-IN) you described in your work. For your convenience, I have attached a PDF file containing images of my KO clones, for your reference.
>
> Given your extensive expertise in the interconversion of neuroblastoma cells, I would greatly appreciate your insights on whether the morphologies of my KO clones align with those of the epithelial-like (SH-EP) or intermediate (SH-IN) clones as described in your influential study.
>
> KO Clone 1 = Intermediate (SH-IN)?
>
> KO Clone 2 = Epithelial-like (SH-EP)?
>
> KO Clone 3 = ? (I'm not sure about this clone)
>
> Thank you very much for considering my inquiry.
>
> --
>
> Best Regards,
> Jong Hui Lan (Grace)
>
> Science Officer
> Postgraduate Laboratories
> M. Kandiah Faculty of Medicine and Health Sciences
> Universiti Tunku Abdul Rahman
> Lot PT21144, Jalan Sungai Long,
> Bandar Sungai Long, Cheras
> 43000 Kajang,
> Selangor, Malaysia
> Phone: +603 - 90860288 Ext. 192 (office) / +6017- 2488365 (handphone)
> - UTAR Website: https://utar.edu.my
> - UTAR Facebook page: https://www.facebook.com/UTARnet
> - UTAR Twitter: https://twitter.com/UTARnet
> - UTAR YouTube: https://www.youtube.com/user/UTARnet

IMAGES (EMAIL ATTACHMENT) SENT TO PROFESSOR ROBERT ROSS

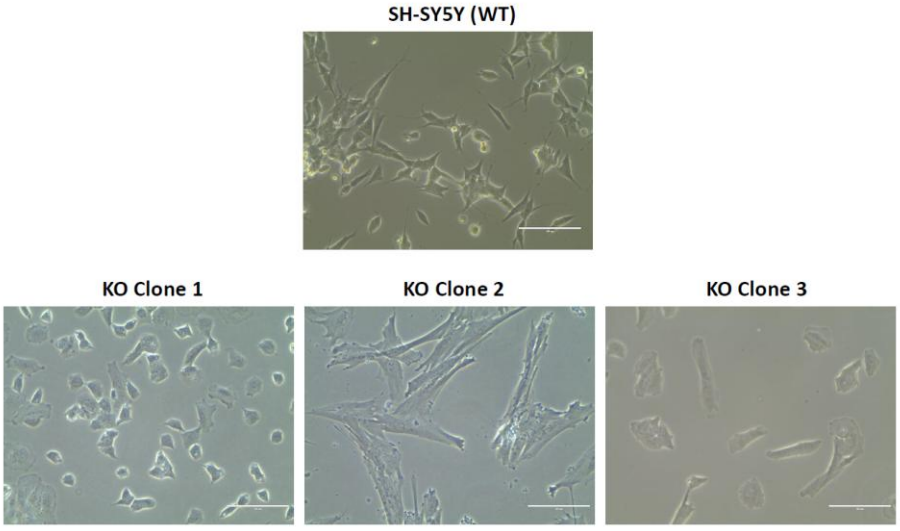

PUBLICATIONS

1. Jong, HL., Yuen, KS., Jin, DY. et al. Generation of Leucine-Rich Repeat Kinase 2 (LRRK2) Knockout Neuroblastoma Cells SH-SY5Y by CRISPR/Cas9-Mediated Genome Editing. Biochem Genet (2025). https://doi.org/10.1007/s10528-025-11174-4 (Published on 2 July 2025; WOS/ Scopus indexed publication)

2. Jong, HL., Yuen, KS., Jin, DY. et al. Leucine-Rich Repeat Kinase 2 (LRRK2) Knockout Induces Spontaneous Interconversion and Senescence in SH-SY5Y Neuroblastoma Cells. (Manuscript has been submitted for peer review)

3. Jong, HL., Lam, SK., Lim, YM. et al. Investigating the Effects of Edible Bird's Nest Extracts on Leucine-Rich Repeat Kinase 2 Knockout SH-SY5Y Neuroblastoma Cells. (Manuscript has been submitted for peer review)

4. Jong, HL., Yuen, KS., Jin, DY. et al. Leucine-Rich Repeat Kinase 2 (LRRK2) Knockout Induces Spontaneous Interconversion and Senescence in SH-SY5Y Neuroblastoma Cells. *The ageing genome: from mechanisms to disease.* European Molecular Biology Laboratory (EMBL), Heidelberg, Germany, 10 – 13 June 2025. pp. 75 (Abstract)

5. Jong, HL., Yuen, KS., Jin, DY. et al. Leucine-Rich Repeat Kinase 2 (LRRK2) Knockout Leads to Senescence-Like Phenotypes in SH-SY5Y Neuroblastoma Cells. Malays J Pathol 2024; 46(3): 495 (Abstract)

6. Jong, HL., Yuen, KS., Jin, DY. et al. Generation of LRRK2 Knockout Neuroblastoma Cells by CRISPR/Cas9-mediated Genome Editing. *16th Federation of Asian and Oceanian Biochemists and Molecular Biologists (FAOBMB) Congress.* Christchurch, New Zealand, 22- 25 November 2021. pp. 236 (Abstract)

PROFESSIONAL BODY MEMBERSHIPS

1. International Union of Biochemistry and Molecular Biology Trainee Initiative (IUBMB TI)
   Role:
   - Regional leader for the Asia and Oceania region (2025 - present)
   - Representative for the Asia and Oceania region & social media coordinator (2024 - 2025)

2. Malaysian Society for Biochemistry and Molecular Biology (MSBMB)
   Role:
   - Ordinary member (2019 – present)

3. Malaysia Board of Technologists (MBOT)
   Role:
   - Graduate technologist (Biotechnology) (2021- present)

FELLOWSHIPS/AWARDS

1. Universiti Tunku Abdul Rahman Staff Scholarship for PhD degree study (2018 – 2022)
2. Federation of Asian and Oceanian Biochemists and Molecular Biologists (FAOBMB) Exchange Fellowship, Travel Grant (2019)
3. Croucher Summer Course in Precision Genome Engineering by CRISPR, The University of Hong Kong, Travel Grant (2018)

Jong, HL., Yuen, KS., Jin, DY. et al. Generation of Leucine-Rich Repeat Kinase 2 (LRRK2) Knockout Neuroblastoma Cells SH-SY5Y by CRISPR/Cas9-Mediated Genome Editing. Biochem Genet (2025). https://doi.org/10.1007/s10528-025-11174-4 (Published on 2 July 2025; WOS/ Scopus indexed publication)

Biochemical Genetics
https://doi.org/10.1007/s10528-025-11174-4

METHODOLOGY ARTICLE

Generation of Leucine-Rich Repeat Kinase 2 (LRRK2) Knockout Neuroblastoma Cells SH-SY5Y by CRISPR/Cas9-Mediated Genome Editing

Hui-Lan Jong[2] · Kit-San Yuen[3,4] · Dong-Yan Jin[3] · Susan Ling Ling Hoe[5] · Aini Ideris[6] · Chee-Hong Tan[7] · Sau-Kuen Lam[2] · Yang-Mooi Lim[2] · Soon-Keng Cheong[1]

Received: 4 January 2025 / Accepted: 17 June 2025

Abstract

Leucine-rich repeat kinase 2 (LRRK2) is associated with Parkinson's disease, despite its low expression in the brain. Pathogenic mutations in LRRK2 enhance kinase activity and contribute to the disease's pathogenesis. Neuroblastoma SH-SY5Y cells, which also exhibit low LRRK2 expression, are extensively used as a model for Parkinson's disease. While less prominent, low-expression genes can play crucial roles in cellular processes, development, and disease. Knocking out such genes poses specific challenges, including difficulties in detection, incomplete knockout, and compensatory mechanisms that can obscure phenotypic changes. This study develops a strategy to knockout low-expression LRRK2 in SH-SY5Y cells effectively. Our approach employs a double-cut and multiple guide RNAs strategy, optimized electroporation parameters to enhance CRISPR/Cas9 plasmid delivery, refined clonal expansion technique, and a sensitive protein detection protocol. We successfully generate LRRK2 knockout SH-SY5Y cells using CRISPR/Cas9, with the knockout efficiency validated by PCR analysis, sequencing, and Western blot analysis.

Extended author information available on the last page of the article

Published online: 02 July 2025

low expression in neuronal tissues (Tolosa et al. 2020; Rocha et al. 2022; Simpson et al. 2022; Taymans et al. 2023). Neuroblastoma cell line SH-SH5Y, a neuronal cell line, is one of the cell lines that exhibit low expression of LRRK2 (Biskup et al. 2007).

The neuroblastoma SH-SY5Y cell line is widely used as a model for Parkinson's disease research due to its human origin and neuronal characteristics (Biedler et al. 1973, 1978). Compared to primary neurons, SH-SY5Y cells are relatively easy and cost-effective to culture, express various human-specific proteins and isoforms absent in rodent primary cells, are amenable to genetic manipulation, and can undergo large-scale expansion before differentiation. In addition, they can be differentiated into dopaminergic neurons, making them particularly relevant for Parkinson's disease studies (Kovalevich et al. 2013; Rodríguez-Losada et al. 2020; Ioghen et al. 2023). These properties make SH-SY5Y cells a valuable tool for investigating Parkinson's disease mechanisms and testing potential therapies. In recent years, various LRRK2 knockout cell models have been developed, including human-induced pluripotent stem cells (iPSCs) (Chen et al. 2020), microglial cells (Zhang et al. 2022), macrophages (Almudimeegh 2022), and human embryonic kidney (HEK-293) cells (Quintero-Espinosa et al. 2023). While iPSCs derived from Parkinson's patient fibroblasts can be differentiated into dopaminergic neurons, making them a physiologically relevant model that retains patient-specific genetic variants, they are costly to maintain, labor-intensive to culture, and require careful handling, despite ongoing efforts to simplify their culturing process and reduce labor demands (Chang et al. 2015; Ghaedi et al. 2016; Cheng et al. 2023). In contrast, the LRRK2 knockout SH-SY5Y cell model generated in this study is significantly more cost-effective and easier to maintain. In addition, SH-SY5Y cells possess neuronal characteristics, making them relevant for Parkinson's disease research, unlike HEK-293 cells, which, while easier to transfect and culture than SH-SY5Y cells, lack neuronal properties (Ioghen et al. 2023). Although LRRK2 knockout microglial cells and macrophages are valuable for studying neuroinflammation-related processes, such as aggregate clearance (Gao et al. 2023), LRRK2 knockout SH-SY5Y cells offer a broader research scope, including synaptic transmission studies. In addition, SH-SY5Y cells are widely used to investigate cellular responses to neurotoxicants and genetic mutations associated with Parkinson's disease (Rakotoarisoa et al. 2019; Ramalingam et al. 2019; Rodríguez-Losada et al. 2020; Zhao et al. 2020; Xu et al. 2021; Luo et al. 2023). Despite their advantages, SH-SY5Y cells have notable limitations, including their cancerous origin, genomic instability (Hoffmann et al. 2023; Ioghen et al. 2023), potential conversion to an epithelial phenotype (Ross et al. 1983; Ioghen et al. 2023), and low expression of certain Parkinson's disease-related proteins, such as LRRK2 (Snoderly-Foster et al. 2022). These factors can limit their applicability in specific studies. However, researchers continue to use SH-SY5Y cells as a valuable and accessible platform for initial screenings and mechanistic studies, bridging the gap between simpler in vitro systems and more complex in vivo models.

Knocking out genes with low expression levels presents several challenges due to their minimal baseline activity and subtle impact on cellular functions. These genes are often difficult to detect and quantify, making it challenging to confirm successful

knockout (Biskup et al. 2007; Fernández et al. 2022). In addition, low-expression genes may not produce easily observable phenotypic changes when disrupted, complicating the assessment of knockout efficacy (Schapansky et al. 2014; Snoderly-Foster et al. 2022). Earlier investigation revealed that the LRRK2 knockout leads to significant changes in the kidney, likely because LRRK2 is normally expressed at approximately 6.2 times higher levels in the kidney compared to the brain and other organs (Tong et al. 2010). Furthermore, compensatory mechanisms within the cell can mask the effects of the knockout by upregulating alternative pathways or redundant genes, thereby obscuring the intended outcomes (El-Brolosy et al. 2017; Giaime et al. 2017; Araki et al. 2018). Previous studies have demonstrated that functions of LRRK2 are redundant, and can be compensated by its homolog LRRK1 (Tong et al. 2010; Giaime et al. 2017; Araki et al. 2018; Erb et al. 2020). In tissues with lower LRRK2 expression, such as the heart and brain, LRRK2 knockout animals show no noticeable endolysosomal pathology (Erb et al. 2020). The inherent difficulties in achieving complete knockout and the potential for compensatory adaptations necessitate carefully optimized techniques and sensitive detection methods to accurately evaluate the impact of disrupting low-expression genes. The challenge of detecting endogenous LRRK2 protein by Western blotting and immunocytochemistry is heightened by the combination of a poorly expressed transcript and an unusually large, seemingly unstable protein, even though LRRK2 is highly soluble (Biskup et al. 2007). LRRK2 knockout models have been established in animals (Lee et al. 2007; Tong et al. 2010, 2012; Hinkle et al. 2012; Baptista et al. 2013; Ness et al. 2013; Østergaard 2024), stem cells (Bahnassawy et al. 2013; Chen et al. 2020), and cell lines (Kim et al. 2019; Quintero-Espinosa et al. 2023). LRRK2 knockout SH-SY5Y models remain rare, despite the widespread use of SH-SY5Y cells in Parkinson's disease research. To the best of our knowledge, only one LRRK2 knockout SH-SY5Y cell line has been reported, generated by Tombesi et al. (Tombesi et al. 2024). However, a detailed, step-by-step protocol for its generation has not been available. This study is the first to provide a comprehensive protocol for generating LRRK2 knockout SH-SY5Y cells, along with essential tips and strategies to overcome associated challenges.

CRISPR/Cas9 is a revolutionary genome editing technology that allows permanent and precise modifications to DNA by harnessing the cellular double-strand breaks repair pathways, i.e., non-homologous end joining or homology-directed repair (Lander 2016; Moon et al. 2019). This tool offers significant advantages, including high specificity, efficiency, ease of use, and versatility, making it widely applicable to genetic research (Moon et al. 2019). Notably, CRISPR/Cas9 has been successfully employed to manipulate genes across various expression levels, including those with low expression (Deleuze et al. 2024). While targeting low-expression genes is challenging due to their subtle effects on cellular phenotypes, CRISPR/Cas9 provides a powerful approach for precise gene modifications. Applying CRISPR/Cas9 in neuronal cells presents both challenges and advantages. One major hurdle is the efficient delivery of CRISPR/Cas9 components. Neurons are post-mitotic and have a limited capacity for plasmid uptake, while certain neuronal cell lines, such as SH-SY5Y, PC12, Neuro-2A, are notoriously difficult to transfect (Jordan et al. 2008; Covello et al. 2014; Yin et al. 2014). Viral vectors, particularly

adeno-associated viruses (AAVs), are commonly used for delivery but have cargo size limitations (Karra et al. 2010). In addition, off-target effects remain a concern, especially in neuronal cells, where precision is critical for maintaining cellular function (Arango et al. 2021). Despite these challenges, CRISPR/Cas9 has proven invaluable for studying neuronal function and disease. Optimizing guide RNA design (Joberty et al. 2020), delivery methods (Lattanzi et al. 2019; Yip 2020; Sinclair et al. 2023), and detection techniques (Deleuze et al. 2024; Navarro-Guerrero et al. 2024) has enhanced its effectiveness, particularly for investigating low-expression genes. CRISPR/Cas9 enables researchers to model neurodegenerative disorders, study gene function, and explore potential therapeutic strategies. Compared to traditional gene editing methods, it is faster, more efficient, and cost-effective (Gupta et al. 2014). Moreover, its adaptability for in vivo studies makes it a powerful tool for neuroscience research (Macarrón Palacios et al. 2024).

The present study aimed to develop an effective strategy for knocking out low-expression LRRK2 in SH-SY5Y cells. We utilized a dual-cut approach with multiple guide RNAs, optimized electroporation parameters to improve CRISPR/Cas9 plasmid delivery, refined clonal expansion techniques, and established a sensitive protein detection protocol. Using this strategy, we successfully generated LRRK2 knockout SH-SY5Y cells, with knockout efficiency validated through PCR analysis, sequencing, and Western blot analysis.

Materials and Methods

The overall workflow for *LRRK2* gene knockout using CRISPR/Cas9 in SH-SY5Y cells is outlined in Fig. 1.

Designing of gRNAs

1. Design the gRNAs using a web tool, CHOPCHOP (https://chopchop.cbu.uib.no/). CHOPCHOP is a tool designed to identify single-gRNA targets for CRISPR/Cas systems. The parameters used to design gRNAs for knockout of the LRRK2 are detailed in Table 1.

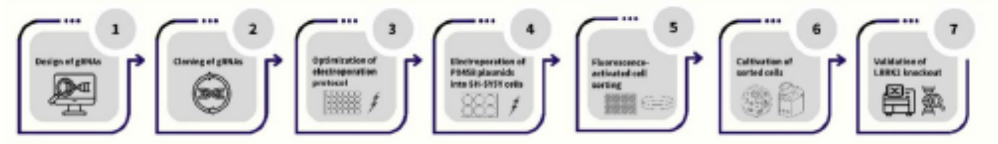

Fig. 1 Workflow for *LRRK2* gene knockout using CRISPR/Cas9 in SH-SY5Y cells. We describe protocols for designing and cloning gRNAs, optimizing the electroporation procedure, electroporating PX458 plasmids into SH-SY5Y cells, conducting fluorescence-activated cell sorting, cultivating sorted cells, and validating the LRRK2 knockout

Table 1 The parameters used to design gRNAs

Parameter	Input
Target	LRRK2
In	Homo sapiens (hg38/ GRCh38)
Using	CRISPR/Cas9
For	Knockout

Tip: There are many web-based tools available for designing gRNAs, each utilizing different algorithms to provide gRNA sequences and predict off-target sites. One of the highly recommended and commonly used tools is CHOPCHOP (Hwang et al. 2021).

2. Select three gRNAs from the list of gRNAs designed by CHOPCHOP (Supplementary File 2) and name them as gRNA1, gRNA2, and gRNA3.

Tip: Select the gRNAs that fulfill the following criteria

i. *20 base pairs in length*
ii. *Target exon(s) in the early coding region*
iii. *Guanine-cytosine (GC) content of 40–60%*
iv. *Low number of mismatches (i.e., number of off-target transcripts that the gRNA may bind to, outside of the target gene).*

Cloning of gRNAs

1. Construct PX458-gRNA1, PX458-gRNA2 and PX458-gRNA3 by inserting the respective gRNA sequence into pSpCas9(BB)-2A-GFP (PX458) plasmids. The PX458 plasmids were a gift from Feng Zhang (Addgene plasmid # 48,138; http://n2t.net/addgene:48138; RRID: Addgene_48138) (Ran et al. 2013).
2. The cloning of gRNAs involves the following steps:
3. Preparation of competent cells
4. Digestion of PX458 plasmids
5. Purification of the digested PX458 plasmids
6. Annealing of gRNA oligos
7. Ligation of gRNA oligos and PX458 plasmids
8. Transformation of ligation products into competent cells
9. Extraction of PX458 plasmids

Preparation of Competent Cells

1. Prepare RF1 and RF2 solutions. The RF1 solution consists of 100 mM potassium chloride (Merck, USA), 50 mM manganese (II) chloride (Merck, USA), 30 mM

potassium acetate (Merck, USA), 10 mM calcium chloride (Merck, USA), and 15%v/v glycerol (MP Biomedicals, USA). The RF2 solution contains 10 mM 3-(4-Morpholino) propane sulfonic acid (MOPS) (Fisher Scientific, USA), 10 mM potassium chloride, 75 mM calcium chloride, and 15%v/v glycerol.

2. Adjust the pH of both RF1 and RF2 solutions to 5.8 using hydrochloric acid (R & M Chemicals, Malaysia).
3. Autoclave the RF2 solution after its preparation.

Tip: You may keep both RF1 and RF2 solutions at room temperature after you prepare them. Chill both solutions in the refrigerator before the preparation of the competent cells.

4. Inoculate a single colony of *E. coli* (commonly used strains are DH5α/ DH10β) into 4 ml LB broth (Condalab, Spain). Incubate the culture at 37 °C with shaking (250 rpm) overnight.
5. Transfer 2 ml overnight culture into 100 ml LB broth.
6. Incubate the culture at 37 °C with shaking (250 rpm) until it reaches an optical density (OD 550) of 0.3–0.5.
7. Transfer the culture into a 50 ml conical tube and centrifuge at 5000 rpm, 5 min, 4 °C.
8. Remove the supernatant and resuspend the pellet in 1/3 volume of ice-cold RF1 solution (e.g., 33 ml ice-cold RF1 solution for 100 ml culture).

Tip: Avoid pipetting up and down. Resuspend by inverting the tube gently.

9. Centrifuge the cells at 5000 rpm, 5 min, 4 °C.
10. Remove the supernatant, resuspend the pellet in 1/12.5 volume of ice-cold RF2 solution (e.g., 8 ml ice-cold RF2 solution for 100 ml culture), and mix.
11. Incubate the cells on ice for 15 min.
12. Aliquot competent cells into 1.5 ml microcentrifuge tubes.
13. Snap freeze the aliquoted competent cells in liquid nitrogen and store them at − 80 °C.

Tip: If liquid nitrogen is not available, you may store the competent cells at − 80 °C directly, but their competency will be lower.

Digestion of PX458 Plasmids

1. Perform restriction enzyme digestion to linearize the PX458 plasmids.
2. For each restriction enzyme digestion reaction, add 1 µg (1 unit) *Bbs*I enzyme (New England Biolabs, USA) into a 1.5 ml microcentrifuge tube containing 5 µg PX458 plasmids and incubate for 16 h at 37 °C.

Purification of the Digested PX458 Plasmids

1. Run digested PX458 plasmids on 1% agarose gel at 80 V for 30 min.
2. Excise the DNA band from the gel.
3. Purify the gel slice (containing the digested PX458 plasmid) using Wizard SV Gel and PCR Clean-Up System (Promega, USA) following the manufacturer's instructions.
4. Keep the purified plasmids at − 20 °C until further use.

Annealing of gRNA Oligos

1. Order single-stranded gRNA oligos from a supplier. The gRNA oligos used in this study were synthesized by Integrated DNA Technologies (IDT, Singapore), the sequences are as in Table 2.
2. Prepare an annealing mix by combining 1.5 µl of 100 µM gRNA oligo (sense), 1.5 µl of 100 µM gRNA oligo (anti-sense), 1.0 µl of 10 X PCR buffer, and 6.0 µl of nuclease-free water (Sigma-Aldrich, USA).

Tip: You may use 10X PCR buffer of any brand.

3. Anneal each pair of gRNA oligos using a thermal cycler (Applied Biosystems, USA) with the following temperature cycle: 95 °C for 5 min, 90 °C for 5 min, 85 °C for 5 min, 80 °C for 5 min, 75 °C for 5 min, 70 °C for 5 min, 65 °C for 5 min and 60 °C for 20 min.

Ligation of gRNA Oligos and PX458 Plasmids

1. Ligate each pair of annealed gRNA oligos into *Bbs*I-digested PX458 plasmids.
2. Prepare a ligation mix which consists of 4.0 µl of 100 µM annealed gRNA oligo, 1.0 µl of *Bbs*I-digested PX458 plasmid, 1.0 µl of 10 X ligation buffer (New England Biolabs, USA), 1.0 µl of T4 DNA ligase (Thermo Fisher Scientific, USA), and 3.0 µl of nuclease-free water.
3. Incubate the ligation mix at room temperature for 10 min.

Table 2 gRNAs sequence

gRNA	Sequence (5'–3')
gRNA 1 sense	CACCGTGTTCACGTACTCCGAGCG
gRNA 1 anti-sense	AAACCGCTCGGAGTACGTGAACAC
gRNA 2 sense	CACCGAGTCCAAGACGATCAACAG
gRNA 2 anti-sense	AAACCTGTTGATCGTCTTGGACTC
gRNA 3 sense	CACCGAGTCAGGCTGAACAATGTCC
gRNA 3 anti-sense	AAACGGACATTGTTCAGCCTGACTC

Transformation of Ligation Products into Competent Cells

1. Add 10 µl ligation product into 100 µl competent cells and incubate on ice for 30 min.
2. Heat-shock the competent cells at 42 °C for 90 s and chill on ice immediately for 3 min.

Tip: The temperature is critical. Confirm the water bath temperature using a thermometer before performing the heat shock.

3. Recover competent cells using LB broth and incubate them at 37 °C with shaking (250 rpm) for 1 h.
4. After recovery, spread the competent cells on an LB agar plate (Condalab, Spain) with Ampicillin (100 µg/ml) (Nacalai Tesque, Japan) and incubate at 37 °C overnight.
5. Pick colonies the next day, inoculate each colony with 1 ml LB broth with Ampicillin (100 µg/ml), and incubate at 37 °C with shaking (250 rpm) for 3 h.
6. After 3 h of incubation, harvest 500 µl culture and send it to the service provider for Sanger sequencing to verify the gRNA sequence in the PX458 plasmids.
7. After verification, inoculate 100 µl culture into 100 ml LB broth with Ampicillin (100 µg/ml) and incubate at 37 °C with shaking (250 rpm) overnight.

Extraction of PX458 Plasmids

1. Extract the plasmids from overnight culture using Nucleobond Xtra Midi Plus (Macherey–Nagel, Germany) following the manufacturer's protocol.
2. Determine the plasmids yield using a NanoQuant Plate on a microplate reader (Tecan, Switzerland).
3. Confirm the plasmids' integrity by running the plasmids on 1% agarose gel at 80 V for 1 h.
4. Keep the extracted plasmids at − 20 °C until further use.

Optimization of Electroporation Protocol

The electroporation protocol is optimized to identify the most effective electroporation parameters for SH-SY5Y cells (ATCC, Manassas, VA, USA, Cat# CRL-2266, RRID: CVCL_0019). This optimization is crucial for ensuring efficient genome editing and high cell viability. Detailed optimization parameters are provided in Table 3.

Table 3 Electroporation optimization parameters

Sample	Well number	Pulse voltage (V)	Pulse width (ms)	Pulse number
1	A1	None (control without electroporation)		
2	A2	1400	20	1
3	A3	1500	20	1
4	A4	1600	20	1
5	A5	1700	20	1
6	A6	1100	30	1
7	B1	1200	30	1
8	B2	1300	30	1
9	B3	1400	30	1
10	B4	1000	40	1
11	B5	1100	40	1
12	B6	1200	40	1
13	C1	1100	20	2
14	C2	1200	20	2
15	C3	1300	20	2
16	C4	1400	20	2
17	C5	850	30	2
18	C6	950	30	2
19	D1	1050	30	2
20	D2	1150	30	2
21	D3	1300	10	3
22	D4	1400	10	3
23	D5	1500	10	3
24	D6	1600	10	3

1. Electroporate the cells using the reagents and consumables provided in the Neon™ Transfection System 10 µL Kit and the Neon Transfection System (Thermo Fisher Scientific, USA), following the manufacturer's protocol.

   Tip:

   i. *Use PX458 plasmids without gRNA for this optimization.*
   ii. *Use* 5×10^4 *cells and 2 µg of plasmids per electroporation reaction*

2. After electroporation, incubate the cells in a CO_2 incubator (Esco, Singapore) for 72 h to allow for recovery.
3. After 72 h recovery, observe the cells using a fluorescence microscope with a FITC filter (Carl Zeiss, Germany), capture an image for each well, and evaluate

electroporation efficiency by estimating the intensity of green fluorescence protein (GFP).
4. Assess cell viability based on cell morphology.
5. Determine the optimal electroporation parameters for SH-SY5Y cells.

Electroporation of PX458 Plasmids into SH-SY5Y Cells

1. Electroporate the cells using the reagents and consumables provided in the Neon™ Transfection System 100 µL Kit and the Neon Transfection System (Thermo Fisher Scientific, USA), following the manufacturer's protocol.

Tip:

i. To electroporate more cells, use the Neon™ Transfection System 100 µL Kit, instead of the 10 µL Kit.
ii. Use 5×10^5 cells per electroporation reaction
iii. Each electroporation reaction for LRRK2 knockout consists of PX458-gRNA1 (6.67 µg), PX458-gRNA2 (6.67 µg) and PX458-gRNA3 (6.67 µg), whereas the mock control contains 20 µg PX458 (without gRNA).
iv. The optimal electroporation parameters for SH-SY5Y cells are 1400 V, 20 ms, and 1 pulse.

2. Incubate the plate containing transfected cells in a CO_2 incubator for 72 h to allow cell recovery.

Fluorescence-Activated Cell Sorting (FACS)

After 72 h recovery in a 6-well plate, the electroporated cells were brought to a cell sorting facility for FACS.

1. Harvest the cells using Accutase (Merck, USA).
2. Wash the cells with 1 X PBS (Amresco, USA) and centrifuge at 300× g for 5 min.
3. Remove the 1 X PBS and resuspend the cell pellet in 1 X sorting buffer. The 1 X sorting buffer consists of 1X Hanks' balanced salt solution (HBSS) (Gibco, USA), 2% fetal bovine serum (FBS) (Gibco, USA) and 10 mM of N-2-hydroxyethylpiperazine-N-ethanesulfonic acid (HEPES) (Sigma-Aldrich, USA).

Tip: Filter the 1 X sorting buffer using a 0.22 µm syringe filter (Whatman, USA) before use.

4. Perform cell count using the trypan blue exclusion method.
5. Stain the cells with 2 µg/ml propidium iodide (PI) (BD Biosciences, USA) per 1×10^6 cells, for 10 min in the dark. Do not wash the stained cells.

Tip: PI was used to differentiate live cells from dead cells during cell sorting.

6. Filter the cells through 40 µm cell strainers (BD Biosciences, USA) to obtain single-cell suspension and transfer the cells to 5 ml polypropylene round-bottom tubes (BD Biosciences, USA).

Tip: Due to budget constraints, we opted for polystyrene tubes as we had remaining stock in the lab. However, it is important to note that cells tend to adhere to polystyrene, and these tubes are more susceptible to breakage under the high pressures from the cell sorters. Therefore, we recommend using polypropylene tubes.

7. Sort the cells using BD FACS Aria SORP cell sorter (BD Biosciences, USA) into a 96-well plate (single cell in each well) and 15 ml conical tube (100 or 200 cells in a tube). Autoclaved and filtered 1 X PBS solution is used as sheath buffer. Collect the PI-negative and GFP-positive cells.

Tip:

i. Based on our observations, SH-SY5Y cells have considerable difficulty proliferating from a single cell. To maximize clone yield, we employed both bulk sorting (sorting 100 or 200 cells into a 15 ml conical tube) and single-cell sorting (sorting individual cells into each well of a 96-well plate).
ii. Alternatively, BD FACSFlow can be used as sheath buffer. It has been shown not to compromise the growth and/or downstream applications of post-sorted cells.

8. Transfer the 96-well plate to the CO_2 incubator once the sorting is completed.
9. Transfer 100 or 200 cells from the 15 ml conical tube to a 10 cm cell culture dish containing supplemented media once the sorting is completed, and return the dish containing 100 or 200 cells to the CO_2 incubator.

Cultivation and Expansion of Clones

Clones from Single-Cell Sorting

1. When the clones grow to an appropriate size, harvest the clones from the 96-well plate using 0.25 % trypsin-EDTA (Gibco, USA).
2. Transfer them to a 24-well plate.
3. Expand the clones by plating them into progressively larger vessels until there are sufficient cells for downstream assay.

Clones from Bulk Sorting

1. When the clones grow to a reasonable size, isolate them using the single-cell isolation technique (filter paper method) as described in Yuen et al. (2017a, 2017b), Section 3.2, Step No. 7 and 8.
2. Expand the clones by plating them into progressively larger vessels until there are sufficient cells for downstream assay.

Verification of LRRK2 Knockout

Extraction of Total Genomic DNA

1. Extract the total genomic DNA using a Wizard Genomic DNA extraction kit (Promega, USA) according to the manufacturer's protocol.
2. Determine the DNA concentration and purity using NanoQuant Plate on a microplate reader (Tecan, Switzerland).
3. Stored the DNA at -20° until further use.

PCR

A pair of primers flanking the target site was used in the PCR:
Forward primer (pLKO_F): 5'-CTGAGCAGCGGACGTTCAT- 3'
Reverse primer (pLKO_R): 5'-CTCTTCATCCCGTTTACATTGCG-3'

1. Prepare a PCR reaction mixture which consists of 12.50 µl of 2X GoTaq Hot Start Master Mix (Promega, USA), 1.25 µl of 10 µM of forward primer, 1.25 µl of 10 µM of reverse primer, 1.0 µl of 100 ng/µl DNA template, and 9.0 µl of nuclease-free water.
2. Mix the PCR reaction gently and centrifuge to bring the solution to the bottom of the tube.
3. Run the PCR on a Veriti 96-well thermal cycler (Thermo Fisher Scientific, USA) using the following cycling parameters: 95 °C for 2 min; 35 cycles of 95 °C for 15 s, 59.3 °C for 30 s, 72 °C for 1 min; followed by final extension at 72 °C for 5 min.

TA Cloning

1. Perform the TA cloning using the pGEM-T vector system (Promega, USA) following the manufacturer's protocol.

2. Spread 20 µl of isopropyl-β-d-thiogalactopyranoside (IPTG) (Biosynth Carbosynth, UK) and 100 µl of 5-bromo-4-chloro-3-indolyl-beta-D-galacto-pyranoside (X-gal) (J & K Scientific, USA) on a LB agar plate with Ampicillin (100 µg/ml).
3. After 1 h of incubation, add the ligation products to 100 µl competent cells.
4. Perform transformation following the steps outlined in the "Transformation of ligation products into competent cells" section.
5. After overnight incubation, pick the white colonies from the plates, inoculate them in 5 ml LB broth with Ampicillin (100 µg/ml), and culture overnight.

Extraction of Plasmids

1. Extract the plasmids from 5 ml culture using FavorPrep™ Plasmid DNA Extraction Mini Kit (Favorgen, Taiwan) following the manufacturer's protocol.
2. Determine the plasmid concentration and purity using NanoQuant Plate on a microplate reader (Tecan, Switzerland).
3. Stored the DNA at − 20 °C until further use.

Sanger Sequencing

1. Send plasmids to a service provider (Apical Pvt. Ltd.) for Sanger sequencing.
2. The primers for sequencing are the same as those listed in the "PCR" section.
3. Analyze the Sanger sequencing results using Molecular Evolutionary Genetics Analysis (MEGA) software version 5.2 by performing manual alignments of sequences from the wild-type and knockout clones.

Extraction of Protein Lysates

1. Extract protein lysates from cells using the NE-PER Nuclear and Cytoplasmic Extraction Reagent (Thermo Fisher Scientific, USA) according to the manufacturer's protocol.
2. Quantify the protein lysate concentration using Pierce 660 nm Protein Assay Reagent (Thermo Fisher Scientific, USA) following the manufacturer's instructions.
3. Store the protein lysates at − 20 °C until further use.

Western Blot

1. Load the 20 µg of each protein lysate and ExcelBand™ 3-color extra range protein marker (SMOBIO, Taiwan) on a 4–20% tris–glycine gel.

Tip: For guidance on hand-casting a gradient gel, please refer to Lorberbaum (2013).

2. Run the gel in 1 X tris–glycine-sodium dodecyl sulfate (TG-SDS) buffer (1st BASE, Singapore) using a vertical polyacrylamide gel electrophoresis system (Bio-Rad, USA) at 20 mA, for 3 h.
3. Transfer the proteins from the gel to a polyvinylidene fluoride (PVDF) membrane (Merck, USA) in 1 X tris–glycine (TG) buffer (1st BASE, Singapore) using a wet transfer system (Bio-Rad, USA) at 30 V, overnight at 4 °C.
4. Disassemble the transfer sandwich and examine that the ExcelBand™ 3-color extra range protein marker has been completely transferred to the membrane.
5. Stain the membrane with Ponceau S staining solution and the gel with Coomassie Blue solution.

Tip:

a. Ensure that there are no or very few protein bands on the Coomassie Blue-stained gel. The presence of protein bands indicates incomplete transfer of proteins from the gel to the membrane.
b. Verify that protein bands are visible on the Ponceau S-stained membrane. The absence or minimal visibility of protein bands suggests that proteins have been either under-transferred or over-transferred.

6. Place the membrane in a clean container and incubate it with 5% bovine serum albumin (BSA) (Merck, USA) in 1 X tris-buffered saline (1 X TBST) at room temperature for 1 h.
7. Cut the membrane and incubate it with the primary antibody [anti-LRRK2 antibody (Abcam Cat# ab133474, RRID: AB_2713963) and anti-GAPDH antibody (Abcam Cat# ab181602, RRID: AB_2630358)] in two different containers (one primary antibody in each of the containers) overnight at 4 °C with rocking. The anti-LRRK2 and anti-GAPDH antibodies were used at dilutions of 1:20,000 and 1:10,000, respectively.
8. Remove the primary antibody solution.
9. Wash the membrane with 1 X TBST 3 times (5 min each).
10. Incubate the membrane with secondary antibody [goat anti-rabbit IgG (H + L) secondary antibody, HRP conjugate (Thermo Fisher Scientific Cat# 31,460, RRID: AB_228341)] at room temperature for 1.5 h. The goat anti-rabbit IgG (H + L) HRP-conjugated secondary antibody was used at a dilution of 1:100,000 for the membrane previously incubated with anti-LRRK2 antibody, and 1:10,000 for that incubated with anti-GAPDH antibody.
11. Remove the secondary antibody solution.
12. Wash the membrane with 1 X TBST 3 times (5 min each).
13. Incubate the membrane with WesternBright Sirius chemiluminescent HRP substrate (Advansta, USA) for 2 min.
14. Capture an image of the membrane using the Azure 600 Gel Imaging System (Azure, USA). In the software, select "Chemi blot" as the protocol type, "Manually image" as the capture type, "3 × 3" for pixel binning, "Manual" for the

Table 4 gRNA2 and gRNA3 potential off-target locations (No.1 and No. 2 to No.7, respectively), number of mismatches, sequences (as predicted by CHOPCHOP) and primers designed for validation, and the annealing temperature

No	Location	Number of mismatches	Sequence (including mismatches*)	Primers	Annealing temperature (°C)
1	chr10:124,442,476	3	aAGaCCAAGACGAcCAACAGAGG	F: GATGTCAAGGCTGCAGTGAG	63.0
				R: GTTCACTCCCTTCTCCCCTC	
2	chr10:75,876,195	3	AGTCAGcCTGAAgAgTGTCCTGG	F: CCTGACTGGGGAACACTGAT	64.5
				R: CCAAGGGAGAACTTCAAGAGCT	
3	chr13:89,431,766	3	AGTgAaGCTGAACAATGTCtAGG	F: GCCAAAATACCAGCAACCTCA	64.7
				R: ACATAGTTGCCTCCTAGCCA	
4	chr4:73,126,296	3	AGTCAGGCTGAAtAATaCCAGG	F: AGGCAGTGCAGAAGAGTGAT	64.3
				R: CACAACTGCTAATTTGGCCCT	
5	chr4:83,762,058	3	CCAGGACATTGcTCAGCCTcACc	F: CAGGGTGCGCACATAAAGAC	64.5
				R: GCTGTGGCCATTTCTGAGCA	
6	chr6:154,976,916	3	CCAcGAtATTGcTCAGCCTGACT	F: ACTCCAGTTACATGCCCAGC	71.1
				R: CTAAGACCACAGGCCAGACG	
7	chr9:27,216,984	3	AGTCAaGCTttACAATGTCCAGG	F: CCCTCAAGTGCTCCTGGTTT	65.1
				R: CACGCATGGTAGTCGGTCAT	

*Mismatches are in lowercase

exposure type, "Chemiluminescence" as the channel name, "Cumulative" for the imaging mode, "30 s" for the exposure interval, "50" as the maximum number of images, "ECL" for the light source, "No filter" for the filter, "Maximum" for the aperture, and "Top shelf" for the tray type.

Verification of gRNAs Off-Targets

Extraction of Total Genomic DNA

Please refer to the protocol in the "Extraction of total genomic DNA" section.

PCR

The off-target locations, number of mismatches and sequences as well as the primer sequences and their annealing temperatures are detailed in Table 4.

1. Prepare a PCR reaction mixture which consists of 10 µl of 2X Phusion High Fidelity PCR master mix (Thermo Fisher Scientific, USA), 2 µl of 10 µM forward primer, 2 µl of 10 µM reverse primer, 1 µl of 100 ng/µl DNA template, and 5 µl of nuclease-free water.
2. Mix the PCR reaction gently and centrifuge to bring the solution to the bottom of the tube.
3. Perform the PCR on a Veriti 96-well thermal cycler (Thermo Fisher Scientific, USA) using the following cycling parameters: 98 °C for 30 s; 35 cycles of 98 °C for 10 s, xx °C for 30 s, 72 °C for 30 s; followed by final extension at 72 °C for 10 min. "xx" is the annealing temperature indicated in Table 4.

Sanger Sequencing

1. Send plasmids to a service provider (Apical Pvt. Ltd.) for Sanger sequencing.
2. The primers for sequencing are listed in Table 4.

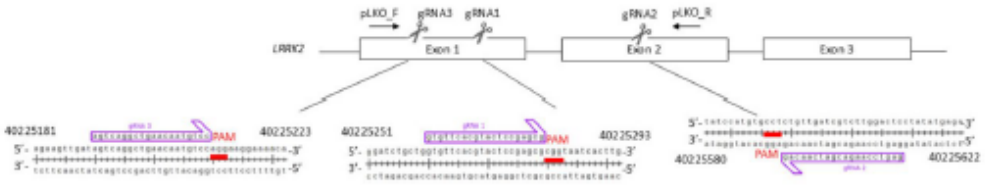

Fig. 2 Sequence and binding sites of gRNA1, gRNA2, and gRNA3 in the exon 1 and 2 of the LRRK2 gene. PAM motifs are highlighted in red color

3. Analyze the Sanger sequencing results using Molecular Evolutionary Genetics Analysis (MEGA) software version 5.2 by performing manual alignments of sequences from the wild-type and knockout clones.

Results

Double-Cut and Multiple gRNAs Strategy

To enhance editing efficiency, we adapted the double-cut approach described by Yuen et al. (Yuen et al. 2017a, 2017b), utilizing two gRNAs to excise the target region rather than relying on the conventional single-gRNA method. In this study, we employed three gRNAs to maximize the likelihood of achieving a complete knockout of the low-expression *LRRK2* gene. To attain complete abrogation of the LRRK2 protein, we selected gRNAs targeting exon 1 and exon 2. Sequences and binding sites of gRNAs are shown in Fig. 2.

The double-cut approach not only improves editing efficiency but also simplifies subsequent screening. The spliced-out target region, approximately 100 bp to 400 bp in length, can be easily detected by conventional PCR. We designed a pair of primers (pLKO_F and pLKO_R) flanking the putative target sites of gRNA 1, gRNA 2, and gRNA 3 for use in PCR analysis (Fig. 2). The amplicon length is determined by the combination of gRNAs that directs CRISPR/Cas9 to the target site for double cutting. CRISPR/Cas9 induces cuts 3 to 4 bp upstream of the PAM sequence, followed by repair via non-homologous end joining (NHEJ) or homology-directed repair (HDR). NHEJ is the canonical pathway used to repair double-stranded breaks in DNA and typically introduces small insertions or deletions, making precise amplicon lengths difficult to predict before Sanger sequencing. The potential amplicon lengths resulting from double cuts led by either two gRNAs are summarized in Table 5.

Table 5 Estimated amplicon length resulting from double cut led by either two gRNAs

Clone	Amplicon length (bp)	gRNAs
WT	746	N/A
Mock	746	N/A
LRRK2 knockout	3xx	gRNA 2 + gRNA 3
	4xx	gRNA 1 + gRNA 2
	6xx	gRNA 1 + gRNA 3

N/A, not applicable

"xx" indicates the approximate value (e.g., 6xx indicates approximately six hundred)

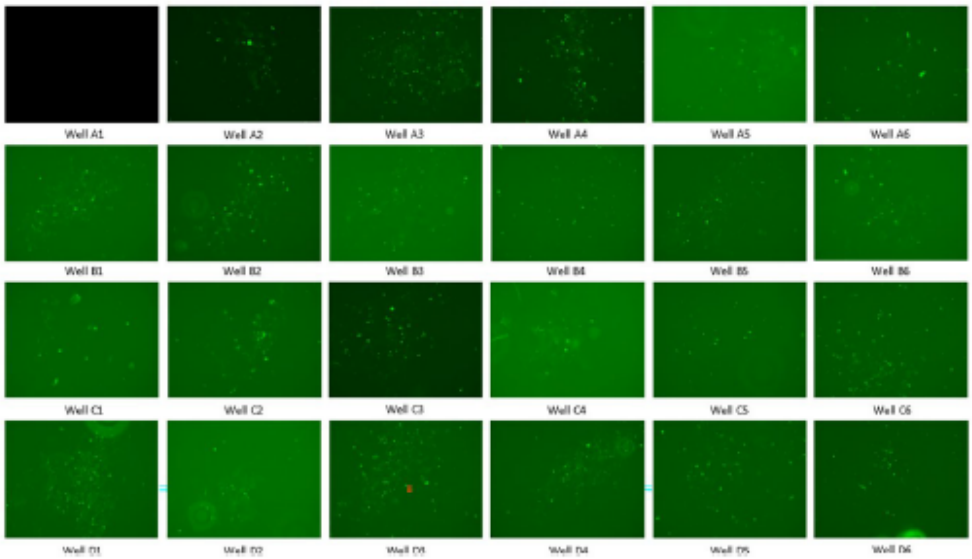

Fig. 3 Optimization of electroporation using the Neon transfection system. Twenty-three different pulse voltages, widths, and numbers were tested. Images of SH-SY5Y cells with GFP signals were captured 48 h post-electroporation (Well A2 to Well D6). Well A1 is a control without electroporation

Optimization of Electroporation Protocol

Delivering large plasmids into mammalian cells is widely recognized as a challenge, especially with hard-to-transfect cells like SH-SY5Y. The CRISPR/Cas9 plasmids used in this study are particularly large, measuring 9288 bp. Since each plasmid contains a single gRNA, this study required the transfection of three individual plasmids in a single reaction. Consequently, our initial focus was to optimize the transfection protocol. Given that chemical transfection reagents are generally less harmful to cells, we first tested Lipofectamine 3000 (Thermo Fisher Scientific, USA) and GeneJuice (Merck, USA). However, based on our visual estimation of the percentage of GFP-expressing cells under the fluorescence microscope, neither reagent yielded a transfection efficiency greater than 1%. As a result, we chose to proceed with the electroporation method, despite its higher cost.

We refined the electroporation protocol by meticulously adjusting three key parameters: pulse voltage, pulse width, and pulse number (Table 3). Based on qualitative assessments of cell viability and GFP intensity (Fig. 3 and Table 6), we identified four promising protocols that demonstrated high GFP levels while maintaining acceptable cell viability, as seen in wells A2, A3, A4, and C3. Ultimately, we selected the protocol yielding the best results: 1400 V, 20 ms, and 1 pulse, which exhibited optimal GFP expression and cell viability for downstream experiments.

Table 6 Qualitative evaluation of cell viability and GFP intensity following electroporation, and the shortlisting of protocol

Well number	% viable cells	GFP intensity	Short-listed protocol (Yes, Y/ No, N)
A1	High	None	N/A
A2	Medium	High	Y
A3	Medium	High	Y
A4	Medium	High	Y
A5	Low	Low	N
A6	Low	Medium	N
B1	High	Low	N
B2	High	Medium	N
B3	Medium	Low	N
B4	Low	Medium	N
B5	Medium	Medium	N
B6	Medium	Medium	N
C1	Low	Medium	N
C2	Medium	Medium	N
C3	Medium	High	Y
C4	Low	Low	N
C5	Low	Medium	N
C6	Medium	Medium	N
D1	High	Medium	N
D2	Low	Low	N
D3	High	Medium	N
D4	Medium	Medium	N
D5	Medium	Medium	N
D6	Low	Medium	N

N/A, not applicable

Table 7 Success rate of the refined clonal expansion technique

Type of cell culture vessel	Number of cells sorted into the vessel (A)	Number of vessels (B)	Total number of cells (C)	Total number of clones (D)	Success rate (E)
96-well plate	1 cell per well	5	480	2	0.4%
10 cm culture dish	100 cells per dish	5	500	21	4.2%
10 cm culture dish	200 cells per dish	2	400	10	2.5%

$C = A * B$

$E = D/C * 100\%$

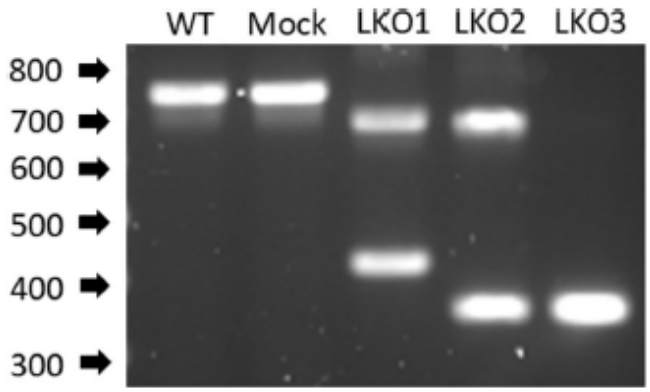

Fig. 4 PCR analysis of LRRK2 knockout (LKO) clones

Table 8 Estimated amplicon length for LRRK2 knockout clones

Clone	Amplicon length (bp)	gRNAs
WT	746	N/A
Mock	746	N/A
LKO1	4xx	gRNA 1+gRNA2
	6xx	gRNA 1+gRNA3
LKO2	3xx	gRNA 2+gRNA3
	6xx	gRNA 1+gRNA3
LKO3	3xx	gRNA 2+gRNA3

N/A, not applicable

Refined Clonal Expansion Technique

Many cell lines struggle to survive as single cells in vitro, and our experience suggests that SH-SY5Y cells may not be an exception, particularly after undergoing multiple stresses such as electroporation, transportation (which required the cells to be outside the CO_2 incubator for several hours, while being transported to a cell sorter facility located approximately 50 km away), and cell sorting. However, to produce homogeneous knockout clones, we need to culture SH-SY5Y cells from single cells post-editing.

To address this challenge, we conducted trials by seeding single cells into each well of a 96-well plate, as well as seeding 100 to 200 cells in a 10 cm culture dish. The trial results indicated that SH-SY5Y cells had difficulty growing into clones from single cells in the 96-well plates. Conversely, isolating clones from 10 cm culture dishes presented a challenge due to potential cross-contamination between clones.

Given these findings, we decided to pursue both methods to maximize the success rate of obtaining homogeneous knockout clones. Ultimately, we were able to obtain a total of 2 clones from 480 cells sorted into 96-well plates, resulting in a success rate of 0.4%. However, the success rate was significantly higher, i.e., 6 to 10 times greater, when we sorted the cells into 10 cm culture dishes, achieving

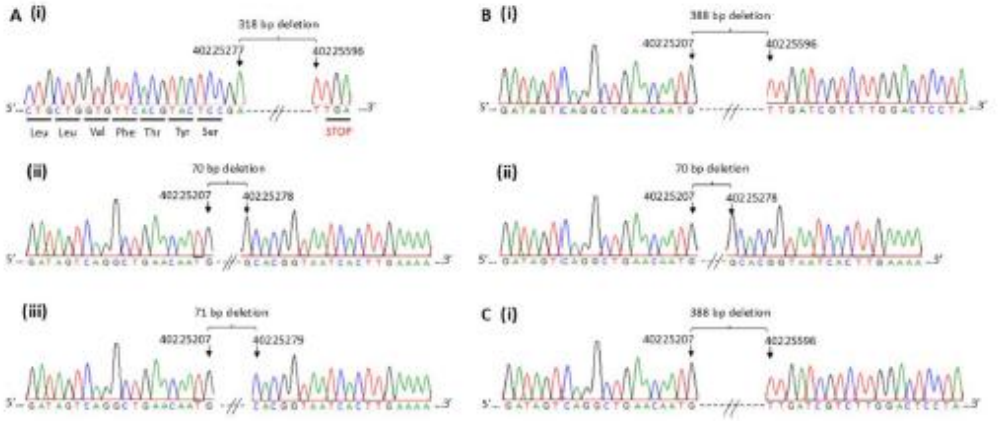

Fig. 5 DNA sequence of the edited *LRRK2* gene in **A** LKO1 where (i) a premature stop codon was generated, (ii) 70 bp or (iii) 71 bp were deleted, respectively; **B** LKO2 where (i) 388 bp or (ii) 70 bp were deleted, respectively; **C** (i) LKO3 where 388 bp were deleted

Table 9 The amplicon length, combination of gRNAs involved in the genome editing, number of bases deleted, and the resulting mutation(s) in LKO1, LKO2 and LKO3

Clone	Amplicon length (bp)	gRNAs	Number of bases deleted	Mutation
WT	746	N/A	N/A	N/A
Mock	746	N/A	N/A	N/A
LKO1	428	gRNA 1 + gRNA2	318	Generation of premature stop codon
	676 or 675	gRNA 1 + gRNA3	70 or 71	Frameshift deletion
LKO2	358	gRNA 2 + gRNA3	388	Frameshift deletion
	676	gRNA 1 + gRNA3	70	Frameshift deletion
LKO3	358	gRNA 2 + gRNA3	388	Frameshift deletion

N/A, not applicable

success rates of 2.5% (for 200 cells per dish) and 4.2% (for 100 cells per dish) (see Table 7). This aligns with the results from our trial run, confirming that sorting 100 cells into a 15 ml conical tube followed by transferring them to a 10 cm dish with supplemented media is the most effective approach.

PCR Analysis

The clones were screened using PCR analysis. From the screening, three representative LRRK2 KO clones (hereafter named LKO1, LKO2 and LKO3) were selected for further validation. LKO1 and LKO3 were derived from bulk sorting (100 and 200 cells per dish, respectively), while LKO2 was obtained from single-cell sorting

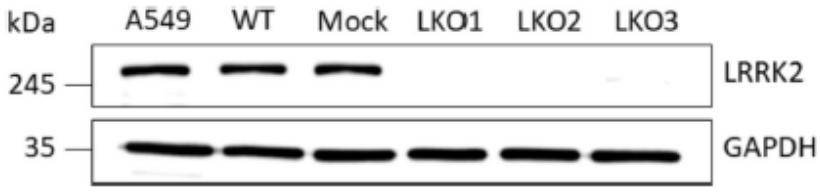

Fig. 6 Western blot validation of LRRK2 knockout (LKO) clones. GAPDH was used as a loading control

(1 cell per well). PCR analysis revealed that the LKO1 clone has two amplicons of 4xx bp and 6xx bp, the LKO2 clone has two amplicons of 3xx bp and 6xx bp, and LKO3 has a single amplicon of 3xx bp (Fig. 4 and Table 8).

TA Cloning and Sanger Sequencing

To verify the DNA sequence editing by CRISPR/Cas9, the PCR products from three representative clones (LKO1, LKO2, and LKO3) were further validated using TA cloning and Sanger sequencing. Sequencing results revealed that the 428 bp amplicon in the LKO1 clone resulted from a 318 bp deletion and the formation of a premature stop codon during rejoining of the double-stranded break, while the 676 bp or 675 bp amplicon arose from a 70 bp or 71 bp deletion [Fig. 5A(i) to (iii) and Table 9]. In the LKO2 clone, the 358 bp and 676 bp amplicons were due to deletions of 388 bp and 70 bp, respectively [Fig. 5B(i) to (ii) and Table 9]. For LKO3, there was a single amplicon of 358 bp, resulting from a 388 bp deletion [Fig. 5C(i) and Table 9].

Optimized Protein Detection Protocol

To confirm the ablation of the LRRK2 protein, we performed the Western blot analysis to verify its absence. The results demonstrated a loss of LRRK2 protein in LKO1, LKO2, and LKO3 (Fig. 6). Detecting low-expression proteins poses well-known challenges, so we optimized several critical steps in the Western blot protocol. This included ensuring efficient protein extraction, effective protein separation, and complete protein transfer. We employed primary antibodies with high specificity and a sensitive chemiluminescent substrate, while carefully adjusting image acquisition parameters to achieve strong signal intensity.

Due to budget constraints, we utilized the remaining protein extraction kit available in the lab. The NE-PER Nuclear and Cytoplasmic Extraction Kit allows for the separation of nuclear and cytoplasmic protein lysates, although it is not necessary in our study, as LRRK2 is expressed in both cellular compartments. To assess the kit's efficacy beyond its expiration date, we compared the lysate obtained with that extracted using fresh reagents. The protein quantification results indicated that both reagents performed equally well. The protein concentration extracted using the expired protein extraction kit is 2092 µg/ml, while the concentration from the new

kit is 2334 µg/ml. In addition, we successfully detected the LRRK2 protein in both the nuclear and cytoplasmic lysates, confirming its presence in both cellular compartments. Since LRRK2 is a low-abundance protein, we recommend concentrating the lysate using the minimum amount of lysis buffer and the maximum number of cells. This approach will allow us to load more protein when running the gel, despite the limited volume we can load per well. LRRK2 is a relatively large protein (286 kDa), while GAPDH, our loading control for normalization in Western blotting, is a smaller protein with a molecular weight of 44 kDa. To ensure effective protein separation, we chose to use a gradient gel. Given the financial constraints, we hand-cast the gradient gel and optimized its concentration by testing several ranges:

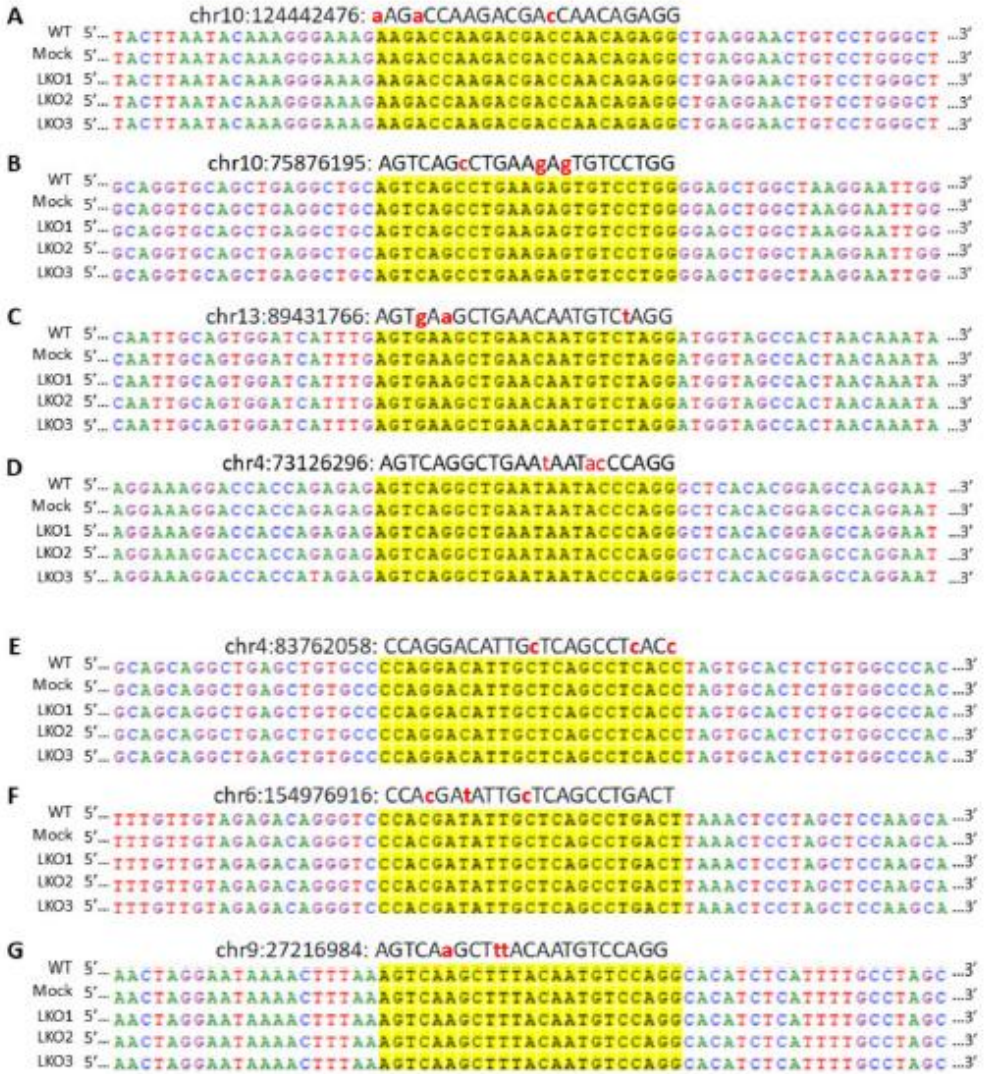

Fig. 7 Evaluation of off-targets. DNA sequences of one (**A**) and six (**B–G**) potential off-target sites of gRNA 2 and gRNA 3, respectively, in WT, mock, LKO1, LKO2 and LKO3. gRNA 1 has no off-target site

4–12%, 6–12%, 4–15%, and 4–20%. Both 4–15% and 4–20% gels provided better protein separation than 4–12% and 6–12%, with good resolution in the 245–310 kDa and 35–45 kDa ranges (Fig. S1). However, considering that the same blot would also be used to detect a 22 kDa protein (data not shown), the 4–20% gel was chosen, as it offered a better resolution in the 20–25 kDa range compared to the 4–15% gel.

To ensure the complete transfer of large LRRK2 protein without over-transferring the small GAPDH protein, we performed Coomassie blue staining on the gel and Ponceau S staining on the membrane after the overnight transfer. We visually verified that no significant amounts of large proteins remained on the Coomassie blue-stained gel. We also confirmed that both large and small proteins were present on the Ponceau S-stained membrane.

The LRRK2 primary antibody used in this study was obtained from a reliable source and demonstrated high specificity (i.e., knockout-validated). The human lung cancer cell line A549, known for its high levels of LRRK2 protein, served as a positive control. To enhance detection sensitivity, we utilized a highly sensitive chemiluminescent substrate from a reputable brand capable of detecting proteins at the femtogram level.

For image acquisition, we employed a digital imaging system with a high-resolution CCD camera. Given the weak signal for low-expression LRRK2 protein, we used a cumulative capture mode, capturing multiple images at set time intervals and combining the signals to generate a final image with increased intensity.

Off-Target Validation

Off-target effects are defined as unintended cleavages or genetic modifications at sites with sequences that are similar, but not identical, to the target site (Modrzejewski et al. 2019). In this study, off-target prediction was performed using a web-based tool, CHOPCHOP (https://chopchop.cbu.uib.no/) (Labun et al. 2019). According to CHOPCHOP, gRNA1 does not have any off-targets, while gRNA2 and gRNA3 have two and six off-targets, respectively. PCR and Sanger sequencing were performed to

Table 10 Off-target prediction by IDT CRISPR Cas9 gRNA checker

gRNA	Sequence	IDT CRISPR Cas9 gRNA checker	
		On-target score	Off-target score
1	gtgttcacgtactccgagcgcgg	44	96
2	gagtccaagacgatcaacagagg	85	76
3	agtcaggctgaacaatgtccagg	64	56

On-target score: The predicted editing performance of the gRNA at the intended target site. A higher value is better

Off-target score: A higher value indicates lower off-target. Score is from 0 to 100

evaluate the off-targets. Sequencing results demonstrated that there was no off-target in LKO1, LKO2, and LKO3 (Fig. 7A–G). In addition to the predicted non-specific binding provided by CHOPCHOP, we also assessed the non-specific binding of the gRNAs using the IDT CRISPR Cas9 gRNA checker (https://sg.idtdna.com/site/order/designtool/index/CRISPR_SEQUENCE) (Table 10).

Discussion

As the global population ages at an unprecedented pace, the community is in dire need of effective treatments for neurodegenerative diseases. Could LRRK2 kinase inhibitor be the long-awaited cure for Parkinson's disease? Previous studies have shown conflicting results. Many studies have observed adverse effects associated with LRRK2 knockout (Lee et al. 2007; Tong et al. 2010, 2012; Hinkle et al. 2012; Baptista et al. 2013; Ness et al. 2013; Pellegrini et al. 2018; Gu et al. 2023). A LRRK2 knockout model is a valuable tool for deciphering the mechanisms underlying the detrimental effects following the loss of LRRK2.

Despite the SH-SY5Y human neuroblastoma cell line being a widely used model for Parkinson's disease, a detailed step-by-step protocol for low-expression gene knockout using CRISPR/Cas9 has not yet been made available for novices. To address this gap, we provide an optimized protocol and strategy for knocking out the low-expression *LRRK2* gene in SH-SY5Y cells. Using CRISPR/Cas9, we successfully edited exons 1 and 2 of the *LRRK2* gene, leading to a premature stop codon and frameshift mutation that resulted in loss of LRRK2 protein expression.

In this study, a double-cut strategy using multiple gRNAs was employed to achieve a complete knockout of the low-expression LRRK2 gene (Yuen et al. 2017a, 2017b). Consistent with previous findings, this approach enables highly efficient gene knockout. Joberty et al. demonstrated that using dual gRNAs to generate knockout clones has synergistic effects compared to the traditional single-gRNA approach. When two gRNAs target sequences in close proximity (ideally within 40–300 bp), the indel rate significantly increases, with allele editing reaching up to 95% in most cases. Moreover, tandem gRNAs enable highly efficient gene knockout even in primary cells, such as T cells, which typically proliferate inefficiently in culture (Joberty et al. 2020). The effectiveness of dual gRNAs has also been demonstrated in plant genome editing. In soybeans, an allotetraploid crop known for its transformation difficulty, dual gRNAs guided Cas9 to cleave two sites 1 kb apart, successfully generating double homozygous mutations in the GmFAD2–1A and GmFAD2–1B genes (Do et al. 2019). In addition, Liu et al. showed that packaging tandem gRNAs along with single-stranded annealing-based surrogate reporter cassettes into CRISPR/Cas9 vectors enhanced gene editing efficiency by up to 6.31-fold (Liu et al. 2018). This study utilized three gRNAs instead of the commonly used two, resulting in three potential double cuts, further enhancing editing efficiency.

Electroporation involves applying high-voltage electric pulses to cells, temporarily disrupting the cell membrane. This increased permeability facilitates the efficient delivery of plasmids into the cells (Fus-Kujawa et al. 2021). Three key parameters i.e., pulse voltage, pulse width, and pulse number, were optimized for

electroporation using the Neon Transfection System. Achieving maximum electroporation efficiency often comes at the expense of cell viability, and vice versa (Skruber et al. 2021). In this study, electroporation efficiency was prioritized over cell viability to ensure the successful delivery of CRISPR/Cas9 plasmids into SH-SY5Y cells. High electroporation efficiency increases the likelihood that a significant proportion of SH-SY5Y cells will take up the CRISPR/Cas9 plasmids, which is crucial for achieving an effective knockout in hard-to-transfect cells. While this approach results in lower cell viability, it is an acceptable trade-off, as generating knockout clones in actively proliferating cells may require only a small number of viable cells. These cells are expected to proliferate post-transfection and can subsequently undergo clonal expansion and screening.

Clonal expansion is a critical yet challenging step in the genome editing workflow. It begins with the isolation of a single edited cell, followed by its expansion to generate a homogeneous cell population (Bernhard et al. 2022). Several common methods for clonal isolation include fluorescence-activated cell sorting (FACS), limiting dilution, and clonal picking, which can be combined to enrich cultures with the desired cell population (Martin 2011). Many cell lines, including SH-SY5Y cells, struggle to survive as single cells in vitro, making clonal expansion particularly difficult. These challenges were further exacerbated in this study, as the edited SH-SY5Y cells were subjected to multiple stresses before clonal expansion, including electroporation, prolonged exposure outside the CO_2 incubator, and FACS sorting. To mitigate these issues, both bulk sorting and single-cell sorting methods were employed. Bulk sorting involved sorting 100 or 200 cells into a 15 ml conical tube, followed by transfer to a 10 cm dish, while single-cell sorting involved isolating individual cells into wells of a 96-well plate. The refined clonal expansion strategy used in this study, i.e., bulk sorting followed by clonal picking in a 10 cm dish, significantly enhanced cell proliferation. This improvement is likely due to the presence of supportive signals or growth factors from neighboring cells, which promote cell attachment and proliferation (Kovalevich et al. 2013; Jiao et al. 2017; Li et al. 2023).

Detection is the final and one of the most critical steps in Western blotting. Chemiluminescence detection is highly sensitive, relying on enzymatic reactions to generate signals. However, because these reactions are dynamic, signal intensity can fluctuate over time. Thus, selecting the appropriate chemiluminescent substrate and optimizing both the reaction duration and imaging process is essential (Mathews et al. 2009). In this study, to maximize signal detection for the low-abundance LRRK2 protein, a highly sensitive chemiluminescent substrate from a reputable brand, capable of detecting proteins at the femtogram level, was used. Imaging was performed using a high-resolution CCD camera, with optimized capture parameters. Specifically, cumulative capture mode was utilized, allowing the merging of multiple images to generate a final image with improved intensity.

The SH-SY5Y cell line is known for its heterogeneity, which may explain the limited publications on genome editing in this model. Numerous studies have documented the bidirectional interconversion of neuroblastoma cells from neuroblastic-like (N-type) to intermediate (I-type) or epithelial-like/ substrate-adherent (S-type) phenotypes (Biedler et al. 1973, 1978; Ross et al. 1983; DeClerck et al. 1987; Ciccarone et al. 1989; La Quaglia et al. 1996). Therefore, it is essential to include mock

controls in genome editing experiments to account for this variability. In addition, mock controls are crucial for ensuring that any downstream functional or phenotypic changes are not the result of off-target effects from CRISPR/Cas9 or stress experienced by the cells during the genome editing workflow.

Our optimized protocol and strategy are particularly well-suited for laboratories with limited funding, as it is cost-effective. We successfully performed many steps in-house at minimal cost, including the preparation of competent cells, cloning of gRNAs into PX458 plasmids, isolation of clones using the filter paper method, and hand-casting gradient gels for Western blot analysis.

Conclusion

Knocking out a gene with low endogenous expression is feasible, but it requires careful planning and consideration of the potential compensatory mechanisms and detection challenges. Advances in genome editing technologies and detection methods have made it increasingly possible to study these challenging genes.

To the best of our knowledge, this study is the first to provide a comprehensive protocol for generating LRRK2 knockout SH-SY5Y cells. Our protocol provides a strategy, along with helpful tips and tricks, to effectively knockout the low-expression *LRRK2* gene in the hard-to-transfect SH-SY5Y cells. This protocol can also be easily adapted for other low-expression genes in different hard-to-transfect cell lines.

Supplementary Information The online version contains supplementary material available at https://doi.org/10.1007/s10528-025-11174-4.

Acknowledgements We extend our heartfelt thanks to the Federation of Asian and Oceanian Biochemists and Molecular Biologists (FAOBMB) and Professor Dong-Yan Jin for awarding the FAOBMB Exchange Fellowship and providing financial support (including a student research assistantship and research funding) to Hui-Lan Jong. This assistance facilitated her laboratory attachment at The University of Hong Kong, where she received advanced training in genome editing from Professor Dong-Yan Jin and Assistant Professor Kit-San Yuen. We also express our gratitude to Dr. Feng Zhang at the Massachusetts Institute of Technology for generously sharing the plasmid.

Author Contributions HLJ: Conceptualization, Methodology, Validation, Formal analysis, Investigation, Data curation and visualization, Resources, Writing—original draft, Writing—review & editing, Funding acquisition, Project administration. KSY: Methodology, Validation, Formal analysis, Investigation, Resources, Writing—review & editing, Supervision. DYJ: Formal analysis, Resources, Writing—review & editing, Funding acquisition, Supervision. SLLH: Methodology, Validation, Formal analysis, Investigation, Resources, Writing—review & editing. AI: Funding acquisition, Project review. CHT: Funding acquisition. SKL: Formal analysis, Writing—review & editing, Supervision. YML: Project conceptualization and initiation, Resources, Funding acquisition, Project administration, Supervision. SKC: Conceptualization, Formal analysis, Resources, Writing—review & editing, Funding acquisition, Project administration, Supervision.

Funding This study was funded by a research grant from Centre of Excellence Swiftlet, University Putra Malaysia (6371400-10301) and University Tunku Abdul Rahman Research Fund (IPSR/RMC/UTARRF/2015-C1/L09 & IPSR/RMC/UTARRF/2015-C2/L10).

Data Availability Enquiries about data availability should be directed to the corresponding author.

Declarations

Competing Interest The authors declare no competing interests.

Ethical Approval This study did not involve human or animal subjects and therefore did not require ethics approval.

References

Almudimeegh S (2022) Modulation of LRRK2 mediated signaling in immune cells, UCL (University College London).

Araki M, Ito G, Tomita T (2018) Physiological and pathological functions of LRRK2: implications from substrate proteins. Neuronal Signal 2(4):NS20180005

Arango D, Bittar A, Esmeral NP, Ocasión C, Muñoz-Camargo C, Cruz JC, Reyes LH, Bloch NI (2021) Understanding the potential of genome editing in Parkinson's disease. Int J Mol Sci 22(17):9241

Bahnassawy LA, Nicklas S, Palm T, Menzl I, Birzele F, Gillardon F, Schwamborn JC (2013) The Parkinson's disease-associated LRRK2 mutation R1441G inhibits neuronal differentiation of neural stem cells. Stem Cells Dev 22(18):2487–2496

Baptista MA, Dave KD, Frasier MA, Sherer TB, Greeley M, Beck MJ, Varsho JS, Parker GA, Moore C, Churchill MJ (2013) Loss of leucine-rich repeat kinase 2 (LRRK2) in rats leads to progressive abnormal phenotypes in peripheral organs. PLoS ONE 8(11):e80705

Beccano-Kelly DA, Kuhlmann N, Tatarnikov I, Volta M, Munsie LN, Chou P, Cao L-P, Han H, Tapia L, Farrer MJ (2014) Synaptic function is modulated by LRRK2 and glutamate release is increased in cortical neurons of G2019S LRRK2 knock-in mice. Front Cell Neurosci 8:301

Bernhard P, Feilen T, Rogg M, Fröhlich K, Cosenza-Contreras M, Hause F, Schell C, Schilling O (2022) Proteome alterations during clonal isolation of established human pancreatic cancer cell lines. Cell Mol Life Sci 79(11):561

Biedler JL, Helson L, Spengler BA (1973) Morphology and growth, tumorigenicity, and cytogenetics of human neuroblastoma cells in continuous culture. Cancer Res 33(11):2643–2652

Biedler JL, Roffler-Tarlov S, Schachner M, Freedman LS (1978) Multiple neurotransmitter synthesis by human neuroblastoma cell lines and clones. Cancer Res 38:3751–3757

Biskup S, Moore DJ, Rea A, Lorenz-Deperieux B, Coombes CE, Dawson VL, Dawson TM, West AB (2007) Dynamic and redundant regulation of LRRK2 and LRRK1 expression. BMC Neurosci 8:1–11

Bravo-San Pedro JM, Niso-Santano M, Gómez-Sánchez R, Pizarro-Estrella E, Aiastui-Pujana A, Gorostidi A, Climent V, López de Maturana R, Sanchez-Pernaute R, López de Munain A, Fuentes JM, González-Polo RA (2013) The LRRK2 G2019S mutant exacerbates basal autophagy through activation of the MEK/ERK pathway. Cell Mol Life Sci 70(1):121–136

Chang M-Y, Oh B, Rhee Y-H, Lee S-H (2015) Doxycycline supplementation allows for the culture of human ESCs/iPSCs with media changes at 3-day intervals. Stem Cell Res 15(3):608–613

Chen S, Luo Z, Ward C, Ibañez DP, Liu H, Zhong X, Sharma NK, Qin B, Fan W, Wang D (2020) Generation of two LRRK2 homozygous knockout human induced pluripotent stem cell lines using CRISPR/Cas9. Stem Cell Res 45:101804

Cheng YS, Xu M, Chen G, Beers J, Chen CZ, Liu C, Zou J, Zheng W (2023) A protocol for culture and characterization of human induced pluripotent stem cells after induction. Curr Protocols 3(8):e866

Choi I, Kim B, Byun J-W, Baik SH, Huh YH, Kim J-H, Mook-Jung I, Song WK, Shin J-H, Seo H (2015) LRRK2 G2019S mutation attenuates microglial motility by inhibiting focal adhesion kinase. Nat Commun 6(1):8255

Ciccarone V, Spengler BA, Meyers MB, Biedler JL, Ross RA (1989) Phenotypic diversification in human neuroblastoma cells: expression of distinct neural crest lineages. Cancer Res 49(1):219–225

Covello G, Siva K, Adami V, Denti MA (2014) An electroporation protocol for efficient DNA transfection in PC12 cells. Cytotechnology 66:543–553

DeClerck YA, Bomann ET, Spengler BA, Biedler JL (1987) Differential collagen biosynthesis by human neuroblastoma cell variants. Cancer Res 47:6505–6510

Deleuze V, Soler E, Andrieu-Soler C (2024) Protocol for efficient CRISPR-Cas9-mediated fluorescent tag knockin in hard-to-transfect erythroid cell lines. STAR Protoc 5(2):103016
Do PT, Nguyen CX, Bui HT, Tran LT, Stacey G, Gillman JD, Zhang ZJ, Stacey MG (2019) Demonstration of highly efficient dual gRNA CRISPR/Cas9 editing of the homeologous GmFAD2–1A and GmFAD2–1B genes to yield a high oleic, low linoleic and α-linolenic acid phenotype in soybean. BMC Plant Biol 19:1–14
El-Brolosy MA, Stainier DY (2017) Genetic compensation: a phenomenon in search of mechanisms. PLoS Genet 13(7):e1006780
Erb ML, Moore DJ (2020) LRRK2 and the endolysosomal system in Parkinson's disease. J Parkinsons Dis 10(4):1271–1291
Fernández B, Chittoor-Vinod VG, Kluss JH, Kelly K, Bryant N, Nguyen APT, Bukhari SA, Smith N, Lara Ordóñez AJ, Fdez E (2022) Evaluation of current methods to detect cellular leucine-rich repeat kinase 2 (LRRK2) kinase activity. J Parkinsons Dis 12(5):1423–1447
Fus-Kujawa A, Prus P, Bajdak-Rusinek K, Teper P, Gawron K, Kowalczuk A, Sieron AL (2021) An overview of methods and tools for transfection of eukaryotic cells in vitro. Front Bioeng Biotechnol 9:701031
Gao C, Jiang J, Tan Y, Chen S (2023) Microglia in neurodegenerative diseases: mechanism and potential therapeutic targets. Signal Transduct Target Ther 8(1):359
Ghaedi M, Niklason LE (2016) Human pluripotent stem cells (iPSC) generation, culture, and differentiation to lung progenitor cells. Organoids: Stem Cells, Structure, and Function. Springer, pp 55–92
Giaime E, Tong Y, Wagner LK, Yuan Y, Huang G, Shen J (2017) Age-dependent dopaminergic neurodegeneration and impairment of the autophagy-lysosomal pathway in LRRK-deficient mice. Neuron 96(4):796-807.e796
Gu Y-Z, Vlasakova K, Miller G, Gatto NT, Ciaccio PJ, Kuruvilla S, Besteman EG, Smith R, Reynolds SJ, Amin RP (2023) Early-onset albuminuria and associated renal pathology in leucine-rich repeat kinase 2 knockout rats. Toxicol Pathol 51(1–2):15–26
Gupta RM, Musunuru K (2014) Expanding the genetic editing tool kit: ZFNs, TALENs, and CRISPR-Cas9. J Clin Invest 124(10):4154–4161
Henry AG, Aghamohammadzadeh S, Samaroo H, Chen Y, Mou K, Needle E, Hirst WD (2015) Pathogenic LRRK2 mutations, through increased kinase activity, produce enlarged lysosomes with reduced degradative capacity and increase ATP13A2 expression. Hum Mol Genet 24(21):6013–6028
Hinkle KM, Yue M, Behrouz B, Dächsel JC, Lincoln SJ, Bowles EE, Beevers JE, Dugger B, Winner B, Prots I (2012) LRRK2 knockout mice have an intact dopaminergic system but display alterations in exploratory and motor co-ordination behaviors. Mol Neurodegener 7:1–17
Hoffmann LF, Martins A, Majolo F, Contini V, Laufer S, Goettert MI (2023) Neural regeneration research model to be explored: SH-SY5Y human neuroblastoma cells. Neural Regen Res 18(6):1265–1266
Hwang G-H, Song B, Bae S (2021) Current widely-used web-based tools for CRISPR nucleases, base editors, and prime editors. Gene Genome Editing 1:100004
Ioghen OC, Ceafalan LC, Popescu BO (2023) SH-SY5Y cell line in vitro models for Parkinson disease research—old practice for new trends. J Integr Neurosci 22(1):20
Jiao Q, Li X, An J, Zhang Z, Chen X, Tan J, Zhang P, Lu H, Liu Y (2017) Cell-cell connection enhances proliferation and neuronal differentiation of rat embryonic neural stem/progenitor cells. Front Cell Neurosci 11:200
Joberty G, Fälth-Savitski M, Paulmann M, Bösche M, Doce C, Cheng AT, Drewes G, Grandi P (2020) A tandem guide RNA-based strategy for efficient CRISPR gene editing of cell populations with low heterogeneity of edited alleles. CRISPR J 3(2):123–134
Jordan ET, Collins M, Terefe J, Ugozzoli L, Rubio T (2008) Optimizing electroporation conditions in primary and other difficult-to-transfect cells. J Biomol Tech: JBT 19(5):328
Juárez-Flores DL, González-Casacuberta I, Ezquerra M, Bañó M, Carmona-Pontaque F, Catalán-García M, Guitart-Mampel M, Rivero JJ, Tobias E, Milisenda JC (2018) Exhaustion of mitochondrial and autophagic reserve may contribute to the development of LRRK2 G2019S-Parkinson's disease. J Transl Med 16:1–13
Karra D, Dahm R (2010) Transfection techniques for neuronal cells. J Neurosci 30(18):6171–6177
Kim J, Pajarillo E, Rizor A, Son D-S, Lee J, Aschner M, Lee E (2019) LRRK2 kinase plays a critical role in manganese-induced inflammation and apoptosis in microglia. PLoS ONE 14(1):e0210248
Kovalevich J, Langford D (2013) Considerations for the use of SH-SY5Y neuroblastoma cells in neurobiology. Methods Mol Biol 1078:9–21

La Quaglia MP, Manchester KM (1996) A comparative analysis of neuroblastic and substrate-adherent human neuroblastoma cell lines. J Pediatr Surg 31(2):315–318
Labun K, Montague TG, Krause M, Torres Cleuren YN, Tjeldnes H, Valen E (2019) CHOP-CHOP v3: expanding the CRISPR web toolbox beyond genome editing. Nucleic Acids Res 47(W1):W171–W174
Lander ES (2016) The heroes of CRISPR. Cell 164(1):18–28
Lattanzi A, Meneghini V, Pavani G, Amor F, Ramadier S, Felix T, Antoniani C, Masson C, Alibeu O, Lee C (2019) Optimization of CRISPR/Cas9 delivery to human hematopoietic stem and progenitor cells for therapeutic genomic rearrangements. Mol Ther 27(1):137–150
Lee SB, Kim W, Lee S, Chung J (2007) Loss of LRRK2/PARK8 induces degeneration of dopaminergic neurons in Drosophila. Biochem Biophys Res Commun 358(2):534–539
Li L, Su H, Ji Y, Zhu F, Deng J, Bai X, Li H, Liu X, Luo Y, Lin B (2023) Deciphering cell-cell interactions with integrative single-cell secretion profiling. Advanced Science 10(19):2301018
Lin C-H, Tsai P-I, Wu R-M, Chien C-T (2010) LRRK2 G2019S mutation induces dendrite degeneration through mislocalization and phosphorylation of tau by recruiting autoactivated GSK3β. J Neurosci 30(39):13138–13149
Liu W, Li S, Zhang Y, Li J, Li Y (2018) Efficient CRISPR-based genome editing using tandem guide RNA s and editable surrogate reporters. FEBS Open Bio 8(7):1167–1175
Lorberbaum T (2013) Pouring a gradient gel. YouTube, Video. https://www.youtube.com/watch?v=zu5a-kpMK8k.
Luo Y, Sakamoto K (2023) Ethyl pyruvate protects SHSY5Y cells against 6-hydroxydopamine-induced neurotoxicity by upregulating autophagy. PLoS ONE 18(2):e0281957
Macarrón Palacios A, Korus P, Wilkens BG, Heshmatpour N, Patnaik SR (2024) Revolutionizing in vivo therapy with CRISPR/Cas genome editing: breakthroughs, opportunities and challenges. Front Genome Editing 6:1342193
Martin BM (2011) Clonal isolation and plating efficiency. eLS. L. Wiley
Mathews ST, Plaisance EP, Kim T (2009) Imaging systems for westerns: chemiluminescence vs. infrared detection. Protein blotting and detection: methods and protocols. Sprinder, pp 499–513
Migheli R, Del Giudice MG, Spissu Y, Sanna G, Xiong Y, Dawson TM, Dawson VL, Galioto M, Rocchitta G, Biosa A (2013) LRRK2 affects vesicle trafficking, neurotransmitter extracellular level and membrane receptor localization. PLoS ONE 8(10):e77198
Modrzejewski D, Hartung F, Sprink T, Krause D, Kohl C, Wilhelm R (2019) What is the available evidence for the range of applications of genome-editing as a new tool for plant trait modification and the potential occurrence of associated off-target effects: a systematic map. Environ Evid 8(1):1–33
Moon SB, Kim DY, Ko J-H, Kim Y-S (2019) Recent advances in the CRISPR genome editing tool set. Exp Mol Med 51(11):1–11
Navarro-Guerrero E, Baronio R, Tay C, Knight JC, Ebner DV (2024) Optimized protocol for CRISPR knockout of human iPSC-derived macrophages. STAR Protoc 5(1):102903
Ness D, Ren Z, Gardai S, Sharpnack D, Johnson VJ, Brennan RJ, Brigham EF, Olaharski AJ (2013) Leucine-rich repeat kinase 2 (LRRK2)-deficient rats exhibit renal tubule injury and perturbations in metabolic and immunological homeostasis. PLoS ONE 8(6):e66164
Østergaard FG (2024) Knocking out the LRRK2 gene increases sensitivity to wavelength information in rats. Sci Rep 14(1):4984
Pellegrini L, Hauser DN, Li Y, Mamais A, Beilina A, Kumaran R, Wetzel A, Nixon-Abell J, Heaton G, Rudenko I (2018) Proteomic analysis reveals co-ordinated alterations in protein synthesis and degradation pathways in LRRK2 knockout mice. Hum Mol Genet 27(18):3257–3271
Plowey ED, Johnson JW, Steer E, Zhu W, Eisenberg DA, Valentino NM, Liu Y-J, Chu CT (2014) Mutant LRRK2 enhances glutamatergic synapse activity and evokes excitotoxic dendrite degeneration. Biochim Biophys Acta 1842(9):1596–1603
Quintero-Espinosa DA, Sanchez-Hernandez S, Velez-Pardo C, Martin F, Jimenez-Del-Rio M (2023) LRRK2 knockout confers resistance in HEK-293 cells to rotenone-induced oxidative stress, mitochondrial damage, and apoptosis. Int J Mol Sci 24(13):10474
Rakotoarisoa M, Angelov B, Garamus VM, Angelova A (2019) Curcumin-and fish oil-loaded spongosome and cubosome nanoparticles with neuroprotective potential against H2O2-induced oxidative stress in differentiated human SH-SY5Y cells. ACS Omega 4(2):3061–3073
Ramalingam M, Huh Y-J, Lee Y-I (2019) The impairments of α-synuclein and mechanistic target of rapamycin in rotenone-induced SH-SY5Y cells and mice model of Parkinson's disease. Front Neurosci 13:1028

Ran F, Hsu PD, Wright J, Agarwala V, Scott DA, Zhang F (2013) Genome engineering using the CRISPR-Cas9 system. Nat Protoc 8(11):2281–2308
Rocha EM, Keeney MT, Di Maio R, De Miranda BR, Greenamyre JT (2022) LRRK2 and idiopathic Parkinson's disease. Trends Neurosci 45(3):224–236
Rodríguez-Losada N, de la Rosa J, Larriva M, Wendelbo R, Aguirre JA, Castresana JS, Ballaz SJ (2020) Overexpression of alpha-synuclein promotes both cell proliferation and cell toxicity in human SH-SY5Y neuroblastoma cells. J Adv Res 23:37–45
Ross RA, Spengler BA, Biedler JL (1983) Coordinate morphological and biochemical interconversion of human neuroblastoma cells. J Natl Cancer Inst 71(4):741–747
Schapansky J, Nardozzi JD, Felizia F, LaVoie MJ (2014) Membrane recruitment of endogenous LRRK2 precedes its potent regulation of autophagy. Hum Mol Genet 23(16):4201–4214
Shutinoski B, Hakimi M, Harmsen IE, Lunn M, Rocha J, Lengacher N, Zhou YY, Khan J, Nguyen A, Hake-Volling Q (2019) Lrrk2 alleles modulate inflammation during microbial infection of mice in a sex-dependent manner. Sci Transl Med 11(511):eaas9292
Simpson C, Vinikoor-Imler L, Nassan FL, Shirvan J, Lally C, Dam T, Maserejian N (2022) Prevalence of ten LRRK2 variants in Parkinson's disease: a comprehensive review. Parkinsonism Relat Disord 98:103–113
Sinclair F, Begum AA, Dai CC, Toth I, Moyle PM (2023) Recent advances in the delivery and applications of nonviral CRISPR/Cas9 gene editing. Drug Deliv Transl Res 13(5):1500–1519
Skruber K, Read T-A, Vitriol EA (2021) Delivering defined amounts of purified protein with high precision into living cells. STAR Protoc 2(1):100272
Snoderly-Foster LJ, Olivas WM (2022) Regulation of Parkinson's disease-associated genes by Pumilio proteins and microRNAs in SH-SY5Y neuronal cells. PLoS ONE 17(9):e0275235
Taymans J-M, Fell M, Greenamyre T, Hirst WD, Mamais A, Padmanabhan S, Peter I, Rideout H, Thaler A (2023) Perspective on the current state of the LRRK2 field. NPJ Parkinsons Dis 9(1):104
Tolosa E, Vila M, Klein C, Rascol O (2020) LRRK2 in Parkinson disease: challenges of clinical trials. Nat Rev Neurol 16(2):97–107
Tombesi G, Kompella S, Favetta G, Chen C, Zhao Y, Sevegnani M, Marte A, Battisti I, Morosin E, Ornaghi M, Iannotta L, Plotegher N, Civiero L, Onofri F, Eickholt BJ, Piccoli G, Arrigoni G, Beccano-Kelly D, Manzoni C, Parisiadou L, Greggio E (2024) LRRK2 regulates synaptic function through BDNF signaling and actin cytoskeleton. eLife. Sciences Publications Ltd
Tong Y, Yamaguchi H, Giaime E, Boyle S, Kopan R, Kelleher RJ III, Shen J (2010) Loss of leucine-rich repeat kinase 2 causes impairment of protein degradation pathways, accumulation of α-synuclein, and apoptotic cell death in aged mice. Proc Natl Acad Sci USA 107(21):9879–9884
Tong Y, Giaime E, Yamaguchi H, Ichimura T, Liu Y, Si H, Cai H, Bonventre JV, Shen J (2012) Loss of leucine-rich repeat kinase 2 causes age-dependent bi-phasic alterations of the autophagy pathway. Mol Neurodegener 7:1–16
Uhlén M, Fagerberg L, Hallström BM, Lindskog C, Oksvold P, Mardinoglu A, Sivertsson Å, Kampf C, Sjöstedt E, Asplund A, Olsson I, Edlund K, Lundberg E, Navani S, Szigyarto CA-K, Odeberg J, Djureinovic D, Takanen JO, Hober S, Alm T, Edqvist P-H, Berling H, Tegel H, Mulder J, Rockberg J, Nilsson P, Schwenk JM, Hamsten M, von Feilitzen K, Forsberg M, Persson L, Johansson F, Zwahlen M, von Heijne G, Nielsen J, Pontén F (2015) Tissue-based map of the human proteome. Science 347(6220):1260419
Xu Z, Yang D, Huang X, Huang H (2021) Astragaloside IV protects 6-hydroxydopamine-induced SH-SY5Y cell model of Parkinson's disease via activating the JAK2/STAT3 pathway. Front Neurosci 15:631501
Yin D, Wells J, Clinton J, Volpe L.-A, Grady K, Curley J (2014) Development of lipid-based transfection reagents for efficient expression of transgenes in hard-to-transfect cell types. Cancer Res., Amer Assoc Cancer Research 615 Chestnut ST, 17th Floor, Philadelphia, PA
Yip BH (2020) Recent advances in CRISPR/Cas9 delivery strategies. Biomolecules 10(6):839
Yuen K-S, Chan C-P, Kok K-H, Jin D-Y (2017a) Mutagenesis and genome engineering of Epstein-Barr virus in cultured human cells by CRISPR/Cas9. In Vitro Mutagenesis: Methods Protocols. https://doi.org/10.1007/978-1-4939-6472-7_2
Yuen K-S, Chan C-P, Kok K-H, Jin D-Y (2017b) Mutagenesis and Genome Engineering of Epstein-Barr Virus in Cultured Human Cells by CRISPR/Cas9. In Vitro mutagenesis: methods and protocols A. Reeves. Springer, pp 23–31
Zhang M, Yi F, Wu J, Tang Y (2022) The efficient generation of knockout microglia cells using a dual-sgRNA strategy by CRISPR/Cas9. Front Mol Neurosci 15:1008827

Zhao J, Geng L, Chen Y, Wu C (2020) SNHG1 promotes MPP+-induced cytotoxicity by regulating PTEN/AKT/mTOR signaling pathway in SH-SY5Y cells via sponging miR-153-3p. Biol Res 53:1–11

Authors and Affiliations

Hui-Lan Jong[2] · Kit-San Yuen[3,4] · Dong-Yan Jin[3] · Susan Ling Ling Hoe[5] · Aini Ideris[6] · Chee-Hong Tan[7] · Sau-Kuen Lam[2] · Yang-Mooi Lim[2] · Soon-Keng Cheong[1]

✉ Soon-Keng Cheong
cheongsk@utar.edu.my

1 Department of Medicine, M. Kandiah Faculty of Medicine and Health Sciences, Universiti Tunku Abdul Rahman, Kajang, Selangor, Malaysia

2 Department of Pre-Clinical Sciences, M. Kandiah Faculty of Medicine and Health Sciences, Universiti Tunku Abdul Rahman, Kajang, Selangor, Malaysia

3 School of Biomedical Sciences, Li Ka Shing Faculty of Medicine, The University of Hong Kong, Pokfulam, Hong Kong, China

4 Present Address: School of Nursing, Tung Wah College, Ma Kam Chan Memorial Building, 31 Wylie Road, Kowloon, Hong Kong, China

5 Molecular Pathology Unit, Cancer Research Centre, Institute for Medical Research, National Institutes of Health Malaysia, Shah Alam, Selangor, Malaysia

6 Department of Veterinary Clinical Studies, Faculty of Veterinary Medicine, Universiti Putra Malaysia, Serdang, Malaysia

7 Inbit Biotech Sdn. Bhd., No. 8, Lorong University B, Seksyen 16, 46350 Petaling Jaya, Selangor, Malaysia

Jong, HL., Yuen, KS., Jin, DY. et al. Leucine-Rich Repeat Kinase 2 (LRRK2) Knockout Induces Spontaneous Interconversion and Senescence in SH-SY5Y Neuroblastoma Cells. The ageing genome: from mechanisms to disease. European Molecular Biology Laboratory (EMBL), Heidelberg, Germany, 10 – 13 June 2025. pp. 75 (Abstract)

59

Leucine-rich repeat kinase 2 (lrrk2) knockout induces spontaneous interconversion and senescence in sh-sy5y neuroblastoma cells

Hui-Lan Jong2, Kit-San Yuen1, Dong-Yan Jin1, Sau-Kuen Lam2, Yang-Mooi Lim2, Soon-Keng Cheong2

1 The University of Hong Kong, Hong Kong
2 University Tunku Abdul Rahman, Malaysia

Presenter: Hui-Lan Jong

An increase in LRRK2 kinase activity contributes to Parkinson's disease (PD) pathogenesis. LRRK2 kinase inhibition is a promising therapeutic approach, but LRRK2 knockout (KO) animal models show abnormal phenotypes. Therefore, evaluating the adverse effects of LRRK2 loss is crucial to ensure the safety of LRRK2 kinase inhibitors. We previously developed LRRK2 KO SH-SY5Y neuroblastoma cells (LKO cells) to gain a deeper understanding of the consequences of LRRK2 loss. This study further characterizes these cells. Morphological changes in LKO cells were assessed, along with cell-substrate adhesion strength. Cumulative population doubling was used to assess cell proliferation. Senescence-associated beta-galactosidase (SA-β-gal) staining and autophagy vacuole detection were performed. Mitochondrial respiration was evaluated using a real-time metabolic analyzer. LKO cells converted into I- and S-type neuroblastoma cells, exhibiting senescence characteristics, including increased size ($p < 0.001$), flattening, loss of neurite-like processes, and stronger adhesion to the substrate compared to wild-type (WT) and mock cells. Over 35 days, LKO cells proliferated slower or ceased to proliferate. Mycoplasma testing confirmed no contamination. The percentage of SA-β-gal positive cells in LKO cells increased significantly ($p < 0.001$). Autophagy and mitochondrial respiration were markedly reduced in LKO cells ($p < 0.001$ and $p < 0.01$, respectively). Loss of LRRK2 may drive neuroblastoma cell interconversion and induce senescence. Future research should investigate transcriptional and epigenetic alterations related to LRRK2 loss to understand its role in these processes.

Jong, HL., Yuen, KS., Jin, DY. et al. Leucine-Rich Repeat Kinase 2 (LRRK2) Knockout Leads to Senescence-Like Phenotypes in SH-SY5Y Neuroblastoma Cells. Malays J Pathol 2024; 46(3): 495 (Abstract)

MEDICAL GENETIC

MG01. Leucine-Rich Repeat Kinase 2 (LRRK2) Knockout Leads to Senescence-Like Phenotypes in SH-SY5Y Neuroblastoma Cells

Hui-Lan Jong[2], Kit-San Yuen[3], Dong-Yan Jin[3], Yang-Mooi Lim[2], Susan Ling Ling Hoe[4], Aini Ideris[5], Chee-Hong Tan[6], Sau-Kuen Lam[2], Soon-Keng Cheong[1]

[1]Department of Medicine, Faculty of Medicine and Health Sciences, University Tunku Abdul Rahman, Selangor, Malaysia; [2]Department of Pre-Clinical Sciences, Faculty of Medicine and Health Sciences, University Tunku Abdul Rahman, Selangor, Malaysia; [3]School of Biomedical Sciences, Li Ka Shing Faculty of Medicine, The University of Hong Kong, Pokfulam, Hong Kong; [4]Molecular Pathology Unit, Cancer Research Centre, Institute for Medical Research, National Institutes of Health Malaysia, Selangor, Malaysia; [5]Department of Veterinary Clinical Studies, Faculty of Veterinary Medicine, University Putra Malaysia, Serdang, Malaysia; [6]Inbit Biotech Sdn. Bhd., No. 8, Lorong University B, Sekyen 16, 46350 Petaling Jaya, Selangor, Malaysia

Introduction: Autosomal dominant missense mutations within the *leucine-rich repeat kinase 2 (LRRK2)* gene are the most common genetic cause of Parkinson's disease (PD). An aberrant increase in LRRK2 activity contributes to the pathogenesis of PD. The present study was undertaken to generate LRRK2 knockout neuroblastoma SH-SY5Y (LKO) cells which can be leveraged to gain comprehensive insights into the impact of LRRK2 loss. *Materials and Methods:* LKO cells were generated using the CRISPR/Cas9 genome editing tool. DNA sequencing and Western blot were performed to confirm the LRRK2 knockout and protein ablation, respectively. Subsequently, cell morphological changes were examined under a cell imaging system, and cell size was measured using an automated cell counter. The cumulative population doubling of cells was calculated to plot the growth kinetics. Senescence-associated beta-galactosidase (SA-β-gal) staining was performed to determine the percentage of the positively stained population. Mitochondrial function was assessed using a real-time cell metabolic analyser. Results: CRISPR/Cas9-mediated the introduction of frameshift mutation and premature stop codon led to knockout of LRRK2. The LKO cells were significantly larger ($p<0.001$), exhibited loss of neurite-like processes, and proliferated slower than WT and mock cells. Besides that, in LKO cells, the percentage of the SA-β-gal positive population increased significantly ($p<0.001$) while mitochondrial respiration reduced markedly ($p<0.01$). *Discussion/ Conclusion:* Loss of LRRK2 led to senescence-like phenotypes in SH-SY5Y. A comprehensive assessment of phenotypic changes resulting from inhibition of LRRK2 is essential to ensure the safety of LRRK2 inhibitors.

Jong, HL., Yuen, KS., Jin, DY. et al. Generation of LRRK2 Knockout Neuroblastoma Cells by CRISPR/Cas9-mediated Genome Editing. *16th Federation of Asian and Oceanian Biochemists and Molecular Biologists (FAOBMB) Congress.* Christchurch, New Zealand, 22- 25 November 2021. pp. 236 (Abstract)

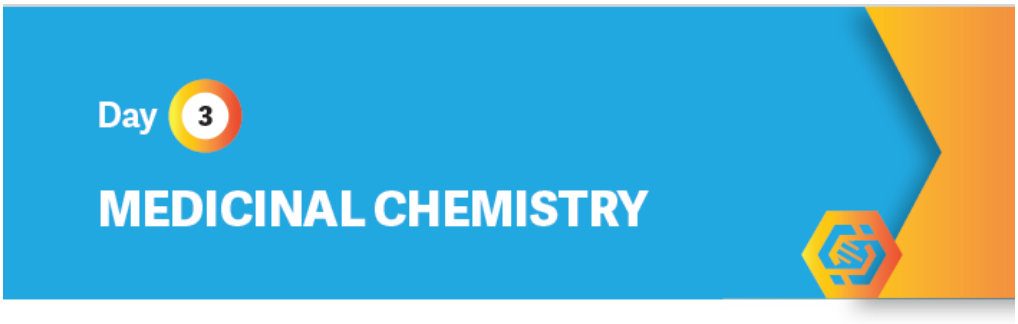

Generation of LRRK2 knockout neuroblastoma cells by CRISPR/Cas9-mediated genome editing

Hui-Lan Jong[2], Kit-San Yuen[3], Dong-Yan Jin[3], Susan Ling Ling Hoe[4] Soon-Keng Cheong[5], Aini Ideris[6], Chee-Hong Tan[7], **Yang-Mooi Lim[1&2]**

[1]*Center for Cancer Research,*

[2]*Department of Pre-Clinical Sciences, Faculty of Medicine and Health Sciences, University Tunku Abdul Rahman, Selangor, Malaysia*

[3]*School of Biomedical Sciences, Li Ka Shing Faculty of Medicine, The University of Hong Kong, Pokfulam, Hong Kong*

[4]*Molecular Pathology Unit, Cancer Research Centre, Institute for Medical Research, National Institutes of Health Malaysia, Selangor, Malaysia*

[5]*Department of Medicine, Faculty of Medicine and Health Sciences, University Tunku Abdul Rahman, Selangor, Malaysia*

[6]*Department of Veterinary Clinical Studies, Faculty of Veterinary Medicine, University Putra Malaysia, Serdang, Malaysia*

[7]*Inbit Biotech Sdn. Bhd., No. 8, Lorong University B, Seksyen 16, 46350 Petaling Jaya, Selangor, Malaysia*

To date, there is no disease-modifying treatment for Parkinson's disease (PD). Abnormal elevation in leucine rich repeat kinase (LRRK2) activity contributes to pathogenesis of PD. The present study was undertaken to generate LRRK2 KO SH-SY5Y cells (hereafter named as LKO cells), which can be used for an in-depth study of adverse effects of loss of LRRK2.

CRISPR/Cas9 was used to generate LKO cells. Sequencing was utilized to confirm the deletion of target region. Cell morphology, size, proliferation rate and number of autophagic vacuoles of wildtype (WT) and LKO cells were assessed. qPCR was performed to evaluate the expression of autophagy, cell cycle and apoptosis markers.

CRISPR/Cas9 removed 69 bp in LRRK2 exon 1. Resulting LKO cells showed altered morphological characteristics, number of autophagic vacuoles and proliferation rate which distinguished them from WT cells. Autophagy markers (BECN1, AMPK, LC3II, p62 and mTOR) expression were dysregulated, hence indicating that LRRK2 might play a role in the regulation of autophagy. mRNA expression of cell cycle markers (CCNA2, CCNB1 and CCND1) were significantly downregulated. This is in line with the lower cell proliferation rate observed in LKO cells. BAX and BCL2 mRNA expression were upregulated and downregulated, respectively. Both CASP3 and CASP9 mRNA expression were upregulated, suggesting that apoptosis might be elevated in LKO cells.

LKO cells are a valuable tool for elucidating the role of LRRK2 in PD. Thorough evaluation of phenotypic changes due to loss of LRRK2 is indispensable to ensure the safety of LRRK2 inhibitors.